

Alterations in network activity and STN beta bursts in Parkinson's disease

Inaugural-Dissertation

zur Erlangung des Doktorgrades
der Mathematisch-Naturwissenschaftlichen Fakultät
der Heinrich-Heine-Universität Düsseldorf

vorgelegt von

Matthias Martin Sure

aus Marburg

Düsseldorf, November 2022

aus dem Institut für Klinische Neurowissenschaften und Medizinische Psychologie
der Heinrich-Heine-Universität Düsseldorf

Gedruckt mit der Genehmigung der
Mathematisch-Naturwissenschaftlichen Fakultät der
Heinrich-Heine-Universität Düsseldorf

Berichterstatter:

1. Prof. Dr. Esther Florin
2. Prof. Dr. Thomas Heinzel

Tag der mündlichen Prüfung: 31.01.2023

Contents

Glossary	7
Summary	8
Zusammenfassung	9
1 General introduction	11
1.1 Brain activity	15
1.1.1 Neural oscillations	15
1.1.2 Neural events	16
1.1.3 Resting-state networks	17
1.2 Measuring brain activity	19
1.2.1 Electrophysiological signal	19
1.2.2 Magnetoencephalography	20
1.2.2.1 Detection of magnetic fields	20
1.2.2.2 Reconstruction of neural activity	23
1.2.3 Local field potentials	28
1.3 Parkinson's disease	29
1.3.1 Clinical characteristics	29
1.3.2 Basal ganglia-cortical loop	30
1.3.3 Subthalamic nucleus	31
1.3.4 Pathology and pathophysiology	31
1.3.5 Therapy	32
2 Objectives	36
3 Study 1: Dopaminergic modulation of spectral and spatial characteristics of parkinsonian STN beta bursts	38
3.1 Abstract	38
3.2 Introduction	39
3.3 Material and methods	40
3.3.1 Subjects and surgery	40
3.3.2 Experimental setup and recordings	41
3.3.3 Signal processing	41
3.3.4 Detection of bursts in the beta-frequency range	42
3.3.5 Statistical analysis	43

3.4	Results	44
3.4.1	Beta power	44
3.4.2	Burst characteristics	44
3.4.3	Clinical relevance of burst characteristics	45
3.5	Discussion	48
3.5.1	Slight directionality of the beta burst amplitude	48
3.5.2	Beta burst activity is frequency specific	48
3.5.3	Burst duration best suited as stimulation trigger in closed-loop DBS . .	49
3.5.4	Limitations	50
3.5.5	Conclusion	50
4	Study 2: Cortical network formation based on subthalamic beta bursts in Parkinson's disease	52
4.1	Abstract	52
4.2	Introduction	53
4.3	Methods	55
4.3.1	Subjects and surgery	55
4.3.2	Experimental setup and recording	55
4.3.3	Signal processing	56
4.3.4	Cortical event-related fields	56
4.3.5	Statistical analysis	58
4.4	Results	60
4.4.1	Cortical activity linked to the onset of STN beta bursts and the maximum	60
4.4.2	Cortical ERFs in areas related to somatosensory/motor processing . . .	61
4.4.3	Cortical ERFs in areas related to associative processing	61
4.4.4	Cortical ERFs in areas related to limbic processing	63
4.4.5	Cortical ERFs in areas related to speech/vision processing	64
4.5	Discussion	66
4.5.1	Neuronal event triggered cortical activity in humans	66
4.5.2	STN beta bursts involved in STN-cortico network formation	66
4.5.3	STN beta bursts and their role in the BGC loop	68
4.5.4	Laterality of the BGC loop impairment	69
4.5.5	Differences between burst characteristics	70
4.5.6	Conclusion	70
5	Study 3: Alterations of resting-state networks of Parkinson's disease patients after subthalamic DBS surgery	72

5.1	Abstract	72
5.2	Introduction	74
5.3	Methods	76
5.3.1	Subjects and surgery	76
5.3.2	Experimental setup and recordings	76
5.3.3	Signal processing	78
5.3.4	Resting-state network estimation	79
5.3.5	Assignment of RSNs of interest	80
5.3.6	Statistical testing between RSNs of the pre- and post-condition	82
5.3.7	Overlap of PD RSNs with healthy RSNs	83
5.3.8	Comparison of the low and high PAC frequencies	83
5.4	Results	85
5.4.1	Patient Characteristics	85
5.4.2	Changes in RSNs	85
5.4.3	Sensory-motor network	86
5.4.4	Visual network	86
5.4.5	Fronto-occipital network	90
5.4.6	Frontal network	90
5.4.7	Comparison of low and high PAC frequencies	92
5.5	Discussion	93
5.5.1	DBS surgery alters RSNs due to the stun effect	93
5.5.2	Alterations in different functional RSNs	93
5.5.3	Higher correspondence of pre-surgery RSNs with healthy RSNs	95
5.5.4	Low frequency components are altered by electrode implantation	96
5.5.5	Limitations	97
5.6	Conclusion	98
6	General discussion	99
6.1	Summary	105
7	Outlook	107
8	References	109
9	Erklärung	138
10	Danksagung	139

11 Appendix	140
11.1 Publications	140
11.2 Supplementary results	141

Glossary

BGC	Basal ganglia-cortical
BOLD	Blood oxygenation level dependent
DBS	Deep brain stimulation
EEG	Electroencephalography
ERF	Event-related fields
fMRI	Functional magnetic resonance imaging
FON	Fronto-occipital network
GABA	γ -aminobutyric acid
GPe	Globus pallidus externus
GPi	Globus pallidus internus
hBB	High beta band
HC	Healthy controls
HPI	Head position indicator
iBP	Individual beta peak frequency
IPG	Implantable pulse generator
lBB	Low beta band
LCMV	Linearly constrained minimum variance
LFP	Local field potential
MEG	Magnetoencephalography
NET	Neuronal-event-triggered
PAC	Phase-amplitude coupling
PD	Parkinson's disease
RSN	Resting-state network
SNr	Substantia nigra
SQUID	Superconducting QUantum Interference Device
SSP	Singal-space projector
STN	Subthalamic nucleus
UPDRS-III	Unified Parkinson's Disease Rating Scale motor score

Summary

Neural oscillations provide a central contribution to the functional states of individual brain regions and the neural communication between brain regions. Large-scale functional networks are usually determined based on temporally extended oscillations, e.g., phase-amplitude cross-frequency coupling between low and high-frequency oscillations. However, neural oscillations can also occur transiently in the form of temporally limited neural events, a temporary power increase in a specific frequency band, and it can be assumed that since neural events can occur synchronously in different brain regions, these events also contribute to network formation.

The central topic of this work is network formation by subcortical oscillatory neural events in humans, on the example of subthalamic beta bursts, which invasive methods can reliably determine. Unfortunately, non-invasive methods do not provide the spatial or temporal resolution to detect subcortical neural events. Therefore, brain activity was recorded from patients with Parkinson's disease undergoing therapeutic deep brain stimulation (DBS) of the subthalamic nucleus (STN), where beta bursts are well-known neural events that have been linked to the pathophysiology of the disease. During a few days after DBS surgery, it was possible to simultaneously record both local field potentials (LFP) in the STN via externalized DBS electrodes and activity at the cortex via magnetoencephalography (MEG) with a high temporal resolution. Recordings were performed during rest, both ON and OFF dopaminergic medication.

The current thesis comprises three empirical studies. In study 1, the spatial and spectral characteristics of STN beta bursts in response to dopaminergic medication were investigated using directional DBS electrodes. The aim was to determine optimal settings for the detection of STN beta bursts. Based on study 1, study 2 investigated network formation by STN beta bursts using combined subcortical LFP and cortical MEG recordings. For network formation, cortical activity temporally coupled to the occurrence of STN beta bursts was examined. Finally, study 3 investigated the effect of DBS electrode implantation on MEG resting-state networks (RSN) to identify potential neurophysiological mechanisms of the stun effect, a transient improvement of motor symptoms following the electrode implantation.

The present work shows that STN beta bursts are involved in forming multifunctional networks between the cortex and the STN. Furthermore, DBS electrode implantation affected the frontal, fronto-occipital, and visual RSN, in addition to the expected changes in the motor network.

Zusammenfassung

Neurale Oszillationen liefern einen zentralen Beitrag zu den Funktionszuständen einzelner Hirnregionen und zur neuronalen Kommunikation zwischen Hirnregionen. Weitreichende funktionelle Netzwerke werden in der Regel auf der Grundlage von zeitlich ausgedehnten Oszillationen bestimmt, z. B. durch Phasen-Amplituden-Kreuzfrequenz-Kopplung zwischen nieder- und hochfrequenten Oszillationen. Neurale Oszillationen können jedoch auch transient in Form von zeitlich begrenzten neuronalen Ereignissen, einer vorübergehenden Erhöhung der Power in einem bestimmten Frequenzband, auftreten. Es ist anzunehmen, dass, da neurale Ereignisse synchron in verschiedenen Hirnregionen auftreten können, diese Ereignisse auch zur Netzwerkbildung beitragen.

Zentrales Thema dieser Arbeit ist die Netzwerkbildung durch subkortikale oszillatorische neurale Ereignisse beim Menschen am Beispiel der subthalamischen Beta-Bursts, die mit invasiven Methoden zuverlässig bestimmt werden können. Leider bieten nicht-invasive Methoden nicht die räumliche oder zeitliche Auflösung, um subkortikale neurale Ereignisse zu erfassen. Daher wurde die Hirnaktivität von Parkinson-Patienten aufgezeichnet, bei denen eine therapeutische tiefe Hirnstimulation (DBS) des Nucleus subthalamicus (STN) durchgeführt wurde, wo Beta-Bursts bekannte neurale Ereignisse sind, die mit der Pathophysiologie der Krankheit in Verbindung gebracht werden. Einige Tage nach der DBS-Operation war es möglich, gleichzeitig sowohl lokale Feldpotentiale (LFP) im STN über externalisierte DBS-Elektroden als auch die Aktivität im Kortex über Magnetoenzephalografie (MEG) mit hoher zeitlicher Auflösung zu messen. Die Aufzeichnungen erfolgten in Ruhe, sowohl nach Einnahme als auch nach Absetzung dopaminerger Medikamente.

Die vorliegende Arbeit umfasst drei empirische Studien. In Studie 1 wurden die räumlichen und spektralen Eigenschaften von STN-Beta-Bursts als Reaktion auf dopaminerge Medikation mithilfe von gerichteten DBS-Elektroden untersucht. Ziel war es, optimale Einstellungen für die Erkennung von STN-Beta-Bursts zu ermitteln. Auf der Grundlage von Studie 1 wurde in Studie 2 die Netzwerkbildung durch STN-Beta-Bursts auf Basis kombinierter subkortikaler LFP- und kortikaler MEG-Messungen untersucht. Für die Netzwerkbildung wurde die kortikale Aktivität untersucht, die zeitlich an das Auftreten von STN-Beta-Bursts gekoppelt ist. Schließlich wurde in Studie 3 die Wirkung der DBS-Elektrodenimplantation auf MEG-Ruhenetzwerke (RSN) untersucht, um mögliche neurophysiologische Mechanismen des Setzeffekts, einer vorübergehenden Verbesserung der motorischen Symptome nach der Elektrodenimplantation, zu identifizieren.

Die vorliegende Arbeit zeigt, dass STN-Beta-Bursts an der Bildung multifunktionaler Netzwerke zwischen dem Kortex und dem STN beteiligt sind. Darüber hinaus beeinflusste die DBS-Elektrodenimplantation neben den erwarteten Veränderungen im motorischen Netzwerk auch das frontale, fronto-okzipitale und visuelle RSN.

1 General introduction

Due to its high prevalence among the elderly (1 % in a population over the age of 60), idiopathic Parkinson’s disease (PD) is a common disease (Tysnes and Storstein, 2017). It is, characterized by debilitating motor and non-motor symptoms (Przedborski, 2017). Key symptoms of PD include depletion and slowing of movement, increased muscle tone, a resting tremor, and a loss of standing reflexes (Hughes et al., 1992). Unfortunately, as of today (2022), there is no cure for this disease, but there are several symptomatic treatments available, including deep brain stimulation (DBS; Deuschl et al., 2006). Although the mechanism of action of DBS is not yet fully understood (Ashkan et al., 2017), this therapy provides a unique opportunity to gain knowledge about DBS-treatable conditions such as PD, along with valuable insights into brain systems (Drummond and Chen, 2020). In particular, during the implantation of DBS electrodes (Fig. 1.1A), one can record local field potentials (LFP) in subcortical target areas with high temporal resolution (i.e., millisecond precision; Maling et al., 2018). In combination with cortical electroencephalographic (EEG)/magnetoencephalographic (MEG; Fig. 1.1B) recordings, functional cortico-subcortical networks can also be delineated with a temporal resolution corresponding to ongoing fluctuations in neural activity. Analyzing such networks can help to understand the working mechanisms of the brain. For this purpose, however, the so-called *stun effect* must be better understood. The *stun effect* describes a temporary improvement of PD symptoms only by implantation of the electrode without stimulation (Chen et al., 2006; Mann et al., 2009). These changes are not yet fully understood and, therefore, an unknown quantity in the analysis of brain activity shortly after electrode implantation.

MEG and EEG are non-invasive functional neuroimaging methods that allow direct recording of electromagnetic brain activity. EEG/MEG measures the electromagnetic signals generated by the postsynaptic potentials of active neural populations. In contrast, functional magnetic resonance imaging (fMRI) indirectly measures brain activity via the concentration of oxygen in the blood, which increases with increased activity of the neural populations. While fMRI can image whole-brain activity with a high spatial resolution (< 1 mm), its temporal resolution is well above the time domain of neural processing (> 500 ms). In contrast, EEG/MEG can temporally resolve the synchronous activity of neuron populations. However, the spatial resolution drops off considerably for subcortical activity (i.e., the magnetic field decreases with the square of the distance, and the electric field decreases linearly with the distance; Hall et al., 2014).

In order to measure whole-brain network activity from subcortical and cortical regions, a carefully constructed experiment can be conducted using LFP and MEG recordings. A straightfor-

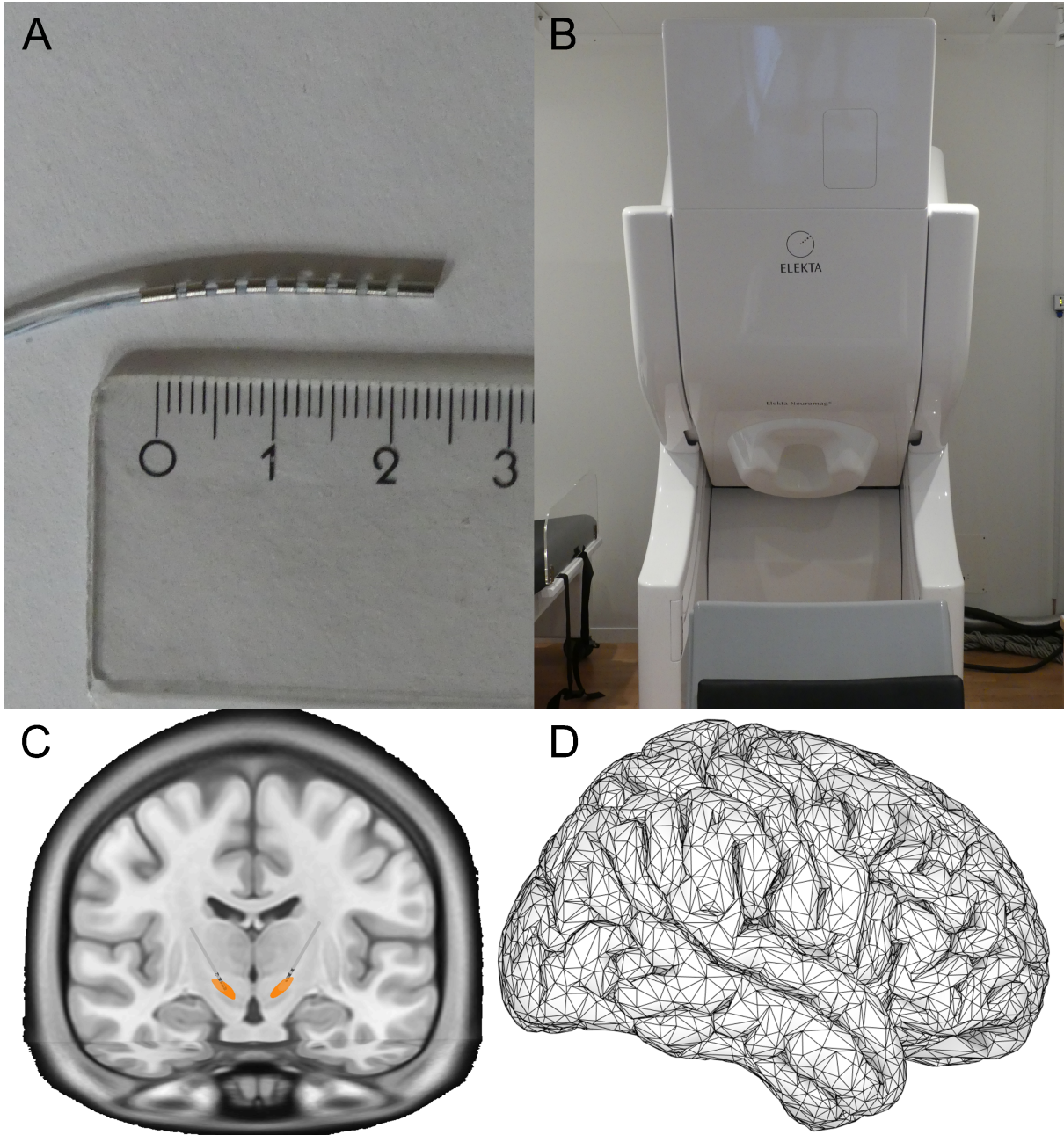


Figure 1.1: Combined MEG and LFP recordings

(A) A macroelectrode (Boston Scientific Corporation, Marlborough, USA) that can be used for DBS as well as LFP recording. Ruler (scale in cm) shown for size comparison. (B) Dewar and gantry of a 306 channel MEG system (Elekta Neuromag, Finland). (C) Reconstructed location of a macroelectrode implanted for DBS and LFP recordings via MRI and CT imaging (created using Lead-DBS). The orange area marks the STN, the target region for the implanted electrode, from where, in this case, subcortical activity is recorded. (D) Triangulated brain model used for MEG source reconstruction (created using Brainstorm). Cortical activity can be reconstructed for each source (indicated by the intersections of the black lines).

ward approach to analyzing network activity based on LFP and MEG recordings is measuring resting-state activity as the subject remains awake at rest and has no particular task to perform. Furthermore, the simplicity of this recording approach facilitates feasibility for different target groups to perform (e.g., patient populations or healthy controls) using various imaging methods. Thus, the evaluation of resting-state activity is suitable for detecting changes in brain activity between measurement groups and time points. Finally, different functional networks can be investigated via a single resting-state recording, as the found resting-state networks (RSN) are hierarchically organized (Cordes et al., 2002; Doucet et al., 2011). RSNs can disappear by actively coping with tasks, like the default mode network, but also RSNs whose topography strongly corresponds to the topography of networks formed by a bandwidth of sensory, motor, and cognitive tasks were shown (Smith et al., 2009; Thomas Yeo et al., 2011). Here, individual regions in the brain can also be assigned to different RSNs simultaneously (Beckmann et al., 2005).

In analyzing brain activity, the concept of oscillatory neural activity, which LFP, EEG, and MEG can measure, plays a central role, as it is crucial for neural communication (Schnitzler and Gross, 2005). The macroscopic oscillatory neural activity refers to a synchronous rhythmic fluctuation of predominantly postsynaptic potentials of a large neural population (Gray and Singer, 1989). In addition to playing a central role in brain communication, neural oscillations are pathologically altered in a disease-specific manner (e.g., in PD; Schnitzler and Gross, 2005). Functionally, the oscillatory activity is divided into different frequency bands (Buzsáki and Draguhn, 2004). In the context of PD, neural oscillations in the range of 3-10 Hz are associated with resting tremors (Bergman et al., 1998; Bergman and Deuschl, 2002), from 60 to 80 Hz are associated with voluntary movement (Brown et al., 2001; Cassidy et al., 2002), and in the beta-band (12-35 Hz) are associated with slowing of movement (Kühn et al., 2004; Marsden et al., 2001). The latter is thus associated with one of the cardinal motor symptoms in PD diagnosis (Little and Brown, 2014).

Beta-band oscillations in PD were investigated in recordings of resting-state activity in subcortical areas via implanted DBS electrodes. In this context, pathologically increased activity in the beta-band in the subthalamic nucleus (STN) has been determined (Kühn et al., 2006; Weinberger et al., 2006) and can be seen as a hallmark of PD. Furthermore, this activity occurs in transient temporal bursts (i.e., beta bursts; Feingold et al., 2015; Lobb, 2014; Tinkhauser et al., 2017a,b), which can be characterized by their duration, frequency of occurrence, and amplitude. The definition of the beta-band frequency range is elementary for determining the beta bursts.

In this work, the occurrence of beta bursts was therefore examined (1) in dependence on three different definitions of the beta-band (e.g., low beta (12-24 Hz), high beta (24-35 Hz), ± 3 Hz around the frequency of the local maximum of the power in the beta-band, i.e., individual beta peak frequency). Furthermore, it was investigated (2) whether the beta bursts occur homogeneously in the STN. For the latter aim, segmented DBS electrodes were used, which allowed for the distinct analysis of contacts distributing current in three directions. As recordings were performed with and without dopaminergic medication, beta bursts will be characterized in terms of their pathological significance for PD and also in a state approximating healthy physiology because of the dopaminergic medication. These findings will be relevant for PD therapy, as STN beta bursts have been recently proposed as promising biomarkers to optimize DBS in terms of spatial and temporal parameters (Tinkhauser et al., 2017a).

The detailed characterization of the beta bursts served as preliminary work to investigate whether STN beta bursts are involved in network formation between the STN and cortex. This research topic is based on four foundations:

1. anatomical connections between cortex and STN via the basal ganglia-cortical (BGC) loop (Fig. 1.2; Albin et al., 1989; Deffains and Bergman, 2019; McGregor and Nelson, 2019)
2. functional connectivity in the beta-band between the STN and the cortex, especially the motor cortex (Cagnan et al., 2019; Hirschmann et al., 2011; Tinkhauser et al., 2018b)
3. the hypothesized pathological significance of beta bursts per se for PD (Tinkhauser et al., 2017a,b)
4. a demonstrated influence on cortical activity by subcortical neural events in nonhuman primates (Logothetis et al., 2012).

Despite the unique opportunity to derive electrophysiological activity from deep brain regions in DBS, the stun effect must be considered in the data analysis. The stun effect is associated with microlesions and edema in the target area caused by the electrode implantation, which can temporarily affect neural activity (Chen et al., 2006; Mann et al., 2009). However, how exactly the stun effect affects brain activity is not known. Therefore, this work used the analysis of classical RSNs detected in cortical MEG data before and after electrode implantation to investigate the influence of the stun effect on different functional networks.

In the context of the pathophysiology of PD, this work aimed to deepen the knowledge about

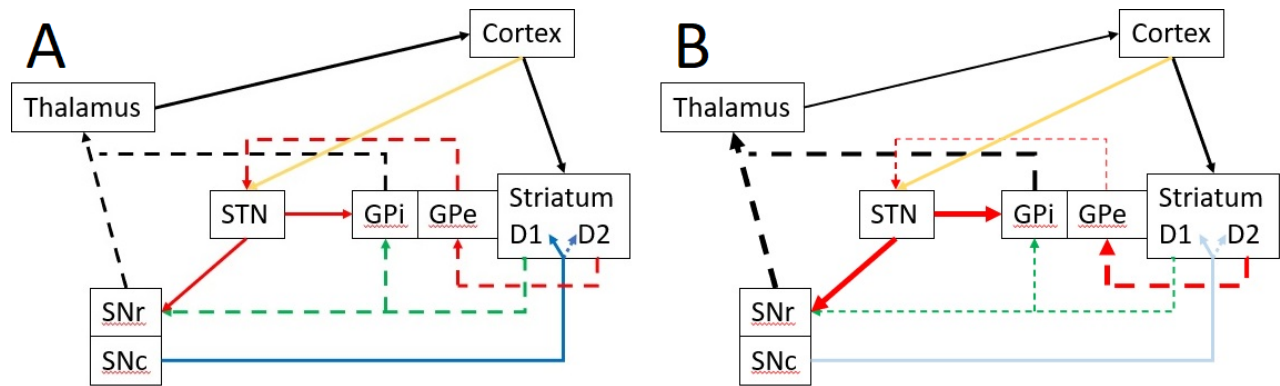


Figure 1.2: Basal ganglia-cortical loop

In (A), the basal ganglia-cortical loop is shown schematically in a healthy state. The direct pathway is marked in green, the indirect pathway in red, the hyperdirect pathway in yellow, and the shared pathways in black. Blue shows the dopamine transport via the nigrostriatal pathway from the substantia nigra pars compacta to the striatum. Solid lines mark excitatory neurons and dashed lines inhibitory neurons. In (B), the parkinsonian state under dopamine deficiency is illustrated. The nigrostriatal pathway is shown bleached out. The connections that are subsequently more activated have a more robust line thickness, and the attenuated connections have a thinner line thickness. Adapted from (DeLong, 1990).

the role of STN beta bursts in network formation. Furthermore, the influence of the implantation of DBS electrodes, which are essential for this work, on brain activity was highlighted to elucidate this therapy form further.

1.1 Brain activity

1.1.1 Neural oscillations

Neural oscillations are central for understanding brain activity, as they are involved in the communication of brain areas and can be pathologically altered specific to different diseases (Schnitzler and Gross, 2005). Oscillatory activity can be detected throughout the central nervous system. Neural oscillations recorded by LFP, EEG, and MEG recordings are mainly caused by synchronous rhythmic fluctuations of the postsynaptic potential of neural populations or by a modulation of the firing probability of individual neurons corresponding to the frequency (Gray and Singer, 1989; Schnitzler and Gross, 2005). These oscillations can be attributed to cellular pacemakers and neural network influences (Bennett and Zukin, 2004; Llinás, 1988; Wang, 2010). Three main parameters characterize neural oscillations:

1. Oscillation frequency indicates the number of cycles per second [measured in Hz] and is the most prevalent of these three quantities. Overall, oscillatory activity covers a spectrum from 0.5 to 500 Hz but is usually divided into different subbands to distinguish

various brain states: delta (< 4 Hz), theta (4-8 Hz), alpha (8-12 Hz), beta (12-35 Hz), low gamma (35-60 Hz), high gamma (60-90 Hz), and high-frequency oscillations (> 100 Hz; Buzsáki and Draguhn, 2004). This rough classification of frequency bands is widely used, but the exact definition is not uniform in the literature. The mentioned frequency bands can also be associated with RSNs (Mantini et al., 2007). In addition, slow oscillations are assumed to have a spatially larger neural population of synchronous neurons than fast oscillations, which thus act more locally (Buzsáki and Draguhn, 2004; Pfurtscheller and Lopes Da Silva, 1999)

2. The oscillation phase, which ranges from $0 - 2\pi$, describes at which point of the cycle the signal currently is (e.g., at a cycle peak or trough).
3. The oscillation power reflects the number of synchronously firing neurons in the population, with measured power inversely related to frequency.

1.1.2 Neural events

Neural oscillations are often considered sustained rhythms of ongoing population-level neuronal activity. However, the notion that sustained oscillations are, at least in part, comprised of transient events (i.e., sequential time-limited periods of synchronous activity with high amplitude) is ever-increasing (Van Ede et al., 2018). While the evaluation of sustained rhythms is most commonly applied for time-averaged or trial-averaged experimental designs, neural events reflect dynamic fluctuations in power, which can be seen at the single trial level (Jones, 2016). These neural events can be described by their duration, rate, or amplitude. In addition, as the power of sustained oscillations could be attributed to the occurring events, an increase in sustained oscillatory power could reflect a higher rate of events (Jones, 2016; Little et al., 2019; Seedat et al., 2020). A common approach for determining neural events is using a threshold value for the power amplitude in a certain frequency band; therefore, the start and end points of the event are determined by exceeding and falling below the threshold value (Feingold et al., 2015; Shin et al., 2017; Tinkhauser et al., 2017a,b).

Frequency-specific neural events can subsequently be evaluated across cortical and subcortical brain regions. For example, K complexes between 0.5-0.9 Hz occur mainly during slow wave sleep in the cortex (Cash et al., 2009; Steriade, 1998). The low-frequency K complexes can be followed by higher-frequency spindle oscillations in the 8-16 Hz range. The spindles also occur in the cortex during non-rapid eye movement sleep but are also found in the thalamus (Contreras et al., 1997; Fernandez and Lüthi, 2020). Neural events are also evident in the high-frequency range (100-200 Hz) as ripples in the hippocampus (Buzsáki et al., 1992;

O’Keefe and Nadel, 1979). For instance, hippocampal ripples occur when a local theta oscillation is suppressed in the hippocampus (Buzsáki, 2002) and are temporally associated with cortical spindles (Axmacher et al., 2006; Siapas and Wilson, 1998). Neural events are also pathologically significant. For example, neural events in the 12-35 Hz range (i.e., beta bursts) are involved in controlling movement in the healthy motor system (Hannah et al., 2020; Little et al., 2019; Wessel, 2020). However, these events are pathologically altered in their duration or the probability of burst occurrence in PD patients and correlate with symptom severity (Pauls et al., 2022; Sure et al., 2021; Tinkhauser et al., 2017b). Beta bursts occur as both cortical and subcortical events in the STN (Feingold et al., 2015; Lobb, 2014; Tinkhauser et al., 2017a,b).

1.1.3 Resting-state networks

In order to examine specific brain functions, specific tasks can be actively performed during the recording of brain activity. However, since 60-80 % of the brain’s energy demand is consumed at rest (Raichle and Mintun, 2006), the analysis of the brain’s resting-state activity is also relevant. While task-linked experiments limit the ability to analyze brain activity to the task-specific functional domain, in resting-state activity, different networks can be determined simultaneously, which occur mainly at rest but also during the processing of specific tasks such as motor or cognitive tasks (Smith et al., 2009; Thomas Yeo et al., 2011). In terms of execution, no task needs to be performed for resting-state activity recordings, and therefore no complicated setup is required. However, participants must sit as calmly and relaxedly as possible, not thinking about anything specific, but at the same time not falling asleep. If this is fulfilled, resting-state recordings can be used to study the physiology but also the pathophysiology of the brain by comparing recordings from different groups of participants (e.g., healthy controls and PD patients; Schneider et al., 2020). The recordings can also be repeated with different imaging methods to record different signal components related to neural activity (Schneider et al., 2020; Pelzer et al., 2021). Furthermore, it has been shown that the brain is functionally active at rest and that for specific functions, different regions interact, thus forming networks (Biswal et al., 1995, 2010; Damoiseaux et al., 2006). The topography of these RSNs resembled the topography of brain networks associated with specific tasks (Smith et al., 2009; Thomas Yeo et al., 2011).

RSNs have been widely studied with fMRI based on the low-frequency fluctuations of the blood oxygenation level dependent (BOLD) signal. Here, increased neural activity leads to a higher BOLD signal (Ogawa et al., 1998; Seitzman et al., 2019), and RSNs were determined via temporal correlations of BOLD signals in separate brain regions (Biswal et al., 1995; Fox

and Raichle, 2007). Still, the BOLD signal reflects the activity of neurons via hemodynamics only indirectly. Contrarily, the activity of neural populations can be measured directly via MEG and can also be used to determine RSNs (Brookes et al., 2011; De Pasquale et al., 2010; Florin and Baillet, 2015). Even though RSNs can be determined with both methods, there are method-related differences. Due to the low temporal resolution of the BOLD signal (< 0.15 Hz), fMRI RSNs cannot be analyzed for their spectral properties (Josephs and Henson, 1999). However, MEG-based RSNs can be determined for different frequencies (Brookes et al., 2011; De Pasquale et al., 2010; Florin and Baillet, 2015). With an appropriate selection of the frequencies, MEG recordings can also show correspondences of the fMRI RSN (Brookes et al., 2011; Pelzer et al., 2021). However, especially for RSNs with an auditory component, noise during an fMRI recording must be considered, which does not occur during a MEG recording and thus may cause differences in RSNs (Pellegrino et al., 2022). While focusing on the time domain, the temporal resolution of MEG is in the range of ms (Hämäläinen et al., 1993). Thus in the order of magnitude of neural events (Cagnan et al., 2019; Tinkhauser et al., 2017a,b; Logothetis et al., 2012), and with fMRI, one is in the range of seconds clearly above that (Glover, 2011). Regarding spatial resolution, the whole brain can be recorded via fMRI at a uniform resolution (Glover, 2011). However, with MEG, resolution decreases with distance from the sensor, and most studies are limited to the cortex (Hämäläinen et al., 1993).

Regardless of the recording technique chosen, functional connectivity between brain regions is sought when determining RSN. While for fMRI RSN, temporal correlations of BOLD signals are sought (Biswal et al., 1995; Fox and Raichle, 2007), for MEG RSN, the connectivity between the time series of the reconstructed cortical sources can be determined via various procedures. Among the procedures are methods that determine connectivity via the correlation of the amplitude of the time series but also via their spectral coherence, the relationship between phases, phase-amplitude coupling, and auto-regressive models (Colclough et al., 2016; Florin and Baillet, 2015). After determining the connectivity via one of these methods, the RSNs can be determined. Again, different methods are suitable for this purpose. One of the first methods was seed-based connectivity, but also singular value decomposition, independent component analysis, and graph theory are widely used to determine RSN. In addition, different RSNs, which are organized hierarchically, can be determined from one data set using the same procedure (Brookes et al., 2011; Doucet et al., 2011).

These methods primarily determine static networks and thus cannot fully represent the brain's communication dynamics. Even though dynamic RSNs have been studied by fMRI (Britz et al., 2010; Chang and Glover, 2010; Zalesky et al., 2014), their temporal resolution is limited

by the low temporal resolution of the BOLD signal. At higher temporal resolution, dynamic networks have been shown for the cortex using EEG and MEG recordings but not for subcortical areas (Britz et al., 2010; Chen et al., 2013; Dimitriadis et al., 2018; Vidaurre et al., 2018). However, networks involving subcortical areas can be expected to emerge at the time scale of neural events; for example, hippocampal ripples are functionally connected to cortical spindles (Axmacher et al., 2006; Siapas and Wilson, 1998), or coupling of cortical and subcortical beta bursts also occurs (Cagnan et al., 2019; Tinkhauser et al., 2018b). Through the method of neural-event-triggered-(NET)-fMRI introduced by Logothetis *et al.* (2012), it was possible to testify, using hippocampal ripples as an example, that extensive network formation occurs triggered by subcortical events. The NET method was also transferred to MEG data (study 2).

1.2 Measuring brain activity

Of the many methods used to measure brain activity, the methods relevant to this work are presented below: MEG and LFP recordings via macroelectrodes.

1.2.1 Electrophysiological signal

For MEG and LFP recordings, the electrophysiological component dominating the recorded signal is thought to be the postsynaptic potential of neurons (Hansen et al., 2010; Pollok and Schnitzler, 2010). In part, action potentials could also contribute to the signal. However, the de- and repolarization of action potentials occur so rapidly that synchronous activation of sufficiently many neurons, which would lead to a measurable signal via the superposition of individual activation, becomes unlikely (Buzsáki et al., 2012). In contrast, both the excitatory and inhibitory postsynaptic potentials proceed more slowly, so the spatial and temporal synchronicity of sufficiently many neurons may provide a measurable signal (Hansen et al., 2010; Pollok and Schnitzler, 2010).

LFP and MEG recordings differ fundamentally in two points despite originating from the same primary signal source. An active neuron conducts an electric current analogous to a current-carrying cable and generates an electromagnetic signal. In LFPs, the electrical component is detected, whereas, in MEG, the magnetic component is detected. Furthermore, the measurement signal from LFPs is spatially very focal and depends mainly on the brain area where the recording electrode was implanted (Katzner et al., 2009). In contrast, MEG has a fixed sensor array that allows whole-brain activity recordings, although signal quality decreases with distance from the sensors (Baillet, 2017). Due to the spatial arrangement of different types of neurons and the folding of the brain, specific neuronal sources contribute

more to the MEG signal than others. Since first, the magnetic field emanating from the neurons, especially the dendritic branches, is always perpendicular to the source, and second, the MEG sensors can best detect magnetic fields perpendicular to the skull, the orientation of the dendritic branches of the neurons must be tangential to the skull (Hämäläinen et al., 1993). This geometry is the case in the walls of the sulci (Fig. 1.3). Of the different types of neurons, the apical dendrites of the pyramidal cells run as parallel fibers to the cortical surface (Hansen et al., 2010; Pollok and Schnitzler, 2010). Therefore, it is assumed that the signal measured by the MEG is mainly generated by the pyramidal cells located in the walls of the sulci. It takes synchronous activity of about 50000 neurons to generate sufficient signal strength to be detected by sensors outside the skull (Proudfoot et al., 2014).

1.2.2 Magnetoencephalography

MEG detects the magnetic field generated by active and thus current-carrying neurons (Fig. 1.3), whereby the temporal dynamics of neural activity can be reflected with high temporal resolution (Hämäläinen et al., 1993; Proudfoot et al., 2014). It is an entirely non-invasive method because the sensors are located outside the skull, and no contrast agent is required. MEG was developed by David Cohen and is based on the SQUID (Superconducting QUantum Interference Device) sensors developed by James Zimmerman (Zimmerman et al., 1970). MEG is a neurophysiological imaging technique and, unlike neurovascular imaging techniques such as fMRI or PET, allows direct measurement of electrical brain activity (Hall et al., 2014). Furthermore, when MEG recordings are combined with structural MRI images, the measured activity can be projected back onto anatomical structures. In the following, two critical points of MEG theory will be highlighted: How the electrophysiological signal is measured and how activity can be sorted to specific brain areas from sensors located outside the brain.

1.2.2.1 Detection of magnetic fields

The magnetic flux density of a single neuron is 0.1 fT and would be too weak to be detected outside of the skull (Buckel and Kleiner, 2012). On the other hand, the detectable flux density of synchronously active neurons is 50-500 fT and thus up to 9 orders of magnitude smaller than the Earth's magnetic field at the equator (31 μ T; Hämäläinen et al., 1993). Considering the orders of magnitude, there are two requirements for the sensors used. First, the sensor must be sensitive enough to measure the magnetic fields of the neurons, and second, external interferences have to be shielded so that they do not overlay the actual signal.

Low-temperature SQUID sensors (commonly cooled with liquid helium at 4.2 K) are widely

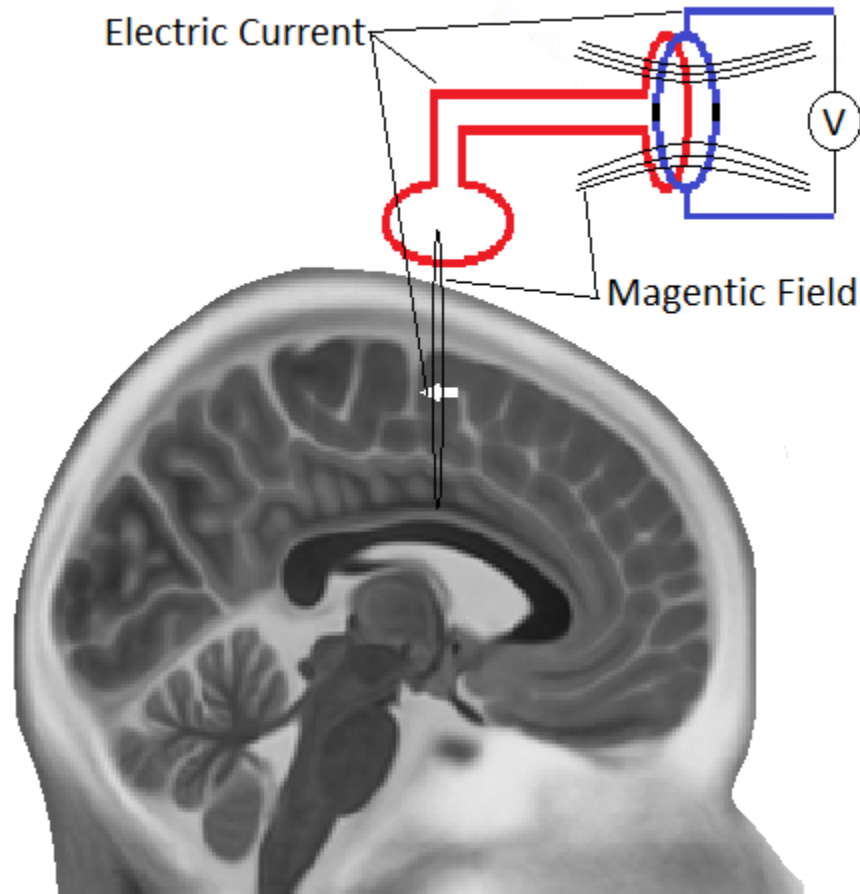


Figure 1.3: MEG signal and source

Schematically, the signal measured by the MEG via a SQUID sensor with a preconnected magnetometer, and the signal source is shown. The white arrow represents an electrical signal generated by simultaneous postsynaptic potentials at the apical dendrites of a sufficient number of pyramidal cells in the cortex. The resulting magnetic field induces an electric current outside the skull in the first coil of a magnetometer (red). This, in turn, generates a new magnetic field in a second coil. The magnetic field generated again induces a ring current in the directly applied SQUID. Since the SQUID is superconducting and a direct current is applied from outside, the induced current at one of the Josephson contacts (black) lengthens the wavelength of the Cooper electrons and shortens it at the other Josephson contact. This results in a measurable voltage drop. It is essential that the magnetic flux at the SQUID can only take on whole multiples of the magnetic flux quantum, and the induced ring current at the SQUID is modulated accordingly.

used in MEG to detect magnetic flux density. These sensors operate in the superconducting state, in which there is no electrical resistance. Standard SQUID sensors consist of a superconducting ring, which is symmetrically divided into two semicircles by electrically insulating oxide layers, so-called Josephson junctions, and a flux transformer (Hämäläinen et al., 1993). The essential theoretical assumptions for the operation of the SQUIDS are:

1. the magnetic flux through a superconducting ring can only take integer multiples of the magnetic flux quantum ($\Phi = \frac{h}{2e} \approx 2.07 \cdot 10^{-15}Vs$; Buckel and Kleiner, 2012).
2. electric current transport in superconductivity occurs via two paired electrons, the Cooper electrons, which can be described as a matter-wave (Buckel and Kleiner, 2012).
3. the wave functions of the Cooper electrons can overlap at the Josephson junctions, allowing the Cooper electrons to tunnel through the insulator. This is described as the Josephson effect and results in a phase jump between the Cooper electrons' wave functions (Buckel and Kleiner, 2012).

The operation of the magnetic flux measurement through a SQUID is outlined as follows (Fig. 1.3; Fagaly, 2006). First, a direct current is applied to the two semicircles of the SQUID to pass the two Josephson contacts in the same flow direction. Next, the magnetic flux is measured via a flux transformer, and a ring current is induced in the SQUID. The current has precisely the magnitude to bring the magnetic flux in the superconducting ring to the nearest multiple of the flux quantum and flows at one of the Josephson junctions with the direct current and the other junction against the direct current. Resulting in a lengthening of the wavelength of the Cooper electrons on one contact and a shortening on the other. This results in a phase difference, which manifests in interference effects with a measurable voltage drop at the contacts. If the voltage is plotted against the magnetic flux, a sinusoidal curve with the magnetic flux quantum as the period is seen (Buckel and Kleiner, 2012; Fagaly, 2006).

Specific detection coils are used in the flux transformer to increase the sensitivity of the sensors. A distinction is made between magnetometers and planar or axial gradiometers (Fagaly, 2006; Hämäläinen et al., 1993). Magnetometers consist of a coil and measure the absolute magnetic flux but have no special spatial orientation. Axial and planar gradiometers each have two coils with counter-rotating windings along the plane's axis or side by side. The resulting gradient gives a greater spatial precision for near sources. Since the magnetic flux of distant sources changes spatially only slowly, no gradient would form here, and no signal would be transmitted.

To prevent the magnetic signal of the brain from being superimposed by stronger external magnetic fields, the entire measuring apparatus is placed in a magnetically shielded room (Fig. 1.4). The shielding can be active or passive. Passive shielding is achieved by the materials used to construct the room. Materials with ferromagnetic properties are suitable to suppress static and low-frequency fields, whereas higher-frequency fields can be suppressed due to paramagnetic properties (Buckel and Kleiner, 2012). Active shielding classically uses an arrangement of magnetic field sensors mounted in the room's wall and compensation coils,

often Helmholtz coils (Hämäläinen et al., 1993). The magnetic field measured by the sensors is compensated by a counter field generated by the compensation coils.



Figure 1.4: Magnetically shielded chamber

Shown here is a 306 channel MEG inside a magnetically shielded chamber. The cross-section of the door to the shielded chamber is shown in the foreground.

Nevertheless, the recorded signal may be contaminated by external, non-brain-related artifacts. For example, the line noise, electrical devices in the measurement chamber, mechanical vibrations, but also muscle movements of the test person can contribute to artifact formation. Such artifacts can be mathematically extracted from the measured signal directly or via reference sensors (Hansen et al., 2010). Established methods used for this purpose include signal space projection (Tesche et al., 1995; Uusitalo and Ilmoniemi, 1997), principal component analysis (Sadasivan and Narayana Dutt, 1996), independent component analysis (Escudero et al., 2007), signal space separation (Taulu and Kajola, 2005), or temporal signal space separation (Taulu and Simola, 2006).

1.2.2.2 Reconstruction of neural activity

Reconstructing the neural activity measured by MEG at the location of its true source requires first solving the forward problem and then the inverse problem (Hämäläinen et al., 1993;

Hansen et al., 2010). In the inverse problem, starting from an observed signal/effect, the underlying source/cause is to be determined. Contrary, given a known source/cause, the resulting signal/effect is predicted in the forward problem. For the forward problem, in MEG source reconstruction, a model of the head and the sensor geometry must be found to determine the signal at the sensor given a known current source (Baillet et al., 2001; Hämäläinen et al., 1993). For the inverse problem, a distribution of neural activity must be found that reflects the signal from the sensors via the solution of the forward problem. However, the solution to the inverse problem is not unique, which makes the inverse problem ill-posed (Baillet et al., 2001; Hämäläinen et al., 1993). The following description of the forward and backward problem is based on the descriptions of Baillet *et al.* (2001), Hämäläinen *et al.* (1993), and Van Veen *et al.* (1997).

Forward problem: The solution to the forward problem is also known as the forward model or head model and describes the modeling of the electromagnetic properties of the head and the sensors. With the solution to this problem, the propagation of the electromagnetic fields can be described starting from a known electrical current using the Maxwell equations. From there, the law of Biot-Savart can be derived, which describes the magnetic flux density \mathbf{B} generated by a current I moving in a length element $d\mathbf{l}$ at a known location \mathbf{r} relative to the location \mathbf{r}' of the current:

$$d\mathbf{B}(\mathbf{r}) = \frac{\mu_0}{4\pi} I d\mathbf{l} \times \frac{\mathbf{r} - \mathbf{r}'}{|\mathbf{r} - \mathbf{r}'|^3}$$

To describe the magnetic fields due to brain activity, the current density distribution in the whole brain must be modeled using the model of current dipoles. A current dipole is an infinitesimal small current segment, which is defined by its dipole moment p and the position \mathbf{r} and thus generates a point-like current density distribution (Hämäläinen et al., 1993):

$$I = p\delta(\mathbf{r})$$

As the superposition principle can be applied to magnetic induction, any magnetic field can be described with a sufficient number of current dipoles.

The current dipoles can be distributed over a previously determined grid (Fig. 1.1D). One or more dipoles with different orientations and weighting are placed at each grid point (Henson et al., 2009; Mosher et al., 1999). The distribution may cover the entire brain or be limited to the cortex, where the signal-to-noise ratio and the sensitivity of the MEG are best (Baillet, 2017; Tadel et al., 2019).

Furthermore, a model has to be found which describes how the electromagnetic field propagates from the neural sources via the different tissue types of the brain to the sensors. The simplest variant is the sphere model, where the head is considered a homogeneous sphere with constant conductivity and a magnetic permeability assumed as in the empty space (Baillet et al., 2001; Huang et al., 1999; Nolte, 2003). A variation of the sphere model is the model of overlapping spheres (Fig. 1.5), where a separate sphere is adapted for each sensor (Huang et al., 1999). There are also much more accurate models, such as the boundary element model, where the interfaces between tissue types (e.g., between brain and cerebrospinal fluid) are more accurately described, or the finite element model, where the entire volume is divided into small units of constant conductivity (Baillet et al., 2001). The latter two methods are more realistic but require significantly more computational effort. Since the magnetic field is less susceptible to head heterogeneity than the electric field and the magnetic permeability of the brain tissue can be approximated to that of free space, the first two methods also achieve sufficient accuracy with less computational effort (Baillet et al., 2001; Huang et al., 1999; Leahy et al., 1998).

If an adequate model for the head is found and spatially aligned to the sensor geometry, then a so-called leadfield operator \mathbf{H} can be determined. Ideally, if the leadfield operator is applied to an arbitrary current density distribution \mathbf{S} , the signal \mathbf{X} measured by the SQUID sensors is obtained (Baillet et al., 2001).

$$\mathbf{X} = \mathbf{H}\mathbf{S}$$

Inverse problem: To solve the inverse problem, the underlying neural activity must be determined from the measured sensor signal. In an ideal setting, one could invert the solution of the forward problem and use it as the solution for the inverse model:

$$\mathbf{H}^{-1}\mathbf{X} = \mathbf{S}$$

As there is no ideal setting, the leadfield operator can only be approximated:

$$\mathbf{W}\mathbf{X} = \hat{\mathbf{S}} \text{ with } \mathbf{W} \sim \mathbf{H}^{-1}$$

Moreover, the sensor noise \mathbf{N} must be taken into account while solving the inverse problem (Baillet et al., 2001):

$$\mathbf{X} = \mathbf{H}\mathbf{S} + \mathbf{N} \Rightarrow \mathbf{W}(\mathbf{X} - \mathbf{N}) = \hat{\mathbf{S}}$$

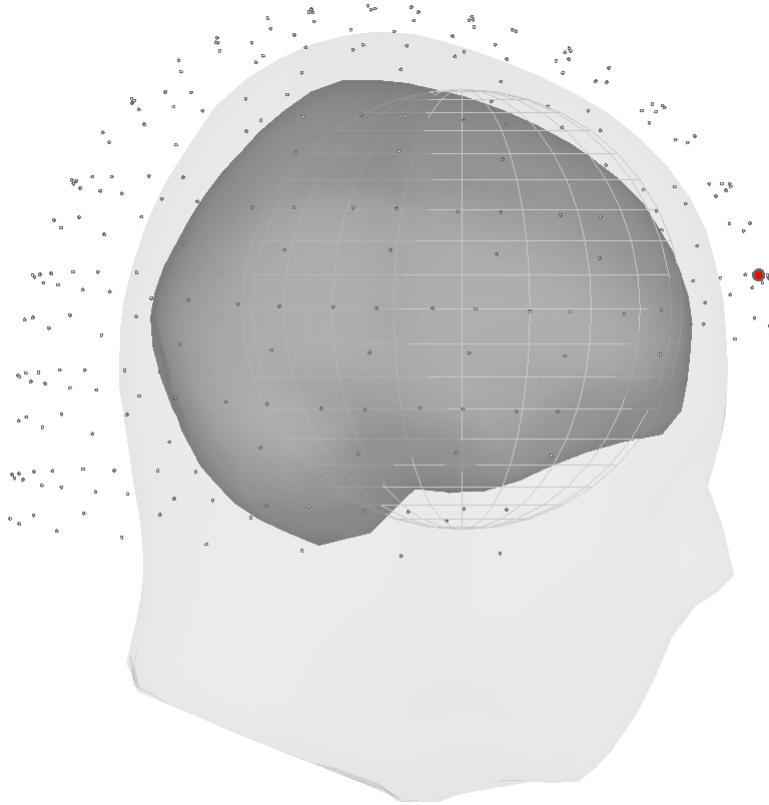


Figure 1.5: Overlapping spheres

Schematic of the head model using overlapping spheres created using Brainstorm. The head (light gray) and the brain (dark gray) are visible, while the surrounding points mark the location of the MEG sensors. For each sensor, a sphere with constant conductivity and magnetic permeability is fitted, describing the propagation of the measured signal. The sphere shown is an example of the sensor marked in red.

Different approaches can solve the inverse problem: single or many dipoles fitting, distributed dipole models, or spatial filters. The solution to the inverse problem using a spatial filter, the Linearly constrained minimum variance (LCMV) beamformer, will be described here as an example (Van Veen et al., 1997). The beamformer acts as a spatial filter to determine the neural activity in electrophysiological data at each previously defined location. Furthermore, using a head model, the filter is weighted for each source to determine the source activity correctly.

Ideally, the spatial filter for a source allows only the activity of that source to pass and blocks the contributions of the other sources (Fig. 1.6). Approximately applies: $\mathbf{S} \sim \hat{\mathbf{S}}$

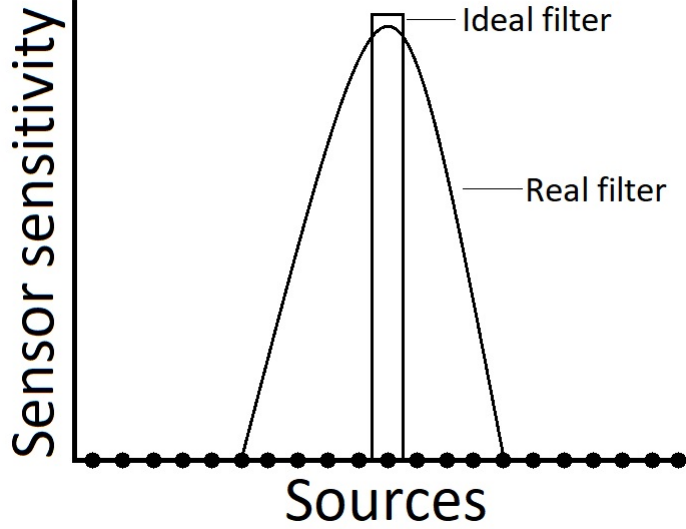


Figure 1.6: Beamformer as spatial filter

Direct comparison shows the sensitivity of sensors to a source using an ideal and a real spatial filter. An ideal filter produces maximum sensitivity to one source while sensitivity to other sources is completely blocked. The sensor is always partially sensitive to unwanted sources with a real filter.

For the source under consideration would apply:

$$\mathbf{X} = \mathbf{H}\mathbf{S} \Rightarrow \mathbf{W}\mathbf{X} = \hat{\mathbf{S}} = \mathbf{W}\mathbf{H}\mathbf{S} \Rightarrow \mathbf{W}\mathbf{H} = 1$$

Ideally, the following would apply to sources A and B:

$$\mathbf{W}_A\mathbf{H}_A = 1; \mathbf{W}_B\mathbf{H}_B = 1 \text{ and } \mathbf{W}_A\mathbf{H}_B = 0$$

Nevertheless, such an ideal filter cannot be fulfilled for all sources. While targeting this problem, the goal of the beamformer technique is to minimize the variance of the sources. Using the LCMV beamformer, the solution to this problem is as follows:

The solution to the inverse problem $\mathbf{X} = \mathbf{H}\mathbf{S} \Rightarrow \mathbf{W}\mathbf{X} = \mathbf{S}$ is to be found by minimizing the variance of \mathbf{S} .

For the variance \mathbf{V} of \mathbf{S} holds:

$$\mathbf{V} = \text{Var}(\mathbf{S}) = \mathbf{S}\mathbf{S}^T = \mathbf{W}\mathbf{X}\mathbf{X}^T\mathbf{W}^T = \mathbf{W}\mathbf{C}\mathbf{W}^T \text{ with the covariance matrix } \mathbf{C}$$

The minimum of \mathbf{V} with $\mathbf{W}\mathbf{H} = 1$ is searched for. The solution for this can be found via

Lagrangian multiplication:

$$\text{Use: } \mathbf{W}\mathbf{H} = 1 = \mathbf{H}^T\mathbf{W}^T \Leftrightarrow \mathbf{H}^T\mathbf{W}^T - 1 = 0$$

$$\text{Minimize: } \mathbf{V} = \mathbf{W}\mathbf{C}\mathbf{W}^T + \lambda(\mathbf{H}^T\mathbf{W}^T - 1)$$

$$\frac{\delta\mathbf{V}}{\delta\mathbf{W}^T} = \mathbf{W}\mathbf{C}\lambda\mathbf{H}^T \stackrel{!}{=} 0 \Leftrightarrow \mathbf{W} = -\lambda\mathbf{H}^T\mathbf{C}^{-1}$$

$$0 = \mathbf{W}\mathbf{H} - 1 = -\lambda\mathbf{H}^T\mathbf{C}^{-1}\mathbf{H} - 1$$

$$\lambda = \frac{-1}{\mathbf{H}^T\mathbf{C}^{-1}\mathbf{H}}$$

$$\mathbf{W} = -\lambda\mathbf{H}^T\mathbf{C}^{-1} = \frac{\mathbf{H}^T\mathbf{C}^{-1}}{\mathbf{H}^T\mathbf{C}^{-1}\mathbf{H}}$$

Thus, there is a solution where the neural activity can be determined with the help of the head model and the sensor activity. Furthermore, the solution can be further optimized using normalization and regularization methods. However, the LCMV beamformer is shown to be disadvantageous to correlated neural sources and sensitive to the head model (Brookes et al., 2007). On the other side, the LCMV beamformer is advantageous over other inverse solutions in the case of simultaneous MEG, and LFP recordings since the artifacts in the MEG data caused by ferromagnetic components of the LFP system have less impact on the reconstruction of neural activity (Litvak et al., 2010).

1.2.3 Local field potentials

The electrophysiological activity of deeper neuron populations can be recorded via measurements of LFPs. LFP is the extracellular electrical signal of neurons and can be measured via electrodes implanted in the brain (Fig. 1.1C; Einevoll et al., 2013). They can be measured using microelectrodes and macroelectrodes, such as those used for DBS. While microelectrodes are also suitable for single-unit recordings, macroelectrodes always map the activity of neural populations. The LFP signal is commonly assumed to be spatially restricted to the location of the electrode, as the signal from contacts only a few hundred micrometers apart can differ (Katzner et al., 2009).

Furthermore, postsynaptic signals are assumed to contribute the most to the measured signal. The fact that the action potentials are not the main component of the measurement signal is likely because its high-frequency nature results in greater attenuation with distance and makes synchrony more difficult for multiple neurons. However, especially for neurons close to the contacts, the action potentials may account for part of the measured signal (Gray et al., 1995). The distance between measurable signal source and electrode contact is between 0.1

mm (Xing et al., 2009) and 5 mm (Kreiman et al., 2006). In addition, contributions from cortical activity through volume conductance to the LFP signal from the basal ganglia are also discussed (Marmor et al., 2017). Further, it can be assumed that the measured signal depends on electrode referencing, as monopolar referencing can pick up signals of cortical activity, whereas bipolar referencing appear resistant to it (Marmor et al., 2017). Lastly, the geometry of the neural generators also matters, as neurons in the STN have a lower degree of order than the pyramid cells of the cortex (i.e., less homogeneous spatial orientation; Marmor et al., 2017).

1.3 Parkinson’s disease

PD is a progressive neurodegenerative disease with a high prevalence in the elderly (1 % in a population over the age of 60; Bennett et al., 1996; De Rijk et al., 1995; Samii et al., 2004; Tysnes and Storstein, 2017). It was first described in 1817 by its name-giver James Parkinson (Goetz, 2011).

1.3.1 Clinical characteristics

The clinical diagnosis of PD is based on the occurrence of bradykinesia, a depletion and slowing of movement, and the occurrence of at least one of the following three symptoms (Hughes et al., 1992):

- **rigidity:** an increase in muscle tone that leads to resistance to passive movement
- **resting tremor:** a rhythmic, oscillatory movement at 3-5 Hz that is present at rest
- **postural instability:** a loss of standing reflexes that results in frequent falls

Depending on the expression of these cardinal motor symptoms, PD can be subdivided into two main clinical subtypes: tremor dominant and akinetic-rigid type (Hughes et al., 1992; Zaidel et al., 2009). In addition, the progression of PD may differ by subtype (e.g., slower disease progression for the tremor dominant subtype; Jankovic and Kapadia, 2001; Moretti et al., 2017; Rajput et al., 2009). Above the four cardinal motor symptoms, PD includes other motor and non-motor symptoms (e.g., deficits of gait, speech, olfaction, sleep; Jellinger, 2015; Moustafa et al., 2016).

PD must be distinguished from atypical and secondary parkinsonian syndromes based on pathogenesis, therapy response, and prognosis. PD is causative for about 75 % of all diagnosed parkinsonian syndromes (Luschnig, 2021).

The further descriptions of the parkinsonian syndrome in this thesis are for idiopathic PD.

1.3.2 Basal ganglia-cortical loop

The BGC loop connects the basal ganglia, thalamus, and cortex and plays a central role in PD therapy and pathology, as the degeneration of dopaminergic neurons in the substantia nigra pars compacta – a pathophysiological hallmark of PD (Antony et al., 2013) – leads to an impairment of the BGC loop (McGregor and Nelson, 2019). The BGC-loop is involved in processing motor and non-motor actions and inhibiting unwanted actions (Alexander et al., 1986; Deffains and Bergman, 2019; McGregor and Nelson, 2019). The basal ganglia nuclei include the corpus striatum (putamen and nucleus caudatus), external and internal globus pallidus, STN, and the pars compacta and pars reticulata of the substantia nigra (Lanciego et al., 2012). The BGC loop can be considered as a model with several parallel loops, where the division of the loops is based on including motor, limbic, and associative functions of the traversing brain regions (Alexander et al., 1986; Deffains and Bergman, 2019; McGregor and Nelson, 2019). In the following four central pathways of the BGC loop will be highlighted (Fig. 1.2):

- **Direct pathway**

γ -aminobutyric acid (GABA)-ergic inhibitory neurons project to the globus pallidus internus (GPi) and the pars reticulata of the substantia nigra (SNr) via D1 receptors located in the striatum. Further, GABAergic inhibitory neurons from GPi and SNr project to the thalamic fasciculus and reach the thalamus. From the thalamus, glutamatergic excitatory neurons project to the cortex. Via disinhibition of the thalamus, this loop activates the cortex. Finally, glutamatergic excitatory neurons from the cortex project back to the striatum. (Description based on Albin et al., 1989; Calabresi et al., 2014)

- **Indirect pathway**

The indirect pathway is similar to the direct pathway, except that from the striatum, a detour is chosen via the globus pallidus externus (GPe) and the STN to the GPi and SNr. Via D2 receptors in the striatum, inhibitory neurons project to the GPe. From here, inhibitory neurons, in turn, project to the STN. From the STN, in contrast, excitatory neurons project to the GPi and SNr, from where the circuitry again resembles the direct pathway. In the indirect pathway, disinhibition of the STN results in inhibition of the thalamus and less activation of the cortex. (Description based on Albin et al., 1989; Calabresi et al., 2014)

- **Hyperdirect pathway**

In the hyperdirect pathway, glutaminergic neurons from the cortex project to the STN directly, bypassing the striatum and GPe. Otherwise, the hyperdirect pathway is similar to the indirect pathway. It leads to an inhibition of the thalamus and, thus, to a lower activation of the cortex at a shorter propagation time. (Description based on Nambu et al., 1996; Oswal et al., 2021)

- **Nigrostriatal pathway**

The nigrostriatal pathway connects pars compacta of the substantia nigra with the striatum via dopaminergic neurons, where it excites the direct pathway and inhibits the indirect pathway. The stimulation of the striatum occurs via the dopaminergic D1 receptors involved in the direct pathway and D2 receptors involved in the indirect pathway. D1 receptors excite downstream neurons, and D2 receptors have an inhibitory effect. Therefore, the nigrostriatal pathway activates the direct pathway via D1 receptors and inhibits the indirect pathway via the D2 receptors. (Description based on Blandini et al., 2000; Ledonne and Mercuri, 2017)

1.3.3 Subthalamic nucleus

The STN is located ventral to the thalamus and is functionally associated with the basal ganglia. Direct neighbors of the STN are anteriorly and laterally the capsula interna, medially Forel's fields and the nucleus ruber, dorsally the zone incerta and the fasciculus lenticularis, and ventrally the substantia nigra (Bosch, 1978; Parent and Hazrati, 1995a). The STN itself can be functionally divided into three areas consistent with the parallel model of the BGC loop. Most of the nucleus toward the dorsolateral border is assigned to motor function, whereas the ventral area is intervened by associative fibers and the medial tip by limbic fibers (Mazzoni et al., 2012; Parent and Hazrati, 1995a; Remy et al., 2005; Vriezen and Moscovitch, 1990).

1.3.4 Pathology and pathophysiology

Central characteristics of PD pathology are the degeneration of dopaminergic neurons in the substantia nigra pars compacta, as well as the inclusion of Lewy bodies, which are aggregates of various proteins, mainly alpha-synuclein and ubiquitin, in the cytoplasm of the neurons (Lang and Lozano, 1998; Pollanen et al., 1993). Furthermore, alpha-synuclein-containing aggregates can also be formed in the neurites and axons (Braak et al., 1999). Although the loss of neurons is mainly limited to the substantia nigra pars compacta, aggregate formation increases in large parts of the brain as PD progresses (Müller et al., 2005).

Degeneration of dopaminergic neurons in the substantia nigra pars compacta results in a deficiency of dopamine in the striatum and functional impairment of the BGC loop (Deffains and Bergman, 2019; McGregor and Nelson, 2019). Now that the D1 and D2 receptors are no longer supplied by dopamine, the direct pathway is less activated, and the indirect pathway is less inhibited. Since the direct pathway contributes to an excitation of the cortex and the indirect pathway to an inhibition, dopamine deficiency finally leads to reduced cortex activation (DeLong, 1990; McGregor and Nelson, 2019). In PD patients, this can be seen in the motor system through the appearance of bradykinesia (Kish et al., 1988).

Activity patterns of neural populations are also pathologically modulated in PD. In PD, changes in oscillatory activity are particularly prominent in the beta-band, with changes also occurring in other frequency bands (Schnitzler and Gross, 2005). For the beta-band, increased activity in the STN that is considered pathological has been found in PD patients when PD medication is discontinued, with a peak at an individual frequency within the beta-band (Kühn et al., 2006; Thompson et al., 2014; Weinberger et al., 2006). This activity is reduced by dopaminergic medication and voluntary movement (Levy et al., 2002). Furthermore, the power of beta activity could also be correlated with symptom severity of akinesia and rigidity (Hammond et al., 2007; Kühn et al., 2006), and functional connections between STN and cortex were shown, especially OFF medication in this frequency band (Cagnan et al., 2019; Hirschmann et al., 2011; Tinkhauser et al., 2018b). Oscillatory beta-band activity can be divided into phases of increased activity (i.e., beta bursts; Fig. 1.7) and phases of low activity (Feingold et al., 2015; Tinkhauser et al., 2017a,b). The evidence here shows that the duration of these beta bursts positively correlates with symptom severity of PD (Sure et al., 2021; Tinkhauser et al., 2017a).

1.3.5 Therapy

As of today (2022), there is no cure for PD, but various therapies alleviate symptoms and significantly improve the overall quality of life (Lee and Yankee, 2022). Therapies include pharmacological, non-pharmacological, and interventional therapy (Lee and Yankee, 2022), with therapy individualized for each patient and adapted to the progression of PD.

Pharmacological therapy primarily targets the lack of dopamine. One way is to prevent the remaining dopamine from being metabolized. For this purpose, the patient is given antagonists for corresponding enzymes. Furthermore, L-dopa, a drug that is the gold standard of PD therapy, is used to increase dopamine availability in the brain. L-dopa is a precursor of dopamine, which can pass the blood-brain barrier and is subsequently converted to dopamine

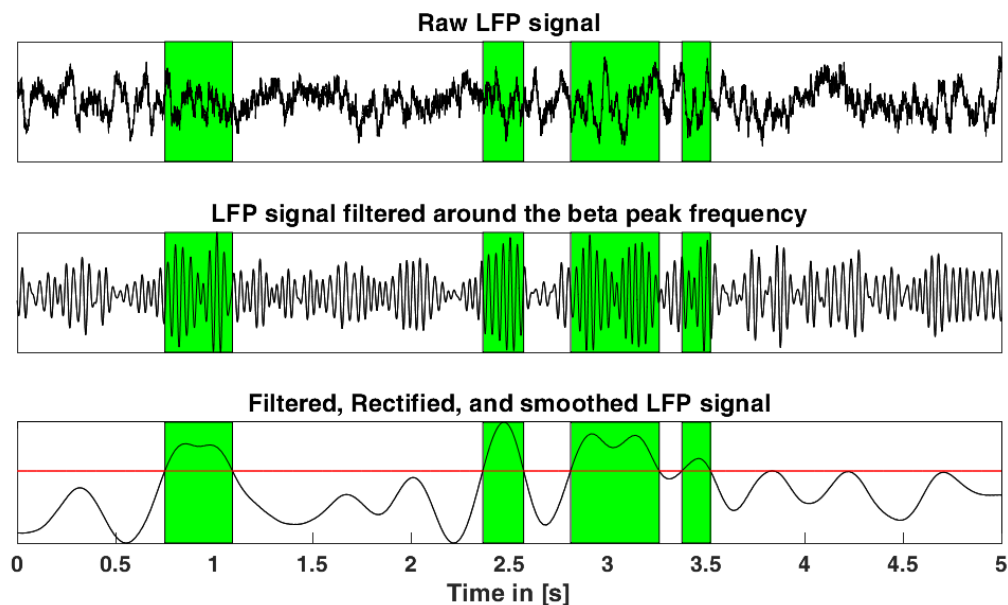


Figure 1.7: Beta burst determination

The three figures show a five-second epoch from a ten-minute LFP measurement in the STN at rest and schematically outline one way to detect beta bursts. The top figure shows the raw signal. In the middle figure, this signal has been filtered ± 3 Hz around the individual beta peak frequency. The bottom figure shows the magnitude of this signal, which was smoothed with 400 ms long Gaussian windows. From this signal, the 75th percentile was used as the threshold for burst detection and plotted as a red line. All time points continuously above this threshold for at least 80 ms were evaluated as beta bursts (colored green).

(Birkmayer and Hornykiewicz, 1962). In addition, dopamine agonists, glutamate antagonists, and anticholinergics are also used therapeutically in PD patients (Armstrong and Okun, 2020). Non-drug therapy includes physical, occupational, and speech therapy (Witt et al., 2017).

For interventional therapy of PD, a distinction is made between intraduodenal infusion of L-dopa, subcutaneous application of apomorphine, lesional procedures, non-invasive brain stimulation procedures, and DBS (Krüger et al., 2016; Witt et al., 2017). Subsequently, only DBS in STN will be discussed. Although other basal ganglia structures can be stimulated for PD therapy, the STN, focusing on the motor area in the dorsal part, is the most common target in German-speaking countries (Hamel et al., 2017). Therefore, an electrode is inserted into the STN (Fig. 1.1C) through stereotactic surgery and connected to an implantable pulse generator (IPG) placed in the clavicle or abdomen for DBS. The nerve cells of the STN are now modulated for therapy by high-frequency (usually 150 Hz; Jakobs et al., 2019) electrical stimulation.

The electrodes used for stimulation vary in size, number, and type of contacts. For ex-

ample, modern segmented electrodes have eight contacts distributed on four levels, with two ring-shaped contacts and six contacts pointing in three different directions (Fig. 1.8). There are several options for choosing the cathode and anode for electrical stimulation. On the one hand, the electrode contacts can be selected for the poles, called bipolar stimulation. On the other hand, the electrode contacts can be the cathode, while the case of the IPG acts as the anode, which is called monopolar stimulation. Several electrode contacts can also be connected to form one pole (Coenen et al., 2015; Kuncel and Grill, 2004).

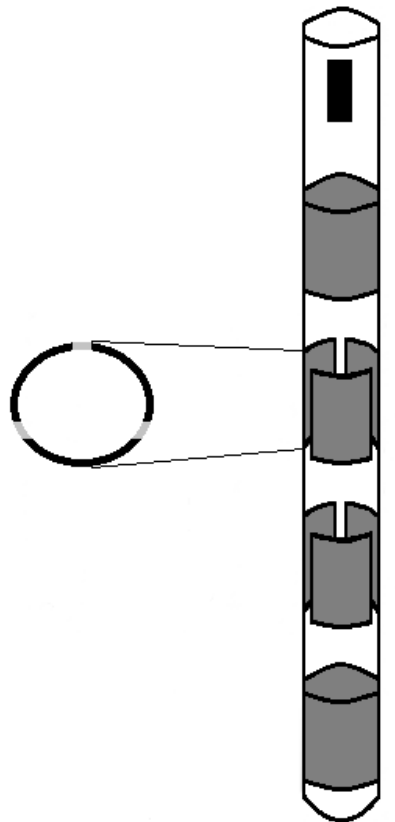


Figure 1.8: Sketch of a directional electrode

A directional electrode for deep brain stimulation is shown (adapted from St. Jude Medical Directional lead 6172; Abbott Laboratories, Lake Bluff, USA). The gray fields mark the stimulation contacts. In this example, the top and bottom contact planes have 360° round contacts, while the two middle planes each have three contacts looking symmetrically in different directions. The black rectangle at the top of the electrode represents a directional marker, which allows the orientation of the electrode contacts to be determined via X-ray or CT imaging.

To ensure the correct placement of the DBS electrodes, planning of the electrode trajectories is performed using modern imaging methods (i.e., MRI, CT), and implantation is performed stereotactically. Intraoperatively, the accuracy of the target area of the DBS electrodes can be verified by measurements of local electrophysiological activity via combined micro-macro

electrodes (Hartmann et al., 2018; Moran et al., 2006; Sterio et al., 2002). Microelectrodes have a small diameter, small surface area, and high impedance and can be used to record single-unit activity and, on a small scale, LFPs. The macroelectrode has a larger diameter and larger surface area but a lower impedance and can be used to record LFPs and to apply intraoperatively electrical stimulation. Microelectrode recording allows the detection of the STN via spiking and background activity (Koirala et al., 2020) and distinguishes the STN from other basal ganglia structures due to differences in the recorded activity (Bour et al., 2010).

Furthermore, the target area can be electrically stimulated via the macroelectrode during surgery, and the electrode can be relocated, if necessary, when the stimulation effect is observed (Walker et al., 2019). The actual DBS electrode can then be moved to the optimal position determined via the micro-macro electrode. There is already a temporary improvement in PD symptoms when the electrode has been implanted, but the stimulation has not yet been turned on. This effect, called the stun effect, is due to microlesions and edema caused by the insertion of the electrode but subsides over time (Chen et al., 2006; Mann et al., 2009). However, as with DBS, the exact mode of action has yet to be clarified.

Stimulating the STN leads to a general improvement of motor symptoms and, with reasonable adjustment, has a favorable side effect profile. DBS is also associated with reducing medication (Deuschl et al., 2006; Vingerhoets et al., 2002). To obtain the best possible outcome, a complex optimization problem has to be solved: The optimal contact for stimulation, the stimulation frequency, pulse amplitude, and duration all have to be adjusted individually (Kringelbach et al., 2007; Kuncel and Grill, 2004). The general positive effect of DBS has been proven, but the exact mechanism still needs to be fully elucidated. To improve the clinical effect of DBS, research is being done on the severity of PD at which DBS should be used, how DBS settings can be optimized, or also whether stimulation should be constant or adaptive at times of pathological events like the STN beta bursts (Abosch et al., 2012; Arlotti et al., 2018; Lettieri et al., 2012; Little et al., 2013; Neumann et al., 2014; Priori et al., 2013; Qasim et al., 2016; Swann et al., 2011; Velisar et al., 2019).

2 Objectives

This work aimed to investigate network formation due to spontaneous brain activity from two points of view. On the one hand, the question arose whether subcortical neural events are involved in the formation of networks in humans and, on the other hand, whether existing RSNs are altered by the insertion of an electrode and the corresponding stun effect.

Since invasive interventions were necessary for both questions, implementation possibilities are limited due to ethical and clinical constraints. In PD patients, implanting an electrode for DBS is one of the standard therapy options. This procedure makes it possible to record activity from the target area, e.g., the STN, and simultaneously record cortical activity via other non-invasive modalities such as MEG. Since burst-like neural events are seen in the STN, especially in PD patients, this work was based on data from PD patients undergoing surgery for DBS.

Study 1 aimed to investigate the spectral and spatial characteristics of STN beta bursts in PD and their response to dopaminergic modulation. Based on this, the optimal setting for detecting subthalamic beta bursts should be determined. In PD patients, STN beta-band activity is pathologically elevated and can be reduced by medication and DBS (Kühn et al., 2009; Ray et al., 2008). Therefore, the STN beta-band activity of PD patients is the subject of many studies. However, the frequency definition of the beta-band is not uniform across studies, and sometimes only a fraction of the beta-band is considered (Kühn et al., 2006; Neumann et al., 2016; Priori et al., 2004). Therefore, study 1 determined the frequency dependence of STN beta bursts with and without medication using three different frequency definitions. That the occurrence of beta bursts differs concerning the frequency definition is expected because, already individually, for each patient, an increased beta activity for a specific frequency in the beta-band can be found (Kühn et al., 2006; Thompson et al., 2014).

Furthermore, segmented DBS electrodes with directional contacts were used in study 1, which provided the opportunity to investigate whether STN beta bursts are evenly distributed in all directions of the STN or occur to be altered in a specific direction. Because beta activity is primarily associated with motor symptoms (Schnitzler and Gross, 2005), we assume an inhomogeneous burst distribution since the STN has functional areas for the limbic and associative systems in addition to motor activity (Haynes and Haber, 2013). Answering these questions could optimize DBS settings in general and adaptive DBS in particular.

Study 2 was built on study 1 and investigated the topology and dynamics of networks associated with STN beta bursts. In an animal study, neural events from the hippocampus

were shown to be involved in network formation (Logothetis et al., 2012), and there are likely other neural events affecting brain activity (Florin et al., 2015). Since STN beta bursts play a prominent role in PD pathology (Sure et al., 2021; Tinkhauser et al., 2017b), they are found in both the STN and cortex (Cagnan et al., 2019; Tinkhauser et al., 2018b, 2017a,b), and there are also functional correlates in both the STN and cortex (i.e., areas for motor, associative and limbic processing; Haynes and Haber, 2013), we hypothesize that beta bursts, possibly via the BGC loop, are involved in network formation between the STN and cortex.

Study 3 studied the effects of STN microlesioning on MEG RSN of PD patients due to DBS electrode implantation. Both dopaminergic medication and DBS can alleviate PD patients' symptoms (Lee and Yankee, 2022) and change RSNs (Oswal et al., 2016; Schneider et al., 2020). In addition, symptom relief was also shown by the stun effect (Chen et al., 2006; Mann et al., 2009). Therefore, an influence on RSNs is also expected. Depending on the function of RSNs, changes caused by the stun effect could lead to conclusions about the mechanisms underlying the stun effect, and it could be helpful in the future planning and application of DBS.

Targeting STN beta bursts in terms of spatial occurrence and frequency dependence could improve clinical effects, especially in applications such as closed-loop DBS. Furthermore, determining the role of STN beta bursts in STN-cortex network formation could be helpful in better understanding the clinical effects and side effects of DBS and the functional role of beta bursts per se. The final comparison of RSN before and after implantation of the electrodes should also help to highlight the role of the stun effect.

3 Study 1: Dopaminergic modulation of spectral and spatial characteristics of parkinsonian STN beta bursts

This work was published under:

Sure, M., Vesper, J., Schnitzler, A., Florin, E., 2021. Dopaminergic modulation of spectral and spatial characteristics of parkinsonian subthalamic nucleus beta bursts. *Front. Neurosci.* 15, 1450. <https://doi.org/10.3389/fnins.2021.724334>

Impact factor (2021): 5.2

Personal Contribution: Concept & study design 10 %; Data acquisition 40 %; Data processing 70 %; Data analyses & figures 100 %; Discussion of results 70 %; Manuscript writing 70 %

3.1 Abstract

In Parkinson's disease (PD), subthalamic (STN) beta burst activity is pathologically elevated. These bursts are reduced by dopamine and deep brain stimulation (DBS). Therefore, these bursts have been tested as a trigger for closed-loop DBS. To provide better targeted parameters for closed-loop stimulation, we investigate the spatial distribution of beta bursts within the STN and if they are specific to a beta sub-band.

Local field potentials (LFP) were acquired in the STN of 27 PD patients while resting. Based on the orientation of segmented DBS electrodes, the LFPs were classified as anterior, postero-medial, and postero-lateral. Each recording lasted 30 minutes with (ON) and without (OFF) dopamine. Bursts were detected in three frequency bands: ± 3 Hz around the individual beta peak frequency, low beta band (lBB), and high beta band (hBB).

Medication reduced the duration and the number of bursts per minute but not the amplitude of the beta bursts. The burst amplitude was spatially modulated, while the burst duration and rate were frequency dependent. Furthermore, the hBB burst duration was positively correlated with the akinetic-rigid UPDRS III subscore.

Overall, these findings on differential dopaminergic modulation of beta burst parameters suggest that hBB burst duration is a promising target for closed-loop stimulation and that burst parameters could guide DBS programming.

3.2 Introduction

Increased beta band activity in the subthalamic nucleus (STN) is considered to be a hallmark of Parkinson’s disease (PD): It correlates with motor symptoms and is reduced by dopaminergic medication or deep brain stimulation (DBS) in the STN (Kühn et al., 2009; Ray et al., 2008). Recent evidence points to beta activity occurring in phasic bursts in the cortex (Feingold et al., 2015; Lobb, 2014) and within the STN (Tinkhauser et al., 2017a,b). These transient bursts have been suggested to indicate episodes of long-range synchronization in the basal ganglia-cortical circuit (Cagnan et al., 2019; Tinkhauser et al., 2018b). Moreover, beta bursts can be used as a feedback signal for closed-loop DBS to improve the stimulation outcome, highlighting their clinical relevance (Arlotti et al., 2018; Velisar et al., 2019). As closed-loop stimulation is still under investigation different approaches for the feedback signal have been proposed (Abosch et al., 2012; Arlotti et al., 2018; Lettieri et al., 2012; Little et al., 2013; Neumann et al., 2014; Priori et al., 2013; Qasim et al., 2016; Swann et al., 2011; Velisar et al., 2019). In the case of beta bursts, it is not known which burst properties lead to the best clinical outcome if they are used as feedback signal for closed-loop DBS.

Using directional DBS leads as opposed to the spatially unspecific omnidirectional leads we investigate the spatial distribution of STN bursts and analyze whether their characteristics differ within the functional subsystems of the STN. Spatially and functionally, the STN itself can be subdivided into three parts corresponding to the motor, limbic, and associative system (Haynes and Haber, 2013). We also aim for a more precise characterization of STN beta bursts along the frequency dimension. Previously it was demonstrated that PD severity as measured by the motor Unified Parkinson’s Disease Rating Scale (UPDRS III) score, on the one hand, correlates positively with the spectral power in the low beta band (lBB) (Neumann et al., 2016). On the other hand, it correlates positively with the temporal stability of the amplitude in the high beta band (hBB) (Little et al., 2012). At the same time, most PD patients have one spectral power peak in the beta band at an individual frequency (iBP).

Finally, we investigate the effect of dopaminergic medication on STN beta bursts and the relation between burst characteristics and the UPDRS III score. As dopamine alleviates the motor symptoms, a change in burst characteristics due to dopamine would highlight their pathological nature. Such pathological burst parameters would be a good target signal for closed-loop DBS and instrumental to optimize closed-loop STN-DBS.

3.3 Material and methods

3.3.1 Subjects and surgery

In total 27 (8 female) PD patients (age: 59.0 ± 8.7 years) undergoing surgery for therapeutic STN-DBS in both hemispheres were recruited for this study. Patients had been selected for DBS treatment according to the guidelines of the German Society for Neurology. The Edinburgh Handedness score (81.1 ± 27.0) showed a clear preference for the right side, whereas the side of the main PD impairment was not lateralized (left = 12, right = 12, equal = 3), which was determined by a laterality score based on the UPDRS part III score (Goetz et al., 2008; Heinrichs-Graham et al., 2017). The UPDRS score was assessed two days before surgery OFF and ON dopaminergic medication (in the following: OFF and ON).

Written informed consent was obtained from all participants. The study was approved by the local ethics committee (study no. 5608R) and conducted in accordance with the Declaration of Helsinki. DBS electrodes with directional leads were implanted within the dorsal part of each STN at the Department of Functional Neurosurgery and Stereotaxy in Düsseldorf. The implanted DBS electrodes used were the St. Jude Medical Directional lead 6172 (Abbott Laboratories, Lake Bluff, USA) and, in one case, the Boston Scientific Vercise segmented lead (Boston Scientific Corporation, Marlborough, USA). To enable LFP measurements, the implanted DBS electrodes were externalized using the St. Jude Medical Directional extension 6373 (Abbott Laboratories, Lake Bluff, USA).

The entry point of the STN was identified based on intraoperative microelectrode recordings (Hartmann et al., 2018; Moran et al., 2006; Sterio et al., 2002). Only the height of directional contacts that matched the STN entry point was selected for further analysis. We thus selected only three out of six possible directional contacts but ensured that the selected contacts were in a comparable anatomic position. Due to a radiopaque marker on the electrode, we identified the segmented contacts facing the anterior, postero-medial, and postero-lateral orientation based on two orthogonal X-ray images. We compared the contacts selected based on the STN entry with the contacts that showed the best clinical outcome. The contact of the best clinical outcome was determined 3-6 months after stimulator implantation and characterized by the best clinical effect due to DBS without any side effects as ascertained by a clinician. In 38 % of the cases, the selected contacts were at the height of the clinically chosen contact for therapeutic DBS.

Subthalamic nucleus recordings of four hemispheres were excluded from further analysis because intraoperative microelectrode measurements showed no typical STN activity or the

electrode orientation was not visible on the available X-ray images. Additionally, the LFPs of one patient could not be included due to excessive artifacts of unknown origin. In the end, we included LFP recordings from 44 STNs of 24 patients in our analysis.

3.3.2 Experimental setup and recordings

The measurement took place 1 to 3 (1.3 ± 0.8) days after surgery. The externalized DBS electrodes were connected to an EEG amplifier. All patients were asked to sit relaxed and still. The data were recorded with a sampling rate of 2400 Hz and a low-pass filter of 800 Hz was applied. The LFP signals were measured against a reference electrode placed at the mastoid. To ensure that patients did not fall asleep we used an eye tracker, tracking the pupil diameter.

We recorded resting-state activity in three consecutive blocks of 10 minutes in two conditions for a total of 60 minutes: once OFF and once ON medication. OFF medication PD oral medication was withdrawn overnight for at least 12 hours. In case a patient had an apomorphine pump, this pump was stopped at least 1 hour before the measurement. After the three OFF measurement blocks, patients received 1.5 times their levodopa morning dose in the form of rapidly acting dispersible levodopa (173.0 ± 48.9 mg). To ensure a stable ON, we waited for at least 30 minutes and tested the clinical symptoms before the second half of the measurement. One patient could only be measured ON medication and one only OFF.

3.3.3 Signal processing

All data processing and analyses were performed using Matlab (version R 2016b; MathWorks, Natick, USA). Custom-written Matlab scripts and the toolbox Brainstorm¹ (Tadel et al., 2011) were used. To ensure artifact-free data, two persons independently inspected the data visually, cleaned artifacts, and compared the cleaned output. In case of differences, the questioned time segment was rejected. The line noise was removed from all channels with a notch filter with a 3-dB bandwidth of 1 Hz at 50, 100, 150, . . . , 550, and 600 Hz. The LFP recordings from the DBS electrode were re-referenced against the mean of all LFP channels. Noisy or flat LFP channels were excluded from further analysis. Time segments containing artifacts were removed from the time series, but if artifacts just occurred frequently in one channel, only this whole channel was removed. All data were high-pass filtered with 1 Hz to remove movement-related artifacts. Furthermore, the data were down-sampled to 1000 Hz. To avoid the influence of different impedance values between patients and recording sessions, we finally calculated the z-transformation of the preprocessed time-series separately for each recording session.

¹<https://neuroimage.usc.edu/brainstorm/>

3.3.4 Detection of bursts in the beta-frequency range

Within the beta band, different activity patterns have been described for the lower and higher beta frequency range (Kühn et al., 2006; Priori et al., 2004). As the definition and segmentation of the beta band differ among research groups, we decided to divide the beta band into a lower and a higher sub-band of equal size (12-24 Hz; 24-35 Hz). Moreover, we considered a ± 3 Hz band around the iBP (Mean \pm SD: 22.1 ± 5.8 Hz) of each patient. The iBP was determined OFF medication based on the beta peak in the individual power spectrum. For this purpose, the power spectrum in the beta band was examined for local maxima. In case the maximum was at the corner frequencies of 12 Hz or 35 Hz, the amplitude at 11 Hz or 36 Hz needed to be lower for the iBP to be considered at 12/35 Hz. The maximum with the highest amplitude in all contacts of one patient was considered as iBP frequency. ON medication the beta peak was generally reduced or vanished completely for some patients. In case a peak was still visible ON medication, it was always within 1 Hz of the OFF peak, i.e. covered by our ± 3 Hz interval. The power spectra were determined based on the z-score normalized time-series with 1 Hz resolution using the Welch method with a window length of 1 s and an overlap of 50 % (Welch, 1967). To compare different spectra, we corrected for the 1/f characteristic of the LFP signal and normalized to the total power of 5-45 Hz and 55-95 Hz analog to Neumann *et al.* (2016).

The preprocessed LFP data were used to detect bursts within the two beta sub-bands and the iBP. Our approach follows Tinkhauser *et al.* (2017a; 2017b), but we determined the bursts based on the z-value normalized data rather than the raw data. Afterward, following the burst detection approach by Tinkhauser *et al.* (2017a; 2017b), Morlet wavelets (Tallon-Baudry et al., 1997) as implemented in Brainstorm were calculated for the lBB, the hBB, and around the iBP. The time-evolving amplitude was smoothed by a 200 ms moving average, followed by a DC-offset correction with a time constant of 20 s to correct for a potential baseline offset. For each patient, channel, and frequency we calculated the 75th percentile of the OFF and ON time-series and took the average of both of them. The separate z-score normalization of the LFP data OFF and ON medication could potentially mask the differences in the burst amplitudes between OFF and ON. Despite the z-value normalization, there were significant differences in beta power. Moreover, the bursts were detected based on a common threshold from the combined ON and OFF recording, which ensures that differences in burst amplitude between OFF and ON can be detected.

For a time-point to be part of a burst in the respective frequency band, the amplitude needed to be higher than the 75th percentile. All consecutive time-points with an amplitude exceed-

ing the threshold were assigned to the same burst. The minimal burst duration was set to 80 ms, which is equivalent to 2 oscillatory cycles at 24 Hz. For every burst, the time-point of the amplitude crossing the threshold and again dropping below were stored. The value of the maximum burst amplitude and its time of occurrence were also stored. Due to the applied burst detection scheme, we are referring to the power based on the z-score transformed time series and not to the power of the raw time series when we are considering the burst amplitude.

3.3.5 Statistical analysis

For the number of bursts per minute which is calculated by the total number of bursts detected for one channel divided by the total recording time in minutes (in the following: burst rate), burst duration, and amplitude we compared the recording orientation of the LFP contacts, frequency band, and the medication state. Therefore, we performed a three-way ANOVA (Yates, 1934) in Matlab. The dependent variables were burst rate, duration, and amplitude, respectively, and the independent variables were directions (anterior, postero-medial, and postero-lateral), frequency bands (iBP, lBB, and hBB), and medication states (OFF and ON). Because the correlation of the burst parameters between the hemispheres was partially significant, but a paired t-test showed no significant differences between hemispheres, the evidence on hemisphere dependence is inconclusive. Following the previous literature (Zavala et al., 2017), we opted to pool both hemispheres. Therefore, the incoming sample size for ANOVA was the total number of good LFP data by orientation (anterior: OFF & ON each 31 LFPs; postero-medial: OFF & ON each 37 LFPs; postero-lateral: OFF 31 LFPs and ON 32 LFPs). For the post-hoc test, a t-test was used, which was corrected for multiple comparisons using the Bonferroni method, again using the Matlab implementation. We corrected for two medication states, three frequency bands, and three contact directions for a total of 18 comparisons.

Finally, the Pearson correlation between the akinetic/rigid (AR) UPDRS III subscore (sum of the 13 items 3.3 a-c, 3.4 ab, 3.5 ab, 3.6 ab, 3.7 ab, 3.8 ab) and the beta burst characteristics, as well as the power values from the power spectra, were calculated OFF medication. All reported correlation p-values are Bonferroni corrected for the three contact orientations and the three frequency bands.

3.4 Results

3.4.1 Beta power

Figure 3.1 displays the average power spectra OFF and ON medication across patients for the three different LFPs at the STN entry from 5-35 Hz. The power spectra are 1/f corrected and normalized to the total power of 5-45 Hz and 55-95 Hz. There were no significant differences between power of the different recording orientations in each medication condition but between the power OFF and ON medication. The difference was significant in the anterior direction from 32-34 Hz, the postero-medial one from 24-28 Hz, and the postero-lateral one from 31-34 Hz. Beta peaks OFF medication occurred mainly around 24 Hz at the anterior and postero-medial contact (Fig. 3.1). As the beta peak frequency differed between the recording directions, we investigate in the following to what extent the recording orientation and frequency band influence beta bursts.

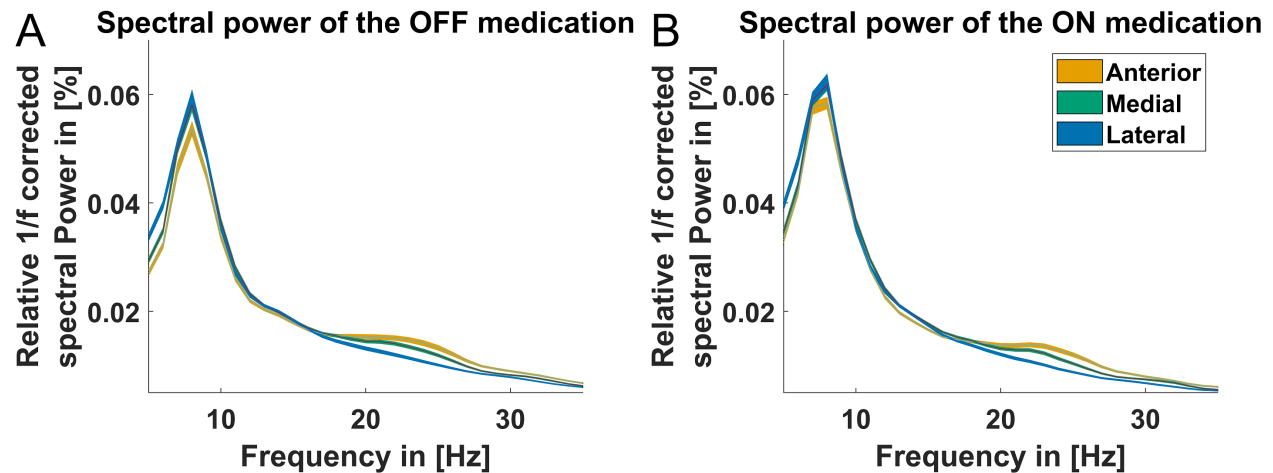


Figure 3.1: Power spectra for three recording directions

The spectra displayed for the contact orientation anterior (orange line), postero-medial (green line), and postero-lateral (blue line) are corrected for the 1/f characteristic of the LFP signal and normalized to the total power from 5-45 Hz and 55-95 Hz. The x-axis presents the frequency from 5-35 Hz. (A) shows the spectra OFF medication and (B) ON medication. The colored shaded areas indicate one standard deviation of the mean.

3.4.2 Burst characteristics

Figure 3.2 illustrates characteristics of STN beta bursts depending on medication state, pre-defined frequency band, and electrode contact orientation. Panel A displays the burst rate for the two medication states, the three contact orientations and frequency bands. Medication had a significant main effect indicating that dopaminergic medication decreased the burst rate for all orientations and frequency bands ($F(1,579) = 97.1$, $p = 2.8E-21$, $\eta^2p = 0.144$). This

was also evident in the post-hoc test for the hBB and iBP in anterior and postero-medial orientation ($p < 0.05$). Thus, a high burst rate seems to be a characteristic of PD pathology. In addition, there was a significant main effect of frequency for the burst rate ($F(2,579) = 283.9$, $p = 1.2E-86$, $\eta^2p = 0.495$) but no significant main effect of the contact orientation. Based on post-hoc tests the hBB burst rate was higher compared to the lBB and the iBP for all contact orientations and both medication states ($p < 1.0E-6$; Fig. 3.2A,B). The rate at the iBP was only significantly higher compared to the lBB OFF medication for the postero-medial and postero-lateral direction and ON medication only for the postero-medial direction ($p < 0.05$; Fig. 3.2A).

Medication had also a significant main effect for burst duration, which was reduced due to dopaminergic medication ($F(1,579) = 4.6$, $p = 0.03$, $\eta^2p = 0.144$), which can be seen in panel B of figure 3.2. Moreover, the burst duration was influenced by the frequency band but not by the contact orientation ($F(2,579) = 341.6$, $p = 1.0E-98$, $\eta^2p = 0.495$). Post-hoc analysis revealed that the burst duration was significantly shorter for the hBB compared to the lBB as well as the iBP in both medication states ($p < 1.0E-7$; Fig. 3.2C,D). The burst duration was also significantly shorter at the iBP compared to the lBB ($p < 0.01$; Fig. 3.2C,D) but only for the postero-medial direction both OFF and ON medication. Interestingly for the burst amplitude, the contact orientation had a significant main effect across medication states and frequency bands ($F(2,579) = 6.7$, $p = 0.001$, $\eta^2p = 0.003$) but not for the medication and frequency itself.

3.4.3 Clinical relevance of burst characteristics

Because a positive correlation between bradykinesia and overall beta oscillations has previously been reported (Ray et al., 2008), we tested whether beta bursts characteristics correlate with the AR UPDRS subscore. We focused on the AR UPDRS subscore, because, based on the UPDRS score, 70.4 % of our patients were of the akinetic-rigid subtype. The OFF hBB burst duration of the postero-medial contact was significantly positively correlated with the OFF AR subscore ($p = 0.03$, $r = 0.48$; Fig. 3.3). For the other contact orientations and frequency bands there was no significant correlation.

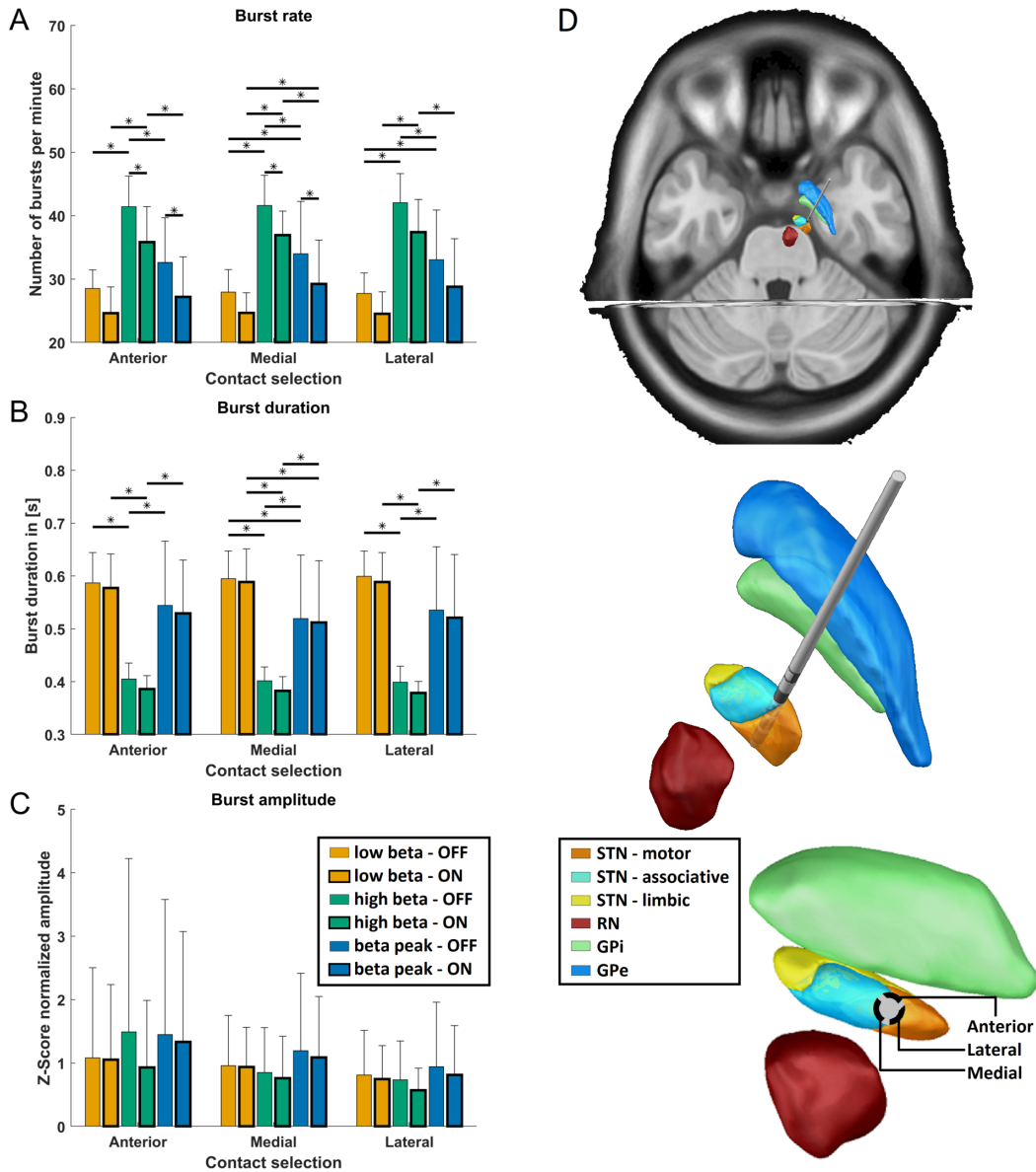


Figure 3.2: Burst characteristics

(A) Shows the mean burst rate, (B) the mean burst duration, (C) the mean burst amplitude, and (D) the exemplary reconstructed electrode position of the right hemisphere. (A - C) The mean values for the three frequency bands (low beta band in orange, high beta band in green, and the individual beta peak frequency in blue) are shown OFF (thin frame) and ON medication (bold frame) grouped on the x-axis for the anterior, postero-medial, and postero-lateral directions for each burst parameter. Error bars depict one standard deviation. Stars indicate significant differences with $p < 0.05$ after Bonferroni corrected post-hoc tests between the respective groups. (D) Shows the reconstructed electrode on top, with focus on the surrounding subcortical structures (STN, subthalamic nucleus divided into motor, associative, and limbic areas; RN, red nucleus; GPi, globus pallidus pars internus; GPe, globus pallidus pars externus). At the bottom the perspective is along the electrode so that the directions of the electrode contacts can be seen.

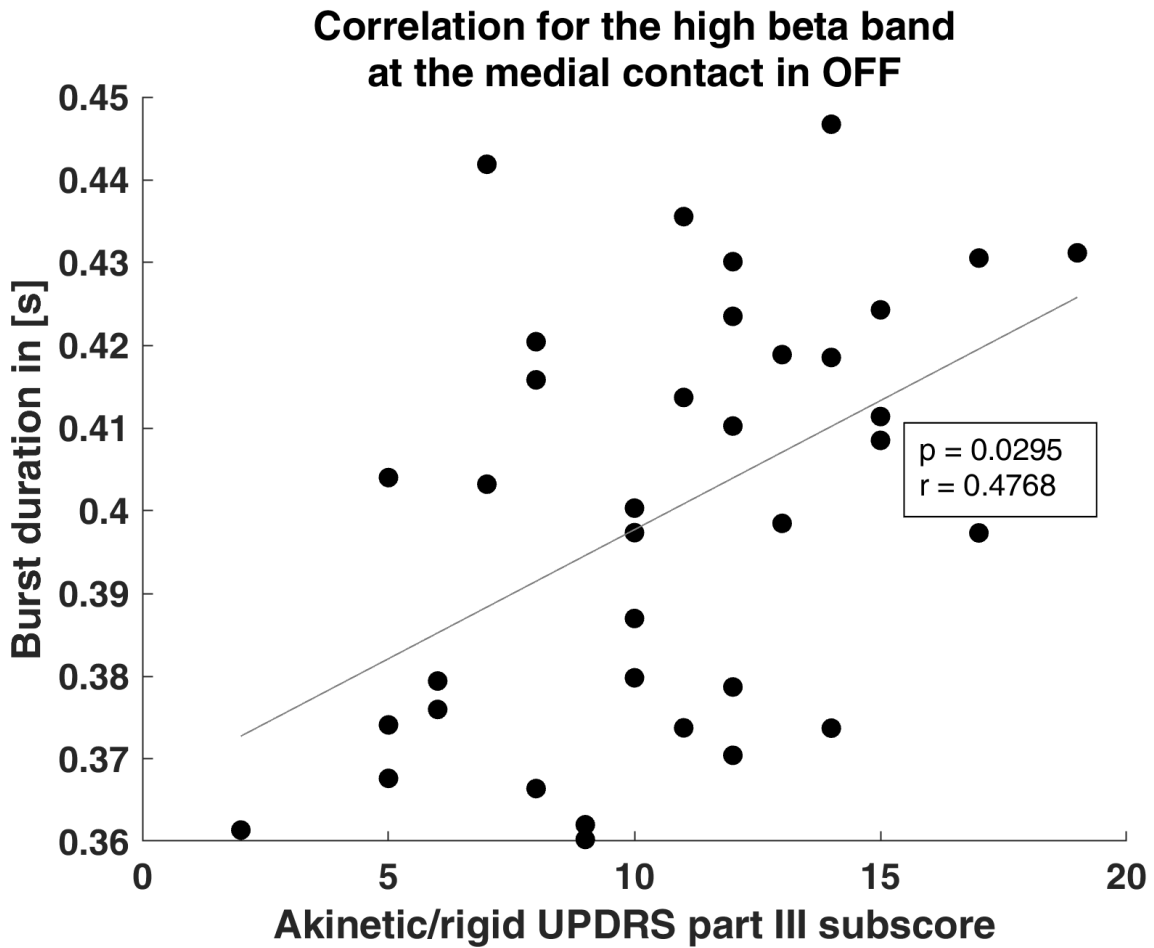


Figure 3.3: Clinical correlation of burst duration

The scatter plot shows the significant correlation of the burst duration and the akinetic/rigid UPDRS part III subscore. The gray line indicates the linear fit.

3.5 Discussion

To our knowledge, this is the first work investigating the spatial characteristics of STN beta bursts recorded with directional electrodes. Spatially, we found a non-homogeneous distribution of the burst amplitude. However, we could not identify any outstanding direction with respect to the amplitude or the rate and duration of the bursts. However, the burst rate and duration in particular are frequency-dependent, which makes frequency selection very important for applications such as closed-loop DBS.

3.5.1 Slight directionality of the beta burst amplitude

It has been shown that for each patient, a preferential contact exists in terms of best clinical outcome, and many patients benefit from directional stimulation (Gordon et al., 2017; Hartmann et al., 2019). Therefore, we wanted to identify whether beta burst properties differ between the three recording orientations and thus could serve as an indicator for stimulation selection. There was a main effect of recording orientation for burst amplitude. However, post-hoc tests did not reveal one prominent direction for amplitude or any other measure. Therefore, based on our analysis, no particular anatomic direction can be recommended for directional DBS. The reason for this could be that all contacts used were placed in the dorsal end of the STN, which is functionally attributed to the motor system (Parent and Hazrati, 1995b). Therefore, a comparable neurophysiological signal at all contact orientations is plausible and suggests a homogeneous structure of this area. In line with this reasoning, the connectivity between STN and cortex is functionally organized based on the functional sub-areas of the STN (Lambert et al., 2012). Nevertheless, there is a significant main effect of direction for the burst amplitude. One possibility is that the anatomical dependence of the bursts will only reveal itself with a larger number of cases.

3.5.2 Beta burst activity is frequency specific

We considered three different frequency bands within the beta band: the lBB, the hBB, and the frequency range around the individual beta peak frequency. The reason for this choice was that previous publications reported results specifically for sub-bands of the beta band (Little et al., 2012; Priori et al., 2004; Tinkhauser et al., 2017a,b). We found that burst characteristics differ depending on the chosen frequency band. The burst rate increases for higher frequencies, while the duration decreases. In line with this finding, the AR score correlated with the burst duration in the hBB but no other frequency band. In addition, duration was significantly reduced by dopaminergic medication only for the hBB and iBP. This suggests that bursts in the hBB are likely linked to the pathophysiology of PD, which is consistent with the results

of Little *et al.* (2012). However, it contrasts with the results of Neumann *et al.* (2016) and Priori *et al.* (2004), but these studies considered beta power, not beta bursts. A pairwise test of power values compared to Priori *et al.* showed significant influence of dopaminergic medication on power in the hBB but not in the IBB.

To further investigate the importance of the frequency band definition, we performed our analysis with a modified frequency band definition, assigning the IBB to 12-20 Hz and the hBB to 21-35 Hz. When comparing the results for the two frequency band definitions, there were no differences with respect to significant findings for the medication dependence or the direction dependence of the burst parameters. However, while for the frequency band separation at 24 Hz there were no significant differences for the burst amplitude between the frequency bands, for the separation at 20 Hz, there were significant differences in the burst amplitude between the IBB and iBP and between hBB and iBP for both medication states and all three directions. In addition, significant differences for burst rate and duration were found between the IBB and iBP. This change in findings based on the beta band separation is most likely due to beta peaks formerly assigned to the IBB now being assigned to the hBB with the separation at 20 Hz. This difference in results suggests that if a beta peak occurs in the power spectra, the frequency band around this peak should be favored for closed-loop stimulation for example; if no peak is present, our results indicate that the hBB could be a good alternative.

3.5.3 Burst duration best suited as stimulation trigger in closed-loop DBS

Burst characteristics OFF medication are linked to the pathology of PD, while those ON medication approximate physiological activity. As expected based on previous publications, we could find an effect of dopaminergic medication on beta bursts (Kühn *et al.*, 2009; Ray *et al.*, 2008; Tinkhauser *et al.*, 2017a,b). Since we could detect a main effect only with respect to the duration and the rate of the bursts, this suggests that these are more pathologically altered by PD than the amplitude of the individual bursts. The burst amplitude is a necessary quantity for the burst detection method employed in the present study. But according to our results, it is less suitable for distinguishing between pathological and physiological bursts.

In contrast, it has previously been described that a long burst duration is being positively and a short burst duration negatively correlated with clinical motor impairment (Tinkhauser *et al.*, 2017a). In our study, only the duration significantly correlated with the AR score and the duration was reduced under medication. Therefore, burst duration seems to be more tightly linked to PD motor symptoms than the burst amplitude and rate. This suggests that

the burst duration is the best candidate for a stimulation trigger in closed-loop DBS. This conjecture is in line with previous results that reduced burst duration is associated with improved movement velocity due to DBS (Kehnemouyi et al., 2021). However, since amplitude is the key parameter in burst detection, further studies are needed to understand the interplay of amplitude and burst duration for detecting pathological bursts and their usefulness as stimulation triggers in closed-loop DBS.

To use electrophysiological signals as control parameters for closed-loop DBS, they should remain stable over months and years. We recorded the LFP signals a few days after electrode implantation, when the tissue is still subject to transient processes, such as inflammation, that may affect recording properties and neural activity. However, previous studies indicate that STN beta band LFP patterns and response profiles stay almost unchanged for years after DBS electrode implantation (Abosch et al., 2012; Giannicola et al., 2012). Moreover, beta activity continues to correlate with severity of PD motor symptoms 8 months after implantation (Neumann et al., 2017). Therefore, it is likely that the duration of beta bursts remains stable over a long period of time and thus provides a valid control parameter for closed-loop DBS. Still, the stability of beta burst duration over longer time periods needs to be investigated in future studies.

3.5.4 Limitations

Because we, at the latest, recorded the LFP data 3 days after the DBS surgery, our recordings might be affected by the stun effect (Chen et al., 2006). Due to the magnitude of the stun effect being unknown and immeasurable, it is impossible to correct the electrophysiological data for it. In line with other studies, the UPDRS values were collected before the DBS surgery and thus do not capture the stun effect on the clinical symptoms. This timing difference likely also influences the calculated correlation between the UPDRS and the beta bursts parameters. A further limitation is our assumption that beta bursts in one STN arise independently from the other STN. Based on our data, the evidence on the STN activity being independent of the hemisphere was inconclusive. Our decision to pool the data follows previous literature treating the LFPs of both STNs as independent (e.g., Zavala et al., 2017).

3.5.5 Conclusion

Using directional contacts, we intended to identify the spatial distribution of beta bursts at the entry point of the STN. However, based on the electrode’s recording orientation, we could not identify one orientation with significantly different burst parameters than the other orientations, even though there was an overall effect of orientation for the burst amplitude.

Still, we could identify a strong frequency dependence of beta bursts. Correlation with the akinesia and rigidity scores indicates, in particular, that hBB burst duration is pathologically increased. In addition, dopaminergic medication influences burst rate and duration. These two findings speak in favor of the hBB bursts as feedback signal for stimulation in closed-loop DBS.

4 Study 2: Cortical network formation based on subthalamic beta bursts in Parkinson's disease

This work was published under:

Sure, M., Vesper, J., Schnitzler, A., Florin, E., 2022. Cortical network formation based on subthalamic beta bursts in Parkinson's disease. *Neuroimage* 263, 119619.<https://doi.org/10.1016/j.neuroimage.2022.119619>

Impact factor (2022): 7.4

Personal Contribution: Concept & study design 30 %; Data acquisition 40 %; Data processing 70 %; Data analyses & figures 100 %; Discussion of results 75 %; Manuscript writing 70 %

4.1 Abstract

Recent evidence suggests that beta bursts in subthalamic nucleus (STN) play an important role in Parkinsonian pathophysiology.

We studied the spatio-temporal relationship between STN beta bursts and cortical activity in 26 Parkinson's disease (PD) patients undergoing deep brain stimulation (DBS) surgery. Post-operatively, we simultaneously recorded STN local field potentials (LFP) from externalized DBS leads and cortical activity using whole-brain magnetoencephalography. Event-related magnetic fields (ERF) were averaged time-locked to STN beta bursts and subjected to source localization.

Our results demonstrate that ERF exhibiting activity significantly different from baseline activity were localized within areas functionally related to associative, limbic, and motor systems as well as regions pertinent for visual and language processing.

Our data suggest that STN beta bursts are involved in network formation between STN and cortex. This interaction is in line with the idea of parallel processing within the basal ganglia-cortex loop, specifically within the functional subsystems of the STN (i.e., associative, limbic, motor, and the related cortical areas). ERFs within visual and language-related cortical areas indicate involvement of beta bursts in STN-cortex networks beyond the associative, limbic, and motor loops. In sum, our results highlight the involvement of STN beta bursts in the formation of multiple STN - cortex loops in patients with PD.

4.2 Introduction

The analysis of resting-state networks (RSN) is a widely used approach to gain insight into the communication between brain regions and various methods have been developed to determine RSNs from neurophysiological recordings (Brookes et al., 2011; Florin and Baillet, 2015; van den Heuvel and Hulshoff Pol, 2010). However, these methods mostly map static networks and thus cannot fully capture the dynamic communication of the brain. Therefore, Logothetis *et al.* (2012) proposed an approach to investigate cortical activity based on neuronal events, thereby investigating more dynamic effects of communication. In the original study, cortical activation determined from functional MRI occurred time-locked with hippocampal ripples, which were identified from simultaneous local field potentials (LFP). Since it can be assumed that other neuronal events are also involved in network formation (Florin et al., 2015), we hypothesize that this is also true for beta bursts in the subthalamic nucleus (STN), due to the present coupling of subcortical and cortical bursts (Tinkhauser et al., 2018b).

Network formation determined via neuronal events would enable the investigation of network dynamics linked to specific prominent activity. Studies on dynamic RSNs with fMRI (Britz et al., 2010; Chang and Glover, 2010; Zalesky et al., 2014), however, have a poor temporal resolution due to the low-frequency blood oxygenation level-dependent signal (< 0.15 Hz; Josephs and Henson, 1999). In contrast, electroencephalography (EEG) and magnetoencephalography (MEG) offer a much better temporal resolution (< 1 ms) for which dynamic networks have already been identified (Britz et al., 2010; Chen et al., 2013; Dimitriadis et al., 2018; Vidaurre et al., 2018). Although EEG and MEG allow for more precise time-resolved recordings of neuronal events, they are mainly limited to cortical interconnectivity. This interconnectivity is often determined via correlation or phase coupling of synchronous activity in different brain areas, thereby not considering specific neuronal events. Recently, Hidden Markov Models (Vidaurre et al., 2018) were used to identify cortical connectivity based on cortical neuronal events (Seedat et al., 2020). In this analysis, connectivity is based on simultaneous or consecutive occurrences of oscillatory bursting events in different areas. In contrast, the method of Logothetis *et al.* (2012) examines the influence of specific local neuronal events on activity in other brain areas, making it well-suited for understanding the impact of individual neuronal events, especially those of pathological nature.

A potential candidate for such neural events are beta bursts in the STN of Parkinson’s disease (PD) patients. During the implantation of deep brain stimulation (DBS) systems, LFPs from electrodes in the STN can be recorded. In PD, STN oscillatory beta band activity is pathologically increased and occurs in the form of phasic bursts in both the STN and the

cortex (Feingold et al., 2015; Lobb, 2014; Tinkhauser et al., 2017a,b). In terms of network formation, extensive coupling between basal ganglia and cortex was demonstrated during the precise timing of the beta bursts (Tinkhauser et al., 2018b). This is in line with the notion that retrograde cortical activity is evoked by electrical stimulation of the STN (Ashby et al., 2001; Ceballos-Baumann et al., 1999; Hartmann et al., 2018; Miocinovic et al., 2018; Walker et al., 2012), demonstrating an electrophysiological connection in parallel with anatomical connections between the STN and motor cortex via the basal ganglia-cortical (BGC) loop (Deffains and Bergman, 2019; McGregor and Nelson, 2019). Furthermore, matching the hypothesized hyperdirect pathway between frontal cortex and STN (Aron et al., 2016), STN and areas on the frontal cortex are synchronized (Cagnan et al., 2019). However, these previous studies used single EEG electrodes to identify long-range coupling between cortex and STN, therefore not allowing a complete cortex coverage with high spatial specificity (Cagnan et al., 2019; Tinkhauser et al., 2018b).

To unveil the relationship between STN beta bursts and whole-brain cortical activation, we employed the neuronal event triggered (NET) approach to simultaneously record STN-LFP-MEG data, which allowed us to sample the whole cortex with high spatial accuracy at the time of neuronal events. In addition, the temporal resolution shifts from seconds to milliseconds compared to the fMRI recordings used in the original NET approach. Because beta activity in the STN appears in event-like phasic bursts and is electrophysiologically connected to cortical activity, we hypothesized that cortical activity patterns evolve time-locked to STN beta bursts. To our knowledge, our study is the first to apply the NET approach to human recordings and further, to show that neural events play a role in network formation. For this purpose, we recorded combined LFP-MEG data of 26 PD patients at rest without dopaminergic medication.

Based on the previous work by Logothetis *et al.* (2012) that neuronal events are involved in network formation in the human brain, we hypothesize that STN beta bursts are involved in forming STN-cortex networks related to the motor, limbic, and associative subdivisions of the STN. Such knowledge will deepen our understanding of whole-brain network effects based on neural events, as hypothesized in Florin *et al.* (2015). Further, these results may improve our understanding of the pathophysiology in PD and the communication between STN and cortex.

4.3 Methods

4.3.1 Subjects and surgery

For this study, 26 (8 female) PD patients were recruited. All patients underwent therapeutic bilateral STN-DBS surgery according to the guidelines of the German Society of Neurology. Written informed consent was obtained from all participants. The study was approved by the local ethics committee (study no. 5608R) and conducted in accordance with the Declaration of Helsinki. According to the Edinburgh Handedness inventory, all patients were right handed (80.4 ± 27.2), whereas the side of main PD impairment was not lateralized to the left ($N = 15$) or right ($N = 11$). The average Unified Parkinson’s Disease Rating Scale motor score OFF medication was 37.8 ± 11.3 .

4.3.2 Experimental setup and recording

Bilateral implantation of DBS electrodes with directional leads (St. Jude Medical Directional lead 6172, Abbott Laboratories, Lake Bluff, USA; in one case the Boston Scientific Vercise segmented lead, Boston Scientific Corporation, Marlborough, USA) was performed at the Department of Functional Neurosurgery and Stereotaxy in Düsseldorf, Germany, targeting the dorsal part of the STN with the center between the outermost contacts of the electrode. Intraoperatively, multi-unit activity was recorded with microelectrodes to ensure that the DBS electrode was placed in the STN. The implanted DBS electrodes have eight contacts distributed at four heights. The top and bottom heights consist of a 360-degree round contact, while the two middle heights consist of three 120-degree directional contacts. The implanted electrodes were connected via the St. Jude Medical Directional extension cable 6373 (Abbott Laboratories, Lake Bluff, United States) to an EEG amplifier integrated into a 306 channel MEG system (Elekta Neuromag, Finland). This allowed us to simultaneously record LFP signals from the STN and MEG signals. The LFP signals were referenced to the mastoid during the recording. To identify the spatial relation between the patient’s head and the MEG-sensors, four head position indicator coils were placed on the patient’s head and their position was digitized using the Polhemus system (Polhemus Isotrack, Colchester, USA). In addition, we digitized about 100 additional points on the head for later co-registration with the individual MRIs.

During the MEG measurement, heartbeat and eye movements were recorded. Patients were seated in the MEG and remained at rest with eyes open. Patients were on a personalized medication regime and were discontinued from their regular oral dopaminergic medication overnight for at least 12 hours before measurement. In patients on continuous subcutaneous

apomorphine, the pump was stopped at least 1 h before the measurement. This practically defined medication OFF state does not necessarily represent the worst OFF condition but is typically used in PD studies. Resting activity was recorded in three consecutive blocks of 10 minutes. At the beginning of each block, the relative position of the patient’s head to the MEG sensors was measured with the four head positioning coils. All data were sampled with a frequency of 2400 Hz with an anti-aliasing low-pass filter of 800 Hz.

4.3.3 Signal processing

All preprocessing and further analyses were done using Matlab (version R 2016b; MathWorks, Natick, USA) and the toolbox Brainstorm (<https://neuroimage.usc.edu/brainstorm/>; Tadel et al., 2011). The customized Matlab code is available at https://github.com/FlorinNeuro/stn_beta_burst_erf. To ensure artifact-free data, all data were independently checked by two MEG experts. If there was disagreement on an artifact, the corresponding segment was marked as an artifact. In a first step, heartbeats and eye blinks and any regularly occurring artifacts were corrected using signal-space projectors as implemented in Brainstorm. More details on the measurement and preprocessing can be found in Sharma *et al.* (2021).

For further analysis, we re-referenced, in each hemisphere, the LFP signal of the top circular contact against the bottom circular contact of the recording electrode. This allows good coverage of the activity in the target area of the STN since the target point for electrode implantation was planned to be the center of the electrode. The distance of the center of the outer contacts to the planned target point was 3 mm. If either the top or the bottom circular contact had to be rejected because of poor signal quality, the re-referencing was performed on the mean of the three adjacent directional contacts. If one of the three contacts necessary to compute the mean also had a poor signal quality, this hemisphere was not included in further analysis. This led to the exclusion of 2 hemispheres of different patients.

4.3.4 Cortical event-related fields

To investigate cortical activation time-locked to STN beta bursts, we detected beta bursts in the re-referenced LFPs of each hemisphere based on an adapted version (Sure et al., 2021) of the approach by Tinkhauser *et al.* (2017a; 2017b). This adapted version includes raw signals that were z-score normalized to correct for possible impedance differences in the contacts. The bipolar re-referencing was used to cover as much of the STN as possible. Moreover, no difference in the rate and duration of beta bursts was found for the different contacts of directed electrodes (Sure et al., 2021). First, we z-score normalized the re-referenced LFP signal separately for each run to account for impedance differences of the contacts between

measurement runs or patients. Next, Morlet wavelets were calculated for the LFP signals within the frequency range ± 3 Hz around the individual beta peak frequency (iBP). The iBP frequency was determined based on the power spectra compensated for the $1/f$ decay using Brainstorms implementation, i.e., each frequency bin is multiplied by the frequency value. A local maximum with a hard-coded peak prominence – the vertical displacement between the peak value and its lowest contour line – of $1e-13$ was searched for in the frequency range of 12-35 Hz. The peak prominence limit was determined using the mean of the peak prominence values of all local maxima in the beta band. The calculation of the prominence values followed the implementation in Matlab. The resulting signal was temporally smoothed using a moving box with a 0.2 s window and additionally corrected with a 20 s moving window for DC offset, where the mean of the box was subtracted from the sample in the center of the box. The burst detection threshold was set as the 75 % percentile of the final amplitude of all runs per patient. A burst was defined as the period of time which continuously exceeded the threshold value. For each hemisphere, the iBP was determined from the power spectrum of the re-referenced LFP signal as the local interior maximum in the beta band (12-35 Hz). If the maximum occurred at either extreme of this beta band (i.e., 12-35 Hz), no iBP would be considered for the corresponding hemisphere and subsequent analyses. This led to the exclusion of an additional 16 hemispheres, resulting in 34 included hemispheres (18 right; 16 left) of 23 patients.

To link cortical activity to STN beta bursts, we calculated source-level activity at the cortex based on the simultaneously acquired MEG data. To do so, the individual cortical surfaces (white matter – gray matter) were extracted from the individual T1-weighted MRI scans (3 T scanner and 1 mm^3 voxel size) using Freesurfer (<http://freesurfer.net>, v.5.3.0). Based on the Polhemus data, the relative MEG sensor positions were imported to Brainstorm and matched to the head surface using the nasion, left, and right pre-auricular point as anatomical landmarks. This initial co-registration was optimized using the additional head points. The forward problem was solved using overlapping spheres as implemented in Brainstorm (Huang et al., 1999). The lead-fields were computed from elementary current dipoles distributed perpendicularly to the cortical surface of each individual. For source reconstruction of broadband brain activity, the linearly constrained minimum variance beamformer, as implemented in Brainstorm, was used (Van Veen et al., 1997). A total of 15002 evenly spaced cortical sources were reconstructed. The cortical triangles had a mean surface area of 7.82 mm^2 . The data covariance matrix was calculated individually for each measurement block of 10 minutes. The noise covariance matrix was obtained from 5-minutes of empty room recording, which were acquired on the day of each patient’s measurement.

To calculate event-related fields (ERF) in relation to STN beta bursts, cortical time-series from -100 ms to +100 ms around the maximum of the beta burst were extracted from the MEG data without restrictions in the frequency range. As a burst state and thus comparable beta activity should be present in the STN for the entire duration of this time window, we set a minimum burst duration of 200 ms. Furthermore, no significant difference was found between the time from burst onset to burst maximum and the time from burst maximum to burst end (paired t-test ($t = -0.06$)). Therefore, a symmetrical temporal profile of the bursts can be assumed. Secondly, as baseline cortical activity from 200 ms to 100 ms before burst onset was used. This baseline was determined for each burst individually. The time-series around the beta burst maximum were baseline-corrected by subtracting the temporal mean of the individual baseline from each burst. ERFs were then obtained for each subject by averaging the extracted time-series across all beta bursts. To ensure better comparability of cortical activity between subjects, we removed high frequency noise while temporally smoothing the cortical ERFs of each subject using a Gaussian kernel with a window length of 5 ms. The cortical activity maps were projected onto a template brain (ICBM152) for group-level comparison using FreeSurfer’s spherical registration (Fonov et al., 2011).

We also repeated the analysis for short bursts (< 300 ms) and long bursts (> 500 ms) because long beta bursts are considered pathological (Tinkhauser et al., 2017b), and thus cortical activity might differ with respect to these two burst groups. In addition, the analysis was also repeated for a time window ± 100 ms around the onset of the burst. This allows an analysis of cortical activity at times before the onset of STN beta bursts.

In the end, we examined cortical activity for twelve different burst characteristics. Regarding burst onset and burst maximum, we considered bursts with a minimum duration of 200 ms, which was congruent with the investigated time range of cortical activity (i.e., central bursts), short bursts with a maximum duration of 300 ms and long bursts with a minimum duration of 500 ms of the left and the right STN.

4.3.5 Statistical analysis

A whole-brain t-test against baseline was computed at the group level, resulting in a matrix containing a p-value for every cortical source and every time-point from -100 ms to +100 ms around the burst maximum. Subsequently, the t-values were spatially smoothed with an FWHM of 1 mm. The significance threshold was determined using a bootstrapping approach with 100 repetitions with the same pipeline for different random time points. Within each

repetition for each measurement run of each patient, cortical activity was averaged from 250 random time points rather than beta bursts. We used 250 random time points due to having an average of 250 beta bursts per measurement run. For each bootstrap repetition, the 97.5th percentile of the absolute value of the t-values of all vertices was determined. Of these 100 critical t-values, the most extreme value of $t = 5.05$ was used as the threshold in the further analysis. Significant sources were only considered if the absolute t-value exceeded 5.05 for at least 5 ms and 10 contiguous sources. We mapped significant changes in cortical activity to areas of the Mindboggle atlas (Klein et al., 2017). The classification was based on the area in which the majority of the vertices of a significant cluster were located.

Finally, we also investigated whether there were differences in cortical activity with respect to the twelve burst characteristics. For this, we used an independent t-test for equal variance and tested the averaged time-series projected onto the standard brain between two burst characteristics. Changes were considered significant with a p-value below 0.05 after using the false discovery rate correction.

4.4 Results

On average, 26.89 ± 6.71 bursts per minute were detected in all 34 STN-LFP recordings. The temporal distribution of the burst duration can be seen in Figure 4.1. Overall, the mean burst duration was 595 ms with a standard deviation of 472 ms. For bursts longer than 200 ms (in the following: central bursts), the mean number of bursts per minute (i.e., rate) was 23.91 ± 5.03 for the right STN and 23.42 ± 5.06 for the left STN. In comparison, the rate for long bursts (> 500 ms) was 12.62 ± 1.79 for the right and 12.10 ± 2.36 for the left STN, whereas short bursts (< 300 ms) had a rate of 6.90 ± 4.31 for the right and 7.30 ± 3.94 for the left STN. For all three burst durations, there was no significant difference in the occurrence of beta bursts in the left and right STN (unpaired t-test; $|t| < 0.40$), so that a comparable number of bursts was used to determine ERFs with respect to the left and right STN.

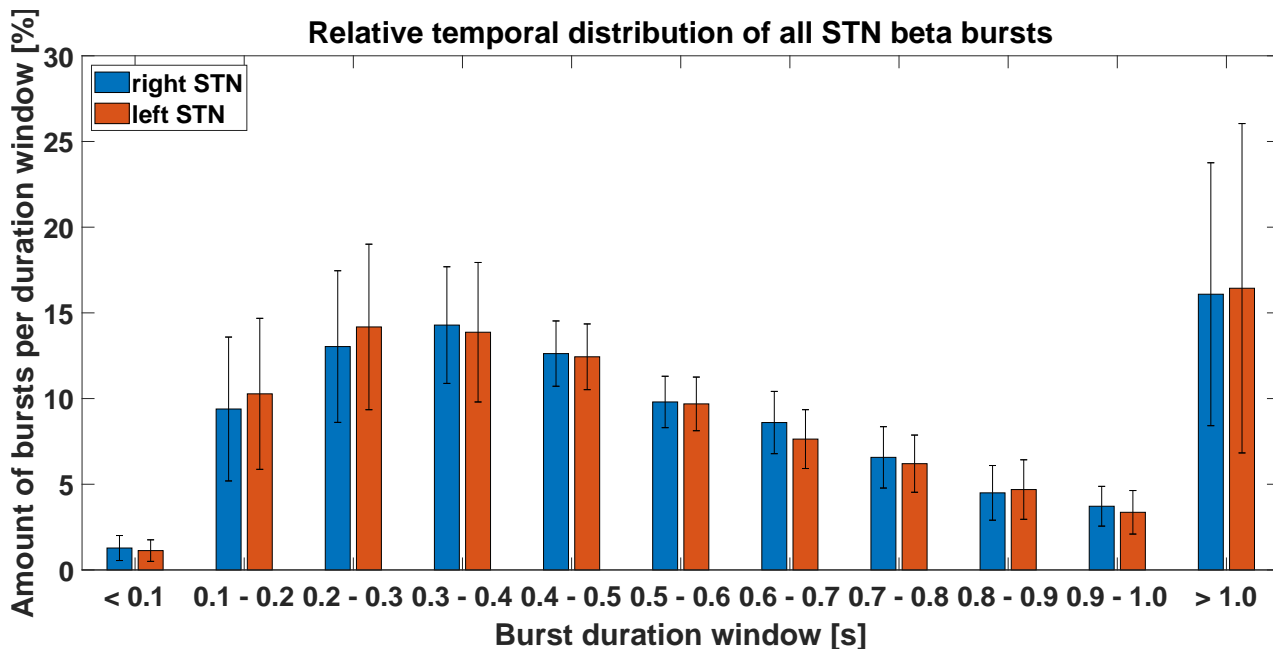


Figure 4.1: Relative temporal distribution of all detected beta bursts

Beta bursts with a minimum duration of 80 ms were detected in LFP recordings of 34 STN from PD patients OFF levodopa. The error bars indicate the standard deviation. No significant differences in beta bursts were detected between the right STN (blue) and left STN (red). At a duration of 300 ms, there is an accumulation of bursts.

4.4.1 Cortical activity linked to the onset of STN beta bursts and the maximum

Cortical activity time-locked to the maximum or the onset of STN beta bursts was significantly changed compared to the baseline activity before the onset of a beta burst. These ERFs occurred for three burst durations, two time points, and two hemispheres. In addition, we

examined the relationship between twelve different burst characteristics and cortical activity. There were differences between the spatial and temporal occurrence of ERFs with respect to the burst characteristics considered (i.e., onset and maximum of central, short, and long bursts, as well as bursts from the left and right STN). However, because the spatial occurrence of ERFs was more consistent than the temporal occurrence across burst characteristics, we sorted the following results according to their spatial occurrence. A direct comparison of the averaged cortical activity based on the different burst characteristics yielded no significant differences. In particular, there was also no significant difference in the cortical activity related to long and short beta bursts.

Cortical sources with significantly changed activity were mainly ipsilateral to the hemisphere of the STN beta burst. The active cortical areas can be broadly subdivided into areas functionally related to associative, limbic, and motor processing, but also speech and vision. We will present the results for each functional domain below.

4.4.2 Cortical ERFs in areas related to somatosensory/motor processing

A modulation of somatosensory and motor cortical activity by STN beta bursts was expected. First, cortical motor activity increased only after the maximum of the long bursts (see Fig. 4.2I; Appendix Fig. 11.5, 11.6E, 11.7, 11.8M). However, in the postcentral gyrus, activity increased during the maxima of the central bursts, first contralateral (-63 to -56 ms) and later ipsilateral (11 - 68 ms; see Appendix Fig. 11.3, 11.4NO). In contrast, during the onset of central bursts and the maxima of long bursts, the cortical activity in the postcentral gyri was attenuated (see Appendix Fig. 11.7, 11.8N, 11.15, 11.16F). Contralateral to the left STN, there was a decrease in activity in the motor areas of the superior frontal gyrus (Goldberg et al., 2006), especially during the maximum of the long and the central bursts but also during the onset of short bursts (see Fig. 4.3I; Appendix Fig. 11.1, 11.2G, 11.5, 11.6F, 11.19, 11.20N). Finally, cortical motor activity increased after the maximum of the long bursts (see Appendix Fig. 11.5, 11.6E, 11.7, 11.8M).

4.4.3 Cortical ERFs in areas related to associative processing

In the precuneus, an area related to associative processing (Cavanna and Trimble, 2006), we observed after the maximum of the short bursts, both attenuated (49 - 58 ms, see Appendix Fig. 11.9, 11.10N) and increased activity contralateral to the respective STN (63 - 68 ms, see Appendix Fig. 11.9, 11.10N). While, only an ERF with decreased activity was present after the onset of short bursts (see Fig. 4.3J; Appendix Fig. 11.19, 11.20M).

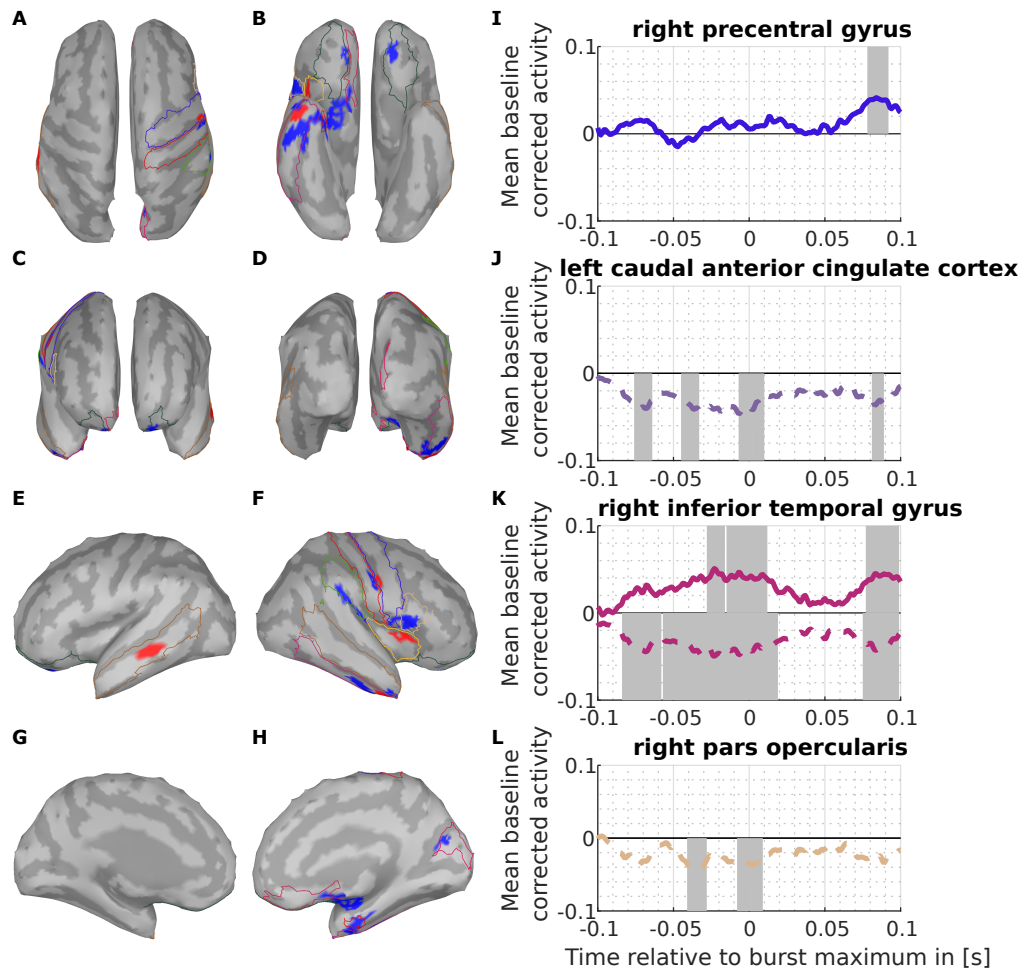


Figure 4.2: Cortical ERFs evoked by beta bursts maxima in the right STN with a minimum duration of 500 ms

The left part of the figure shows the spatial extent of the event-related fields evoked by beta bursts from the right STN on the standard ICBM152 brain (A-H), and the right part shows the corresponding temporal dynamics for four ERFs: (I) right precentral gyrus, (J) left caudal anterior cingulate cortex, (K) right inferior temporal gyrus, and (L) pars opercularis of the right inferior frontal gyrus. In the cortical figure on the left, all vertices are color-coded, which differed significantly with $|t| > 5.05$ from baseline for at least 5 ms and 10 vertices in the period from 100 ms before to 100 ms after the burst maximum. Vertices with a positive deviation from the baseline in the time period under consideration were marked red, and those with a negative deviation were marked blue. The time-series on the right, with the burst maximum at time 0 ms, show the baseline corrected cortical activity averaged on the beta peak for these exemplary clusters. These averaged time-series were then averaged across the vertices belonging to one cluster. Clusters were assigned to cortical regions using the Mindboogle atlas, with the primary location of the significant vertices being the determining factor. The cortical areas with significant t-values have a colored outline corresponding to the color of the associated time-series on the right. The plotted time-series were averaged across all subjects and averaged separately across the vertices with a positive deviation (solid line) from baseline and a negative deviation (dashed line). The time periods significantly deviating from baseline are highlighted in gray.

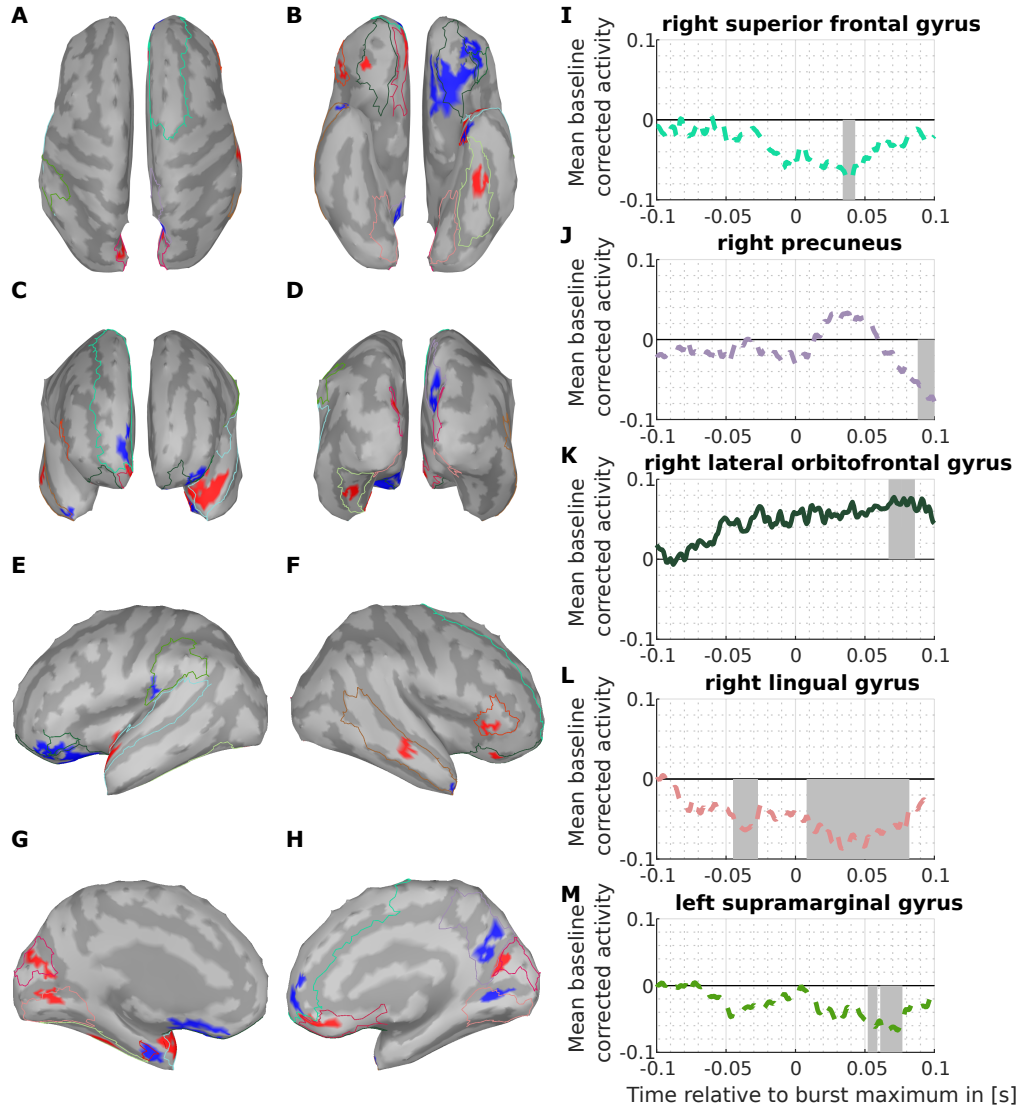


Figure 4.3: Cortical ERFs evoked by beta bursts onset in the left STN with a maximum duration of 300 ms

The left part of the figure shows the spatial extent of the event-related fields evoked by beta bursts from the left STN on the standard ICBM152 brain (A-H), and the right part shows the corresponding temporal dynamics for five ERFs: (I) right superior frontal gyrus, (J) right precuneus, (K) left lateral orbitofrontal gyrus, (L) right lingual gyrus, and (M) left supramarginal. The time-series on the right, with the burst onset at time 0 ms, represent the baseline corrected cortical activity averaged on the beta peak for these exemplary clusters. The time windows with a significant deviation from the baseline are highlighted in gray. For detailed description, please refer to Figure 4.2.

4.4.4 Cortical ERFs in areas related to limbic processing

Cortical ERFs are also temporally related to STN beta bursts in regions pertinent to limbic processing, including the orbitofrontal gyrus (Rolls et al., 2020), the insular cortex (Augustine, 1996), and the cingulate cortex (Hadland et al., 2003). Around the onset of short and cen-

tral bursts, activity increased contralaterally and decreased ipsilaterally in the orbitofrontal gyrus (see Fig. 4.3K; Appendix Fig. 11.15, 11.16DE, 11.19, 11.20EFI, 11.21, 11.22A). For the cingulate gyrus, we observed increased and decreased activity around the onset of the central bursts (see Appendix Fig. 11.13, 11.14ABG, 11.15, 11.16A), albeit divergent activity was also evident surrounding the burst maximum for all burst durations investigated (see Appendix Fig. 11.1, 11.2ADF, 11.3, 11.4E, 11.5, 11.6A, 11.7, 11.8AD, 11.9, 11.10ADO). Additionally, activity also increased in the ipsilateral insular cortex during the burst maximum of the right STN for all three burst durations (see Fig. 4.2K; Appendix Fig. 11.3, 11.4D, 11.7, 11.8E, 11.11, 11.12A). Moreover, in the bilateral orbitofrontal gyrus, activity decreased for all burst durations around the burst maximum from the right STN, while it increased with respect to the left STN (see Fig. 4.2J; Appendix Fig. 11.3, 11.4FGIJ, 11.7, 11.8FGH, 11.9, 11.10GJ, 11.11, 11.12BC).

4.4.5 Cortical ERFs in areas related to speech/vision processing

STN beta bursts of all durations led to altered activity in cortical areas associated with language and visual processing. This was especially pertinent around the burst maximum, rather than the onset of the burst. Related to visual processing, activation was observed in six areas. There was increased and decreased activity, (1) in the ipsilateral inferior temporal gyrus (see Fig. 4.2K; Appendix Fig. 11.3, 11.4C, 11.7, 11.8D, 11.15, 11.16B, 11.17, 11.18A), part of the ventral visual pathway (Conway, 2018), (2) in the bilateral cuneus (see Appendix Fig. 11.7, 11.8B, 11.9, 11.10B, 11.19, 11.20AB), involved in basic visual processing (Parker et al., 2014), and in (3) the bilateral lingual gyri, an area important for visual decoding (see Fig. 4.3L; Appendix Fig. 11.1, 11.2BC, 11.3, 11.4H, 11.9, 11.10HI, 11.13, 11.14C, 11.19, 11.20GH; Machielsen et al., 2000). Additionally, there was increased activity in (4) the ipsilateral lateral occipital cortex, containing retinotopic visual fields (see Appendix Fig. 11.9, 11.10E; Larsson and Heeger, 2006), in (5) the left fusiform gyrus (see Appendix Fig. 11.3, 11.4B, 11.9, 11.10C, 11.19, 11.20D), a key area of object recognition (Weiner and Zilles, 2016), and in (6) the ipsilateral peri-calcarine cortex (see Appendix Fig. 11.13, 11.14F), whose thickness plays a role in blindsight (Georgy et al., 2020).

Furthermore, there was an alteration in activity in various cortical areas linked to language processing. During STN beta bursts, activity increased and decreased at the bilateral superior temporal gyrus (see Appendix Fig. 11.1, 11.2H, 11.3, 11.4P, 11.5, 11.6G, 11.9, 11.10PQ, 11.19, 11.20O), which is part of a network important for language comprehension (Turken and Dronkers, 2011), the ipsilateral supramarginal cortex (see Fig. 4.3M; Appendix Fig. 11.3, 11.4Q, 11.7, 11.8N, 11.19, 11.20P), involved in phonological decisions (Hartwigsen et al., 2010), the

bilateral middle temporal gyrus (see Appendix Fig. 11.3, 11.4K, 11.5, 11.6B, 11.7, 11.8IJ, 11.9, 11.10K, 11.13, 11.14E, 11.19, 11.20J), involved in semantic cognition (Davey et al., 2016), and the pars orbitalis of the ipsilateral inferior frontal gyrus (see Appendix Fig. 11.3, 11.4M, 11.11, 11.12E, 11.19, 11.20K), also involved in language processing (De Carli et al., 2007). In addition, the activity decreased at the right pars opercularis of the inferior frontal gyrus (see Fig. 4.2L; Appendix Fig. 11.3, 11.4L, 11.7, 11.8K, 11.9, 11.10L, 11.11, 11.12D), an area pertinent for phonological processing (Roskies et al., 2001).

4.5 Discussion

We investigated cortical ERFs associated with STN beta bursts of PD patients. By translating the NET approach for combined fMRI-LFP data in non-human primates (Logothetis et al., 2012) to human MEG-LFP data, we were to our knowledge the first to demonstrate cortical network formation effects based on sub-cortical neural events in humans. This is consistent with the conjecture by Florin *et al.* (2015), where it was predicted that other neuronal events besides the hippocampal ripples described by Logothetis *et al.* (2012), play a role in network formation. In line with our hypotheses, STN beta bursts were associated with activity in motor, limbic, and associative cortical areas but also in areas of language and visual processing, highlighting the multifunctionality of beta bursts. In the following, we will consider the results separately with respect to these functional systems but also in the context of the BGC loop.

4.5.1 Neuronal event triggered cortical activity in humans

First, it should be emphasized that our results indicate that the method presented by Logothetis *et al.* (2012) based on LFP and fMRI measurements in non-human primates can be transferred to humans. Furthermore, in contrast to the original NET approach, by switching from fMRI to MEG, we were able to enhance the temporal resolution from seconds to milliseconds, effectively capturing the temporal evolution of neuronal events in both cortical and subcortical areas. Thus, especially in combination with modalities like MEG or EEG, dynamic network information can be investigated with the NET approach due to the millisecond temporal resolution.

4.5.2 STN beta bursts involved in STN-cortico network formation

In the context of PD, we identified motor cortex activity evoked by beta bursts in the STN, which corroborates previous publications describing beta coherence and coupling of beta bursts between STN and the ipsilateral motor cortex in the OFF state (Hirschmann et al., 2011; Tinkhauser et al., 2018b). This activity increased mainly ipsilaterally to the respective STN. Still, some activity also occurred later and, to a smaller extent, on the contralateral side. The bilateral cortical activity in relation to beta bursts could be due to interhemispheric connections that facilitate interhemispheric communication either directly between the STNs (Hohlefeld et al., 2014; Tinkhauser et al., 2018b) or at the cortical level (Roland et al., 2017). Furthermore, pathologically altered sensory processing in PD can be linked to the altered dopamine levels (Conte et al., 2013), which could explain our findings of activation linked to occurrence of STN beta bursts in somatosensory areas in addition to the motor area. With regard to the pathological occurrence of STN beta bursts in PD, our results suggest that STN beta bursts

are involved in the network formation between STN and cortical motor areas.

In addition, we identified ERFs time-locked to STN beta bursts in associative cortical areas, especially in areas involved in decision making. PD patients ON medication tend to make more impulsive and error-prone decisions (Herz et al., 2016; Mimura et al., 2006). Because we measured our patient’s OFF medication, we cannot distinguish whether the ERFs in associative cortical areas are of physiological or pathological origin. This will require further investigations, for instance by comparing ON and OFF dopaminergic medication states. Presence of ERFs in areas of the limbic system was hypothesized based on parts of the STN being associated with limbic processing. Indeed we detected ERFs in the insular and cingulate cortex, which are both associated with limbic tasks (Augustine, 1996; Hadland et al., 2003).

With regard to the pathology of PD, a functional link via the limbic part of the BGC loop through beta bursts could be explained by the following observations: (1) STN beta bursts are considered pathologically increased in PD (Sure et al., 2021; Tinkhauser et al., 2017a,b), and (2), PD-specific alterations in the development of depression involves the limbic system (Remy et al., 2005). However, further investigation of such a putative link between beta bursts and depression is required. Nevertheless, these results suggest a broader functional spectrum for STN beta bursts than commonly thought. While motor processes in PD are associated with beta band activity, associative and limbic processes are primarily associated with the alpha and theta bands (Brücke et al., 2007; Buot et al., 2021; Mazzoni et al., 2018; Rosa et al., 2013; Zavala et al., 2015; Zénon et al., 2016). Combined with our results, this could imply that while beta bursts play an important role at rest in general, additional recruitment of oscillatory activity in different frequency bands (e.g., gamma > 30 Hz) is required for specific tasks. However, if a task is already actively performed, the influence of beta bursts may be lower because, e.g., movement preparation leads to decreased beta activity (Tzagarakis et al., 2010). This suppression is modulated by age- and disease-related pathologies (e.g., healthy aging – stronger suppression, Parkinson’s disease – diminished suppression; Heinrichs-Graham et al., 2014; Heinrichs-Graham and Wilson, 2016; McCusker et al., 2021), leading to improvements and deteriorations in performance, respectively. At rest, in line with our initial hypothesis, cortical ERFs occurred time-locked to STN beta bursts in areas corresponding to each of the functional subareas of the STN. Thus, STN beta bursts seem relevant for network formation within those functional systems. As the beta bursts were detected in the dorsal (i.e., motor) area of the STN, cortical ERFs were expected to primarily occur within motor areas. Nevertheless, as there is evidence that the functional regions in the STN overlap (Haynes and Haber, 2013), detected beta bursts might also relay to non-motor regions of the STN, poten-

tially causing cortical ERFs in associative and limbic areas. This might not be due to either direct links or mediation via different subcortical and cortical areas. Still, the functional or pathophysiological role of these beta bursts in the non-motor loops of the STN is not clear and will require further investigation.

Furthermore, ERFs occurred within cortical areas related to visual and language processing, which are not part of the BGC loop model. Nevertheless, there is evidence for functional connections between the STN and language/visual areas. For example, in rats, the STN responds to visual stimuli (Coizet et al., 2009), while in PD patients, STN-DBS can affect speech (Hammer et al., 2010; Wertheimer et al., 2014). For example, PD has been shown to affect voice control and the related cortical areas (Huang et al., 2016). Even though DBS leads to subcortical language impairments, our results suggest that STN beta bursts are involved in the interaction between STN and cortical visual and language fields. Supporting this finding, cortical oscillatory activity in the low beta band plays a crucial role in the audiovisual speech perception network (Biau and Kotz, 2018). For the visual system, the authors are not aware of reported links to beta activity or a functionally equivalent field in the STN. However, this finding could indicate that STN beta bursts have far-reaching influences on the cortex beyond the three functional fields found in the STN. This would be analogous to the extensive modulation of cortical activity shown for hippocampal ripples by Logothetis *et al.* (2012).

4.5.3 STN beta bursts and their role in the BGC loop

The presence of both increases and decreases in cortical activity related to STN beta bursts suggests two different roles of beta bursts. First, beta bursts could arise primarily due to hyperdirect pathway projections from the cortex to the STN. Since this pathway is comprised of excitatory neurons (Tillage et al., 2020), increased cortical activity could induce beta bursts in the STN. This fits with the fact that time-series of synchronized spike discharges of local neuronal populations in the STN are phase-locked to the beta band activity in frontal cortex (Cagnan et al., 2019). It must be noted that in animal models, cortical input to the STN decreases in PD (Chu et al., 2017; Mathai et al., 2015), but activation of the STN via cortical activity still exists. Alternatively, reduced cortical activity associated with STN beta bursts could be due to cortical inhibition via the indirect pathway of the BGC loop. In this case, beta bursts in the STN would stimulate the indirect pathway, leading to inhibition of the cortex, for example, as shown for the caudal part of the anterior cingulate gyrus via the globus pallidus pars interna/substantia nigra and the thalamus (Calabresi et al., 2014). The BGC loop also includes a direct pathway, which, in contrast to the indirect pathway, leads to activation of the cortex. However, in PD patients, the direct pathway is pathologically sup-

pressed, while the indirect pathway is enhanced (Calabresi et al., 2014; McGregor and Nelson, 2019). Thus, because we studied PD patients OFF medication, the indirect pathway is likely over-active compared to the direct pathway, making the hypothesized role of STN beta bursts as stimulators of the indirect pathway and the subsequent reduced cortical activity more likely.

However, we detected both decreased and increased cortical activation around the maximum of the STN beta burst. In general, we could not determine whether these directionalities preceded the other one in time. Therefore, these processes could also occur simultaneously, making the beta burst-stimulated STN-cortex communication not a closed circuit, hence STN beta bursts are also subject to other influences. Even if we extended our analysis to the burst onset, we could not determine on the basis of our data whether the activity change happens first at the cortex or only after the beta bursts in the STN. However, the occurrence of decreases and increases in cortical activity associated with STN beta bursts suggests that both can occur as described above.

Furthermore, the time courses of the ERFs were heterogeneous. This heterogeneity could be due to the high variability of STN burst durations and/or to the inherently imprecisely defined trigger time point within the STN burst. Consequently, the analysis performed here demonstrates network formation via STN beta bursts, but inference on the temporal evolution of the ERFs is less precise.

4.5.4 Laterality of the BGC loop impairment

Visually, we detected more widespread cortical ERFs on the right hemisphere (9.17 ± 9.17 [mean over the burst characteristics \pm std]) than on the left hemisphere (4.08 ± 3.68). However, we could not detect any laterality of PD impairment in our patient population that would explain this. Furthermore, there were no differences in the rate of STN beta bursts between the hemispheres. In addition, it has been reported that unilateral stimulation of the STN contralateral to the clinically more affected side may be sufficient to alleviate symptoms (Castrioto et al., 2011; Rizzone et al., 2017). This could indicate a hemisphere-specific impairment of the BGC loop. Therefore, the difference in the beta-related ERFs for the hemispheres could be related to the dominant STN for DBS. Moreover, there is also evidence for interhemispheric interaction between STNs (Darvas and Hebb, 2014; Walker et al., 2011), which may also affect the STN-cortical correlation seen in this study.

We consider it highly unlikely for the accumulation of ERFs on the right hemisphere to be due to cable artifacts. First, the Abbott extension cable is non-magnetic and suitable for use

in the MEG, and care was taken to avoid loops in the cable. Second, the ERFs also appeared in frontal and occipital brain regions, which are spatially separated from the cable location. Third, the cable was actually routed over the left hemisphere. Nevertheless, it could be possible that the cables create artifacts that mask the ERFs generated by STN beta bursts, which would explain why fewer ERFs were found within the left hemisphere.

4.5.5 Differences between burst characteristics

As there were no significant differences between the burst characteristics, we can only refer to the occurrence of ERFs at this point. Overall, more significant ERFs occurred around the burst maximum (20.00 ± 10.02 [mean over the burst characteristics \pm std]) than around the burst onset (6.50 ± 8.19). This could indicate that interaction between STN and cortex is more likely to occur at higher frequencies within the beta rhythm. This leads to the question of whether the bursts detected by the percentile-dependent method of Tinkhauser *et al.* (2017a; 2017b) are all functionally relevant or whether a minimum amplitude is required. Our results suggest that a minimum amplitude must be present, but we cannot clarify this conclusively. This, together with the fact that beta bursts are temporally extended with a high variance in duration and are not singular temporal events, complicates the analysis of whether the change in cortical activity or the STN beta burst occurs first. Re-analysis with a larger sample size could be helpful here, as it would allow us to limit the burst duration to a narrower time window and thus have more comparable time points for averaging the events.

When comparing ERFs based on different burst durations, ERFs at the motor cortex occurred only for long bursts, consistent with the correlation between long beta bursts and symptom severity (Sure *et al.*, 2021; Tinkhauser *et al.*, 2017b). Otherwise, the differences in the occurrence of ERFs between the burst characteristics were not striking, which suggests that burst duration is relevant only for certain functional domains, such as motor function, and that beta bursts are more generally involved in network formation regardless of their duration.

4.5.6 Conclusion

Our results on event-related cortical activity time-locked to STN beta bursts indicate that beta bursts play a role in network formation between STN and cortex. Consistent with our hypotheses, the identified connections align with the BGC loops connecting the STN with cortical areas. This allowed us to show that neuronal events could also be used in humans to identify dynamic networks. In our case, the evoked cortical fields were mainly located in brain regions related to the functional subareas of the STN: motor, limbic, and associative but

also vision and speech related areas. Due to the OFF medication state, this broad functional involvement of beta bursts on cortical activity highlights the importance of beta bursts. To see if this role is related to the pathology of PD, further tests ON medication would be necessary. As we found increased and decreased cortical activity linked to STN beta bursts they are likely involved in two pathways of the BGC loop: (1) STN beta bursts are a result of the hyperdirect pathway from the cortex to the STN and (2) a cause of the indirect pathway from the STN to the cortex. In conclusion, our results support cortical network formation by STN beta bursts.

5 Study 3: Alterations of resting-state networks of Parkinson's disease patients after subthalamic DBS surgery

This work was published under:

Sure, M., Mertiens, S., Vesper, J., Schnitzler, A., Florin, E., 2023. Alterations of resting-state networks of Parkinson's disease patients after subthalamic DBS surgery. *Neuroimage Clin.* 37, 103317. <https://doi.org/10.1016/j.nicl.2023.103317>

Impact factor (2023): 4.9

Personal Contribution: Concept & study design 50 %; Data acquisition 30 %; Data processing 60 %; Data analyses & figures 100 %; Discussion of results 75 %; Manuscript writing 70 %

5.1 Abstract

The implantation of deep brain stimulation (DBS) electrodes in Parkinson's disease (PD) patients can lead to a temporary improvement in motor symptoms, known as the stun effect. However, the network alterations induced by the stun effect are not well characterized. As therapeutic DBS is known to alter resting-state networks (RSN) and subsequent motor symptoms in patients with PD, we aimed to investigate whether the DBS-related stun effect also modulated RSNs.

Therefore, we analyzed RSNs of 27 PD patients (8 females, 59.0 ± 8.7 years) using magnetoencephalography and compared them to RSNs of 24 age-matched healthy controls (8 females, 62.8 ± 5.1 years). We recorded 30 minutes of resting-state activity two days before and one day after implantation of the electrodes with and without dopaminergic medication. RSNs were determined by use of phase-amplitude coupling between a low frequency phase and a high gamma amplitude and examined for differences between conditions (i.e., pre vs. post surgery).

We identified four RSNs across all conditions: sensory-motor, visual, fronto-occipital, and frontal. Each RSN was altered due to electrode implantation. Importantly, these changes were not restricted to spatially close areas to the electrode trajectory.

Interestingly, pre-operative RSNs corresponded better with healthy control RSNs regarding the spatial overlap, although the stun effect is associated with motor improvement.

Our findings reveal that the stun effect induced by implantation of electrodes exerts brain

wide changes in different functional RSNs.

5.2 Introduction

Parkinson’s disease (PD) is a neurodegenerative disorder that is characterized mainly by motor symptoms (Poewe et al., 2017). The neuropathological hallmark of PD is the degeneration of dopaminergic neurons in the substantia nigra pars compacta (Mullin and Schapira, 2015). As PD progresses motor fluctuations occur and symptoms cannot be well controlled by medical treatment. In these cases, deep brain stimulation (DBS) of the subthalamic nucleus (STN) is an option to alleviate motor symptoms (Deuschl et al., 2006). It is known, that the sole implantation of the electrodes into STN without stimulation already leads to a temporary alleviation of symptoms. This effect is called *stun effect* and is probably caused by inflammatory processes and edema (Chen et al., 2006; Mann et al., 2009). To date, only one prior fMRI study has revealed altered cortical and subcortical functional connectivity due to the *stun effect* (Luo et al., 2021). Thus, detailed investigation of changes in functional networks is missing.

Analyzing electrophysiological resting-state networks (RSN) should lead to a better understanding of the *stun effect*. Changes in functional networks represent a prime candidate measure, as altered RSNs have been associated with PD (de Schipper et al., 2018; Göttlich et al., 2013) and with dopaminergic medication RSNs of PD patients align better with the RSNs of healthy controls (Schneider et al., 2020). In addition, DBS modulates spatially and spectrally segregated STN - cortical RSNs in PD patients (Oswal et al., 2016). Furthermore, RSN alterations have been related to PD symptoms, cognitive impairment (Tessitore et al., 2012b), and freezing of gait (Tessitore et al., 2012a).

It has been shown that brain activity at rest is organized in different hierarchically structured functional networks (Cordes et al., 2002; Doucet et al., 2011) that are associated with a range of motor and cognitive tasks (Smith et al., 2009; Thomas Yeo et al., 2011). Thus, analysis of RSNs provides the opportunity to study brain network alterations without subjecting patients to complex motor or cognitive tasks.

The *stun effect* is of clinical relevance because its occurrence has been linked to the subsequent effectiveness of DBS (Maltête et al., 2008; Tykocki et al., 2013), although reports on this are inconsistent (Granziera et al., 2008). To better understand the link between *stun effect* and DBS effect, it is eminent to investigate which functional areas are affected by the *stun effect*. Therefore, the question arises whether the *stun effect* is related to the areas impaired by the electrode trajectory.

If the stun effect modulates functional networks, the electrode position-specific side effects of DBS could be described even better. In a further step, stimulation parameter-dependent side effects (Dayal et al., 2017; Hartmann et al., 2019) could be optimally linked to RSN changes induced by DBS electrode implantation. Thus, initial DBS settings could be optimized based on RSN changes induced by the stun effect.

To tackle these questions, we recorded the cortical activity of 27 PD patients via magnetoencephalography (MEG) both before (in the following: pre) and after (in the following: post) DBS surgery. On each measurement day, patients were recorded at rest OFF-stimulation once OFF- and once ON-medication for 30 minutes. We identified four networks present in each of the four conditions: sensory-motor, visual, frontal, and fronto-occipital. RSN connectivity measures for each network were compared between the pre- and post-measurement for both medication states.

The megPAC approach used here is one of many methods (e.g., amplitude correlation, spectral coherence, and autoregressive models; Colclough et al., 2016; Florin and Baillet, 2015) that can determine networks based on cortical time series determined via MEG. The phase-amplitude coupling (PAC; Özkurt and Schnitzler, 2011) used here is particularly suitable for determining RSNs in the context of PD patients, as the PAC correlates positively with PD motor symptoms and can also be reduced by therapeutic interventions (De Hemptinne et al., 2013, 2015; Tanaka et al., 2022). Furthermore, RSNs based on PAC have been shown to be comparable to fMRI-RSN (Pelzer et al., 2021).

As the stun effect has been related to the alleviation of motor symptoms in PD, we hypothesized that the sensory-motor RSN will be altered due to electrode implantation, and further, that these implantation-related changes in the sensory-motor RSN will be linked to changes in clinical scores of motor symptom severity. Due to the wide-spread effects of DBS, we also expect the stun effect to induce alterations within RSNs not traditionally linked to the electrode trajectory (i.e., outside sensory-motor brain areas).

5.3 Methods

5.3.1 Subjects and surgery

A total of 27 (8 female) PD patients (age: 59.0 ± 8.7 years [mean \pm std]) were included in this study (see Table 5.1). The patients were identical to the sample reported in Sure *et al.* (2021). Furthermore, a control group of 24 (8 female) healthy age-matched participants (HC; 62.8 ± 5.1 years) was recruited. Written informed consent was obtained from all patients and HC subjects prior to study participation. Patients had been selected for DBS treatment according to the guidelines of the German Society for Neurology (Deutsche Gesellschaft für Neurologie e.V., 2016). The study was approved by the local ethics committee (study no. 5608R) and conducted in accordance with the Declaration of Helsinki.

The measurements prior to DBS electrode implantation were usually acquired two days before surgery (2, 1-141 days [median, range]. Of note, surgery had to be rescheduled for 2 of the 27 patients, which may lead to confounding variability due to discrepant surgical timelines. To address this concern, these two patients were excluded from all subsequent analyses (time prior to DBS surgery for remaining cohort: 2, 1-3 [median, range]). Measurements after DBS electrode implantation were acquired one day after surgery (1, 1-4 days, [median, range]). The DBS electrodes were bilaterally implanted in the dorsal part of the subthalamic nucleus (STN) at the Department of Functional Neurosurgery and Stereotaxy in Düsseldorf. In one case, the Boston Scientific Vercise segmented lead (Boston Scientific Corporation, Marlborough, MA, USA) was implanted, and in all other cases the St. Jude Medical Directional lead 6172 (Abbott Laboratories, Lake Bluff, IL, USA). During the measurements, electrodes were externalized using the St. Jude Medical Directional extension 6373 (Abbott Laboratories, Lake Bluff, IL, USA) and connected to the EEG amplifier integrated in a 306 channel MEG system (Elekta Neuromag, Helsinki, Finland). No electrical stimulation was applied during any of the measurements.

5.3.2 Experimental setup and recordings

The MEG measurement took place in a magnetically shielded room. Patients were seated in the MEG and remained at rest with their eyes open. During the entire measurement, the patients were asked to look at a black fixation cross on a white poster. An eye tracker (iView X 2.2, SensoMotoric Instruments, Teltow, Germany) was used to ensure that the eyes were consistently kept open. On each of the two measurement days, there were three consecutive measurement blocks of 10 minutes OFF medication and three 10-minute blocks ON medication, resulting in a total measurement duration of 120 minutes per patient (60 minutes for

Subject	Age	Sex	UPDRS pre-OFF	UPDRS pre-ON	UPDRS post-OFF	UPDRS post-ON	Days before/after surgery	Electrode	Levodopa dose [mg] pre/post
1	68	male	-	41	48	38	2/1	Abbott Infinity	125/250
2	56	male	62	28	25	23	22/1	Abbott Infinity	150/150
3	64	male	43	37	31	25	2/1	Abbott Infinity	200/200
4	62	female	27	12	22	24	1/4	Abbott Infinity	200/200
5	69	male	44	37	33	32	3/4	Abbott Infinity	150/150
6	45	male	22	13	22	10	2/1	Abbott Infinity	200/200
7	55	male	33	21	21	18	2/1	Abbott Infinity	200/200
8	77	male	46	17	58	-	2/2	Abbott Infinity	200/200
9	54	male	40	14	-	9	2/1	Abbott Infinity	150/150
10	60	female	22	21	32	28	2/1	Abbott Infinity	200/150
11	46	male	21	9	15	11	141/1	Abbott Infinity	200/150
12	56	male	45	43	31	19	2/1	Boston Scientific	150/150
13	58	male	54	26	25	14	2/1	Abbott Infinity	150/150
14	67	male	28	16	21	12	2/1	Abbott Infinity	200/200
15	54	male	49	45	37	27	2/1	Abbott Infinity	150/200
16	41	male	35	7	34	16	2/2	Abbott Infinity	300/300
17	58	female	23	8	25	13	2/2	Abbott Infinity	100/50
18	65	female	32	17	20	12	2/1	Abbott Infinity	100/100
19	72	female	28	19	42	35	2/1	Abbott Infinity	150/150
20	44	female	59	16	42	14	3/3	Abbott Infinity	225/225
21	68	male	38	20	49	27	2/3	Abbott Infinity	Best med on/
22	53	male	30	14	17	8	3/1	Abbott Infinity	150/150
23	58	male	41	24	33	25	1/1	Abbott Infinity	150/
24	69	male	42	31	33	29	10/1	Abbott Infinity	250/200
25	62	female	33	18	26	17	2/1	Abbott Infinity	150/150
26	55	female	39	32	43	30	2/1	Abbott Infinity	150/150
27	58	male	36	17	14	11	2/1	Abbott Infinity	Best med on/150

Table 5.1: Patient details

each pre and post electrode implantation). To ensure that patients were in their medication OFF state, oral PD medication was discontinued overnight for at least 12 hours. For patients with an apomorphine pump, the pump was stopped at least 1 hour before the start of the measurement. After the OFF measurements, patients received a standardized dose of fast-acting soluble levodopa (1.5 times their morning levodopa dose). To ensure a stable medication ON state, we waited until a significant clinical improvement occurred, i.e., for at least 30 minutes after ingestion. The Unified Parkinson’s Disease Rating Scale (UPDRS III) motor score was assessed for each of the 30-minute measurement blocks and tested for differences between the recording conditions (i.e., pre-OFF, pre-ON, post-OFF, and post-ON) using a paired sample t-test.

The MEG data were recorded with a sampling frequency of 2400 Hz and a low-pass filter of 800 Hz. To identify artifacts caused by heartbeat or eye movements, an electrocardiogram and an electrooculogram were acquired. To determine the relative position of the MEG sensors to the brain, four head position indicator (HPI) coils were placed on the subject’s head and digitized via the Polhemus system (Polhemus Isotrack, Colchester, VT, USA). For subsequent co-registration with individual T1 weighted anatomical MRI scans (depending on scanner availability: 3 T Trio Tim, 3 T Prisma, 1.5 T Avanto, 1.5 T Avanto-fit, 1.5 T Sola; all with 1 mm³ voxel size), 100 points distributed over the skull surface were additionally digitized.

5.3.3 Signal processing

Preprocessing and further analysis of the MEG data was done using Matlab (version R 2016b; The MathWorks, Inc, Natick, MA, USA) and the Matlab based toolbox Brainstorm (<https://neuroimage.usc.edu/brainstorm/>; Tadel et al., 2011). Identification of artifacts was independently performed by two people. If no consensus was achieved for a time segment, this time segment was considered artefactual and discarded from further analysis. The signal-space projectors (SSP) supplied by the Neuromag system were applied by default. In addition, frequent artifacts following the same pattern like eye blinks or cardiac artifacts were removed via custom-made SSPs. Time periods with irregular artifacts like movement artifacts were removed from all channels. Due to excessive artifacts, the data of two patients had to be excluded for the pre-OFF and pre-ON conditions. In addition, the data of one further patient had to be excluded for all four conditions.

Subsequently, time series activity of the artifact-cleaned sensor data was projected to the source level. For this purpose, the cortical surfaces of the individual T1-MRI images were ex-

tracted for each patient using Freesurfer (<http://freesurfer.net>, v.5.3.0). The individual cortex sheet was down-sampled to ~ 15000 vertices within brainstorm. The MEG sensor data and the anatomical data of each patient were transformed into one coordinate system in Brainstorm using the Polhemus data as well as the anatomical landmarks (nasion, left and right pre-auricular point). The forward problem was solved via the overlapping spheres method implemented in Brainstorm (Huang et al., 1999). The lead-fields were computed based on one elementary current dipole for each vertex with an orientation perpendicular to the cortex. For the inverse solution, the linearly constrained minimum variance beamformer implemented in Brainstorm was employed (Van Veen et al., 1997). The necessary individual data covariance matrix was calculated for each measurement block and a separate noise covariance matrix for each measurement day. The separate noise covariance matrix was determined from a 5-minute empty room recording at the end of each measurement day after subject recordings.

5.3.4 Resting-state network estimation

To determine electrophysiological RSNs, we chose the data-driven megPAC approach of Florin and Baillet (2015) which is based on the concept of a synchronized gating between low- and high-frequency information and has been shown to be capable of matching fMRI-RSNs (Pelzer et al., 2021). First, PAC is calculated for each reconstructed cortical source. Then the frequency pair with the highest coupling between the low-frequency phase from 2 to 30 Hz and the high-frequency amplitude from 80 to 150 Hz, is determined. Next, the amplitude of the high-frequency signal is interpolated between the peaks and troughs of the low-frequency signal, resulting in a new time series referred to as megPAC. This time series is generated for each cortical source in the individual anatomy-based source space, sampled down to 10 Hz, and projected onto the standard ICBM152 brain with 15002 vertices using FreeSurfer’s spherical registration (Fonov et al., 2011). On the standard brain, the megPAC time series is spatially smoothed using a Gaussian kernel with a full width at half maximum of 7 mm as implemented in Brainstorm. Downsampling and spatial smoothing were performed to increase comparability with the data processing of more commonly used fMRI-RSNs (e.g., Brookes et al., 2011) and to align with the original methods of Florin and Baillet (2015). To extract the group-level RSNs, the megPAC time series of all available patients are concatenated and the correlation between all cortical time series are calculated, resulting in a 15002 by 15002 correlation matrix. This dimensionality of this matrix was reduced by using a subset of 1175 evenly distributed sources over the cortical surface template. Based on noise data with the same length as the original data and the same preprocessing steps, a projector was defined to remove noise from the correlation matrix. Finally, using a singular value decomposition, the RSNs were determined as principal modes of this noise cleaned correlation matrix. This

resulted in cortical maps with values between 0 and 1, which are further referred to as coupling strength. For further details on the computation please refer to Florin and Baillet (2015). We then selected the 10 principal components that explained the most variability in the data.

5.3.5 Assignment of RSNs of interest

We used the megPAC approach to calculate RSNs for each condition: pre-OFF, pre-ON, post-OFF, and post-ON. Within the set of ten RSNs computed for each condition, we identified four RSNs of interest consistently in all conditions: the sensory-motor, visual, frontal, and fronto-occipital network (FON). The key criterion for selecting these four RSNs was that they were present in all conditions. To support this selection of RSNs, we also successfully identified these four RSNs in an age-matched control group (Fig. 5.1), which highlights the physiological significance of these RSNs.

To compare the RSNs between the recording conditions we used a Jackknife approach with a leave one out technique (Stute, 1996). The RSNs were calculated for each condition separately. For a condition with N patients, we performed N Jackknife runs, omitted one patient at a time. This results in N sets containing ten RSNs each. To determine changes for a given RSN between conditions, the corresponding RSN had to be assigned in the Jackknife runs. The assignment of the four RSNs of interest from each Jackknife run was done separately for each recording condition. As templates for this assignment, we used the RSNs of each condition determined across all participants. For the four template RSNs of each condition, the best matching network was determined for each Jackknife run of the corresponding recording condition. For the purpose of assignment, the cortical map of both the template RSNs and the Jackknife RSNs were thresholded at 40 % of the maximum coupling strength for comparability with the methods of Florin and Baillet (2015). This results in a binary vertex mask.

To quantify the correlation between the binary vertex masks of each of the four template RSNs and the ten RSNs of a Jackknife run, we employ the Phi coefficient also known as Mean Square Contingency Coefficient (Yule, 1912). Based on the Phi coefficient, a one-to-one matching was made between the RSNs of a jackknife run and the four template RSNs. Assignment was made with a minimum phi coefficient of 0.6 (RSN: mean phi coefficient \pm std, minimum; Sensory-Motor: 0.95 ± 0.03 , 0.79; Visual: 0.96 ± 0.03 , 0.80; Frontal: 0.94 ± 0.07 , 0.62; FON: 0.96 ± 0.03 , 0.88).

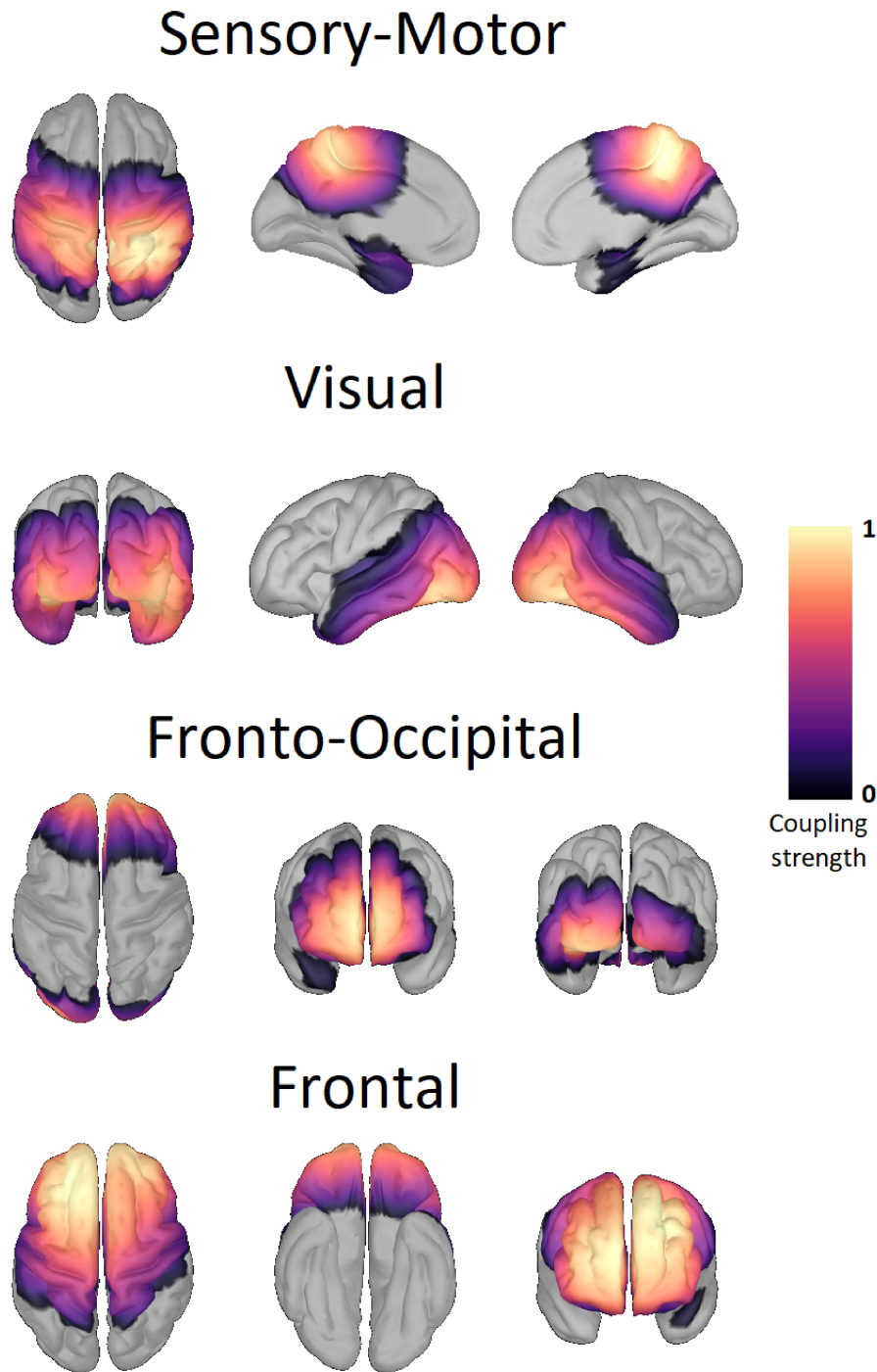


Figure 5.1: Template resting-state networks based on healthy controls

Shown here are the four template resting-state networks (RSN) of the healthy controls. The same RSN are also found in the four PD conditions. The rows display the sensory-motor, visual, fronto-occipital, and frontal RSN. The color scale marks the coupling strength from 0 to 1, with a warmer color indicating a higher coupling strength. No threshold was applied.

5.3.6 Statistical testing between RSNs of the pre- and post-condition

Based on this assignment, the RSNs of the Jackknife runs of the pre- and post-condition of the same RSN were statistically compared with a two-tailed unequal variance t-test, separately for both medication states.

To compare across conditions, we performed the following steps:

1. Separately for both conditions a pseudo value Δ_i was calculated for a RSN of the i -th Jackknife run Θ_i .

$$\Delta_i = N \cdot \Theta_0 - (N - 1) \cdot \Theta_i$$

Where Θ_0 is the baseline estimator without leaving one out.

2. The set of N pseudo values allows computing the mean value

$$\hat{\Delta} = \frac{1}{N} \cdot \sum_{i=1}^n \Delta_i$$

and its the standard deviation

$$\sigma = \frac{1}{N - 1} \cdot \sum_{i=1}^n (\Delta_i - \hat{\Delta})^2.$$

3. Step 2 allows evaluating significance of the difference across conditions 1 and 2 via a t-test:

$$t = \frac{\hat{\Delta}_1 - \hat{\Delta}_2}{\sqrt{\frac{\hat{\sigma}_1}{N_1} - \frac{\hat{\sigma}_2}{N_2}}}$$

4. The associated p-value follows from Student's t cumulative distribution function:

$$p = 2 \cdot (1 - tcdf(t, dof))$$

with degrees of freedom dof:

$$dof = \frac{(N_1 - 1) \cdot (N_2 - 1)}{(N_2 - 1) \cdot C^2 + (1 - C)^2 \cdot (N_1 - 1)}$$

where

$$C = \frac{\frac{\sigma_1^2}{N_1}}{\frac{\sigma_1^2}{N_1} + \frac{\sigma_2^2}{N_2}}$$

This comparison was calculated separately for each vertex within each RSN, i.e. only vertices belonging to a specific RSN were considered. Following (Florin and Baillet, 2015), we only

considered vertices with a coupling strength of at least 0.4 in at least one of the two RSNs to be compared. The p-values determined for these vertices were corrected for the number of vertices, the four RSNs, and the four conditions using the Bonferroni correction implemented in Brainstorm. Reported results are significant after correction at the 0.05 level.

5.3.7 Overlap of PD RSNs with healthy RSNs

To quantitatively assess whether electrode implantation brings the RSNs closer to the physiological state, we evaluated the spatial correspondence between the PD RSNs of the individual jackknife runs in the four conditions and the corresponding HC RSNs based on threshold-constrained coupling strength. The spatial overlap was estimated using the Phi coefficient, which was calculated for each Jackknife run in each condition and the corresponding HC RSNs. For this the coupling strength of the RSNs were again thresholded at 40 %. Using a two-tailed t-test and Bonferroni correction, we examined whether there were significant condition-wise differences in the Phi coefficients between pre- and post-surgery PD RSNs and HC RSNs.

5.3.8 Comparison of the low and high PAC frequencies

Next, we tested whether the driving frequencies in PAC differed between conditions, as alterations of the dopaminergic tone can lead to frequency shifts in beta oscillations (Iskhakova et al., 2021). For this purpose, we determined the low and the high frequency based on the highest PAC value from each vertex of each patient and PD condition. We then examined the low and high frequencies within the four RSNs. Here, separately for each condition, we selected all vertices that belonged to each of the RSN of interest which were determined across all subjects within the same condition. For each RSN of interest, the median of the low and high frequency was determined for each patient in each condition. Subsequently, a 3-factor ANOVA was calculated separately for the low and the high frequencies with the following factors: RSN, medication state, and electrode implantation. For this purpose, Matlab's implementation with associated post-hoc analysis including Bonferroni correction was used.

Finally, we also investigated the total spectral power between the pre- and post-recordings in five standard frequency bands (delta: 1-4 Hz, theta: 4-8 Hz, alpha: 8-12 Hz, beta: 12-35 Hz, gamma: 35-100 Hz). For this purpose, power spectra were calculated at source level for each reconstructed time series using Welch's method (Welch, 1967). A window length of 4 s with an overlap of 50 % was selected. These power spectra were projected onto a standard brain (ICBM 152). To ensure better comparability between runs, the 1/f characteristics of the power spectra were corrected by multiplying each power value with the corresponding frequency and normalized to the total power of 1-45 Hz and 55-95 Hz. To limit dimensionality,

the first principal component of all vertices belonging to a scout from the Mindboggle atlas (Klein et al., 2017) was only considered in the further analysis. Power differences between the conditions were determined with an independent t-test with subsequent Bonferroni correction for 62 scouts and 5 frequency bands.

Furthermore, the local maximum was obtained for each frequency band in the power spectra. We tested for a shift in peak frequency due to electrode implantation with an independent t-test with subsequent Bonferroni correction.

5.4 Results

5.4.1 Patient Characteristics

We assessed the UPDRS-III score in each recording condition. After Bonferroni correction, the UPDRS-III score was significantly higher in the pre-OFF condition (37.45 ± 11.11) compared to the pre-ON condition (22.30 ± 10.71 , $p = 1.72e-7$, $t = 7.74$, $df = 25$). Similarly, scores were higher in the post-OFF condition (30.96 ± 11.49) compared to the post-ON condition (20.61 ± 9.07 , $p = 3.45e-6$, $t = 6.57$, $df = 24$). Notably, there was a significant reduction in UPDRS-III score from the pre-OFF condition to the post-OFF condition ($p = 0.04$, $t = -2.81$, $df = 24$), which can be attributed to the stun effect. In contrast, there was no significant difference between pre-ON and post-ON.

5.4.2 Changes in RSNs

Across all patients and healthy controls, we identified four distinct RSNs of cortical activity (Fig. 5.1, 5.2, 5.3). The sensory-motor RSN extended from the precentral gyrus over the post-central and paracentral gyrus to the precuneus, superior parietal lobules, and supramarginal gyrus. Also, parts of the temporal lobe and cingulate gyrus were included in the sensory-motor RSN. The visual network was centered on the lateral occipital sulcus and traversed across the cuneus, precuneus, inferior and superior parietal lobule, the parahippocampal, lingual, and fusiform gyrus, as well as the pericalcarine cortex, and parts of the temporal lobe. The frontal network extended from the orbitofrontal gyrus across the inferior, medial, and superior frontal gyri to the paracentral, precentral, and postcentral gyri. Furthermore, it also includes parts of the cingulate gyrus. The fronto-occipital network (FON) spanned across the orbitofrontal cortex, rostral parts of the inferior, medial, and superior frontal gyrus, as well as the cingulate gyrus. The occipital area of the FON included lateral occipital sulcus, the lingual, fusiform, and pericalcarine gyrus. For each of these RSNs, we investigated the influence of the stun effect on the coupling strength of the RSNs and furthermore tested if the spatial overlap of the RSNs with HC RSNs differed between the PD conditions. We did not find any correlation between the changes in PD RSNs and changes in UPDRS-III scores.

5.4.3 Sensory-motor network

For the sensory-motor RSN, both in the OFF- and ON-medication condition the post-recording showed higher coupling strength in the pre and postcentral gyri mostly near the longitudinal fissure but also in the anterior parts of the temporal lobe (Fig. 5.4A,B). This alteration in the coupling strength was bilateral when patients were OFF medication and primarily left-lateralized during ON medication conditions. In contrast, the pre-recording showed a higher coupling strength in the right supplementary motor area, which extended to the pre and postcentral gyri when patients were ON medication.

Regarding the correspondence between PD and HC sensory-motor RSN, the spatial overlap was higher prior to surgery than after (Fig. 5.5; ON-Medication: pre $\Phi = 0.761 \pm 0.015$ [mean \pm std], post $\Phi = 0.433 \pm 0.018$; $p = 8.0e-26$; $t = 69.43$; $df = 23$; OFF: pre $\Phi = 0.699 \pm 0.016$, post $\Phi = 0.535 \pm 0.036$; $p = 3.55e-14$; $t = 21.17$; $df = 23$).

5.4.4 Visual network

For the visual RSN, there was increased coupling mainly in the bilateral cuneus and the left parietal lobule for the post-recording compared to the pre-recording (Fig. 5.4C,D) and decreased coupling at the right lateral occipital lobule and right temporal lobe during OFF-medication. During ON-medication, an increase in coupling strength for the post-recording was present at the bilateral cuneus and the right occipital and parietal lobule, whereas the coupling strength at the left occipital lobule and left temporal lobe was decreased.

Finally, the spatial overlap between the PD visual RSN and HC RSN was also higher for the pre- than the post-condition (Fig. 5.5; ON-Medication: pre $\Phi = 0.824 \pm 0.007$, post $\Phi = 0.585 \pm 0.039$; $p = 1.0e-17$; $t = 30.56$; $df = 23$; OFF: pre $\Phi = 0.916 \pm 0.015$, post $\Phi = 0.542 \pm 0.038$; $p = 1.2e-21$; $t = 45.64$; $df = 23$).

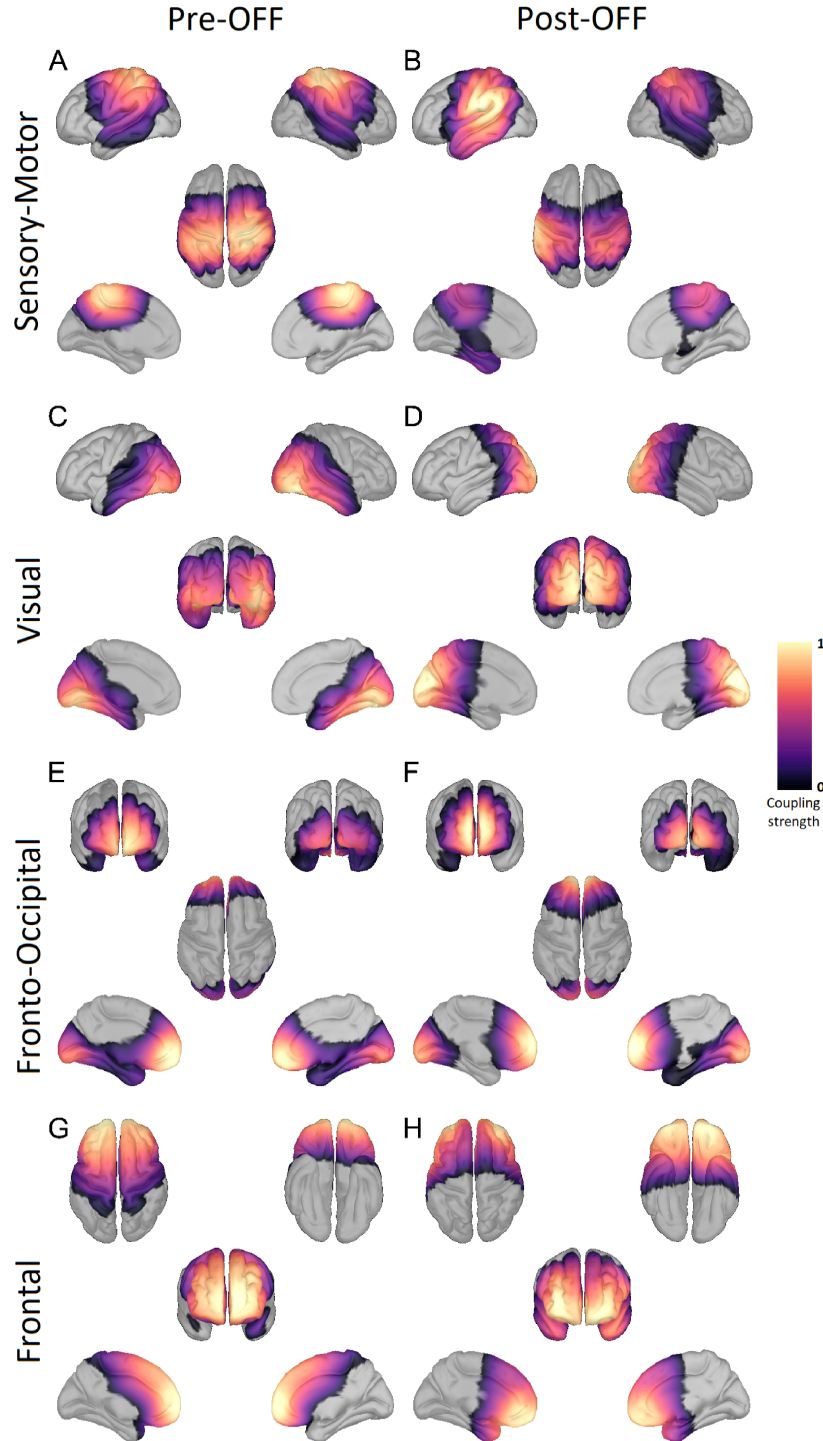


Figure 5.2: Resting-state networks based on Parkinson patients OFF medication

Shown here are the four resting-state networks (RSN) determined across all PD patients OFF medication before electrode implantation (left column) and after electrode implantation (right column). The rows display the sensory-motor, visual, fronto-occipital, and frontal RSN. The color scale marks the coupling strength from 0 to 1, with a warmer color indicating a higher coupling strength. These RSNs were also found ON medication and in the HC data. No threshold was applied.

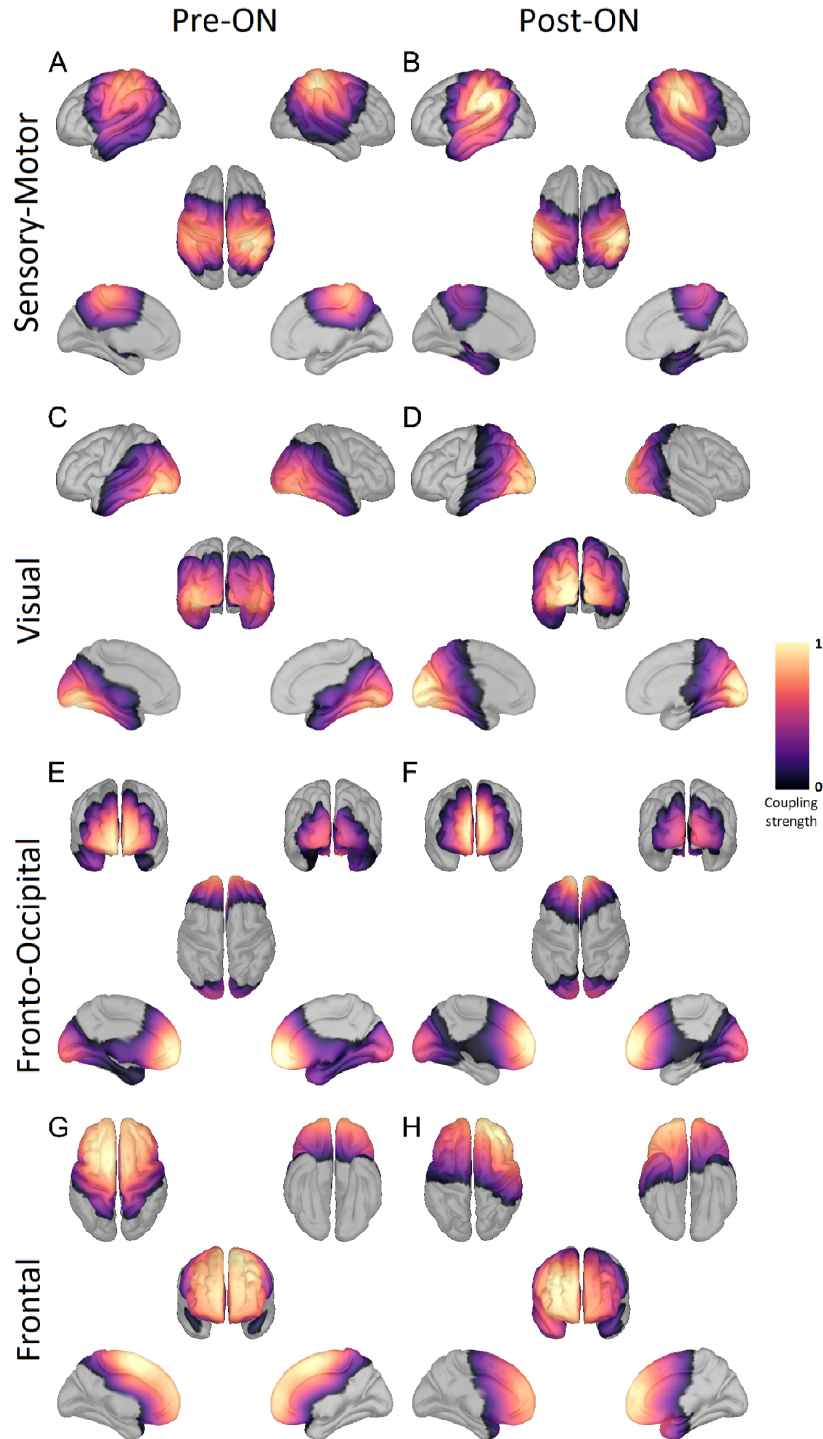


Figure 5.3: Resting-state networks based on Parkinson patients ON medication

Shown here are the four resting-state networks (RSN) determined across all PD patients ON medication before electrode implantation (left column) and after electrode implantation (right column). The rows display the sensory-motor, visual, fronto-occipital, and frontal RSN. The color scale marks the coupling strength from 0 to 1, with a warmer color indicating a higher coupling strength. These RSNs were also found OFN medication and in the HC data. No threshold was applied.

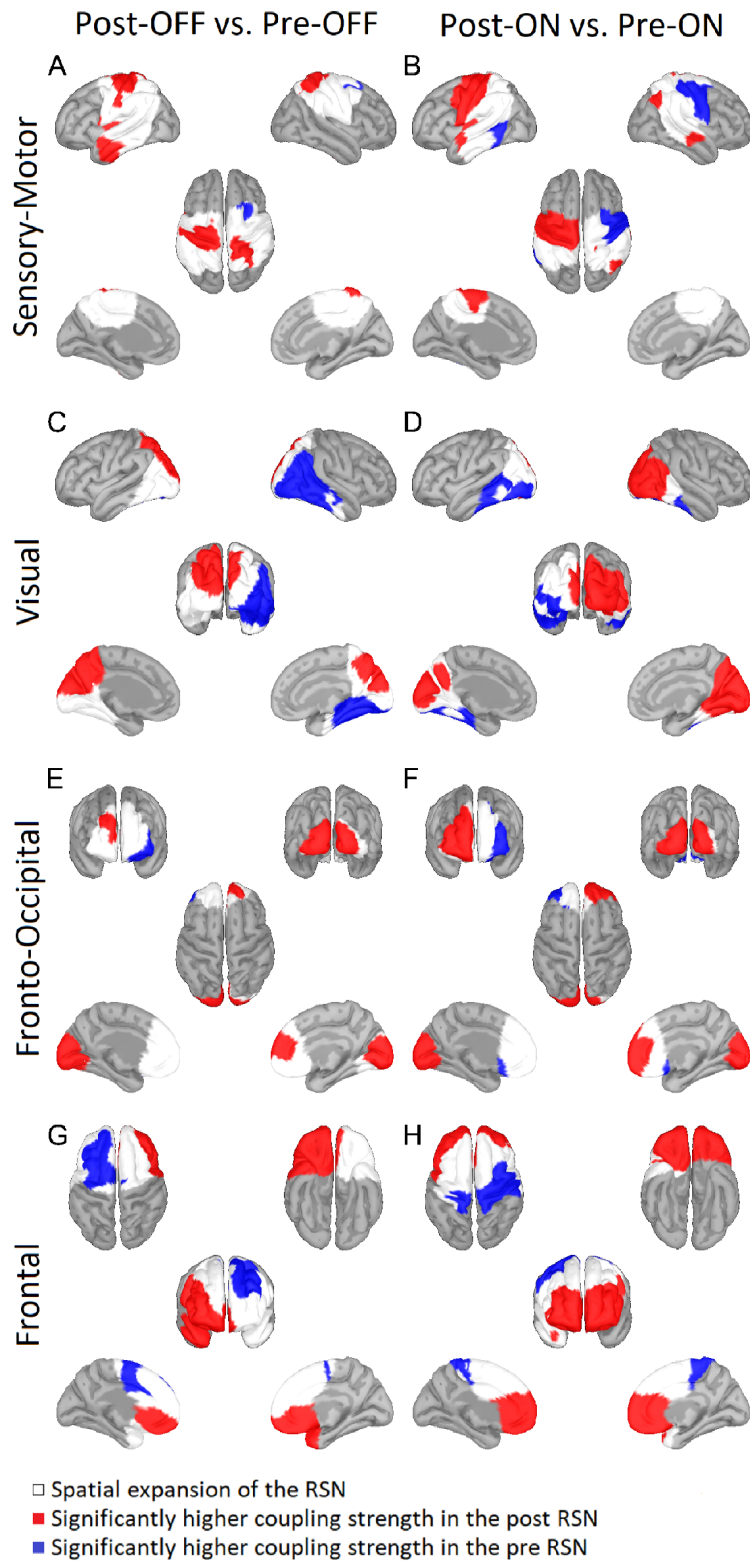


Figure 5.4: (see next page)

Figure 5.4 (*previous page*): Comparison of resting-state networks before and after electrode implantation

The comparison of resting-state networks (RSN) post-OFF vs. pre-OFF (left column) and post-ON vs. pre-ON (right column) revealed significant differences for the sensory-motor (first row), visual (second row), fronto-occipital (third row), and frontal (bottom row) RSN. Areas belonging to either RSN in post- and/or pre-recording are marked in white. Only areas of the RSNs where the coupling strength in one of the two conditions was at least 0.4 are displayed. Red indicates a significantly higher coupling strength in post-recordings, while blue denotes a significantly higher coupling strength in pre-recording. Significance is given at a p-value below 0.05 after Bonferroni correction for the number of vertices, networks, and conditions.

For the sensory-motor RSN, the comparisons post-OFF vs. pre-OFF (A) and post-ON vs. pre-ON (B) revealed significantly stronger coupling in post-recordings at the somatomotor area. Significant differences between the post-OFF vs. pre-OFF conditions (C) and the post-ON vs. pre-ON (D) conditions for the visual RSN were present at the visual cortex and the temporal lobe. For the fronto-occipital RSN, significant differences between the post-OFF vs. pre-OFF conditions (E) and post-ON vs. pre-ON conditions (F) were found, especially in the frontal region of the network at the frontal pole and in the occipital region at the occipital gyrus. For the frontal RSN, the comparison of the post-OFF vs. pre-OFF conditions (G) and the post-ON vs. pre-ON conditions (H) revealed significantly higher coupling strength at the frontal gyrus during post-recordings. A higher coupling strength in pre-recordings is present OFF medication at the left frontal gyrus and ON medication at the bilateral pre and postcentral gyrus.

5.4.5 Fronto-occipital network

In both the frontal and the occipital parts of the FON, there were differences between pre- and post-recordings (Fig. 5.4E,F). Specifically, coupling strength was increased in the recording post surgery- compared to the pre-surgery in the right frontal gyrus and bilateral lateral occipital lobule for both medication states. In addition, increases in coupling strength in the right orbitofrontal gyrus were observed during the ON medication state. For the pre-recording, increased coupling strength was present regardless of medication status in the left frontal and orbitofrontal gyrus.

For the FON, we only found a significantly higher overlap with the HC RSN for the pre-condition compared to the post-condition ON Medication (Fig. 5.5; ON-medication: pre $\Phi = 0.806 \pm 0.014$, post $\Phi = 0.632 \pm 0.011$; $p = 1.37e-21$; $t = 45.31$; $df = 23$; OFF: pre $\Phi = 0.705 \pm 0.031$, post $\Phi = 0.708 \pm 0.009$; $t = 0.41$; $df = 23$).

5.4.6 Frontal network

For the frontal RSN, we found significant differences between the post- and the pre-recordings in both medication states (Fig. 5.4G,H). During the OFF medication state, a significantly higher coupling strength for the pre-recording session was present in the left superior frontal gyrus. In contrast, coupling strengths were higher in an area encompassing the bilateral

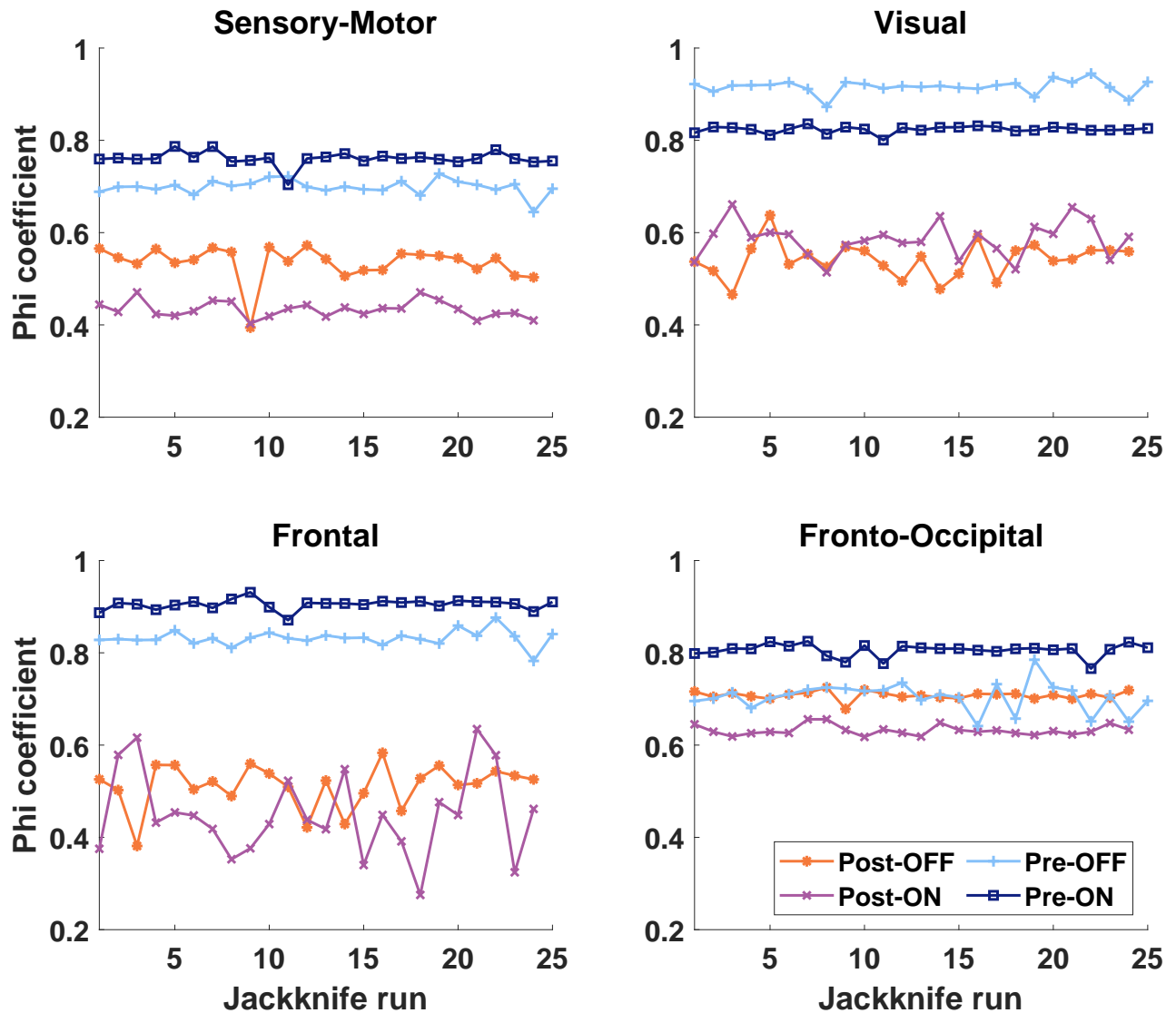


Figure 5.5: Spatial correspondence between HC-RSN and PD-RSN

The spatial correspondence calculated with the phi-coefficient based on the thresholded and then binarized coupling strength between the resting-state networks (RSN) of PD conditions (post-OFF, line indicator: asterisk; post-ON, x; pre-OFF, +; pre-ON, square) and the healthy controls is plotted for each jackknife run (x-axis). In case of the pre-surgery results there were 25 jackknife runs and in case of the post-surgery results there were 26 runs.

anterior cingulate gyrus, left frontal and orbitofrontal gyri up to the right temporal pole during post-recording sessions. In regard to the ON medication state, we identified a higher coupling strength for the post- compared to the pre-recording bilaterally in the orbitofrontal and frontal gyrus. In contrast, coupling strength increased in the pre-recording within the pre and postcentral gyri.

Finally, the PD frontal RSN had a higher spatial overlap with the HC RSN before electrode implantation both OFF and ON medication (Fig. 5.5; ON-medication: pre $\Phi = 0.905 \pm$

0.011, post Phi = 0.449 ± 0.092 , $p = 3.23e-15$; $t = 23.61$; $df = 23$; OFF: pre Phi = 0.832 ± 0.017 , post Phi = 0.511 ± 0.048 ; $p = 4.2e-18$; $t = 31.78$; $df = 23$).

5.4.7 Comparison of low and high PAC frequencies

Using a 3-factor ANOVA (factors: RSN, medication state, and electrode implantation), we examined whether the low- and high-frequencies of the maximal PAC values changed. We found significant main effects for both low- and high-frequencies. For the low-frequencies, we identified a significant main effect for the factor RSN ($F(3,392) = 7.50$; $p = 6.8e-5$; $\eta^2p = 0.054$), as well as for the factor electrode implantation ($F(1,392) = 4.58$; $p = 0.033$; $\eta^2p = 0.012$). No significant main effect was present for the factor medication state. Post-hoc tests revealed that the low-frequency in the pre-ON recording was higher for the sensory-motor RSN compared to the visual and the FON RSN ($p < 0.05$). For the high-frequencies, a significant main effect for the factor RSN ($F(3,392) = 11.58$; $p = 2.7e-7$; $\eta^2p = 0.081$) was present in the pre-ON condition, with significant post-hoc tests indicating higher frequencies for the sensory-motor RSN compared to the other three RSNs ($p < 0.05$).

When analyzing the spectral power before and after electrode implantation, it differed significantly for some cortical regions within the five frequency bands considered. Delta and theta band power was higher after electrode implantation (Appendix Fig. 11.23; $|t| > 4.07$, $df = 145$) in the OFF medication condition. For the ON medication condition delta band power was higher after electrode implantation and in alpha band before implantation (Appendix Fig. 11.24; $|t| > 4.09$, $df = 146$). In addition, power increased in the beta band in the pericalcarine cortex after electrode implantation, and power decreased in the caudal middle frontal gyrus. Cortical areas with significant power changes were spatially located partly within and outside the considered RSN regions (Appendix Fig. 11.25). Regarding the peak frequencies, for the gamma band the peak frequency shifted to a lower peak frequency for only two cortical regions (right pericalcarine cortex and right isthmus of the cingulate gyrus) after electrode implantation OFF medication and ON medication the peak frequency was downshifted for the beta band only in the left posterior cingulate gyrus (OFF: Appendix Fig. 11.26; $|t| > 4.09$, $df = 145$ and ON: Appendix Fig. 11.27; $|t| = 4.17$, $df = 146$). Again, without a clear spatial relation to the RSNs.

5.5 Discussion

In the present paper, we demonstrate that cortical RSNs from PD patients are altered by the mere insertion of a DBS electrode into the STN before any electrical stimulation is applied. At the same time, RSNs in the pre-operative state more closely resembled the ones of healthy controls.

5.5.1 DBS surgery alters RSNs due to the stun effect

Interestingly, we only found a significant reduction in motor symptoms assessed by the UPDRS-III after DBS surgery in the OFF-medication state but not in the ON-medication state, which could be due to medication already significantly reducing the UPDRS-III, rendering further improvement minor and more difficult to detect. Therefore, the changes in RSNs OFF-medication between pre- and post-recordings could reflect the PD severity measured by the UPDRS-III score (Skorvanek et al., 2017). Nevertheless, we detected alterations in the RSNs between pre- and post-recordings also ON-medication, suggesting that the stun effect affects brain communication subthreshold too, or is not necessarily related to clinical improvement. This finding is in line with the results of Mueller *et al.* (2018; 2020), who found different brain connectivity patterns between PD patients treated with DBS or dopaminergic medication. The association with clinical outcomes may also be very specific. For example, using simultaneous MEG-DBS recordings in PD patients, Boon *et al.* observed that rigidity and bradykinetic symptoms correlated with the whole-brain functional connectivity patterns, including connections between cortical and subcortical sensorimotor regions, albeit these patterns did not relate to tremor symptoms (Boon et al., 2020). However, as we could detect significant changes in all four RSNs of interest, this suggests a wide-spread influence of the stun effect and supports the report of the stun effect not being limited to motor function (Rozanski et al., 2012). Furthermore, the alteration of RSNs in disparate functional domains could be a predictor of side effects induced by STN-DBS (Tamma et al., 2002).

5.5.2 Alterations in different functional RSNs

Within the sensory-motor RSN the coupling strength increased after electrode implantation, especially in the somatomotor area. This finding is compatible with increased excitability of the supplementary motor area (Casarotto et al., 2019) and increased motor cortex activity after dopamine administration (Burciu and Vaillancourt, 2018). Similarly, motor effects induced by DBS correlated positively with functional connectivity, especially in the sensorimotor cortices (Boon et al., 2020). This increased coupling is mirrored by clinical improvement after DBS surgery as measured with the UPDRS-III and potentially due to the stun effect. As

the stun effect is associated with an improvement of motor symptoms in PD patients, it was expected that the stun effect would also be reflected in changes of the sensory-motor RSN. As the UPDRS-III from pre- to post-recordings was significantly reduced OFF- but not ON-medication, we surprisingly found similar alterations OFF- and ON-medication between post- and pre-RSNs. This could indicate that medication had a stronger effect than the stun effect on the UPDRS-III, i.e., masking in the clinical assessment of the stun effect, while the more subtle brain wide network effects were still discernible even with medication.

Assuming that the stun effect and DBS are improving PD symptoms, focusing on the visual RSN, the increased coupling within V1 could be associated with the reported shortening of saccade latency under DBS (Temel et al., 2008) and that a shorter saccade latency also leads to a faster response of V1 neurons (Kim and Lee, 2017). Interestingly, however, the sole electrode insertion can increase saccade latency (Antoniades et al., 2012), which fits the reduced coupling strength we found in the visual RSN. These opposing results indicate that the stun effect can lead to the obvious alterations known in DBS, such as the improvements in UPDRS-III, but can also lead to other less obvious alterations, which may be early indications of possible side effects of DBS. Nevertheless, it is striking that the better overlap of the visual RSN for the pre- than post-recording with the HC network was only evident ON- and not OFF-medication because dopaminergic medication in PD patients did not affect cognitive vision tasks (line-, object-, facial-discrimination, visual working memory, and object rotation; Anderson and Stegemöller, 2020). It is possible that this is a task-specific finding that is not transferable to resting activity.

In the frontal and occipital parts of the FON, we also observed alterations after electrode implantation. As this network is based on direct anatomical connections via the fronto-occipital fasciculus (Forkel et al., 2014), it is likely that this fiber tract is functionally affected by the stun effect (Pantazatos et al., 2012). Such a disturbance of the fronto-occipital fasciculus could be due to the spatial proximity to the trajectory of the DBS electrode. However, the cortical areas of the network are clearly separated from the trajectory, as is the visual RSN. Yet they are altered by the stun effect. Only the sensory-motor and frontal RSN encompassed anatomical areas near the trajectory of the DBS electrode. This underscores that the influence of the stun effect on cortical RSNs is not limited to the vicinity of the DBS electrode. In addition, it is well understood that the cortex is connected to the STN, i.e., the target of the DBS electrode, via the basal ganglia-cortical (BGC) loop (Deffains and Bergman, 2019; McGregor and Nelson, 2019). Already the implantation of the electrode in the STN leads to a change in metabolism in parts of the BGC loop (Pourfar et al., 2009), which may influ-

ence cortico-subthalamic communication. Together, with the notion that the BGC loop can be functionally subdivided (McGregor and Nelson, 2019), these data might provide potential explanations for the various network changes associated with electrode implantation.

The frontal RSN in our study corresponds to the default mode network detected in previous electrophysiology studies (Brookes et al., 2011; Mantini et al., 2007) and has been associated with self-referential mental activities (D’Argembeau et al., 2005). Thus, the alterations of the frontal RSN due to the implantation of the electrodes align well with the stun effect influencing cognitive functions (Le Goff et al., 2015). In addition, the higher coupling for the pre-recordings could indicate a possible disruption of cognitive networks due to electrode implantation.

5.5.3 Higher correspondence of pre-surgery RSNs with healthy RSNs

Surprisingly, even though the UPDRS-III score was lower during the post-recording compared to the pre-recording, the pre-RSNs had a higher spatial correspondence based on a threshold-constrained coupling strength with the HC-RSNs compared to the post-RSNs. However, in a previous study, RSNs ON-medication – a state with a low UPDRS-III score – had a better correspondence with the RSNs of healthy controls than RSNs OFF-medication, which corresponds to a higher UPDRS-III score (Schneider et al., 2020). Consistent with this finding, the overlap between the PD pre-recording and HC-recording was higher ON-medication than OFF-medication for the sensory-motor, frontal, and FON RSN ($p < 1.0e-8$). Based on the improved UPDRS-III score we expected even higher overlaps of the RSNs in the post-recording compared to the HC-RSNs than those observed in the pre-recording. This opposing trajectory suggests that the stun effect triggered by inflammatory processes and edema (Chen et al., 2006; Mann et al., 2009), not only modulates the RSNs as shown here, but also masks the potential link between RSNs and UPDRS-III motor symptom severity.

This conjecture is supported by the UPDRS-III score being unrelated to any of the investigated factors. Most surprisingly there was no link between the UPDRS-III and sensory-motor RSNs, albeit motor symptoms improved after electrode implantation. Future studies should determine whether RSNs alterations remain after the stun effect has subsided, or whether alterations of the RSNs under the stun effect have predictive power for the effect of DBS, which may ultimately prove useful for determining an initial stimulation settings for DBS.

5.5.4 Low frequency components are altered by electrode implantation

The low and high frequencies corresponding to the maximal PAC value at each vertex differed between networks. In particular, if the mean low frequency of the maximal PAC value of a RSN was higher in network A than in network B, this was concomitant with the high frequency of the maximal PAC value. This allowed the RSNs to be discriminated based on the low as well as the high frequencies of the maximal PAC values. However, electrode implantation only changed the low frequencies of the maximal PAC value, but not the high frequencies. Nevertheless, because comparable RSNs were found before and after electrode implantation, this suggests that the networks are robust to moderate shifts in frequencies. Furthermore, even though the shifts in the low-frequency band did not result in the RSNs vanishing, spatial changes in coupling strength were evident simultaneously. Since the high frequencies were not changed, this could imply a more important role of the low frequencies in network formation. Similar results were found for a motor task (Jech et al., 2012) and in a resting-state fMRI study that found amplitude changes of low-frequency fluctuations in many brain regions (Luo et al., 2021).

No significant main effect was found for the factor electrode implantation at the higher frequencies, nor was there a significant difference in the power of high frequencies before and after electrode implantation. However, low and high frequencies were modulated when DBS was turned on (Cao et al., 2017). This could indicate that the stun effect is weaker than the DBS effect, or alternatively, that the stun effect attenuates with increasing frequency, which is consistent with the more wide-spread propagation of low frequencies. This aligns well with our findings that electrode implantation cortically modulates mainly the low frequencies of the maximal PAC value.

Especially in the delta band power increased after electrode implantation and ON medication, only three cortical regions showed a decrease in beta band power. Overall, this suggests a frequency-specific modulation of power by electrode implantation. In addition, this could influence the observed differences in RSNs, although we assume a minor role for two reasons. First, power changes were not spatially specific with respect to the RSNs. If the power changes were to shift the low-frequency component of the PAC signal significantly, this would have been expected to occur in the spatial region of the RSNs. Second, the power changes in the delta/theta band occurred mainly OFF medication, although changes due to electrode implantation were detected in RSNs in both medication conditions. Furthermore, the shifts of the peak frequencies occurred so sparsely that a substantial influence on the power or the frequency components of the PAC signal is not to be expected.

5.5.5 Limitations

A caveat of our study is that it is impossible to eliminate all potential confounders. Since the second measurement usually takes place the day after surgery, patients may still be fatigued, generally weakened, or also affected by anesthesia. This is relevant because recovery of cognitive abilities after anesthesia takes time (Mashour et al., 2021), and fatigue can have an influence on cortical networks (Zhang et al., 2020). To prevent fatigue, patients could take breaks between measurement blocks. Since increased alpha power has been associated with increased fatigue (Craig et al., 2012), we calculated the alpha power in both lateral occipital sulci, the inferior, and superior parietal lobule based on the Mindboggle atlas. We did not find a significant change in alpha power between the first and last run for any of the four conditions or selected brain areas ($|t| < 2.22$, df: post recordings = 25; pre recordings = 23) and between conditions ($|t| < 3.18$, df: post OFF vs ON = 150; pre OFF vs ON = 142; OFF post vs pre = 146; ON post vs pre = 146).

The long measurement duration combined with increasing fatigue also poses the risk of the head moving away from the sensors over time. However, before the start of each measurement block, the position of the head was adjusted if necessary. Then the position of the HPI coils was determined at the beginning of each measurement run, which did not allow a continuous position verification. However, the relative position of the HPI coils to the MEG sensors along the z-axis did not significantly differ between the individual measurement runs of a measurement condition ($|t| < 2.51$, df: post recordings = 25; pre recordings = 23) and between conditions ($|t| < 2.30$, df: post OFF vs ON = 150; pre OFF vs ON = 142; OFF post vs pre = 146; ON post vs pre = 146). Thus, it can be assumed that the individual measurement blocks for each condition provided comparable data quality.

Besides the aforementioned limitations of conducting MEG measurements closely following electrode implantation (e.g., < 3 days), earlier measurements do offer a clear advantage. Since the impact of the stun effect decreases over days to weeks following DBS implantation (Maltête et al., 2008; Singh et al., 2012), the impact of the stun effect on the present data is presumed to be the most severe. At a later time point, the stun effect might not be detectable, not even in the UPDRS-III score. As a result, longitudinal measurements designed to track the stun effect decay and its subsequent impact on RSNs would be necessary to better describe the consequences of the stun effect.

5.6 Conclusion

The stun effect of DBS electrode implantation induces changes within different functional RSNs of PD patients that are not spatially limited to the vicinity of the DBS electrode trajectory. These effects are partially modulated by the state of dopaminergic medication. In line with our main hypothesis, the stun effect did not only influence the sensory-motor network, but also other functional networks. However, contrary to our hypothesis, stun effect-induced changes in RSNs exhibited no clear-cut relationship to induced clinical improvements in the UPDRS-III. Although stun effect-induced RSN changes partially matched RSN changes due to dopamine or DBS reported in other studies, the missing link to the UPDRS-III indicates that the stun effect is not restricted to clinically assessed PD symptoms. Our hypothesis for this missing link is that inflammatory processes caused by electrode implantation alter brain activity extensively but not strongly enough to induce changes in specific functional networks and general clinical scores, i.e., the UPDRS. Further insights might be obtained when investigating these RSNs after the stun effect has subsided and under the influence of DBS. Such an analysis could reveal the connection between stun effect and DBS effects, in addition to whether the RSNs measured directly after DBS surgery can be used to choose a first DBS setting and estimate side effects.

6 General discussion

This work has investigated neural network formation from two viewpoints:

1. are subcortical neural events involved in subcortical-cortical network formation in humans?
2. are long-range neural networks modulated by the implantation of a DBS electrode?

As PD patients have DBS electrodes implanted as a form of therapy and have prominent subcortical neural events with STN beta bursts, we investigated both questions in a corresponding cohort of patients.

Due to results presented in papers on STN beta activity in PD for different beta subbands (Kühn et al., 2006; Neumann et al., 2016; Priori et al., 2004), we investigated in study 1 whether there should be a frequency restriction for STN beta burst detection. Furthermore, using electrodes with directional contacts made it possible to examine whether there should also be a spatial restriction. While a frequency restriction for detecting beta bursts seems preferable, we did not find a preferred anatomical direction. Due to high beta-band synchrony in the STN and at the cortex (Cagnan et al., 2019; Tinkhauser et al., 2018b), we assumed and could demonstrate in study 2 that the network formation by subcortical events shown in primates (Logothetis et al., 2012) is also evident in humans, using STN beta bursts. Finally, study 3 indicated, in addition to an alteration in PD symptomatology (Chen et al., 2006; Mann et al., 2009), an alteration in wide-ranging neural networks due to electrode implantation.

The choice of imaging is crucial for analyzing network formation based on subcortical events. For example, fMRI can record cortical and subcortical activity at the same spatial resolution (Glover, 2011). However, fMRI does not provide the ability to capture the temporal dynamics of neural activity because the temporal resolution is on the order of seconds (Glover, 2011). Subcortical events, with durations in the range of milliseconds, can be recorded using macro-electrodes, such as the DBS electrodes (Buzsáki et al., 2012). With externalized cables from the DBS electrodes, recording of subcortical activity was possible even after surgery for electrode implantation.

We achieved a temporal resolution in the ms range for cortical activity using MEG (Lopes da Silva, 2013). As the temporal resolution of MEG and EEG is comparable, spatial resolution is better for MEG than for EEG recordings because of less spatial leakage (Hari, 2012). However, increasing spatial resolution by combining EEG and MEG (Sharon et al., 2007) would not have been reasonable for the patients on the day after DBS surgery due to the additional

time required to place the EEG electrodes. In addition, we expected that due to the individually externalized electrodes, an identical layout for the EEG electrodes could only be used in some patients, making it difficult to compare the results across patients. For recording cortical activity, also fMRI could be used analogously to Logothetis *et al.* (2012), but the temporal resolution of cortical activity would be significantly worse than that of subcortical activity. Nevertheless, a replication of study 2 with fMRI recordings would provide complementary findings to study 2.

Due to the necessary use of macroelectrodes for LFP measurement, it was only possible to measure subcortical events in patients admitted for DBS implantation. The wide usage of DBS in PD allowed for a sufficiently large patient cohort for this study. Even if there are different neural events like hippocampal ripples and beta and gamma bursts, they have to occur in the target area of the DBS electrode to be measured. In German-speaking countries, the STN is mainly chosen for stimulation in PD patients (Hamel *et al.*, 2017). For three reasons, the beta bursts detectable in the STN are well suited for analyzing network formation by neural events in PD patients:

1. STN activity in the beta-band is pathologically increased (Kühn *et al.*, 2009; Ray *et al.*, 2008)
2. there is a synchronous activity in the STN and the cortex in the beta-band (Cagnan *et al.*, 2019; Hirschmann *et al.*, 2011, 2013; Tinkhauser *et al.*, 2018b)
3. beta activity in the STN, as well as in the cortex, can be divided into phases of high and low activity, and the phases of increased activity can be described as temporary events, the beta bursts (Feingold *et al.*, 2015; Lobb, 2014; Tinkhauser *et al.*, 2017a,b)

However, a central problem is how and where the beta bursts are detected.

Most methods for detecting beta bursts are threshold-based (Feingold *et al.*, 2015; Lobb, 2014; Tinkhauser *et al.*, 2017a,b) but can also be data-driven when using a hidden Markov model (HMM; Quinn *et al.*, 2019; Seedat *et al.*, 2020). However, HMM-based methods have the disadvantage that although they find states in the beta-band, we have to show afterward that the state is an STN beta burst and not, for example, a state of high coherence with another region. Threshold-based methods are more direct in this regard. Among the threshold-based methods, the method of Tinkhauser *et al.* (2017a; 2017b) has widespread use. We used this method to allow high comparability towards other studies but introduced a modification. During the measurements for studies 1 and 2, we disconnected the externalized electrode cables from the signal amplifier during breaks. Therefore, differences in impedance

could occur. However, to ensure that the amplitude of the LFP signal was comparable between the individual measurement blocks, the signal was z-score normalized. Otherwise, individual measurement blocks with a strongly deviating impedance could have shifted the threshold for burst detection.

A fundamental issue in threshold-based burst detection is the definition of the frequency band. Previous publications on the pathology of the beta-band in PD have shown results specific to subbands of the beta-band while using an inconsistent definition (Kühn et al., 2006; Neumann et al., 2016; Priori et al., 2004). In study 1, we investigated different definitions of the beta-band in the context of beta burst detection. Here, we directly compared the ± 3 Hz band around the individual beta peak frequency (iBP), the low beta band (lBB), and the high beta band (hBB). Furthermore, we repeated the analysis with two different frequency band definitions for lBB and hBB (1. run: lBB: 12-24 Hz, hBB 24-35 Hz; 2. run: 12-20 Hz hBB: 24-35 Hz). There were no decisive differences between the two runs. Overall, we showed a change due to dopaminergic medication for beta bursts and the power of the overall LFP signal, especially in hBB and iBP.

Additionally, we showed only for hBB a positive correlation of burst duration with clinical parameters. The direct comparison of frequency bands showed that a subdivision into hBB and lBB is essential and attributes a higher significance to hBB in pathology. We found comparable as well as contradictory results in papers that did not perform a direct comparison of frequency bands. These inconsistencies in reported results may be due to patient selection. Because the patient selection in comparable studies was not always selective for PD subtype, it could be that the pathological significance of lBB and hBB differs by PD subtype. Alternatively, the exact spectral position of the iBP could be substantial. For the power at the iBP, a reduction by dopaminergic medication could be shown and related to symptom expression (Neumann et al., 2017), suggesting a pathological significance for iBP. However, iBP can be located in either hBB or lBB or, if there are multiple beta peaks, in both. Assuming that iBP is the dominant pathological signal, then either the lBB or the hBB could be pathological, depending on the location of iBP. Because we also examined channels without a beta peak in study 1, we assume that the hBB is the pathological band in case of doubt. However, in the presence of a beta peak, the iBP should be used to consider the pathological changes.

The second central question to be answered by study 1 was whether beta bursts occur in a specific STN area. The dorsal part of the STN, assigned to the motor system, is considered the primary source of beta oscillations (Tamir et al., 2020; Weinberger et al., 2006). There-

fore, we examined this area for the spatial distribution of beta activity via directional contacts. This revealed a significant main effect for the contact orientation only for the burst amplitude. However, post-hoc, there was no significant difference between directions.

This result was surprising because DBS patients usually have a clinically most effective contact and generally benefit from directional stimulation (Gordon et al., 2017; Hartmann et al., 2019). However, it could be that spatial discrimination of beta activity is only possible with a larger sample size. This result raises the question of whether beta activity is the correct marker for DBS. However, it has been shown that beta activity correlates with best clinical contact (Tinkhauser et al., 2018a), which argues in favor of using beta activity as a marker. Combined with our results, this could mean that there is no dominant anatomical direction in pathological STN beta activity but that beta activity is spatially modulated individually.

Combining the results of study 1 with known literature, we defined constraints for detecting STN beta bursts for study 2. Because of the dominant pathological nature, we used the frequency definition of iBP and selected only LFPs for which a beta peak was detectable. In addition, without prior knowledge of the best clinical contact, we opted for a direction-independent bipolar recording. We based this decision on the fact that a contribution of cortical activity to the bipolar LFP signal was less likely (Marmor et al., 2017). Overall, to focus the interpretation of the results on the pathology of STN beta bursts and to increase the number of beta bursts and thus the signal-to-noise ratio, study 2 was performed OFF medication rather than the ON, since the burst rate is reduced by dopaminergic medication (Sure et al., 2021).

By detecting ERFs based on STN beta bursts, we demonstrated that STN beta bursts are involved in network formation. In conjunction with the results of Logothetis *et al.* (2012), which already showed network formation by hippocampal ripples, we can thus support the hypothesis of Florin *et al.* (2015) that different neural events may be involved in network formation. Therefore, the analysis method introduced by Logothetis *et al.* (2012) and used in study 2 could be used to investigate the functional significance of neural events, as shown here for beta bursts in PD. In general, this method could improve the understanding of individual symptoms, especially in the case of events relevant to diseases, and specify therapeutic procedures.

While applying the NET approach to STN beta bursts in PD in study 2, we found more cortical regions involved than we predicted because, in addition to motor, associative, and limbic areas, which have functional counterparts in the STN, areas of vision and language also

exhibited ERFs. These extended findings argue for extensive network formation by STN beta bursts and suggest that the functional influence of STN beta bursts is not limited to motor activity. Although STN beta bursts in PD are primarily associated with motor symptoms (Sure et al., 2021; Tinkhauser et al., 2017a,b), study 2 suggests that STN beta bursts may also play a role in other functional systems and, thus, symptoms. The analysis method used here, using broadband cortical activity, thus revealed a much broader functional circuitry of STN beta bursts than previously shown by methods restricted to the beta-band (Cagnan et al., 2019; Tinkhauser et al., 2018b).

Furthermore, the network formation seems to be amplitude-dependent. At least in study 2, more ERFs appeared around the burst maximum than around the burst onset and, thus, at the time of high amplitude. This may indicate that network formation increases in probability as the beta burst amplitude increases. It may be analogous to synaptic stimulus propagation, where a threshold must be reached to propagate the signal to the next neuron. As the LFP signal, from which the STN beta bursts are also determined, is based on high synchronicity of neurons, this could mean that a sufficient number of neurons must be active in the beta rhythm for the beta burst to become functionally relevant.

The burst maximum should be a good marker for this analysis since this can be objectively determined for each burst and should mark the time of maximal synaptic activity synchronicity in the beta-band. However, another crucial parameter is the duration of the bursts. As in the case of beta bursts, a distinction in terms of pathology is thought to exist for short and long bursts (Tinkhauser et al., 2017a). Nevertheless, the duration of the bursts is significantly dependent on the threshold value set for burst detection. Therefore, regardless of whether a burst is healthy or pathological, it would be desirable to determine functionally active bursts. For this purpose, a modification of the threshold value determination used here and presented by Tinkhauser *et al.* (2017a; 2017b) for beta burst detection would be necessary. However, determining a functional threshold for this would require further data collection.

ERFs showed up for long and short bursts, so it can be assumed that STN beta bursts are generally involved in network formation. However, no significant differences were shown in these ERFs. Thus, it was not possible with the analysis used to check whether network formation is also pathologically altered by long bursts. This could change with a longer measurement duration and a concomitant increase in beta burst rate. This would lead to more averaging and thus improve the signal-to-noise ratio. However, on the other hand, the network formation itself could remain unchanged, and only the occurrence of the network formation could change.

Because the ERFs showed increased and decreased activity compared to baseline, network formation based on STN beta bursts should generally form via the BGC loop. This is because, via the indirect pathway (Albin et al., 1989; Calabresi et al., 2014), beta bursts could lead to a decrease in cortical activity, and via the hyperdirect pathway (Nambu et al., 1996; Oswal et al., 2021), an increased cortical activity could stimulate beta bursts in the STN. This hypothesis is also based on work considering a general involvement of the BGC loop in beta activity (Brittain et al., 2014; Cagnan et al., 2019; Diesburg et al., 2021; Oswal et al., 2021; Yu et al., 2021).

The results of study 2 and study 1 must be considered in light of the results of study 3, as the stun effect could influence the respective parameters. In general, it is known that inflammation and edema develop over the implantation of the electrode, which can lead to a temporary improvement of PD symptoms (Chen et al., 2006; Mann et al., 2009). However, it is unclear how widespread this stun effect is. Often, though, LFP data are collected during a period in which the stun effect has not yet subsided. Since the impact of the stun effect in general and its particular patient-specific manifestation is not fully known, corresponding results are not corrected for this.

Nevertheless, study 3 shows a modification of different functional RSNs due to the implantation of the electrodes in the STN and thus probably due to the stun effect. Because the modifications were extensive, we assumed that specific neural events, such as STN beta bursts, are also affected. Furthermore, as the stun effect, like DBS and dopaminergic medication, attenuates PD symptoms (Chen et al., 2006; Kühn et al., 2009; Mann et al., 2009; Ray et al., 2008), the influence on STN beta bursts could be analogous to the influence of DBS and dopaminergic medication. Thus, for the network formation shown in study 2, which affects different functional domains as in study 3, an influence of the stun effect can also be assumed. However, to determine whether the results of studies 1 and 2 are indeed affected by the stun effect, it would be necessary to repeat the measurement after attenuation of the stun effect.

Crucial for interpreting network changes is the plausibility of the methods from study 3. Compared to MEG-based RSN determination, methods based on fMRI data are more frequently in use. However, the comparability of MEG and fMRI RSN was demonstrated previously (Pelzer et al., 2021). Based on this, MEG methods offer the advantage of also using high-frequency signals for RSN determination. The method used here is based on phase-amplitude coupling between a low-frequency and a high-frequency component. Although, as in PD, a modulation could be shown for the phase-amplitude coupling (De Hemptinne et al., 2013), and the beta

band was covered by the low-frequency phase component (2-30 Hz), we expected that this method is sensitive to network changes in PD.

Studies 2 and 3 show the importance of both STN beta bursts and the stun effect beyond the motor system. These findings fit with modulations of beta activity found for different cortical areas and functions, and generally, beta bursts were found across the cortex (Betti et al., 2021; Miller et al., 2018; Seedat et al., 2020; Wang, 2010). Moreover, for the motor cortex, synchronicity with STN beta bursts has already been shown (Tinkhauser et al., 2018b). Based on study 2, we expect this synchronicity to be found in other cortical regions, but the degree of the synchronicity might differ. In any case, beta bursts should be investigated more for their correlation to clinical non-motor symptoms, such as visual impairment (Jellinger, 2015). Also, beta bursts should be considered in terms of side effects in DBS. This might emphasize the importance of beta activity in steering the DBS setting even more than the relation to motor symptoms already does, i. e., beta activity could be used to reduce non-motor side effects of DBS. Also, the changes in the various RSNs due to electrode implantation may indicate the later effects of DBS. Thus, an analysis of RSNs in combination with the later DBS outcome could be helpful for individual DBS adjustment.

Finally, in study 3, it was noticed that RSNs before implantation had a better agreement with RSNs from healthy subjects than after implantation, although clinical symptoms improved after implantation. This finding suggests that the stun effect modulates RSNs and alters their association with the Unified Parkinson’s Disease Rating Scale motor score (UPDRS-III). This could explain why we found no correlation to the UPDRS-III in the network formation of study 2. In principle, this also raises the question of how correlations in STN beta activity to UPDRS-III, as shown in study 1, should be evaluated. However, since correlations to the UPDRS-III were shown for STN beta activity and, in particular, for beta bursts (Kühn et al., 2006; Lofredi et al., 2019; O’Keeffe et al., 2020; Thompson et al., 2014; Tinkhauser et al., 2017b; Weinberger et al., 2006), the influence of the stun effect on subcortical neural events should be less severe than on long-range networks.

6.1 Summary

Key findings of this work are that both STN beta bursts and the stun effect take on multi-functional roles. However, for the analysis of STN beta bursts, study 1 demonstrated that the parameters for burst detection need to be carefully determined and highlighted a clear frequency dependence for the bursts. Besides the connection to the motor system, study 2 revealed the involvement of STN beta bursts in extensive network formation. At the cortical

level, areas were involved, which also have functional counterparts in the STN and visual and linguistic fields. Results as in studies 1 and 2 were only possible by LFP measurements, which are possible close in time to the implantation of DBS electrodes. However, study 3 showed that despite the specificity of these data, the stun effect plays a role and should be addressed. Changes in RSNs were evident as a result of electrode implantation. Since different functional RSN were affected, study 3 demonstrated that besides the known connection to the motor system, the stun effect also plays a role in other functional systems.

7 Outlook

This work showed that STN beta bursts are involved in long-range network formation. Thus, the concept of Logothetis *et al.* (2012) of NET activity could be successfully applied to humans. However, when considering subcortical events, this method is limited to patient groups with DBS as a treatment option because invasive procedures are currently required to detect subcortical events. In appropriate patient groups, the examination of events detected in LFP data and cortical activity reconstructed via MEG measurements forms an opportunity for high temporal resolution analysis of functional connectivity between cortex and respective subcortical areas. In addition, neural events could be better characterized as potential electrophysiological markers of disease states. Since neural events, such as beta bursts or spindles, can also be found in the cortex (Axmacher et al., 2006; Feingold et al., 2015), neural events can be detected in healthy participants via pure MEG/EEG measurements and examined for their influence on cortical network formation. However, an additional combined LFP/fMRI or EEG/fMRI measurement would be helpful to extend the network formation based on neural events to all subcortical areas. This is because, complementary to the temporally high-resolution networks detected via MEG/EEG, via fMRI, more static networks, extending across the entire brain, could be detected by averaging the BOLD signal on neural events (Logothetis et al., 2012).

The demonstrated network formation by STN beta bursts allowed a better functional description of STN beta bursts. Since STN beta bursts are considered a possible marker for adaptive DBS in PD patients (Tinkhauser et al., 2017a), these results could help better understand the therapeutic and possible side effects caused by DBS. However, it would be helpful to repeat study 2 with PD patients receiving dopaminergic medication to investigate a possible pathological change in network formation. Furthermore, the network formation shown in study 2 was very heterogeneous, which may have resulted from the high variability in the duration of STN beta bursts. Therefore, to describe the network formation more precisely, a repetition of the analysis with STN beta bursts more restricted in burst duration would be necessary. In this case, however, longer measurement durations would be required not to worsen the signal-to-noise ratio.

So far, network formation by STN beta bursts has been studied in the resting-state. Still, since beta bursts are primarily associated with the motor system (Hannah et al., 2020; Little et al., 2019; Wessel, 2020), an investigation of network formation by STN beta bursts in the context of a movement exercise would be helpful. However, because study 2 found a change in activity at the time of STN beta bursts in cortical areas that are functional counterparts

(motor, limbic, associative) to all three functional domains of the STN, network formation should also be examined in the context of tasks for the limbic and associative systems. This would further reveal the functional significance of STN beta bursts when STN beta bursts alter network formation in a task-bound manner. Further, whether cortical beta bursts like subthalamic beta bursts are involved in long-range network formation should be investigated, as coupling of cortical and subthalamic beta bursts has already been shown (Tinkhauser et al., 2018b). This could also help better to understand the information flow between STN and cortex.

Repeating the measurement for network formation by STN beta bursts after the stun effect has subsided also seems reasonable, given the results of study 3. This is because study 3 showed that RSNs are altered shortly after electrode implantation. Also, the comparison of RSNs should be repeated months after electrode implantation and, thus, after the stun effect has worn off. If the RSNs months after electrode implantation again more closely resemble the RSNs before electrode implantation, this would prove that the changes shown in the RSNs are due to the stun effect. In this case, studies with LFP measurements using permanently implanted electrodes, such as studies 1 and 2, should be performed after the stun effect has subsided to ensure that the measured activity was not modulated by electrode implantation. This would be possible with DBS systems that allow recording LFPs and a non-invasive data readout even after electrode implantation (Cummins et al., 2021).

Overall, it could be shown that the implantation of an electrode into the brain alone can affect the measured brain activity, at least in the short term. However, to better describe this stun effect and especially to detect a decrease of this stun effect, measurements before implantation, directly after implantation, and significantly after implantation of the electrodes would be necessary. Furthermore, it could be demonstrated unambiguously from STN beta bursts that neural events in humans are involved in network formation. This result motivates to perform this analysis also for other neural events. Finally, this work extends the already extensive knowledge of network formation in humans by using a high temporal resolution method applicable to various neural events.

8 References

- Abosch, A., Lanctin, D., Onaran, I., Eberly, L., Spaniol, M., and Ince, N. F. (2012). Long-term recordings of local field potentials from implanted deep brain stimulation electrodes. *Neurosurgery*, 71(4):804–814.
- Albin, R. L., Young, A. B., and Penney, J. B. (1989). The functional anatomy of basal ganglia disorders. *Trends Neurosci.*, 12(10):366–375.
- Alexander, G. E., DeLong, M. R., and Strick, P. L. (1986). Parallel organization of functionally segregated circuits linking basal ganglia and cortex. *Annu. Rev. Neurosci.*, VOL. 9:357–381.
- Anderson, S. and Stegemöller, E. L. (2020). Effects of Levodopa on Impairments to High-Level Vision in Parkinson’s Disease. *Front. Neurol.*, 11:708.
- Antoniades, C. A., Buttery, P., FitzGerald, J. J., Barker, R. A., Carpenter, R. H., and Watts, C. (2012). Deep brain stimulation: Eye movements reveal anomalous effects of electrode placement and stimulation. *PLoS One*, 7(3):e32830.
- Antony, P. M., Diederich, N. J., Krüger, R., and Balling, R. (2013). The hallmarks of Parkinson’s disease. *FEBS J.*, 280(23):5981–5993.
- Arlotti, M., Marceglia, S., Foffani, G., Volkmann, J., Lozano, A. M., Moro, E., Cogiamanian, F., Prenassi, M., Bocci, T., Cortese, F., Rampini, P., Barbieri, S., and Priori, A. (2018). Eight-hours adaptive deep brain stimulation in patients with Parkinson disease. *Neurology*, 90(11):e971–e976.
- Armstrong, M. J. and Okun, M. S. (2020). Diagnosis and Treatment of Parkinson Disease: A Review. *JAMA - J. Am. Med. Assoc.*, 323(6):548–560.
- Aron, A. R., Herz, D. M., Brown, P., Forstmann, B. U., and Zaghoul, K. (2016). Frontosubthalamic circuits for control of action and cognition. *J. Neurosci.*, 36(45):11489–11495.
- Ashby, P., Paradiso, G., Saint-Cyr, J. A., Chen, R., Lang, A. E., and Lozano, A. M. (2001). Potentials recorded at the scalp by stimulation near the human subthalamic nucleus. *Clin. Neurophysiol.*, 112(3):431–437.
- Ashkan, K., Rogers, P., Bergman, H., and Ughratdar, I. (2017). Insights into the mechanisms of deep brain stimulation. *Nat. Rev. Neurol.*, 13(9):548–554.
- Augustine, J. R. (1996). Circuitry and functional aspects of the insular lobe in primates including humans. *Brain Res. Rev.*, 22(3):229–244.

- Axmacher, N., Mormann, F., Fernández, G., Elger, C. E., and Fell, J. (2006). Memory formation by neuronal synchronization. *Brain Res. Rev.*, 52(1):170–182.
- Baillet, S. (2017). Magnetoencephalography for brain electrophysiology and imaging. *Nat. Neurosci.*, 20(3):327–339.
- Baillet, S., Mosher, J. C., and Leahy, R. M. (2001). Electromagnetic brain mapping. *IEEE Signal Process. Mag.*, 18(6):14–30.
- Beckmann, C. F., DeLuca, M., Devlin, J. T., and Smith, S. M. (2005). Investigations into resting-state connectivity using independent component analysis. *Philos. Trans. R. Soc. B Biol. Sci.*, 360(1457):1001–1013.
- Bennett, D. A., Beckett, L. A., Murray, A. M., Shannon, K. M., Goetz, C. G., Pilgrim, D. M., and Evans, D. A. (1996). Prevalence of Parkinsonian Signs and Associated Mortality in a Community Population of Older People. *N. Engl. J. Med.*, 334(2):71–76.
- Bennett, M. V. and Zukin, R. S. (2004). Electrical Coupling and Neuronal Synchronization in the Mammalian Brain. *Neuron*, 41(4):495–511.
- Bergman, H. and Deuschl, G. (2002). Pathophysiology of parkinson’s disease: From clinical neurology to basic neuroscience and back. *Mov. Disord.*, 17(SUPPL. 3).
- Bergman, H., Raz, A., Feingold, A., Nini, A., Nelken, I., Hansel, D., Ben-Pazi, H., and Reches, A. (1998). Physiology of MPTP tremor. *Mov. Disord.*, 13(SUPPL. 3):29–34.
- Betti, V., Della Penna, S., de Pasquale, F., and Corbetta, M. (2021). Spontaneous Beta Band Rhythms in the Predictive Coding of Natural Stimuli. *Neuroscientist*, 27(2):184–201.
- Biau, E. and Kotz, S. A. (2018). Lower beta: A central coordinator of temporal prediction in multimodal speech. *Front. Hum. Neurosci.*, 12:434.
- Birkmayer, W. and Hornykiewicz, O. (1962). Der L-Dioxyphenylalanin (=L-DOPA)-Effekt beim Parkinson-Syndrom des Menschen: Zur Pathogenese und Behandlung der Parkinson-Akinese. *Arch. für Psychiatr. und Nervenkrankheiten Ver. mit Zeitschrift für die Gesamte Neurol. und Psychiatr.*, 203(5):560–574.
- Biswal, B., Zerrin Yetkin, F., Haughton, V. M., and Hyde, J. S. (1995). Functional connectivity in the motor cortex of resting human brain using echo-planar mri. *Magn. Reson. Med.*, 34(4):537–541.

- Biswal, B. B., Mennes, M., Zuo, X. N., Gohel, S., Kelly, C., Smith, S. M., Beckmann, C. F., Adelstein, J. S., Buckner, R. L., Colcombe, S., Dogonowski, A. M., Ernst, M., Fair, D., Hampson, M., Hoptman, M. J., Hyde, J. S., Kiviniemi, V. J., Kötter, R., Li, S. J., Lin, C. P., Lowe, M. J., Mackay, C., Madden, D. J., Madsen, K. H., Margulies, D. S., Mayberg, H. S., McMahon, K., Monk, C. S., Mostofsky, S. H., Nagel, B. J., Pekar, J. J., Peltier, S. J., Petersen, S. E., Riedl, V., Rombouts, S. A., Rypma, B., Schlaggar, B. L., Schmidt, S., Seidler, R. D., Siegle, G. J., Sorg, C., Teng, G. J., Veijola, J., Villringer, A., Walter, M., Wang, L., Weng, X. C., Whitfield-Gabrieli, S., Williamson, P., Windischberger, C., Zang, Y. F., Zhang, H. Y., Castellanos, F. X., and Milham, M. P. (2010). Toward discovery science of human brain function. *Proc. Natl. Acad. Sci. U. S. A.*, 107(10):4734–4739.
- Blandini, F., Nappi, G., Tassorelli, C., and Martignoni, E. (2000). Functional changes of the basal ganglia circuitry in Parkinson’s disease. *Prog. Neurobiol.*, 62(1):63–88.
- Boon, L. I., Hillebrand, A., Potters, W. V., de Bie, R. M., Prent, N., Bot, M., Schuurman, P. R., Stam, C. J., van Rootselaar, A. F., and Berendse, H. W. (2020). Motor effects of deep brain stimulation correlate with increased functional connectivity in Parkinson’s disease: An MEG study. *NeuroImage Clin.*, 26:102225.
- Bosch, D. (1978). Atlas for stereotaxy of the human brain. *Clin. Neurol. Neurosurg.*, 80(4):299.
- Bour, L. J., Contarino, M. F., Foncke, E. M., De Bie, R. M., Van Den Munckhof, P., Speelman, J. D., and Schuurman, P. R. (2010). Long-term experience with intraoperative microrecording during DBS neurosurgery in STN and GPi. *Acta Neurochir. (Wien)*, 152(12):2069–2077.
- Braak, H., Sandmann-Keil, D., Gai, W., and Braak, E. (1999). Extensive axonal Lewy neurites in Parkinson’s disease: A novel pathological feature revealed by α -synuclein immunocytochemistry. *Neurosci. Lett.*, 265(1):67–69.
- Brittain, J. S., Sharott, A., and Brown, P. (2014). The highs and lows of beta activity in cortico-basal ganglia loops. *Eur. J. Neurosci.*, 39(11):1951–1959.
- Britz, J., Van De Ville, D., and Michel, C. M. (2010). BOLD correlates of EEG topography reveal rapid resting-state network dynamics. *Neuroimage*, 52(4):1162–1170.
- Brookes, M. J., Stevenson, C. M., Barnes, G. R., Hillebrand, A., Simpson, M. I., Francis, S. T., and Morris, P. G. (2007). Beamformer reconstruction of correlated sources using a modified source model. *Neuroimage*, 34(4):1454–1465.
- Brookes, M. J., Woolrich, M., Luckhoo, H., Price, D., Hale, J. R., Stephenson, M. C., Barnes, G. R., Smith, S. M., and Morris, P. G. (2011). Investigating the electrophysiological basis

- of resting state networks using magnetoencephalography. *Proc. Natl. Acad. Sci. U. S. A.*, 108(40):16783–16788.
- Brown, P., Oliviero, A., Mazzone, P., Insola, A., Tonali, P., and Di Lazzaro, V. (2001). Dopamine dependency of oscillations between subthalamic nucleus and pallidum in Parkinson’s disease. *J. Neurosci.*, 21(3):1033–1038.
- Brücke, C., Kupsch, A., Schneider, G. H., Hariz, M. I., Nuttin, B., Kopp, U., Kempf, F., Trottenberg, T., Doyle, L., Chen, C. C., Yarrow, K., Brown, P., and Kühn, A. A. (2007). The subthalamic region is activated during valence-related emotional processing in patients with Parkinson’s disease. *Eur. J. Neurosci.*, 26(3):767–774.
- Buckel, W. and Kleiner, R. (2012). *Supraleitung*. Wiley-VCH Verlag GmbH & Co. KGaA.
- Buot, A., Karachi, C., Lau, B., Belaid, H., Fernandez-Vidal, S., Welter, M. L., and Mallet, L. (2021). Emotions Modulate Subthalamic Nucleus Activity: New Evidence in Obsessive-Compulsive Disorder and Parkinson’s Disease Patients. *Biol. Psychiatry Cogn. Neurosci. Neuroimaging*, 6(5):556–567.
- Burciu, R. G. and Vaillancourt, D. E. (2018). Imaging of Motor Cortex Physiology in Parkinson’s Disease. *Mov. Disord.*, 33(11):1688–1699.
- Buzsáki, G. (2002). Theta oscillations in the hippocampus. *Neuron*, 33(3):325–340.
- Buzsáki, G., Anastassiou, C. A., and Koch, C. (2012). The origin of extracellular fields and currents-EEG, ECoG, LFP and spikes. *Nat. Rev. Neurosci.*, 13(6):407–420.
- Buzsáki, G. and Draguhn, A. (2004). Neuronal oscillations in cortical networks. *Science (80-.)*, 304(5679):1926–1929.
- Buzsáki, G., Horváth, Z., Urioste, R., Hetke, J., and Wise, K. (1992). High-frequency network oscillation in the hippocampus. *Science (80-.)*, 256(5059):1025–1027.
- Cagnan, H., Mallet, N., Moll, C. K., Gulberti, A., Holt, A. B., Westphal, M., Gerloff, C., Engel, A. K., Hamel, W., Magill, P. J., Brown, P., and Sharott, A. (2019). Temporal evolution of beta bursts in the parkinsonian cortical and basal ganglia network. *Proc. Natl. Acad. Sci. U. S. A.*, 116(32):16095–16104.
- Calabresi, P., Picconi, B., Tozzi, A., Ghiglieri, V., and Di Filippo, M. (2014). Direct and indirect pathways of basal ganglia: A critical reappraisal. *Nat. Neurosci.*, 17(8):1022–1030.

- Cao, C. Y., Zeng, K., Li, D. Y., Zhan, S. K., Li, X. L., and Sun, B. M. (2017). Modulations on cortical oscillations by subthalamic deep brain stimulation in patients with Parkinson disease: A MEG study. *Neurosci. Lett.*, 636:95–100.
- Casarotto, S., Turco, F., Comanducci, A., Perretti, A., Marotta, G., Pezzoli, G., Rosanova, M., and Isaias, I. U. (2019). Excitability of the supplementary motor area in Parkinson’s disease depends on subcortical damage. *Brain Stimul.*, 12(1):152–160.
- Cash, S. S., Halgren, E., Dehghani, N., Rossetti, A. O., Thesen, T., Wang, C. M., Devinsky, O., Kuzniecky, R., Doyle, W., Madsen, J. R., Bromfield, E., Eross, L., Halász, P., Karmos, G., Csercsa, R., Wittner, L., and Ulbert, I. (2009). The human K-complex represents an isolated cortical down-state. *Science (80-.)*, 324(5930):1084–1087.
- Cassidy, M., Mazzone, P., Oliviero, A., Insola, A., Tonali, P., Di Lazzaro, V., and Brown, P. (2002). Movement-related changes in synchronization in the human basal ganglia. *Brain*, 125(6):1235–1246.
- Castrioto, A., Meaney, C., Hamani, C., Mazzella, F., Poon, Y. Y., Lozano, A. M., Hodaie, M., and Moro, E. (2011). The Dominant-STN phenomenon in bilateral STN DBS for Parkinson’s disease. *Neurobiol. Dis.*, 41(1):131–137.
- Cavanna, A. E. and Trimble, M. R. (2006). The precuneus: A review of its functional anatomy and behavioural correlates. *Brain*, 129(3):564–583.
- Ceballos-Baumann, A. O., Boecker, H., Bartenstein, P., Von Falkenhayn, I., Riescher, H., Conrad, B., Moringlane, J. R., and Alesch, F. (1999). A positron emission tomographic study of subthalamic nucleus stimulation in Parkinson disease: Enhanced movement-related activity of motor-association cortex and decreased motor cortex resting activity. *Arch. Neurol.*, 56(8):997–1003.
- Chang, C. and Glover, G. H. (2010). Time-frequency dynamics of resting-state brain connectivity measured with fMRI. *Neuroimage*, 50(1):81–98.
- Chen, C. C., Pogosyan, A., Zrinzo, L. U., Tisch, S., Limousin, P., Ashkan, K., Yousry, T., Hariz, M. I., and Brown, P. (2006). Intra-operative recordings of local field potentials can help localize the subthalamic nucleus in Parkinson’s disease surgery. *Exp. Neurol.*, 198(1):214–221.
- Chen, J. L., Ros, T., and Gruzelier, J. H. (2013). Dynamic changes of ICA-derived EEG functional connectivity in the resting state. *Hum. Brain Mapp.*, 34(4):852–868.

- Chu, H. Y., McIver, E. L., Kovaleski, R. F., Atherton, J. F., and Bevan, M. D. (2017). Loss of Hyperdirect Pathway Cortico-Subthalamic Inputs Following Degeneration of Midbrain Dopamine Neurons. *Neuron*, 95(6):1306–1318.e5.
- Coenen, V. A., Amtage, F., Volkmann, J., and Schläpfer, T. E. (2015). Deep brain stimulation in neurological and psychiatric disorders. *Dtsch. Arztebl. Int.*, 112(31-32):519–526.
- Coizet, V., Graham, J. H., Moss, J., Bolam, J. P., Savasta, M., McHaffie, J. G., Redgrave, P., and Overton, P. G. (2009). Short-latency visual input to the subthalamic nucleus is provided by the midbrain superior colliculus. *J. Neurosci.*, 29(17):5701–5709.
- Colclough, G. L., Woolrich, M. W., Tewarie, P. K., Brookes, M. J., Quinn, A. J., and Smith, S. M. (2016). How reliable are MEG resting-state connectivity metrics? *Neuroimage*, 138:284–293.
- Conte, A., Khan, N., Defazio, G., Rothwell, J. C., and Berardelli, A. (2013). Pathophysiology of somatosensory abnormalities in Parkinson disease. *Nat. Rev. Neurol.*, 9(12):687–697.
- Contreras, D., Destexhe, A., Sejnowski, T. J., and Steriade, M. (1997). Spatiotemporal patterns of spindle oscillations in cortex and thalamus. *J. Neurosci.*, 17(3):1179–1196.
- Conway, B. R. (2018). The organization and operation of inferior temporal cortex. *Annu. Rev. Vis. Sci.*, 4(1):381.
- Cordes, D., Haughton, V., Carew, J. D., Arfanakis, K., and Maravilla, K. (2002). Hierarchical clustering to measure connectivity in fMRI resting-state data. *Magn. Reson. Imaging*, 20(4):305–317.
- Craig, A., Tran, Y., Wijesuriya, N., and Nguyen, H. (2012). Regional brain wave activity changes associated with fatigue. *Psychophysiology*, 49(4):574–582.
- Cummins, D. D., Kochanski, R. B., Gilron, R., Swann, N. C., Little, S., Hammer, L. H., and Starr, P. A. (2021). Chronic Sensing of Subthalamic Local Field Potentials: Comparison of First and Second Generation Implantable Bidirectional Systems Within a Single Subject. *Front. Neurosci.*, 15:725797.
- Damoiseaux, J. S., Rombouts, S. A., Barkhof, F., Scheltens, P., Stam, C. J., Smith, S. M., and Beckmann, C. F. (2006). Consistent resting-state networks across healthy subjects. *Proc. Natl. Acad. Sci. U. S. A.*, 103(37):13848–13853.

- D'Argembeau, A., Collette, F., Van Der Linden, M., Laureys, S., Del Fiore, G., Degueldre, C., Luxen, A., and Salmon, E. (2005). Self-referential reflective activity and its relationship with rest: A PET study. *Neuroimage*, 25(2):616–624.
- Darvas, F. and Hebb, A. O. (2014). Task specific Inter-Hemispheric coupling in human subthalamic nuclei. *Front. Hum. Neurosci.*, 8(SEP):701.
- Davey, J., Thompson, H. E., Hallam, G., Karapanagiotidis, T., Murphy, C., De Caso, I., Krieger-Redwood, K., Bernhardt, B. C., Smallwood, J., and Jefferies, E. (2016). Exploring the role of the posterior middle temporal gyrus in semantic cognition: Integration of anterior temporal lobe with executive processes. *Neuroimage*, 137:165–177.
- Dayal, V., Limousin, P., and Foltynie, T. (2017). Subthalamic nucleus deep brain stimulation in Parkinson's disease: The effect of varying stimulation parameters. *J. Parkinsons. Dis.*, 7(2):235–245.
- De Carli, D., Garreffa, G., Colonnese, C., Giulietti, G., Labruna, L., Briselli, E., Ken, S., Macrì, M. A., and Maraviglia, B. (2007). Identification of activated regions during a language task. *Magn. Reson. Imaging*, 25(6):933–938.
- De Hemptinne, C., Ryapolova-Webb, E. S., Air, E. L., Garcia, P. A., Miller, K. J., Ojemann, J. G., Ostrem, J. L., Galifianakis, N. B., and Starr, P. A. (2013). Exaggerated phase-amplitude coupling in the primary motor cortex in Parkinson disease. *Proc. Natl. Acad. Sci. U. S. A.*, 110(12):4780–4785.
- De Hemptinne, C., Swann, N. C., Ostrem, J. L., Ryapolova-Webb, E. S., San Luciano, M., Galifianakis, N. B., and Starr, P. A. (2015). Therapeutic deep brain stimulation reduces cortical phase-amplitude coupling in Parkinson's disease. *Nat. Neurosci.*, 18(5):779–786.
- De Pasquale, F., Della Penna, S., Snyder, A. Z., Lewis, C., Mantini, D., Marzetti, L., Belardinelli, P., Ciancetta, L., Pizzella, V., Romani, G. L., and Corbetta, M. (2010). Temporal dynamics of spontaneous MEG activity in brain networks. *Proc. Natl. Acad. Sci. U. S. A.*, 107(13):6040–6045.
- De Rijk, M. C., Breteler, M. M., Graveland, G. A., Ott, A., Grobbee, D. E., Van Der Meche, F. G., and Hofman, A. (1995). Prevalence of parkinson's disease in the elderly: The rotterdam study. *Neurology*, 45(12):2143–2146.
- de Schipper, L. J., Hafkemeijer, A., van der Grond, J., Marinus, J., Henselmans, J. M., and van Hilten, J. J. (2018). Altered whole-brain and network-based functional connectivity in Parkinson's disease. *Front. Neurol.*, 9(JUN).

- Deffains, M. and Bergman, H. (2019). Parkinsonism-related β oscillations in the primate basal ganglia networks – Recent advances and clinical implications. *Park. Relat. Disord.*, 59:2–8.
- DeLong, M. R. (1990). Primate models of movement disorders of basal ganglia origin. *Trends Neurosci.*, 13(7):281–285.
- Deuschl, G., Schade-Brittinger, C., Krack, P., Volkmann, J., Schäfer, H., Bötzel, K., Daniels, C., Deuschländer, A., Dillmann, U., Eisner, W., Gruber, D., Hamel, W., Herzog, J., Hilker, R., Klebe, S., Kloß, M., Koy, J., Krause, M., Kupsch, A., Lorenz, D., Lorenzl, S., Mehdorn, H. M., Moringlane, J. R., Oertel, W., Pinski, M. O., Reichmann, H., Reuß, A., Schneider, G.-H., Schnitzler, A., Steude, U., Sturm, V., Timmermann, L., Tronnier, V., Trottenberg, T., Wojtecki, L., Wolf, E., Poewe, W., and Voges, J. (2006). A Randomized Trial of Deep-Brain Stimulation for Parkinson’s Disease. *N. Engl. J. Med.*, 355(9):896–908.
- Deutsche Gesellschaft für Neurologie e.V. (2016). Idiopathisches Parkinson-Syndrom. *Dtsch. Gesellschaft für Neurol. e.V.*
- Diesburg, D. A., Greenlee, J. D., and Wessel, J. R. (2021). Cortico-subcortical β burst dynamics underlying movement cancellation in humans. *Elife*, 10.
- Dimitriadis, S. I., Routley, B., Linden, D. E., and Singh, K. D. (2018). Reliability of static and dynamic network metrics in the resting-state: A MEG-beamformed connectivity analysis. *Front. Neurosci.*, 12(AUG):506.
- Doucet, G., Naveau, M., Petit, L., Delcroix, N., Zago, L., Crivello, F., Jobard, G., Tzourio-Mazoyer, N., Mazoyer, B., Mellet, E., and Joliot, M. (2011). Brain activity at rest: A multiscale hierarchical functional organization. *J. Neurophysiol.*, 105(6):2753–2763.
- Drummond, N. M. and Chen, R. (2020). Deep brain stimulation and recordings: Insights into the contributions of subthalamic nucleus in cognition. *Neuroimage*, 222:117300.
- Einevoll, G. T., Kayser, C., Logothetis, N. K., and Panzeri, S. (2013). Modelling and analysis of local field potentials for studying the function of cortical circuits. *Nat. Rev. Neurosci.*, 14(11):770–785.
- Escudero, J., Hornero, R., Abasolo, D., Fernandez, A., and Lopez-Coronado, M. (2007). Artifact removal in magnetoencephalogram background activity with independent component analysis. *IEEE Trans. Biomed. Eng.*, 54(11):1965–1973.
- Fagaly, R. L. (2006). Superconducting quantum interference device instruments and applications. *Rev. Sci. Instrum.*, 77(10):101101.

- Feingold, J., Gibson, D. J., Depasquale, B., and Graybiel, A. M. (2015). Bursts of beta oscillation differentiate postperformance activity in the striatum and motor cortex of monkeys performing movement tasks. *Proc. Natl. Acad. Sci. U. S. A.*, 112(44):13687–13692.
- Fernandez, L. M. and Lüthi, A. (2020). Sleep spindles: Mechanisms and functions. *Physiol. Rev.*, 100(2):805–868.
- Florin, E. and Baillet, S. (2015). The brain’s resting-state activity is shaped by synchronized cross-frequency coupling of neural oscillations. *Neuroimage*, 111:26–35.
- Florin, E., Watanabe, M., and Logothetis, N. K. (2015). The role of sub-second neural events in spontaneous brain activity. *Curr. Opin. Neurobiol.*, 32:24–30.
- Fonov, V., Evans, A. C., Botteron, K., Almli, C. R., McKinstry, R. C., and Collins, D. L. (2011). Unbiased average age-appropriate atlases for pediatric studies. *Neuroimage*, 54(1):313–327.
- Forkel, S. J., Thiebaut de Schotten, M., Kawadler, J. M., Dell’Acqua, F., Danek, A., and Catani, M. (2014). The anatomy of fronto-occipital connections from early blunt dissections to contemporary tractography. *Cortex*, 56:73–84.
- Fox, M. D. and Raichle, M. E. (2007). Spontaneous fluctuations in brain activity observed with functional magnetic resonance imaging. *Nat. Rev. Neurosci.*, 8(9):700–711.
- Georgy, L., Lewis, J. D., Bezgin, G., Diano, M., Celeghin, A., Evans, A. C., Tamietto, M., and Ptito, A. (2020). Changes in peri-calcarine cortical thickness in blindsight. *Neuropsychologia*, 143:107463.
- Giannicola, G., Rosa, M., Servello, D., Menghetti, C., Carrabba, G., Pacchetti, C., Zangaglia, R., Cogliamarian, F., Scelzo, E., Marceglia, S., Rossi, L., and Priori, A. (2012). Subthalamic local field potentials after seven-year deep brain stimulation in Parkinson’s disease. *Exp. Neurol.*, 237(2):312–317.
- Glover, G. H. (2011). Overview of functional magnetic resonance imaging. *Neurosurg. Clin. N. Am.*, 22(2):133–139.
- Goetz, C. G. (2011). The history of Parkinson’s disease: Early clinical descriptions and neurological therapies. *Cold Spring Harb. Perspect. Med.*, 1(1).
- Goetz, C. G., Tilley, B. C., Shaftman, S. R., Stebbins, G. T., Fahn, S., Martinez-Martin, P., Poewe, W., Sampaio, C., Stern, M. B., Dodel, R., Dubois, B., Holloway, R., Jankovic, J., Kulisevsky, J., Lang, A. E., Lees, A., Leurgans, S., LeWitt, P. A., Nyenhuis, D., Olanow,

- C. W., Rascol, O., Schrag, A., Teresi, J. A., van Hilten, J. J., LaPelle, N., Agarwal, P., Athar, S., Bordelan, Y., Bronte-Stewart, H. M., Camicioli, R., Chou, K., Cole, W., Dalvi, A., Delgado, H., Diamond, A., Dick, J. P., Duda, J., Elble, R. J., Evans, C., Evidente, V. G., Fernandez, H. H., Fox, S., Friedman, J. H., Fross, R. D., Gallagher, D., Goetz, C. G., Hall, D., Hermanowicz, N., Hinson, V., Horn, S., Hurtig, H., Kang, U. J., Kleiner-Fisman, G., Klepitskaya, O., Kompoliti, K., Lai, E. C., Leehey, M. L., Leroi, I., Lyons, K. E., McClain, T., Metzger, S. W., Miyasaki, J., Morgan, J. C., Nance, M., Nemeth, J., Pahwa, R., Parashos, S. A., Schneider, J. S., Sethi, K., Shulman, L. M., Siderowf, A., Silverdale, M., Simuni, T., Stacy, M., Stern, M. B., Stewart, R. M., Sullivan, K., Swope, D. M., Wadia, P. M., Walker, R. W., Walker, R., Weiner, W. J., Wiener, J., Wilkinson, J., Wojcieszek, J. M., Wolfrath, S., Wooten, F., Wu, A., Zesiewicz, T. A., and Zweig, R. M. (2008). Movement Disorder Society-Sponsored Revision of the Unified Parkinson’s Disease Rating Scale (MDS-UPDRS): Scale presentation and clinimetric testing results. *Mov. Disord.*, 23(15):2129–2170.
- Goldberg, I. I., Harel, M., and Malach, R. (2006). When the Brain Loses Its Self: Prefrontal Inactivation during Sensorimotor Processing. *Neuron*, 50(2):329–339.
- Gordon, E. M., Laumann, T. O., Gilmore, A. W., Newbold, D. J., Greene, D. J., Berg, J. J., Ortega, M., Hoyt-Drazen, C., Gratton, C., Sun, H., Hampton, J. M., Coalson, R. S., Nguyen, A. L., McDermott, K. B., Shimony, J. S., Snyder, A. Z., Schlaggar, B. L., Petersen, S. E., Nelson, S. M., and Dosenbach, N. U. (2017). Precision Functional Mapping of Individual Human Brains. *Neuron*, 95(4):791–807.e7.
- Göttlich, M., Münte, T. F., Heldmann, M., Kasten, M., Hagenah, J., and Krämer, U. M. (2013). Altered Resting State Brain Networks in Parkinson’s Disease. *PLoS One*, 8(10):e77336.
- Granziera, C., Pollo, C., Russmann, H., Staedler, C., Ghika, J., Villemure, J. G., Burkhard, P. R., and Vingerhoets, F. J. (2008). Sub-acute delayed failure of subthalamic DBS in Parkinson’s disease: The role of micro-lesion effect. *Park. Relat. Disord.*, 14(2):109–113.
- Gray, C. M., Maldonado, P. E., Wilson, M., and McNaughton, B. (1995). Tetrodes markedly improve the reliability and yield of multiple single-unit isolation from multi-unit recordings in cat striate cortex. *J. Neurosci. Methods*, 63(1-2):43–54.
- Gray, C. M. and Singer, W. (1989). Stimulus-specific neuronal oscillations in orientation columns of cat visual cortex. *Proc. Natl. Acad. Sci. U. S. A.*, 86(5):1698–1702.
- Hadland, K. A., Rushworth, M. F., Gaffan, D., and Passingham, R. E. (2003). The effect of cingulate lesions on social behaviour and emotion. *Neuropsychologia*, 41(8):919–931.

- Hall, E. L., Robson, S. E., Morris, P. G., and Brookes, M. J. (2014). The relationship between MEG and fMRI. *Neuroimage*, 102(P1):80–91.
- Hämäläinen, M., Hari, R., Ilmoniemi, R. J., Knuutila, J., and Lounasmaa, O. V. (1993). Magnetoencephalography theory, instrumentation, and applications to noninvasive studies of the working human brain. *Rev. Mod. Phys.*, 65(2):413–497.
- Hamel, W., Köppen, J. A., Alesch, F., Antonini, A., Barcia, J. A., Bergman, H., Chabardes, S., Contarino, M. F., Cornu, P., Demmel, W., Deuschl, G., Fasano, A., Kühn, A. A., Limousin, P., McIntyre, C. C., Mehdorn, H. M., Pilleri, M., Pollak, P., Rodríguez-Oroz, M. C., Rumià, J., Samuel, M., Timmermann, L., Valldeoriola, F., Vesper, J., Visser-Vandewalle, V., Volkman, J., and Lozano, A. M. (2017). Targeting of the Subthalamic Nucleus for Deep Brain Stimulation: A Survey Among Parkinson Disease Specialists. *World Neurosurg.*, 99:41–46.
- Hammer, M. J., Barlow, S. M., Lyons, K. E., and Pahwa, R. (2010). Subthalamic nucleus deep brain stimulation changes speech respiratory and laryngeal control in Parkinson’s disease. *J. Neurol.*, 257(10):1692–1702.
- Hammond, C., Bergman, H., and Brown, P. (2007). Pathological synchronization in Parkinson’s disease: networks, models and treatments. *Trends Neurosci.*, 30(7):357–364.
- Hannah, R., Muralidharan, V., Sundby, K. K., and Aron, A. R. (2020). Temporally-precise disruption of prefrontal cortex informed by the timing of beta bursts impairs human action-stopping. *Neuroimage*, 222:117222.
- Hansen, P., Kringelbach, M., and Salmelin, R. (2010). *MEG: An introduction to methods*. Oxford University Press.
- Hari, R. (2012). Magnetoencephalography: Methods and applications. *Niedermeyer’s Electroencephalogr. Basic Princ. Clin. Appl. Relat. Fields*, pages 865–900.
- Hartmann, C. J., Fliegen, S., Groiss, S. J., Wojtecki, L., and Schnitzler, A. (2019). An update on best practice of deep brain stimulation in Parkinson’s disease. *Ther. Adv. Neurol. Disord.*, 12.
- Hartmann, C. J., Hirschmann, J., Vesper, J., Wojtecki, L., Butz, M., and Schnitzler, A. (2018). Distinct cortical responses evoked by electrical stimulation of the thalamic ventral intermediate nucleus and of the subthalamic nucleus. *NeuroImage Clin.*, 20:1246–1254.
- Hartwigsen, G., Baumgaertner, A., Price, C. J., Koehnke, M., Ulmer, S., and Siebner, H. R. (2010). Phonological decisions require both the left and right supramarginal gyri. *Proc. Natl. Acad. Sci. U. S. A.*, 107(38):16494–16499.

- Haynes, W. I. and Haber, S. N. (2013). The organization of prefrontal-subthalamic inputs in primates provides an anatomical substrate for both functional specificity and integration: Implications for basal ganglia models and deep brain stimulation. *J. Neurosci.*, 33(11):4804–4814.
- Heinrichs-Graham, E., Santamaria, P. M., Gendelman, H. E., and Wilson, T. W. (2017). The cortical signature of symptom laterality in Parkinson’s disease. *NeuroImage Clin.*, 14:433–440.
- Heinrichs-Graham, E. and Wilson, T. W. (2016). Is an absolute level of cortical beta suppression required for proper movement? Magnetoencephalographic evidence from healthy aging. *Neuroimage*, 134:514–521.
- Heinrichs-Graham, E., Wilson, T. W., Santamaria, P. M., Heithoff, S. K., Torres-Russotto, D., Hutter-Saunders, J. A., Estes, K. A., Meza, J. L., Mosley, R. L., and Gendelman, H. E. (2014). Neuromagnetic evidence of abnormal movement-related beta desynchronization in Parkinson’s disease. *Cereb. Cortex*, 24(10):2669–2678.
- Henson, R. N., Mattout, J., Phillips, C., and Friston, K. J. (2009). Selecting forward models for MEG source-reconstruction using model-evidence. *Neuroimage*, 46(1):168–176.
- Herz, D. M., Bogacz, R., and Brown, P. (2016). Neuroscience: Impaired Decision-Making in Parkinson’s Disease. *Curr. Biol.*, 26(14):R671–R673.
- Hirschmann, J., Özkurt, T. E., Butz, M., Homburger, M., Elben, S., Hartmann, C. J., Vesper, J., Wojtecki, L., and Schnitzler, A. (2011). Distinct oscillatory STN-cortical loops revealed by simultaneous MEG and local field potential recordings in patients with Parkinson’s disease. *Neuroimage*, 55(3):1159–1168.
- Hirschmann, J., Özkurt, T. E., Butz, M., Homburger, M., Elben, S., Hartmann, C. J., Vesper, J., Wojtecki, L., and Schnitzler, A. (2013). Differential modulation of STN-cortical and cortico-muscular coherence by movement and levodopa in Parkinson’s disease. *Neuroimage*, 68:203–213.
- Hohlefeld, F. U., Huchzermeyer, C., Huebl, J., Schneider, G. H., Brücke, C., Schönecker, T., Kühn, A. A., Curio, G., and Nikulin, V. V. (2014). Interhemispheric functional interactions between the subthalamic nuclei of patients with Parkinson’s disease. *Eur. J. Neurosci.*, 40(8):3273–3283.

- Huang, M. X., Mosher, J. C., and Leahy, R. M. (1999). A sensor-weighted overlapping-sphere head model and exhaustive head model comparison for MEG. *Phys. Med. Biol.*, 44(2):423–440.
- Huang, X., Chen, X., Yan, N., Jones, J. A., Wang, E. Q., Chen, L., Guo, Z., Li, W., Liu, P., and Liu, H. (2016). The impact of parkinson’s disease on the cortical mechanisms that support auditory–motor integration for voice control. *Hum. Brain Mapp.*, 37(12):4248–4261.
- Hughes, A. J., Daniel, S. E., Kilford, L., and Lees, A. J. (1992). Accuracy of clinical diagnosis of idiopathic Parkinson’s disease: A clinico-pathological study of 100 cases. *J. Neurol. Neurosurg. Psychiatry*, 55(3):181–184.
- Iskhakova, L., Rappel, P., Deffains, M., Fonar, G., Marmor, O., Paz, R., Israel, Z., Eitan, R., and Bergman, H. (2021). Modulation of dopamine tone induces frequency shifts in cortico-basal ganglia beta oscillations. *Nat. Commun.*, 12(1):1–17.
- Jakobs, M., Fomenko, A., Lozano, A. M., and Kiening, K. L. (2019). Cellular, molecular, and clinical mechanisms of action of deep brain stimulation—a systematic review on established indications and outlook on future developments. *EMBO Mol. Med.*, 11(4):e9575.
- Jankovic, J. and Kapadia, A. S. (2001). Functional decline in Parkinson disease. *Arch. Neurol.*, 58(10):1611–1615.
- Jech, R., Mueller, K., Uργοšík, D., Sieger, T., Holiga, Š., Růžička, F., Dušek, P., Havránková, P., Vymazal, J., and Růžička, E. (2012). The Subthalamic Microlesion Story in Parkinson’s Disease: Electrode Insertion-Related Motor Improvement with Relative Cortico-Subcortical Hypoactivation in fMRI. *PLoS One*, 7(11):e49056.
- Jellinger, K. A. (2015). Neuropathobiology of non-motor symptoms in Parkinson disease. *J. Neural Transm.*, 122(10):1429–1440.
- Jones, S. R. (2016). When brain rhythms aren’t ‘rhythmic’: implication for their mechanisms and meaning. *Curr. Opin. Neurobiol.*, 40:72–80.
- Josephs, O. and Henson, R. N. (1999). Event-related functional magnetic resonance imaging: Modelling, inference and optimization. *Philos. Trans. R. Soc. B Biol. Sci.*, 354(1387):1215–1228.
- Katzner, S., Nauhaus, I., Benucci, A., Bonin, V., Ringach, D. L., and Carandini, M. (2009). Local Origin of Field Potentials in Visual Cortex. *Neuron*, 61(1):35–41.

- Kehnemouyi, Y. M., Wilkins, K. B., Anidi, C. M., Anderson, R. W., Afzal, M. F., and Bronte-Stewart, H. M. (2021). Modulation of beta bursts in subthalamic sensorimotor circuits predicts improvement in bradykinesia. *Brain*, 144(2):473–486.
- Kim, K. and Lee, C. (2017). Activity of primate V1 neurons during the gap saccade task. *J. Neurophysiol.*, 118(2):1361–1375.
- Kish, S. J., Shannak, K., and Hornykiewicz, O. (1988). Uneven Pattern of Dopamine Loss in the Striatum of Patients with Idiopathic Parkinson’s Disease. *N. Engl. J. Med.*, 318(14):876–880.
- Klein, A., Ghosh, S. S., Bao, F. S., Giard, J., Häme, Y., Stavsky, E., Lee, N., Rossa, B., Reuter, M., Chaibub Neto, E., and Keshavan, A. (2017). Mindboggling morphometry of human brains. *PLoS Comput. Biol.*, 13(2):e1005350.
- Koirala, N., Serrano, L., Paschen, S., Falk, D., Anwar, A. R., Kuravi, P., Deuschl, G., Groppa, S., and Muthuraman, M. (2020). Mapping of subthalamic nucleus using microelectrode recordings during deep brain stimulation. *Sci. Rep.*, 10(1):1–12.
- Kreiman, G., Hung, C. P., Kraskov, A., Quiroga, R. Q., Poggio, T., and DiCarlo, J. J. (2006). Object selectivity of local field potentials and spikes in the macaque inferior temporal cortex. *Neuron*, 49(3):433–445.
- Kringelbach, M. L., Jenkinson, N., Owen, S. L., and Aziz, T. Z. (2007). Translational principles of deep brain stimulation. *Nat. Rev. Neurosci.*, 8(8):623–635.
- Krüger, R., Hilker, R., Winkler, C., Lorrain, M., Hahne, M., Redecker, C., Lingor, P., and Jost, W. H. (2016). Advanced stages of PD: interventional therapies and related patient-centered care. *J. Neural Transm.*, 123(1):31–43.
- Kühn, A. A., Doyle, L., Pogosyan, A., Yarrow, K., Kupsch, A., Schneider, G. H., Hariz, M. I., Trottenberg, T., and Brown, P. (2006). Modulation of beta oscillations in the subthalamic area during motor imagery in Parkinson’s disease. *Brain*, 129(3):695–706.
- Kühn, A. A., Tsui, A., Aziz, T., Ray, N., Brücke, C., Kupsch, A., Schneider, G. H., and Brown, P. (2009). Pathological synchronisation in the subthalamic nucleus of patients with Parkinson’s disease relates to both bradykinesia and rigidity. *Exp. Neurol.*, 215(2):380–387.
- Kühn, A. A., Williams, D., Kupsch, A., Limousin, P., Hariz, M., Schneider, G. H., Yarrow, K., and Brown, P. (2004). Event-related beta desynchronization in human subthalamic nucleus correlates with motor performance. *Brain*, 127(4):735–746.

- Kuncel, A. M. and Grill, W. M. (2004). Selection of stimulus parameters for deep brain stimulation. *Clin. Neurophysiol.*, 115(11):2431–2441.
- Lambert, C., Zrinzo, L., Nagy, Z., Lutti, A., Hariz, M., Foltynie, T., Draganski, B., Ashburner, J., and Frackowiak, R. (2012). Confirmation of functional zones within the human subthalamic nucleus: Patterns of connectivity and sub-parcellation using diffusion weighted imaging. *Neuroimage*, 60(1):83–94.
- Lanciego, J. L., Luquin, N., and Obeso, J. A. (2012). Functional neuroanatomy of the basal ganglia. *Cold Spring Harb. Perspect. Med.*, 2(12).
- Lang, A. E. and Lozano, A. M. (1998). Parkinson’s disease. First of two parts. *N. Engl. J. Med.*, 339(15):1044–53.
- Larsson, J. and Heeger, D. J. (2006). Two retinotopic visual areas in human lateral occipital cortex. *J. Neurosci.*, 26(51):13128–13142.
- Le Goff, F., Derrey, S., Lefaucheur, R., Borden, A., Fetter, D., Jan, M., Wallon, D., and Maltête, D. (2015). Decline in verbal fluency after subthalamic nucleus deep brain stimulation in Parkinson’s disease: A microlesion effect of the electrode trajectory? *J. Parkinsons. Dis.*, 5(1):95–104.
- Leahy, R. M., Mosher, J. C., Spencer, M. E., Huang, M. X., and Lewine, J. D. (1998). A study of dipole localization accuracy for MEG and EEG using a human skull phantom. *Electroencephalogr. Clin. Neurophysiol.*, 107(2):159–173.
- Ledonne, A. and Mercuri, N. B. (2017). Current concepts on the physiopathological relevance of dopaminergic receptors. *Front. Cell. Neurosci.*, 11:27.
- Lee, T. K. and Yankee, E. L. (2022). A review on Parkinson’s disease treatment. *Neuroimmunol. Neuroinflammation*, 8:222.
- Lettieri, C., Rinaldo, S., Devigili, G., Pualetto, G., Verriello, L., Budai, R., Fadiga, L., Oliynyk, A., Mondani, M., D’Auria, S., Skrap, M., and Eleopra, R. (2012). Deep brain stimulation: Subthalamic nucleus electrophysiological activity in awake and anesthetized patients. *Clin. Neurophysiol.*, 123(12):2406–2413.
- Levy, R., Ashby, P., Hutchison, W. D., Lang, A. E., Lozano, A. M., and Dostrovsky, J. O. (2002). Dependence of subthalamic nucleus oscillations on movement and dopamine in Parkinson’s disease. *Brain*, 125(6):1196–1209.

- Little, S., Bonaiuto, J., Barnes, G., and Bestmann, S. (2019). Human motor cortical beta bursts relate to movement planning and response errors. *PLoS Biol.*, 17(10):e3000479.
- Little, S. and Brown, P. (2014). The functional role of beta oscillations in Parkinson’s disease. *Park. Relat. Disord.*, 20(SUPPL.1):S44–S48.
- Little, S., Pogosyan, A., Kuhn, A. A., and Brown, P. (2012). Beta band stability over time correlates with Parkinsonian rigidity and bradykinesia. *Exp. Neurol.*, 236(2):383–388.
- Little, S., Pogosyan, A., Neal, S., Zavala, B., Zrinzo, L., Hariz, M., Foltynie, T., Limousin, P., Ashkan, K., FitzGerald, J., Green, A. L., Aziz, T. Z., and Brown, P. (2013). Adaptive deep brain stimulation in advanced Parkinson disease. *Ann. Neurol.*, 74(3):449–457.
- Litvak, V., Eusebio, A., Jha, A., Oostenveld, R., Barnes, G. R., Penny, W. D., Zrinzo, L., Hariz, M. I., Limousin, P., Friston, K. J., and Brown, P. (2010). Optimized beamforming for simultaneous MEG and intracranial local field potential recordings in deep brain stimulation patients. *Neuroimage*, 50(4):1578–1588.
- Llinás, R. R. (1988). The intrinsic electrophysiological properties of mammalian neurons: Insights into central nervous system function. *Science (80-.)*, 242(4886):1654–1664.
- Lobb, C. J. (2014). Abnormal bursting as a pathophysiological mechanism in Parkinson’s disease. *Basal Ganglia*, 3(4):187–195.
- Lofredi, R., Tan, H., Neumann, W. J., Yeh, C. H., Schneider, G. H., Kühn, A. A., and Brown, P. (2019). Beta bursts during continuous movements accompany the velocity decrement in Parkinson’s disease patients. *Neurobiol. Dis.*, 127:462–471.
- Logothetis, N. K., Eschenko, O., Murayama, Y., Augath, M., Steudel, T., Evrard, H. C., Besserve, M., and Oeltermann, A. (2012). Hippocampal-cortical interaction during periods of subcortical silence. *Nature*, 491(7425):547–553.
- Lopes da Silva, F. (2013). EEG and MEG: Relevance to neuroscience. *Neuron*, 80(5):1112–1128.
- Luo, B., Lu, Y., Qiu, C., Dong, W., Xue, C., Zhang, L., Liu, W., and Zhang, W. (2021). Altered Spontaneous Neural Activity and Functional Connectivity in Parkinson’s Disease With Subthalamic Microlesion. *Front. Neurosci.*, 15:913.
- Luschnig, M. (2021). Parkinson-Krankheit und atypische Parkinson-Syndrome. *Psychopraxis. Neuropraxis*, 24(3):184–191.

- Machielsen, W. C., Rombouts, S. A., Barkhof, F., Scheltens, P., and Witter, M. P. (2000). fMRI of visual encoding: Reproducibility of activation. *Hum. Brain Mapp.*, 9(3):156–164.
- Maling, N., Lempka, S. F., Blumenfeld, Z., Bronte-Stewart, H., and McIntyre, C. C. (2018). Biophysical basis of subthalamic local field potentials recorded from deep brain stimulation electrodes. *J. Neurophysiol.*, 120(4):1932–1944.
- Maltête, D., Derrey, S., Chastan, N., Debono, B., Gérardin, E., Fréger, P., Mihout, B., Menard, J. F., and Hannequin, D. (2008). Microsubthalamotomy: An immediate predictor of long-term subthalamic stimulation efficacy in Parkinson disease. *Mov. Disord.*, 23(7):1047–1050.
- Mann, J. M., Foote, K. D., Garvan, C. W., Fernandez, H. H., Jacobson IV, C. E., Rodriguez, R. L., Haq, I. U., Siddiqui, M. S., Malaty, I. A., Morishita, T., Hass, C. J., and Okun, M. S. (2009). Brain penetration effects of microelectrodes and DBS leads in STN or GPi. *J. Neurol. Neurosurg. Psychiatry*, 80(7):794–797.
- Mantini, D., Perrucci, M. G., Del Gratta, C., Romani, G. L., and Corbetta, M. (2007). Electrophysiological signatures of resting state networks in the human brain. *Proc. Natl. Acad. Sci. U. S. A.*, 104(32):13170–13175.
- Marmor, O., Valsky, D., Joshua, M., Bick, A. S., Arkadir, D., Tamir, I., Bergman, H., Israel, Z., and Eitan, R. (2017). Local vs. Volume conductance activity of field potentials in the human subthalamic nucleus. *J. Neurophysiol.*, 117(6):2140–2151.
- Marsden, J. F., Limousin-Dowsey, P., Ashby, P., Pollak, P., and Brown, P. (2001). Subthalamic nucleus, sensorimotor cortex and muscle interrelationships in Parkinson’s disease. *Brain*, 124(2):378–388.
- Mashour, G. A., Palanca, B. J., Basner, M., Li, D., Wang, W., Blain-Moraes, S., Lin, N., Maier, K., Muench, M., Tarnal, V., Vanini, G., Ochroch, E. A., Hogg, R., Schwartz, M., Maybrier, H., Hardie, R., Janke, E., Golmirzaie, G., Picton, P., McKinstry-Wu, A. R., Avidan, M. S., and Kelz, M. B. (2021). Recovery of consciousness and cognition after general anesthesia in humans. *Elife*, 10.
- Mathai, A., Ma, Y., Paré, J. F., Villalba, R. M., Wichmann, T., and Smith, Y. (2015). Reduced cortical innervation of the subthalamic nucleus in MPTP-treated parkinsonian monkeys. *Brain*, 138(4):946–962.

- Mazzoni, A., Rosa, M., Carpaneto, J., Romito, L. M., Priori, A., and Micera, S. (2018). Subthalamic neural activity patterns anticipate economic risk decisions in gambling. *eNeuro*, 5(1).
- Mazzoni, P., Shabbott, B., and Cortés, J. C. (2012). Motor control abnormalities in Parkinson’s disease. *Cold Spring Harb. Perspect. Med.*, 2(6).
- McCusker, M. C., Wiesman, A. I., Spooner, R. K., Santamaria, P. M., McKune, J., Heinrichs-Graham, E., and Wilson, T. W. (2021). Altered neural oscillations during complex sequential movements in patients with Parkinson’s disease. *NeuroImage Clin.*, 32:102892.
- McGregor, M. M. and Nelson, A. B. (2019). Circuit Mechanisms of Parkinson’s Disease. *Neuron*, 101(6):1042–1056.
- Miller, E. K., Lundqvist, M., and Bastos, A. M. (2018). Working Memory 2.0. *Neuron*, 100(2):463–475.
- Mimura, M., Oeda, R., and Kawamura, M. (2006). Impaired decision-making in Parkinson’s disease. *Park. Relat. Disord.*, 12(3):169–175.
- Miocinovic, S., de Hemptinne, C., Chen, W., Isbaine, F., Willie, J. T., Ostrem, J. L., and Starr, P. A. (2018). Cortical potentials evoked by subthalamic stimulation demonstrate a short latency hyperdirect pathway in humans. *J. Neurosci.*, 38(43):9129–9141.
- Moran, A., Bar-Gad, I., Bergman, H., and Israel, Z. (2006). Real-time refinement of subthalamic nucleus targeting using Bayesian decision-making on the root mean square measure. *Mov. Disord.*, 21(9):1425–1431.
- Moretti, R., Milner, V., Caruso, P., Gazzin, S., and Rumiati, R. (2017). Frontal Tasks and Behavior in Rigid or Tremor-Dominant Parkinson Disease. *Am. J. Alzheimers. Dis. Other Demen.*, 32(5):300–306.
- Mosher, J. C., Leahy, R. M., and Lewis, P. S. (1999). EEG and MEG: Forward solutions for inverse methods. *IEEE Trans. Biomed. Eng.*, 46(3):245–259.
- Moustafa, A. A., Chakravarthy, S., Phillips, J. R., Gupta, A., Keri, S., Polner, B., Frank, M. J., and Jahanshahi, M. (2016). Motor symptoms in Parkinson’s disease: A unified framework. *Neurosci. Biobehav. Rev.*, 68:727–740.
- Mueller, K., Jech, R., Růžička, F., Holiga, Š., Ballarini, T., Bezdicek, O., Möller, H. E., Vymazal, J., Růžička, E., Schroeter, M. L., and Urgošík, D. (2018). Brain connectivity changes

- when comparing effects of subthalamic deep brain stimulation with levodopa treatment in Parkinson’s disease. *NeuroImage Clin.*, 19:1025–1035.
- Mueller, K., Urgošik, D., Ballarini, T., Holiga, Š., Möller, H. E., Růžička, F., Roth, J., Vymazal, J., Schroeter, M. L., Růžička, E., and Jech, R. (2020). Differential effects of deep brain stimulation and levodopa on brain activity in Parkinson’s disease. *Brain Commun.*, 2(1).
- Müller, C. M., De Vos, R. A., Maurage, C. A., Thal, D. R., Tolnay, M., and Braak, H. (2005). Staging of sporadic Parkinson disease-related α -synuclein pathology: Inter- and intra-rater reliability. *J. Neuropathol. Exp. Neurol.*, 64(7):623–628.
- Mullin, S. and Schapira, A. H. (2015). Pathogenic Mechanisms of Neurodegeneration in Parkinson Disease. *Neurol. Clin.*, 33(1):1–17.
- Nambu, A., Takada, M., Inase, M., and Tokuno, H. (1996). Dual somatotopical representations in the primate subthalamic nucleus: Evidence for ordered but reversed body-map transformations from the primary motor cortex and the supplementary motor area. *J. Neurosci.*, 16(8):2671–2683.
- Neumann, W. J., Degen, K., Schneider, G. H., Brücke, C., Huebl, J., Brown, P., and Kühn, A. A. (2016). Subthalamic synchronized oscillatory activity correlates with motor impairment in patients with Parkinson’s disease. *Mov. Disord.*, 31(11):1748–1751.
- Neumann, W. J., Huebl, J., Brücke, C., Gabriëls, L., Bajbouj, M., Merkl, A., Schneider, G. H., Nuttin, B., Brown, P., and Kühn, A. A. (2014). Different patterns of local field potentials from limbic DBS targets in patients with major depressive and obsessive compulsive disorder. *Mol. Psychiatry*, 19(11):1186–1192.
- Neumann, W. J., Staub-Bartelt, F., Horn, A., Schanda, J., Schneider, G. H., Brown, P., and Kühn, A. A. (2017). Long term correlation of subthalamic beta band activity with motor impairment in patients with Parkinson’s disease. *Clin. Neurophysiol.*, 128(11):2286–2291.
- Nolte, G. (2003). The magnetic lead field theorem in the quasi-static approximation and its use for magnetoencephalography forward calculation in realistic volume conductors. *Phys. Med. Biol.*, 48(22):3637–3652.
- Ogawa, S., Menon, R. S., Kim, S. G., and Ugurbil, K. (1998). On the characteristics of functional magnetic resonance imaging of the brain. *Annu. Rev. Biophys. Biomol. Struct.*, 27:447–474.

- O’Keefe, J. and Nadel, L. (1979). Précis of O’Keefe & Nadel’s The hippocampus as a cognitive map. *Behav. Brain Sci.*, 2(4):487–494.
- O’Keefe, A. B., Malekmohammadi, M., Sparks, H., and Pouratian, N. (2020). Synchrony drives motor cortex beta bursting, waveform dynamics, and phase-amplitude coupling in parkinson’s disease. *J. Neurosci.*, 40(30):5833–5846.
- Oswal, A., Beudel, M., Zrinzo, L., Limousin, P., Hariz, M., Foltynie, T., Litvak, V., and Brown, P. (2016). Deep brain stimulation modulates synchrony within spatially and spectrally distinct resting state networks in Parkinson’s disease. *Brain*, 139(5):1482–1496.
- Oswal, A., Cao, C., Yeh, C. H., Neumann, W. J., Gratwicke, J., Akram, H., Horn, A., Li, D., Zhan, S., Zhang, C., Wang, Q., Zrinzo, L., Foltynie, T., Limousin, P., Bogacz, R., Sun, B., Husain, M., Brown, P., and Litvak, V. (2021). Neural signatures of hyperdirect pathway activity in Parkinson’s disease. *Nat. Commun.*, 12(1):1–14.
- Özkurt, T. E. and Schnitzler, A. (2011). A critical note on the definition of phase-amplitude cross-frequency coupling. *J. Neurosci. Methods*, 201(2):438–443.
- Pantazatos, S. P., Yanagihara, T. K., Zhang, X., Meitzler, T., and Hirsch, J. (2012). Frontal–Occipital Connectivity During Visual Search. *Brain Connect.*, 2(3):164–175.
- Parent, A. and Hazrati, L. N. (1995a). Functional anatomy of the basal ganglia. I. The cortico-basal ganglia-thalamo-cortical loop. *Brain Res. Rev.*, 20(1):91–127.
- Parent, A. and Hazrati, L. N. (1995b). Functional anatomy of the basal ganglia. II. The place of subthalamic nucleus and external pallidum in basal ganglia circuitry. *Brain Res. Rev.*, 20(1):128–154.
- Parker, J. G., Zalusky, E. J., and Kirbas, C. (2014). Functional MRI mapping of visual function and selective attention for performance assessment and presurgical planning using conjunctive visual search. *Brain Behav.*, 4(2):227–237.
- Pauls, K. A. M., Korsun, O., Nenonen, J., Nurminen, J., Liljeström, M., Kujala, J., Pekkonen, E., and Renvall, H. (2022). Cortical beta burst dynamics are altered in Parkinson’s disease but normalized by deep brain stimulation. *Neuroimage*, 257:119308.
- Pellegrino, G., Schuler, A. L., Arcara, G., Di Pino, G., Piccione, F., and Kobayashi, E. (2022). Resting state network connectivity is attenuated by fMRI acoustic noise. *Neuroimage*, 247:118791.

- Pelzer, E. A., Sharma, A., and Florin, E. (2021). Evaluation of data-driven MEG analysis approaches for the extraction of fMRI resting state networks. *bioRxiv*, page 2021.04.29.441916.
- Pfurtscheller, G. and Lopes Da Silva, F. H. (1999). Event-related EEG/MEG synchronization and desynchronization: Basic principles. *Clin. Neurophysiol.*, 110(11):1842–1857.
- Poewe, W., Seppi, K., Tanner, C. M., Halliday, G. M., Brundin, P., Volkman, J., Schrag, A. E., and Lang, A. E. (2017). Parkinson disease. *Nat. Rev. Dis. Prim.*, 3(1):1–21.
- Pollanen, M. S., Dickson, D. W., and Bergeron, C. (1993). Pathology and biology of the lewy body. *J. Neuropathol. Exp. Neurol.*, 52(3):183–191.
- Pollok, B. and Schnitzler, A. (2010). Grundlagen und Anwendung der Magnetenzephalographie. *Neurophysiologie-Labor*, 32(2):109–121.
- Pourfar, M., Tang, C., Lin, T., Dhawan, V., Kaplitt, M. G., and Eidelberg, D. D. (2009). Assessing the microlesion effect of subthalamic deep brain stimulation surgery with FDG PET: Clinical article. *J. Neurosurg.*, 110(6):1278–1282.
- Priori, A., Foffani, G., Pesenti, A., Tamma, F., Bianchi, A. M., Pellegrini, M., Locatelli, M., Moxon, K. A., and Villani, R. M. (2004). Rhythm-specific pharmacological modulation of subthalamic activity in Parkinson’s disease. *Exp. Neurol.*, 189(2):369–379.
- Priori, A., Foffani, G., Rossi, L., and Marceglia, S. (2013). Adaptive deep brain stimulation (aDBS) controlled by local field potential oscillations. *Exp. Neurol.*, 245:77–86.
- Proudfoot, M., Woolrich, M. W., Nobre, A. C., and Turner, M. R. (2014). Magnetoencephalography. *Pract. Neurol.*, 14(5):336–343.
- Przedborski, S. (2017). The two-century journey of Parkinson disease research. *Nat. Rev. Neurosci.*, 18(4):251–259.
- Qasim, S. E., de Hemptinne, C., Swann, N. C., Miocinovic, S., Ostrem, J. L., and Starr, P. A. (2016). Electrocorticography reveals beta desynchronization in the basal ganglia-cortical loop during rest tremor in Parkinson’s disease. *Neurobiol. Dis.*, 86:177–186.
- Quinn, A. J., van Ede, F., Brookes, M. J., Heideman, S. G., Nowak, M., Seedat, Z. A., Vidaurre, D., Zich, C., Nobre, A. C., and Woolrich, M. W. (2019). Unpacking Transient Event Dynamics in Electrophysiological Power Spectra. *Brain Topogr.*, 32(6):1020–1034.
- Raichle, M. E. and Mintun, M. A. (2006). Brain work and brain imaging. *Annu. Rev. Neurosci.*, 29:449–476.

- Rajput, A. H., Voll, A., Rajput, M. L., Robinson, C. A., and Rajput, A. (2009). Course in parkinson disease subtypes: A 39-year clinicopathologic study. *Neurology*, 73(3):206–212.
- Ray, N. J., Jenkinson, N., Wang, S., Holland, P., Brittain, J. S., Joint, C., Stein, J. F., and Aziz, T. (2008). Local field potential beta activity in the subthalamic nucleus of patients with Parkinson’s disease is associated with improvements in bradykinesia after dopamine and deep brain stimulation. *Exp. Neurol.*, 213(1):108–113.
- Remy, P., Doder, M., Lees, A., Turjanski, N., and Brooks, D. (2005). Depression in Parkinson’s disease: Loss of dopamine and noradrenaline innervation in the limbic system. *Brain*, 128(6):1314–1322.
- Rizzone, M. G., Ferrarin, M., Lanotte, M. M., Lopiano, L., and Carpinella, I. (2017). The dominant-subthalamic nucleus phenomenon in bilateral deep brain stimulation for Parkinson’s disease: Evidence from a gait analysis study. *Front. Neurol.*, 8(OCT):575.
- Roland, J. L., Snyder, A. Z., Hacker, C. D., Mitra, A., Shimony, J. S., Limbrick, D. D., Raichle, M. E., Smyth, M. D., and Leuthardt, E. C. (2017). On the role of the corpus callosum in interhemispheric functional connectivity in humans. *Proc. Natl. Acad. Sci. U. S. A.*, 114(50):13278–13283.
- Rolls, E. T., Cheng, W., and Feng, J. (2020). The orbitofrontal cortex: Reward, emotion and depression. *Brain Commun.*, 2(2).
- Rosa, M., Fumagalli, M., Giannicola, G., Marceglia, S., Lucchiari, C., Servello, D., Franzini, A., Pacchetti, C., Romito, L., Albanese, A., Porta, M., Pravettoni, G., and Priori, A. (2013). Pathological gambling in Parkinson’s disease: Subthalamic oscillations during economics decisions. *Mov. Disord.*, 28(12):1644–1652.
- Roskies, A. L., Fiez, J. A., Balota, D. A., Raichle, M. E., and Petersen, S. E. (2001). Task-dependent modulation of regions in the left inferior frontal cortex during semantic processing. *J. Cogn. Neurosci.*, 13(6):829–843.
- Rozanski, V. E., Lieb, M., Vollmar, C., Mehrkens, J. H., and Bötzel, K. (2012). Evidence of a non-motor microlesion effect following deep brain surgery: A case report. *Acta Neurochir. (Wien)*, 154(5):835–838.
- Sadasivan, P. K. and Narayana Dutt, D. (1996). SVD based technique for noise reduction in electroencephalographic signals. *Signal Processing*, 55(2):179–189.
- Samii, A., Nutt, J. G., and Ransom, B. R. (2004). Parkinson’s disease. *Lancet*, 363(9423):1783–1793.

- Schneider, L., Seeger, V., Timmermann, L., and Florin, E. (2020). Electrophysiological resting state networks of predominantly akinetic-rigid Parkinson patients: Effects of dopamine therapy. *NeuroImage Clin.*, 25:102147.
- Schnitzler, A. and Gross, J. (2005). Normal and pathological oscillatory communication in the brain. *Nat. Rev. Neurosci.*, 6(4):285–296.
- Seedat, Z. A., Quinn, A. J., Vidaurre, D., Liuzzi, L., Gascoyne, L. E., Hunt, B. A., O’Neill, G. C., Pakenham, D. O., Mullinger, K. J., Morris, P. G., Woolrich, M. W., and Brookes, M. J. (2020). The role of transient spectral ‘bursts’ in functional connectivity: A magnetoencephalography study. *Neuroimage*, 209:116537.
- Seitzman, B. A., Snyder, A. Z., Leuthardt, E. C., and Shimony, J. S. (2019). The State of Resting State Networks. *Top. Magn. Reson. Imaging*, 28(4):189–196.
- Sharma, A., Vidaurre, D., Vesper, J., Schnitzler, A., and Florin, E. (2021). Differential dopaminergic modulation of spontaneous cortico–subthalamic activity in parkinson’s disease. *Elife*, 10.
- Sharon, D., Hämäläinen, M. S., Tootell, R. B., Halgren, E., and Belliveau, J. W. (2007). The advantage of combining MEG and EEG: Comparison to fMRI in focally stimulated visual cortex. *Neuroimage*, 36(4):1225–1235.
- Shin, H., Law, R., Tsutsui, S., Moore, C. I., and Jones, S. R. (2017). The rate of transient beta frequency events predicts behavior across tasks and species. *Elife*, 6.
- Siapas, A. G. and Wilson, M. A. (1998). Coordinated interactions between hippocampal ripples and cortical spindles during slow-wave sleep. *Neuron*, 21(5):1123–1128.
- Singh, A., Kammermeier, S., Mehrkens, J. H., and Bötzel, K. (2012). Movement kinematic after deep brain stimulation associated microlesions. *J. Neurol. Neurosurg. Psychiatry*, 83(10):1022–1026.
- Skorvanek, M., Martinez-Martin, P., Kovacs, N., Rodriguez-Violante, M., Corvol, J. C., Taba, P., Seppi, K., Levin, O., Schrag, A., Foltynie, T., Alvarez-Sanchez, M., Arakaki, T., Aschermann, Z., Aviles-Olmos, I., Benchetrit, E., Benoit, C., Bergareche-Yarza, A., Cervantes-Arriaga, A., Chade, A., Cormier, F., Datieva, V., Gallagher, D. A., Garretto, N., Gdovnova, Z., Gershanik, O., Grofik, M., Han, V., Huang, J., Kadastik-Eerme, L., Kurtis, M. M., Mangone, G., Martinez-Castrillo, J. C., Mendoza-Rodriguez, A., Minar, M., Moore, H. P., Muldmaa, M., Mueller, C., Pinter, B., Poewe, W., Rallmann, K., Reiter, E., Rodriguez-Blazquez, C., Singer, C., Tilley, B. C., Valkovic, P., Goetz, C. G., and Stebbins, G. T.

- (2017). Differences in MDS-UPDRS Scores Based on Hoehn and Yahr Stage and Disease Duration. *Mov. Disord. Clin. Pract.*, 4(4):536–544.
- Smith, S. M., Fox, P. T., Miller, K. L., Glahn, D. C., Fox, P. M., Mackay, C. E., Filippini, N., Watkins, K. E., Toro, R., Laird, A. R., and Beckmann, C. F. (2009). Correspondence of the brain’s functional architecture during activation and rest. *Proc. Natl. Acad. Sci. U. S. A.*, 106(31):13040–13045.
- Steriade, M. (1998). Slow sleep oscillation, rhythmic K-complexes, and their paroxysmal developments. *J. Sleep Res.*, 7(SUPPL. 1):30–35.
- Sterio, D., Zonenshayn, M., Mogilner, A. Y., Rezai, A. R., Kiproviski, K., Kelly, P. J., and Beric, A. (2002). Neurophysiological refinement of subthalamic nucleus targeting. *Neurosurgery*, 50(1):58–67.
- Stute, W. (1996). The jackknife estimate of variance of a Kaplan-Meier integral. *Ann. Stat.*, 24(6):2679–2704.
- Sure, M., Vesper, J., Schnitzler, A., and Florin, E. (2021). Dopaminergic Modulation of Spectral and Spatial Characteristics of Parkinsonian Subthalamic Nucleus Beta Bursts. *Front. Neurosci.*, 15:1450.
- Swann, N., Poizner, H., Houser, M., Gould, S., Greenhouse, I., Cai, W., Strunk, J., George, J., and Aron, A. R. (2011). Deep brain stimulation of the subthalamic nucleus alters the cortical profile of response inhibition in the beta frequency band: A scalp EEG study in parkinson’s disease. *J. Neurosci.*, 31(15):5721–5729.
- Tadel, F., Baillet, S., Mosher, J. C., Pantazis, D., and Leahy, R. M. (2011). Brainstorm: A user-friendly application for MEG/EEG analysis. *Comput. Intell. Neurosci.*, 2011:879716.
- Tadel, F., Bock, E., Niso, G., Mosher, J. C., Cousineau, M., Pantazis, D., Leahy, R. M., and Baillet, S. (2019). MEG/EEG group analysis with brainstorm. *Front. Neurosci.*, 13(FEB):76.
- Tallon-Baudry, C., Bertrand, O., Delpuech, C., and Pernier, J. (1997). Oscillatory γ -band (30-70 Hz) activity induced by a visual search task in humans. *J. Neurosci.*, 17(2):722–734.
- Tamir, I., Wang, D., Chen, W., Ostrem, J. L., Starr, P. A., and de Hemptinne, C. (2020). Eight cylindrical contact lead recordings in the subthalamic region localize beta oscillations source to the dorsal STN. *Neurobiol. Dis.*, 146:105090.

- Tamma, F., Caputo, E., Chiesa, V., Egidi, M., Locatelli, M., Rampini, P., Cinnante, C., Pesi, A., and Priori, A. (2002). Anatomico-clinical correlation of intraoperative stimulation-induced side-effects during HF-DBS of the subthalamic nucleus. *Neurol. Sci.*, 23(SUPPL. 2):s109–s110.
- Tanaka, M., Yanagisawa, T., Fukuma, R., Tani, N., Oshino, S., Mihara, M., Hattori, N., Kajiyama, Y., Hashimoto, R., Ikeda, M., Mochizuki, H., and Kishima, H. (2022). Magnetoencephalography detects phase-amplitude coupling in Parkinson’s disease. *Sci. Rep.*, 12(1):1–14.
- Taulu, S. and Kajola, M. (2005). Presentation of electromagnetic multichannel data: The signal space separation method. *J. Appl. Phys.*, 97(12):124905.
- Taulu, S. and Simola, J. (2006). Spatiotemporal signal space separation method for rejecting nearby interference in MEG measurements. *Phys. Med. Biol.*, 51(7):1759–1768.
- Temel, Y., Visser-Vandewalle, V., and Carpenter, R. H. (2008). Saccadic latency during electrical stimulation of the human subthalamic nucleus. *Curr. Biol.*, 18(10):R412–R414.
- Tesche, C. D., Uusitalo, M. A., Ilmoniemi, R. J., Huotilainen, M., Kajola, M., and Salonen, O. (1995). Signal-space projections of MEG data characterize both distributed and well-localized neuronal sources. *Electroencephalogr. Clin. Neurophysiol.*, 95(3):189–200.
- Tessitore, A., Amboni, M., Esposito, F., Russo, A., Picillo, M., Marcuccio, L., Pellicchia, M. T., Vitale, C., Cirillo, M., Tedeschi, G., and Barone, P. (2012a). Resting-state brain connectivity in patients with Parkinson’s disease and freezing of gait. *Park. Relat. Disord.*, 18(6):781–787.
- Tessitore, A., Esposito, F., Vitale, C., Santangelo, G., Amboni, M., Russo, A., Corbo, D., Cirillo, G., Barone, P., and Tedeschi, G. (2012b). Default-mode network connectivity in cognitively unimpaired patients with Parkinson disease. *Neurology*, 79(23):2226–2232.
- Thomas Yeo, B. T., Krienen, F. M., Sepulcre, J., Sabuncu, M. R., Lashkari, D., Hollinshead, M., Roffman, J. L., Smoller, J. W., Zöllei, L., Polimeni, J. R., Fisch, B., Liu, H., and Buckner, R. L. (2011). The organization of the human cerebral cortex estimated by intrinsic functional connectivity. *J. Neurophysiol.*, 106(3):1125–1165.
- Thompson, J. A., Lanctin, D., Ince, N. F., and Abosch, A. (2014). Clinical implications of local field potentials for understanding and treating movement disorders. *Stereotact. Funct. Neurosurg.*, 92(4):251–263.

- Tillage, R. P., Wilson, G. E., Cameron Liles, L., Holmes, P. V., and Weinschenker, D. (2020). Chronic environmental or genetic elevation of galanin in noradrenergic neurons confers stress resilience in mice. *J. Neurosci.*, 40(39):7464–7474.
- Tinkhauser, G., Pogosyan, A., Debove, I., Nowacki, A., Shah, S. A., Seidel, K., Tan, H., Brittain, J. S., Petermann, K., di Biase, L., Oertel, M., Pollo, C., Brown, P., and Schuepbach, M. (2018a). Directional local field potentials: A tool to optimize deep brain stimulation. *Mov. Disord.*, 33(1):159–164.
- Tinkhauser, G., Pogosyan, A., Little, S., Beudel, M., Herz, D. M., Tan, H., and Brown, P. (2017a). The modulatory effect of adaptive deep brain stimulation on beta bursts in Parkinson’s disease. *Brain*, 140(4):1053–1067.
- Tinkhauser, G., Pogosyan, A., Tan, H., Herz, D. M., Kühn, A. A., and Brown, P. (2017b). Beta burst dynamics in Parkinson’s disease off and on dopaminergic medication. *Brain*, 140(11):2968–2981.
- Tinkhauser, G., Torrecillos, F., Duclos, Y., Tan, H., Pogosyan, A., Fischer, P., Carron, R., Welter, M. L., Karachi, C., Vandenberghe, W., Nuttin, B., Witjas, T., Régis, J., Azulay, J. P., Eusebio, A., and Brown, P. (2018b). Beta burst coupling across the motor circuit in Parkinson’s disease. *Neurobiol. Dis.*, 117:217–225.
- Turken, A. U. and Dronkers, N. F. (2011). The neural architecture of the language comprehension network: Converging evidence from lesion and connectivity analyses. *Front. Syst. Neurosci.*, 5(FEBRUARY 2011):1.
- Tyckocki, T., Nauman, P., Koziara, H., and Mandat, T. (2013). Microlesion Effect as a Predictor of the Effectiveness of Subthalamic Deep Brain Stimulation for Parkinson’s Disease. *Stereotact. Funct. Neurosurg.*, 91(1):12–17.
- Tysnes, O. B. and Storstein, A. (2017). Epidemiology of Parkinson’s disease. *J. Neural Transm.*, 124(8):901–905.
- Tzagarakis, C., Ince, N. F., Leuthold, A. C., and Pellizzer, G. (2010). Beta-band activity during motor planning reflects response uncertainty. *J. Neurosci.*, 30(34):11270–11277.
- Uusitalo, M. A. and Ilmoniemi, R. J. (1997). Signal-space projection method for separating MEG or EEG into components. *Med. Biol. Eng. Comput.*, 35(2):135–140.
- van den Heuvel, M. P. and Hulshoff Pol, H. E. (2010). Exploring the brain network: A review on resting-state fMRI functional connectivity. *Eur. Neuropsychopharmacol.*, 20(8):519–534.

- Van Ede, F., Chekroud, S. R., Stokes, M. G., and Nobre, A. C. (2018). Decoding the influence of anticipatory states on visual perception in the presence of temporal distractors. *Nat. Commun.*, 9(1):1–12.
- Van Veen, B. D., Van Drongelen, W., Yuchtman, M., and Suzuki, A. (1997). Localization of brain electrical activity via linearly constrained minimum variance spatial filtering. *IEEE Trans. Biomed. Eng.*, 44(9):867–880.
- Velisar, A., Syrkin-Nikolau, J., Blumenfeld, Z., Trager, M. H., Afzal, M. F., Prabhakar, V., and Bronte-Stewart, H. (2019). Dual threshold neural closed loop deep brain stimulation in Parkinson disease patients. *Brain Stimul.*, 12(4):868–876.
- Vidaurre, D., Hunt, L. T., Quinn, A. J., Hunt, B. A., Brookes, M. J., Nobre, A. C., and Woolrich, M. W. (2018). Spontaneous cortical activity transiently organises into frequency specific phase-coupling networks. *Nat. Commun.*, 9(1):1–13.
- Vingerhoets, F. J., Villemure, J. G., Temperli, P., Pollo, C., Pralong, E., and Ghika, J. (2002). Subthalamic DBS replaces levodopa in Parkinson’s disease: Two-year follow-up. *Neurology*, 58(3):396–401.
- Vriezen, E. R. and Moscovitch, M. (1990). Memory for temporal order and conditional associative-learning in patients with Parkinson’s disease. *Neuropsychologia*, 28(12):1283–1293.
- Walker, H. C., Faulk, J., Rahman, A. K., Gonzalez, C. L., Roush, P., Nakhmani, A., Crowell, J. L., and Guthrie, B. L. (2019). Awake testing during deep brain stimulation surgery predicts postoperative stimulation side effect thresholds. *Brain Sci.*, 9(2):44.
- Walker, H. C., Huang, H., Gonzalez, C. L., Bryant, J. E., Killen, J., Cutter, G. R., Knowlton, R. C., Montgomery, E. B., Guthrie, B. L., and Watts, R. L. (2012). Short latency activation of cortex during clinically effective subthalamic deep brain stimulation for Parkinson’s disease. *Mov. Disord.*, 27(7):864–873.
- Walker, H. C., Watts, R. L., Schrandt, C. J., Huang, H., Guthrie, S. L., Guthrie, B. L., and Montgomery, E. B. (2011). Activation of subthalamic neurons by contralateral subthalamic deep brain stimulation in parkinson disease. *J. Neurophysiol.*, 105(3):1112–1121.
- Wang, X. J. (2010). Neurophysiological and computational principles of cortical rhythms in cognition. *Physiol. Rev.*, 90(3):1195–1268.

- Weinberger, M., Mahant, N., Hutchison, W. D., Lozano, A. M., Moro, E., Hodaie, M., Lang, A. E., and Dostrovsky, J. O. (2006). Beta oscillatory activity in the subthalamic nucleus and its relation to dopaminergic response in Parkinson’s disease. *J. Neurophysiol.*, 96(6):3248–3256.
- Weiner, K. S. and Zilles, K. (2016). The anatomical and functional specialization of the fusiform gyrus. *Neuropsychologia*, 83:48–62.
- Welch, P. D. (1967). The Use of Fast Fourier Transform for the Estimation of Power Spectra: A Method Based on Time Averaging Over Short, Modified Periodograms. *IEEE Trans. Audio Electroacoust.*, 15(2):70–73.
- Wertheimer, J., Gottuso, A. Y., Nuno, M., Walton, C., Duboille, A., Tuchman, M., and Ramig, L. (2014). The impact of STN deep brain stimulation on speech in individuals with Parkinson’s disease: The patient’s perspective. *Park. Relat. Disord.*, 20(10):1065–1070.
- Wessel, J. R. (2020). B-Bursts Reveal the Trial-To-Trial Dynamics of Movement Initiation and Cancellation. *J. Neurosci.*, 40(2):411–423.
- Witt, K., Kalbe, E., Erasmi, R., and Ebersbach, G. (2017). Nichtmedikamentöse Therapieverfahren beim Morbus Parkinson. *Nervenarzt*, 88(4):383–390.
- Xing, D., Yeh, C. I., and Shapley, R. M. (2009). Spatial spread of the local field potential and its laminar variation in visual cortex. *J. Neurosci.*, 29(37):11540–11549.
- Yates, F. (1934). The Analysis of Multiple Classifications with Unequal Numbers in the Different Classes. *J. Am. Stat. Assoc.*, 29(185):51–66.
- Yu, Y., Sanabria, D. E., Wang, J., Hendrix, C. M., Zhang, J., Nebeck, S. D., Amundson, A. M., Busby, Z. B., Bauer, D. L., Johnson, M. D., Johnson, L. A., and Vitek, J. L. (2021). Parkinsonism alters beta burst dynamics across the basal ganglia-motor cortical network. *J. Neurosci.*, 41(10):2274–2286.
- Yule, G. U. (1912). On the Methods of Measuring Association Between Two Attributes. *J. R. Stat. Soc.*, 75(6):579.
- Zaidel, A., Arkadir, D., Israel, Z., and Bergman, H. (2009). Akineto-rigid vs. tremor syndromes in Parkinsonism. *Curr. Opin. Neurol.*, 22(4):387–393.
- Zalesky, A., Fornito, A., Cocchi, L., Gollo, L. L., and Breakspear, M. (2014). Time-resolved resting-state brain networks. *Proc. Natl. Acad. Sci. U. S. A.*, 111(28):10341–10346.

- Zavala, B., Damera, S., Dong, J. W., Lungu, C., Brown, P., and Zaghoul, K. A. (2015). Human subthalamic nucleus theta and beta oscillations entrain neuronal firing during sensorimotor conflict. *Cereb. Cortex*, 27(1):496–508.
- Zavala, B. A., Jang, A. I., and Zaghoul, K. A. (2017). Human subthalamic nucleus activity during non-motor decision making. *Elife*, 6.
- Zénon, A., Duclos, Y., Carron, R., Witjas, T., Baunez, C., Régis, J., Azulay, J. P., Brown, P., and Eusebio, A. (2016). The human subthalamic nucleus encodes the subjective value of reward and the cost of effort during decision-making. *Brain*, 139(6):1830–1843.
- Zhang, S., Sun, J., and Gao, X. (2020). The effect of fatigue on brain connectivity networks. *Brain Sci. Adv.*, 6(2):120–131.
- Zimmerman, J. E., Thiene, P., and Harding, J. T. (1970). Design and operation of stable rf-biased superconducting point-contact quantum devices, and a note on the properties of perfectly clean metal contacts. *J. Appl. Phys.*, 41(4):1572–1580.

9 Erklärung

Ich versichere an Eides Statt, dass die Dissertation von mir selbständig und ohne unzulässige fremde Hilfe unter Beachtung der „Grundsätze zur Sicherung guter wissenschaftlicher Praxis an der Heinrich-Heine-Universität Düsseldorf“ erstellt worden ist. Die Dissertation wurde in der vorliegenden oder in ähnlicher Form noch bei keiner anderen Institution eingereicht. Ich habe bisher keine erfolglosen Promotionsversuche unternommen.

Düsseldorf, den

Matthias Martin Sure

10 Danksagung

Zuvorderst möchte ich mich bei meiner Doktormutter und Mentorin Frau Prof. Dr. Esther Florin für die Möglichkeit bedanken, dass ich meine Promotion in Ihrer Arbeitsgruppe durchführen durfte. Sowie für die Unterstützung, die ich von Ihr für die Weiterentwicklung meiner wissenschaftlichen Fähigkeiten erhielt. Für die wunderbare Arbeitsumgebung, die sie in Ihrer Arbeitsgruppe geschaffen hat, möchte mich ebenfalls bei Ihr bedanken.

Weiterhin möchte ich mich bei Herrn Prof. Dr. Thomas Heinzl für die Zweitbetreuung der vorliegenden Doktorarbeit bedanken.

Ich möchte mich beim gesamten Team des Instituts für Klinische Neurowissenschaften und Medizinische Psychologie der Heinrich-Heine-Universität Düsseldorf bedanken, das durch die Herzlichkeit und den wohlwollenden Umgang erreicht hat, das es mir eine Freude war, jeden Tag zur Arbeit zu kommen. An dieser Stelle möchte ich mich auch bei dem Institutsleiter Herr Prof. Dr. Alfons Schnitzler für die vielen hilfreichen Kommentare zu allen meinen Publikationen bedanken. Bei Herrn Prof. Dr. Markus Butz bedanke ich mich dafür, dass er mich schon zur Bachelorarbeit ans Institut gelotst hat und mich die ganze Zeit mit seinem Enthusiasmus begleitet hat. Bei Herrn Dr. Thomas Baumgarten möchte ich mich für seine vielfältigen Hilfen, von Beginn meiner Bachelorarbeit bis zum Ende meiner Dissertation, herzlich bedanken. Und für die ganze Unterstützung bei allem organisatorischen möchte ich mich auch bei Frau Anke Golbs und Frau Susanne Claßen bedanken. Auch wenn seine Karriere ihn mittlerweile nach Bonn verschlagen hat, möchte ich mich für die ganzen Späße bei der Arbeit zu Beginn unserer Wissenschaftskarriere in den Neurowissenschaften und der bunten Diskussion im weiteren Verlauf auch bei ihm, Herr Mitjan Morr, bedanken.

Im Weiteren möchte ich mich bei allen Patienten bedanken, die sich die Zeit genommen haben an meinen Experimenten teilzunehmen, denn ohne diese Einsatzbereitschaft wäre diese Dissertation nicht möglich gewesen.

Mein Dank gilt auch im Besonderen allen, die meine Dissertation, aber auch all meine Publikation Korrektur gelesen haben und somit direkt am Gelingen beteiligt waren.

Abschließend möchte ich mich bei meiner Familie und meinen Freunden dafür bedanken, dass ihr mir den Raum und die Zeit gegeben habt, die ich für meine Promotion brauchte, die anhaltende Unterstützung und dafür, dass ich mich nach einem tollen Arbeitstag auf den Feierabend freuen konnte.

11 Appendix

11.1 Publications

The dissertation at hand is based on:

Study 1:

Sure, M., Vesper, J., Schnitzler, A., Florin, E., 2021. Dopaminergic modulation of spectral and spatial characteristics of parkinsonian subthalamic nucleus beta bursts. Front. Neurosci. 15, 1450. <https://doi.org/10.3389/fnins.2021.724334>

Impact factor (2021): 5.2

Personal Contribution: Concept & study design 10 %; Data acquisition 40 %; Data processing 70 %; Data analyses & figures 100 %; Discussion of results 70 %; Manuscript writing 70 %

Study 2:

Sure, M., Vesper, J., Schnitzler, A., Florin, E., 2022. Cortical network formation based on subthalamic beta bursts in Parkinson's disease. Neuroimage 263, 119619.<https://doi.org/10.1016/j.neuroimage.2022.119619>

Impact factor (2022): 7.4

Personal Contribution: Concept & study design 30 %; Data acquisition 40 %; Data processing 70 %; Data analyses & figures 100 %; Discussion of results 75 %; Manuscript writing 70 %

Study 3:

Sure, M., Mertiens, S., Vesper, J., Schnitzler, A., Florin, E., 2023. Alterations of resting-state networks of Parkinson's disease patients after subthalamic DBS surgery. Neuroimage Clin. 37, 103317. <https://doi.org/10.1016/j.nicl.2023.103317>

Impact factor (2023): 4.9

Personal Contribution: Concept & study design 50 %; Data acquisition 30 %; Data processing 60 %; Data analyses & figures 100 %; Discussion of results 75 %; Manuscript writing 70 %

11.2 Supplementary results

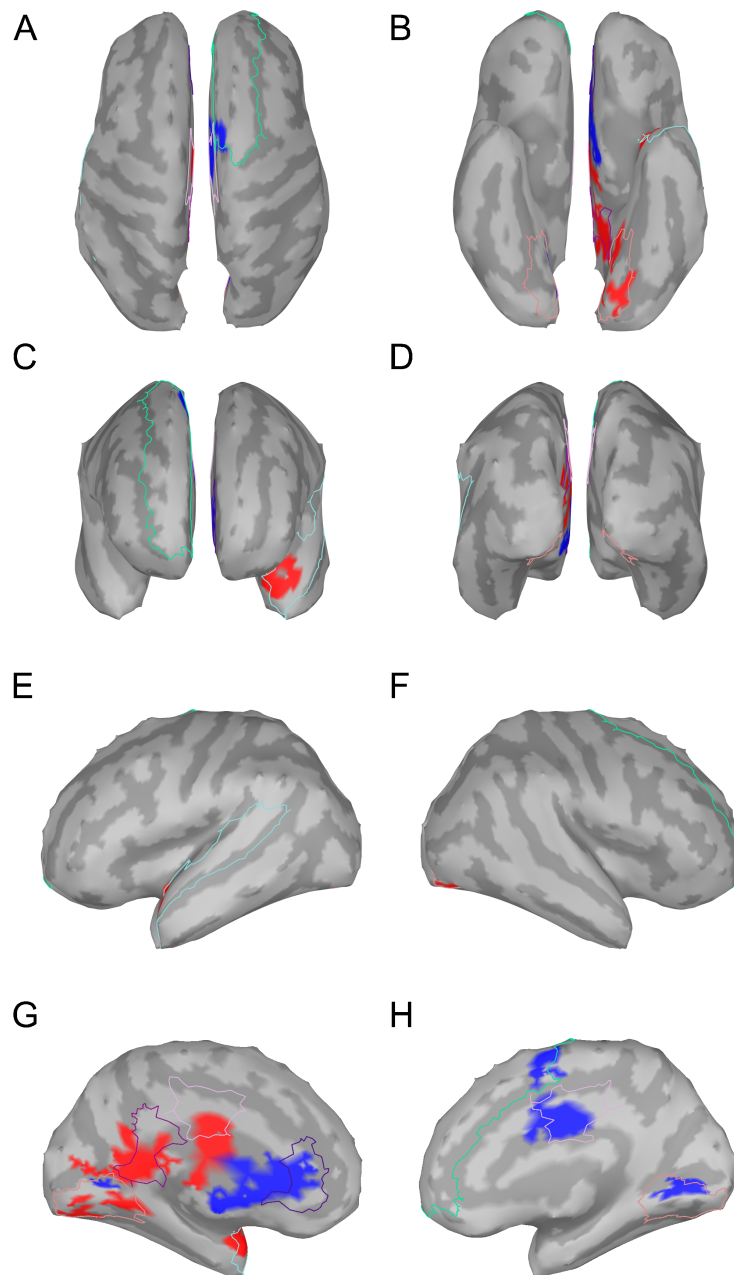


Figure 11.1: Cortical ERFs evoked by beta bursts maximum in the left STN with a minimum duration of 200 ms

The figure shows the spatial extent of the event-related fields evoked by beta bursts from the left STN on the standard brain ICBM152. All vertices are color-coded, which, in a cluster of at least 10 vertices for at least 5 ms, differed significantly with $|t| > 5.05$ from baseline in the period from 100 ms before to 100 ms after the burst maximum. Vertices with a positive deviation from the baseline were marked red and those with a negative deviation were marked blue.

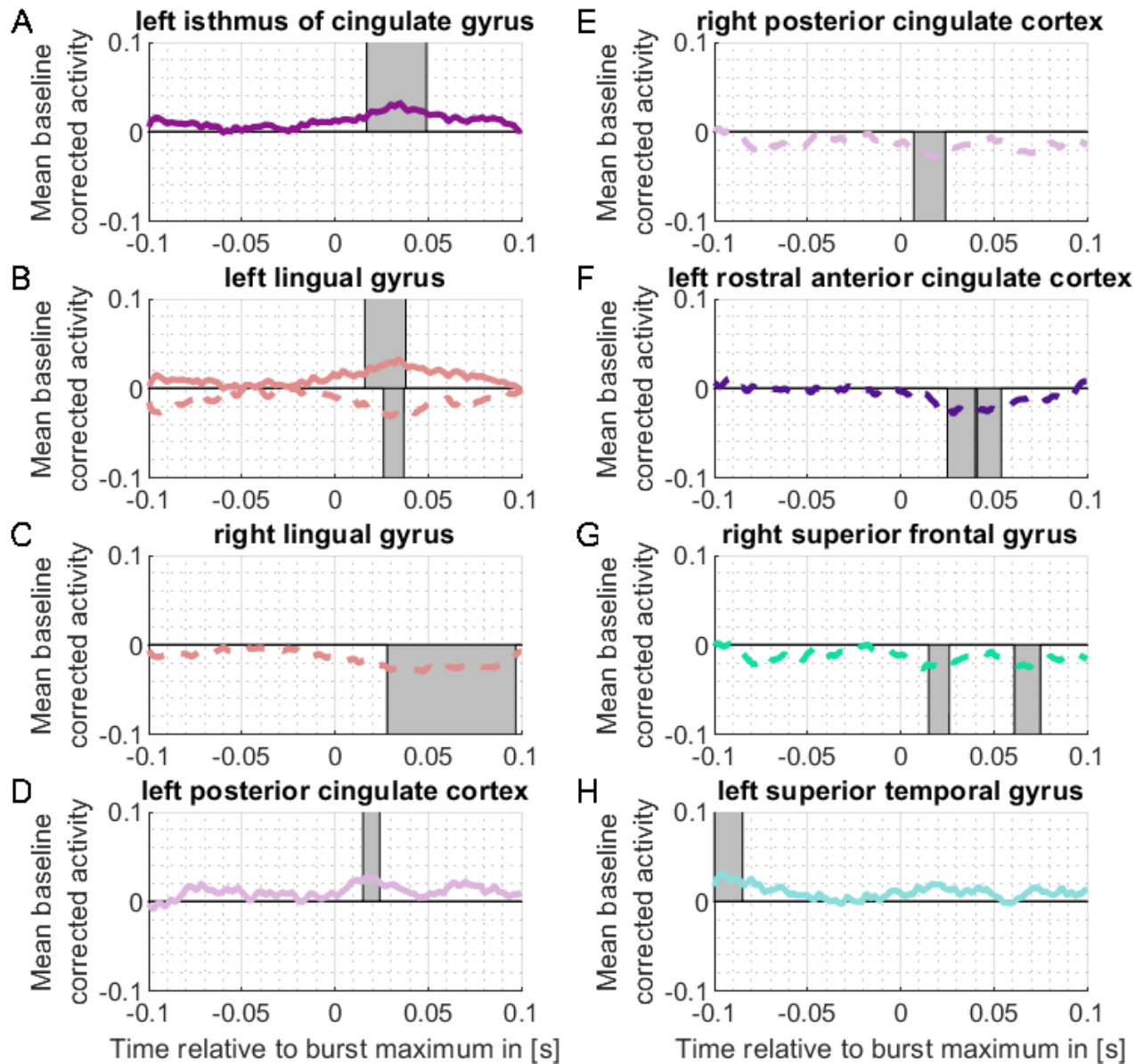


Figure 11.2: Cortical ERFs evoked by beta bursts maximum in the left STN with a minimum duration of 200 ms

The figure shows temporal dynamics of the ERFs. To each ERF belongs a cluster of at least 10 vertices for at least 5 ms, differed significantly with $|t| > 5.05$ from baseline in the period from 100 ms before to 100 ms after the burst maximum. The time-series, with the burst maximum at $t = 0$ ms, show for these clusters, the cortical activity averaged on the beta peak and baseline corrected. These averaged time-series were then further averaged across the vertices belonging to one cluster. Clusters were assigned to cortical regions using the Mindboogle atlas, with the primary location of the significant vertices being the determining factor. The plotted time-series were averaged across all subjects and averaged separately across the vertices with a positive deviation (solid line) from baseline and a negative deviation (dashed line). The time windows with a significant deviation from the baseline are highlighted in gray.

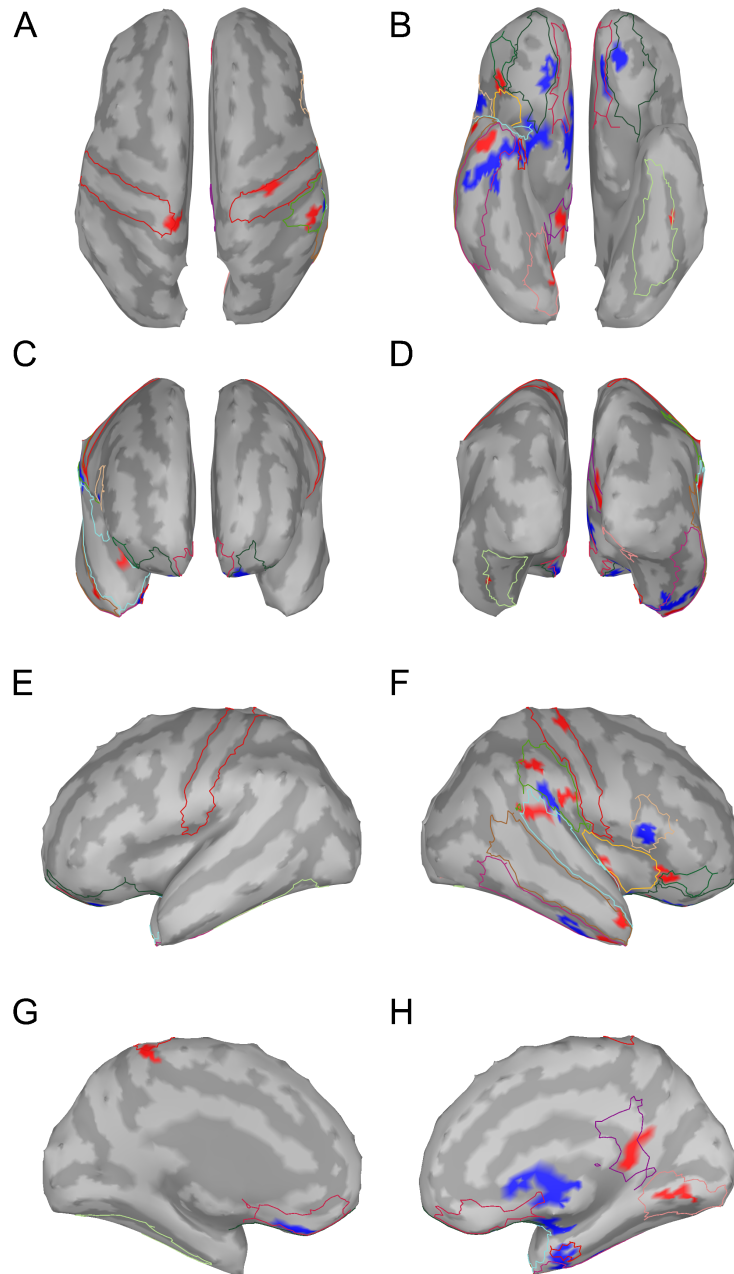


Figure 11.3: Cortical ERFs evoked by beta bursts maximum in the right STN with a minimum duration of 200 ms

For detailed description, please refer to Figure 11.1.

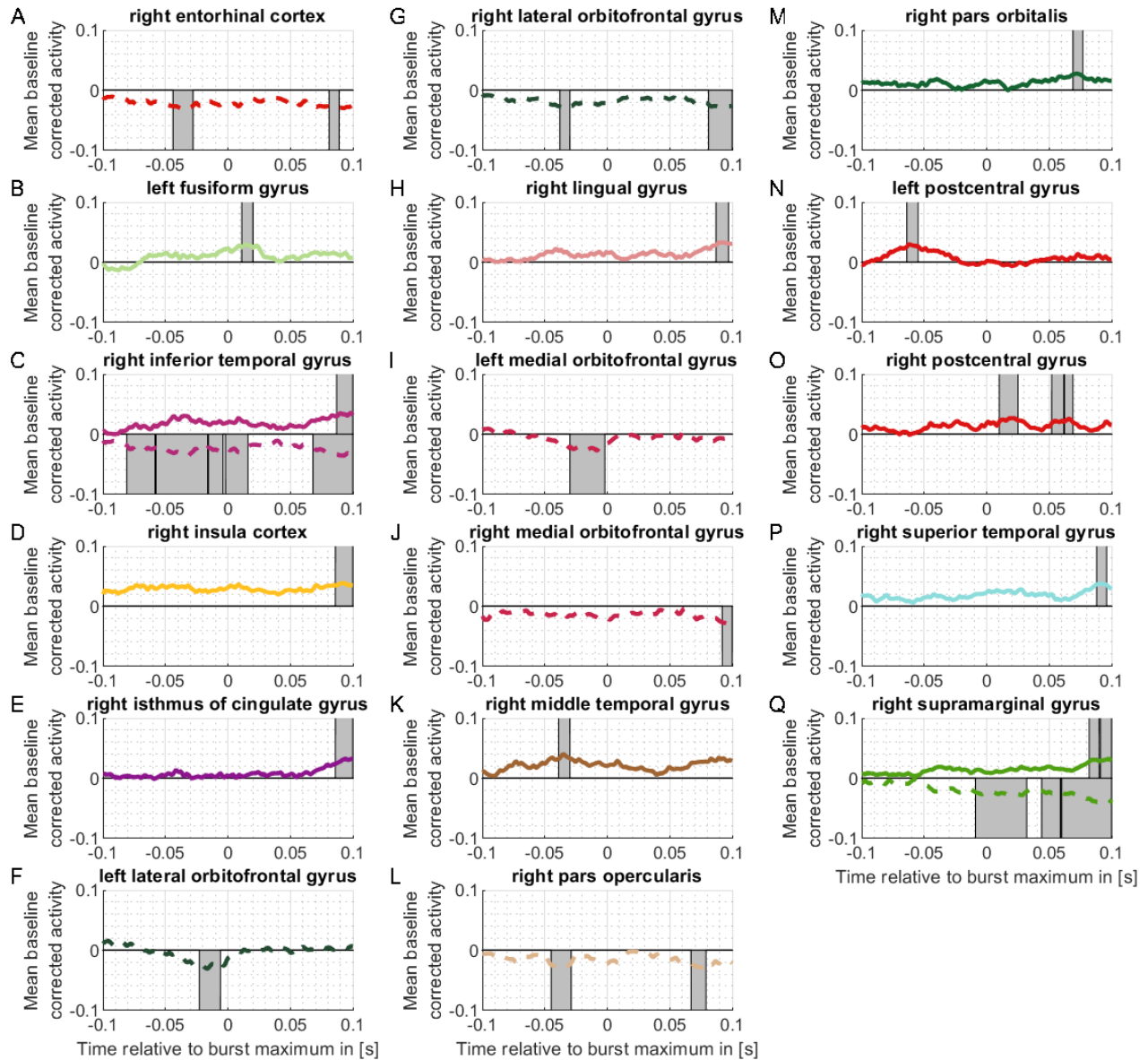


Figure 11.4: Cortical ERFs evoked by beta bursts maximum in the right STN with a minimum duration of 200 ms

For detailed description, please refer to Figure 11.2.

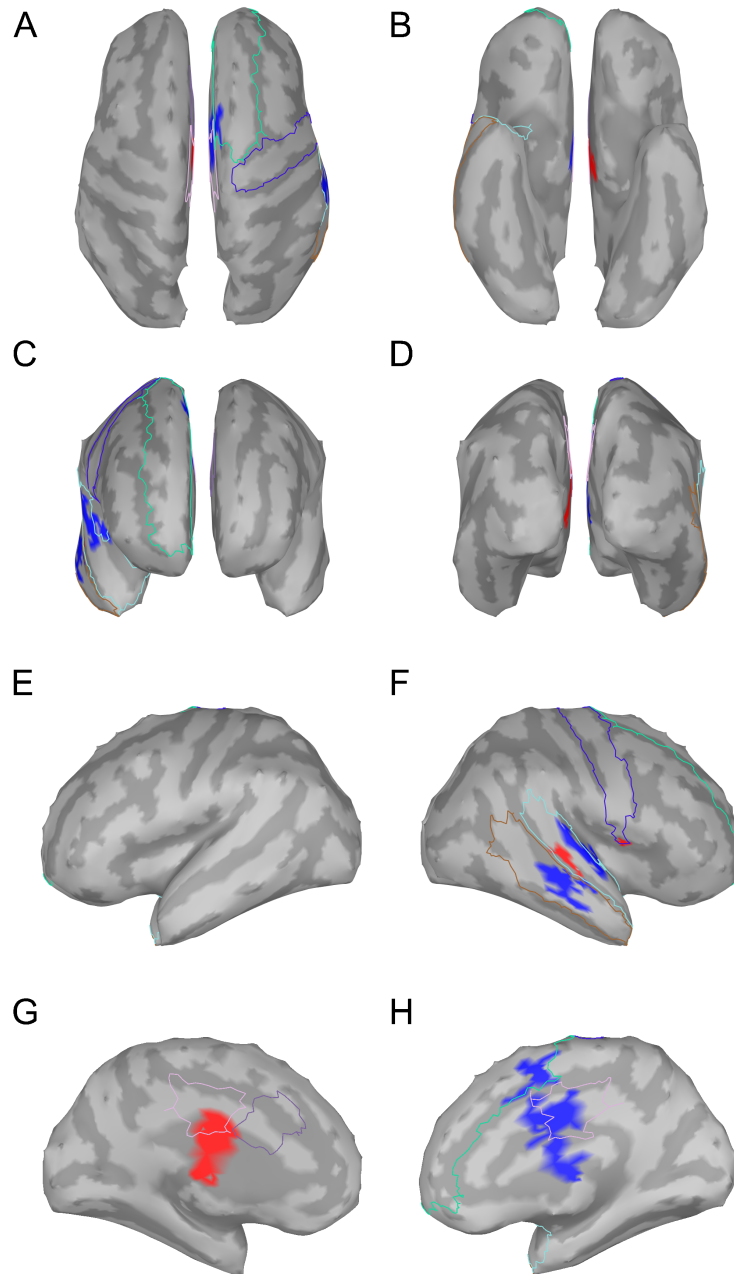


Figure 11.5: Cortical ERFs evoked by beta bursts maximum in the left STN with a minimum duration of 500 ms

For detailed description, please refer to Figure 11.1.

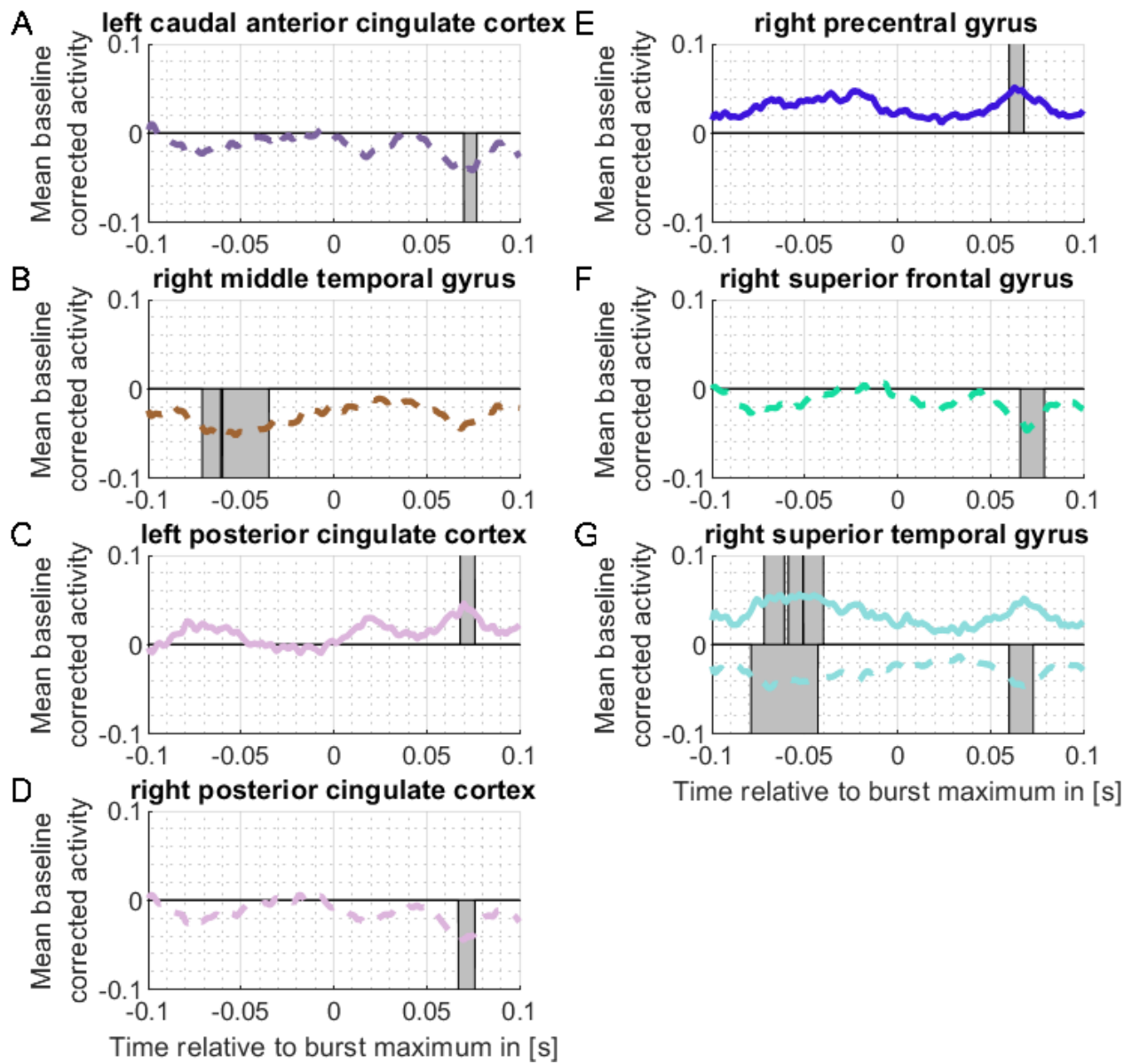


Figure 11.6: Cortical ERFs evoked by beta bursts maximum in the left STN with a minimum duration of 500 ms

For detailed description, please refer to Figure 11.2.

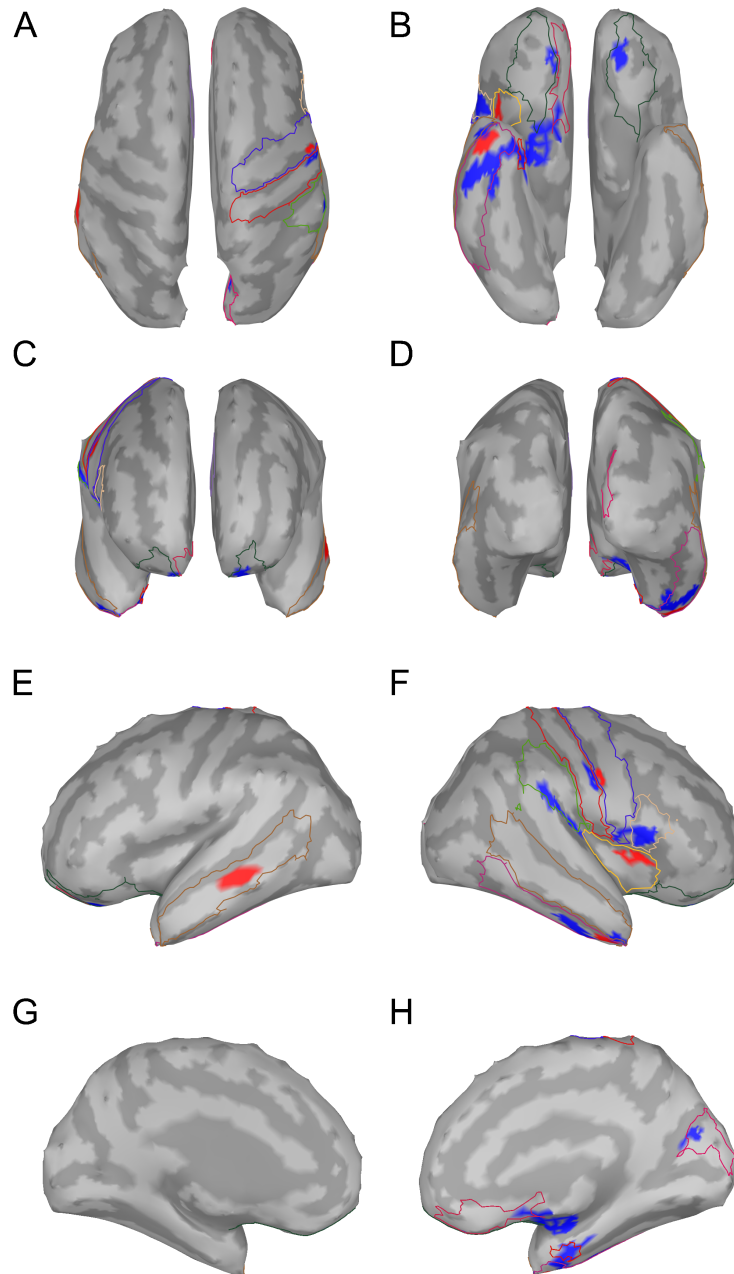


Figure 11.7: Cortical ERFs evoked by beta bursts maximum in the right STN with a minimum duration of 500 ms

For detailed description, please refer to Figure 11.1.

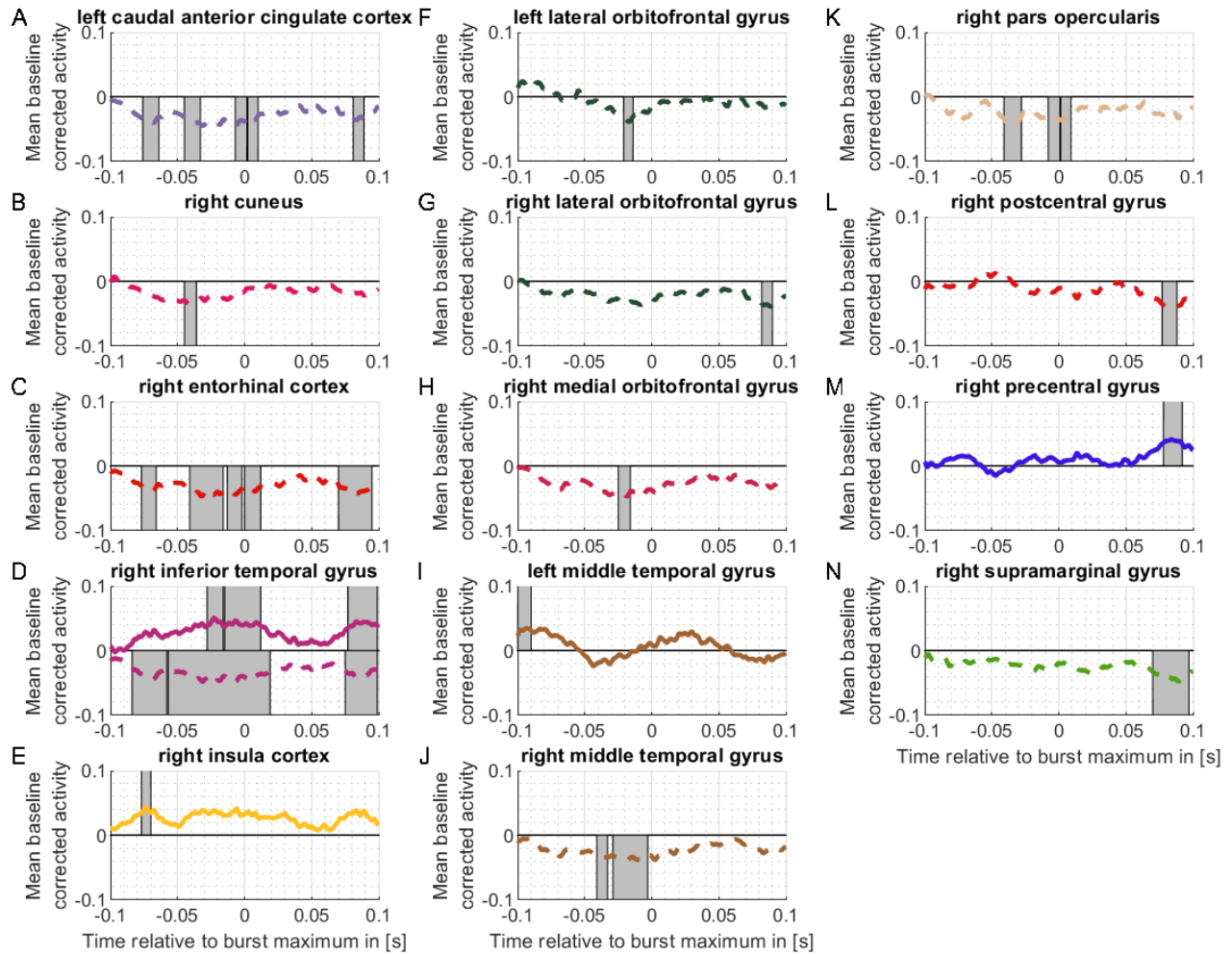


Figure 11.8: Cortical ERFs evoked by beta bursts maximum in the right STN with a minimum duration of 500 ms

For detailed description, please refer to Figure 11.2.

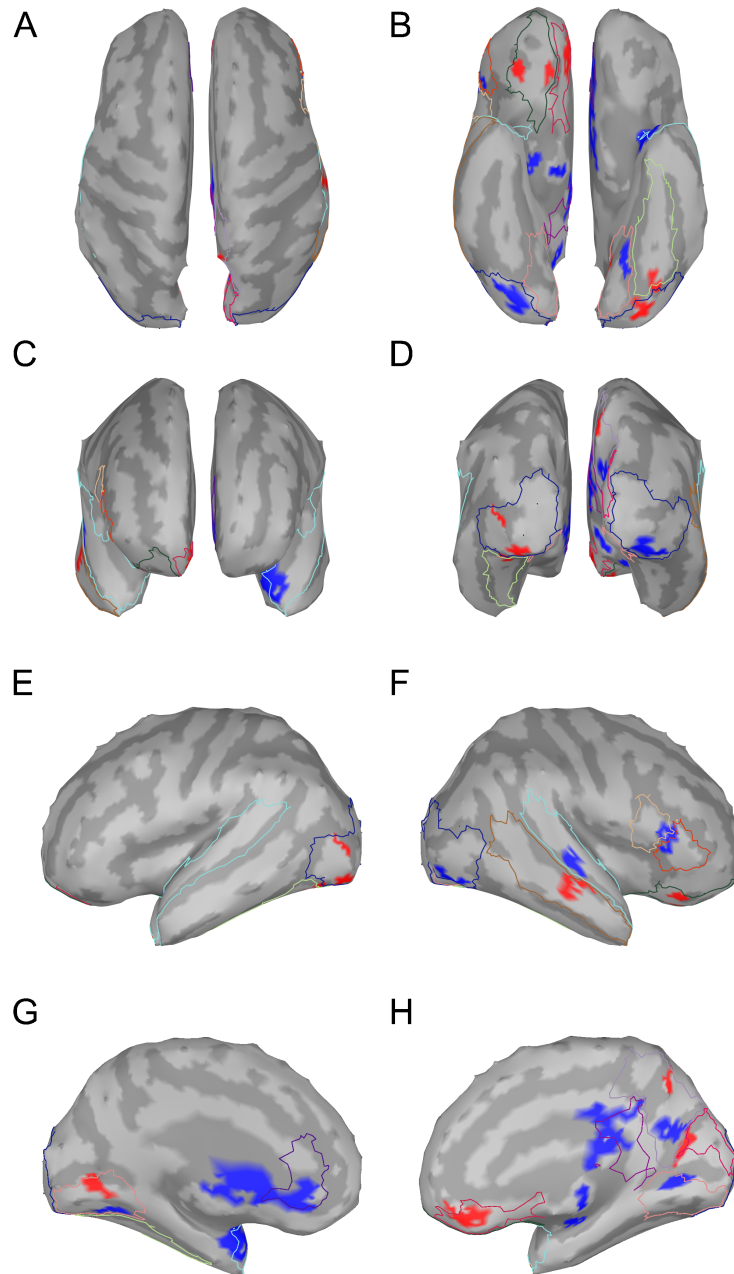


Figure 11.9: Cortical ERFs evoked by beta bursts maximum in the left STN with a maximum duration of 300 ms

For detailed description, please refer to Figure 11.1.

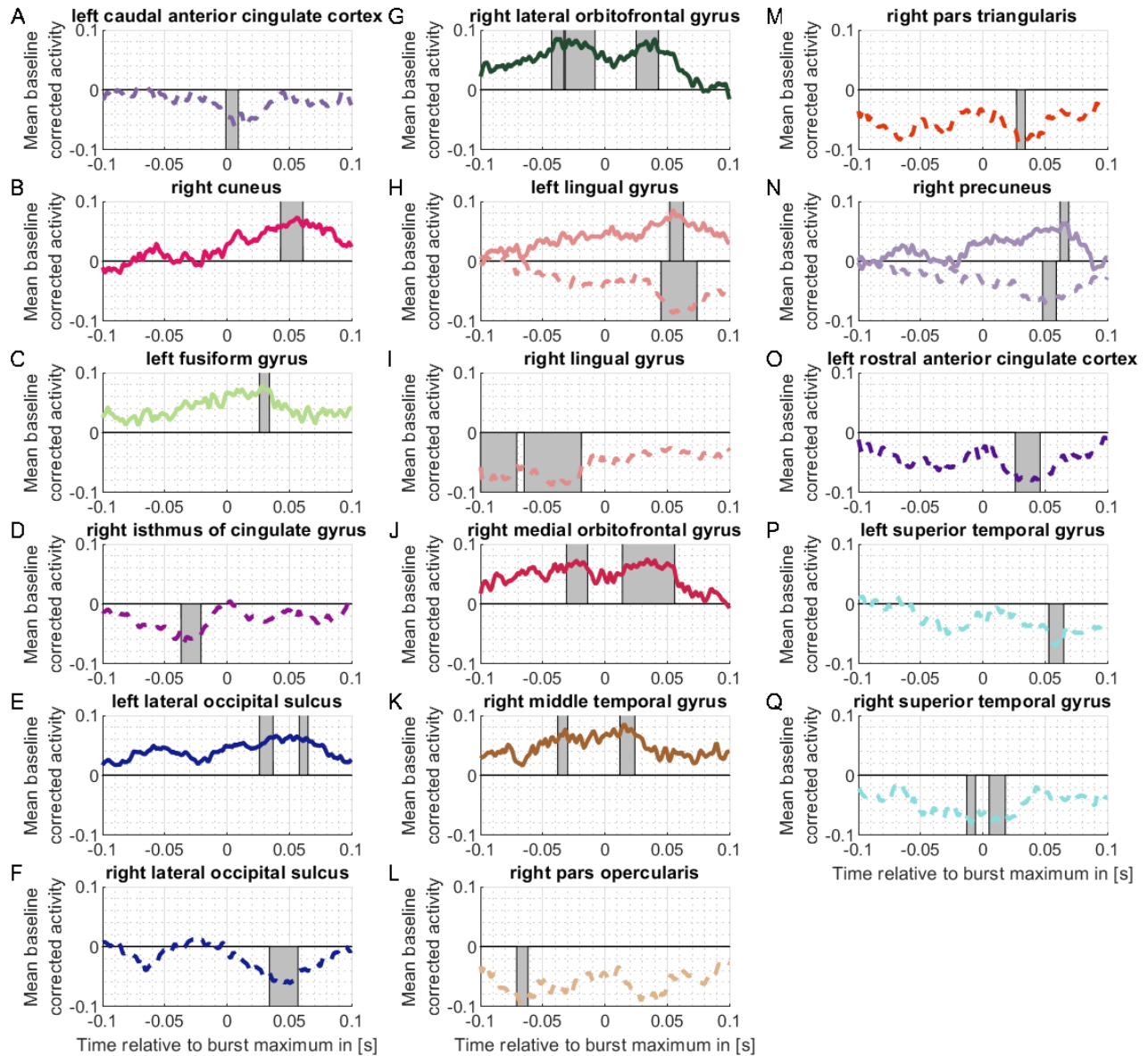


Figure 11.10: Cortical ERFs evoked by beta bursts maximum in the left STN with a maximum duration of 300 ms

For detailed description, please refer to Figure 11.2.

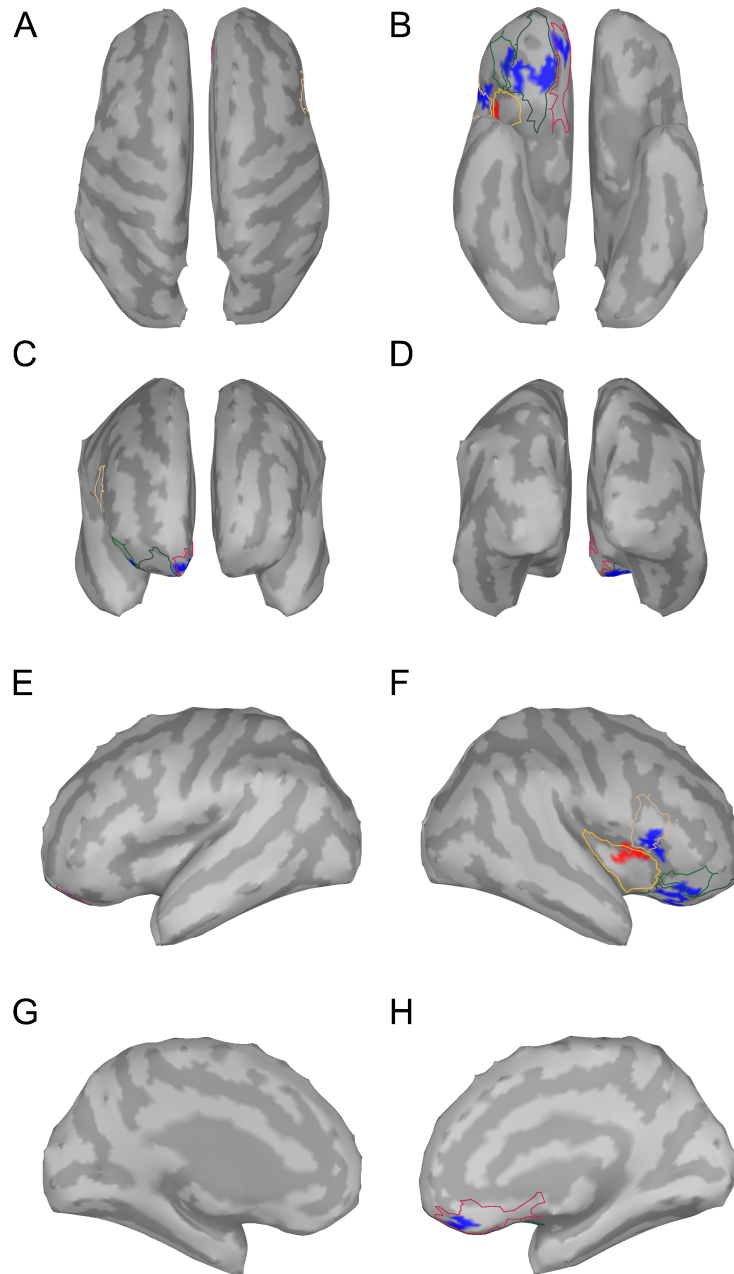


Figure 11.11: Cortical ERFs evoked by beta bursts maximum in the right STN with a maximum duration of 300 ms

For detailed description, please refer to Figure 11.1.

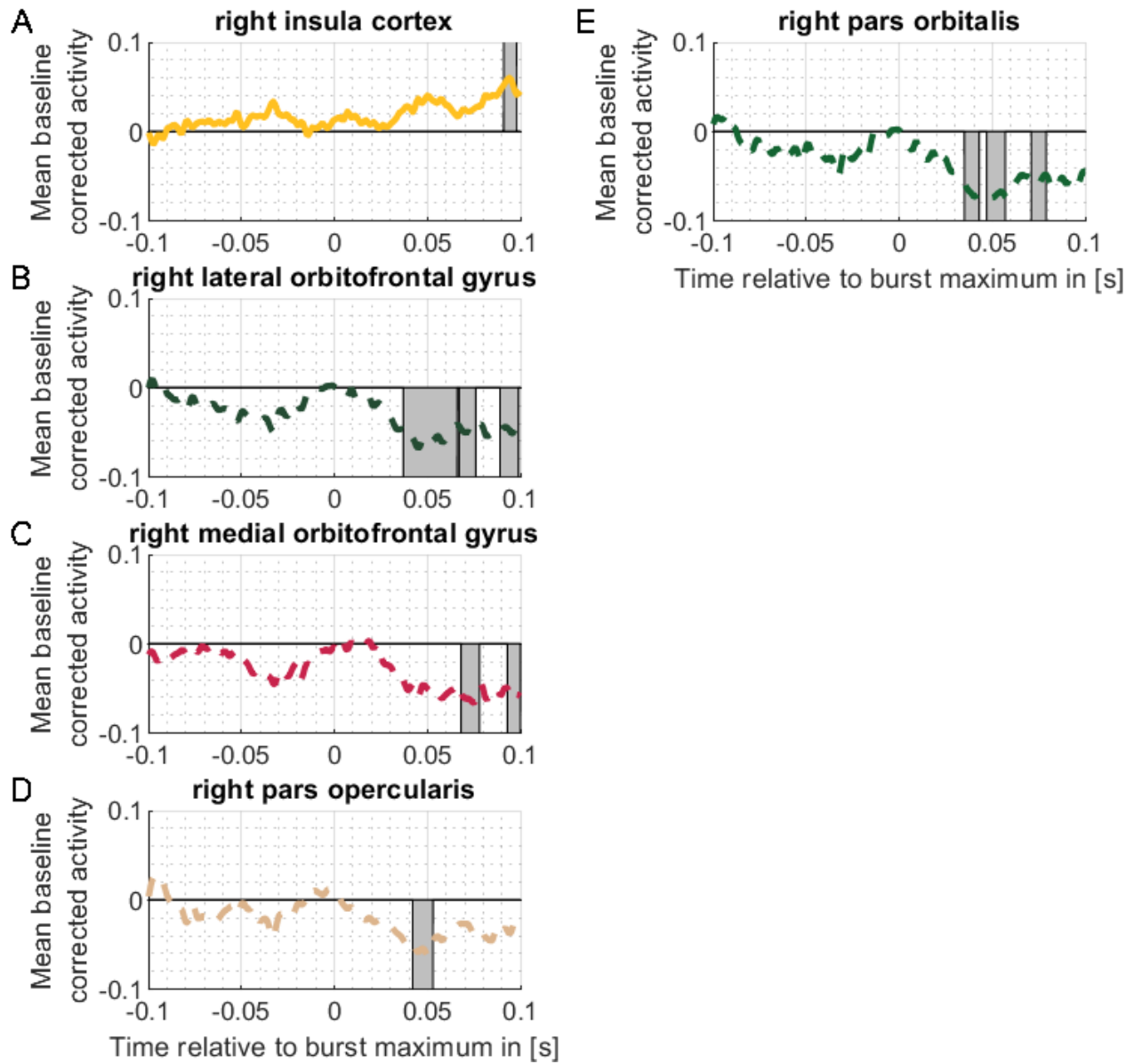


Figure 11.12: Cortical ERFs evoked by beta bursts maximum in the right STN with a maximum duration of 300 ms

For detailed description, please refer to Figure 11.2.

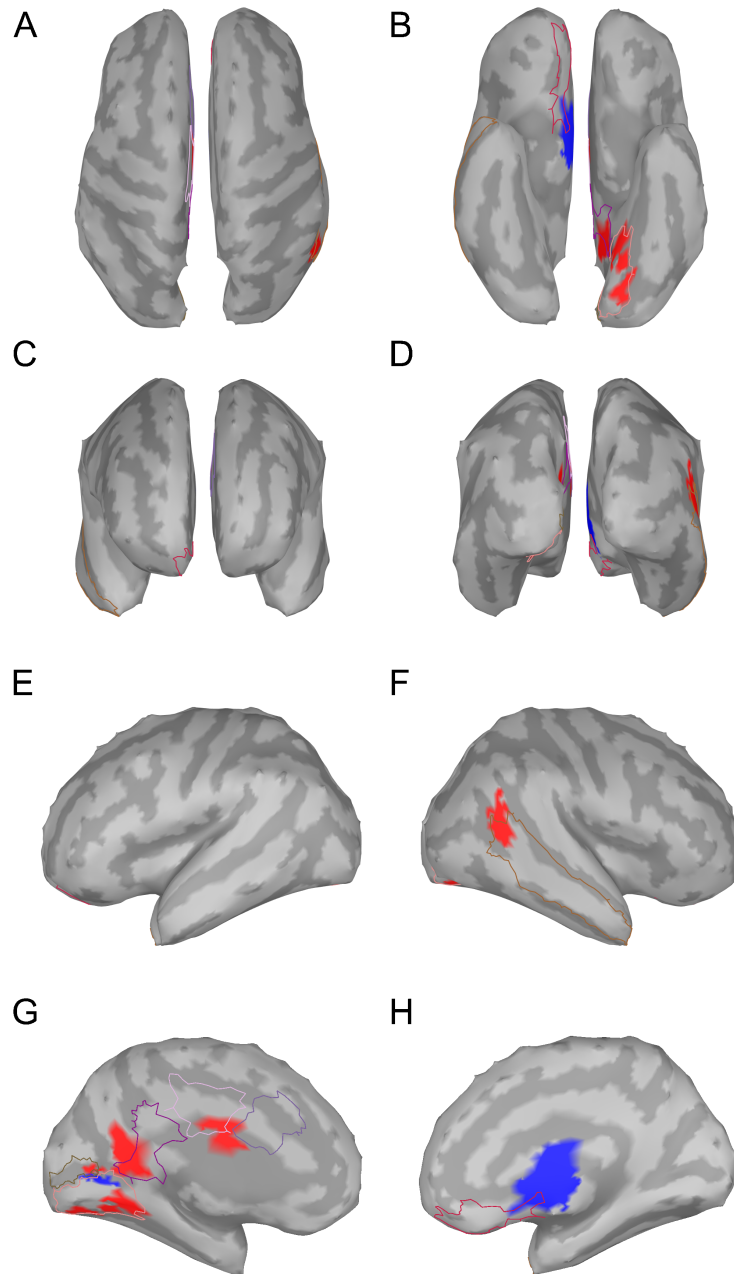


Figure 11.13: Cortical ERFs evoked by beta bursts onset in the left STN with a minimum duration of 200 ms

The figure shows the spatial extent of the event-related fields evoked by beta bursts from the left STN on the standard brain ICBM152. All vertices are color-coded, which, in a cluster of at least 10 vertices for at least 5 ms, differed significantly with $|t| > 5.05$ from baseline in the period from 100 ms before to 100 ms after the burst onset. Vertices with a positive deviation from the baseline were marked red and those with a negative deviation were marked blue.

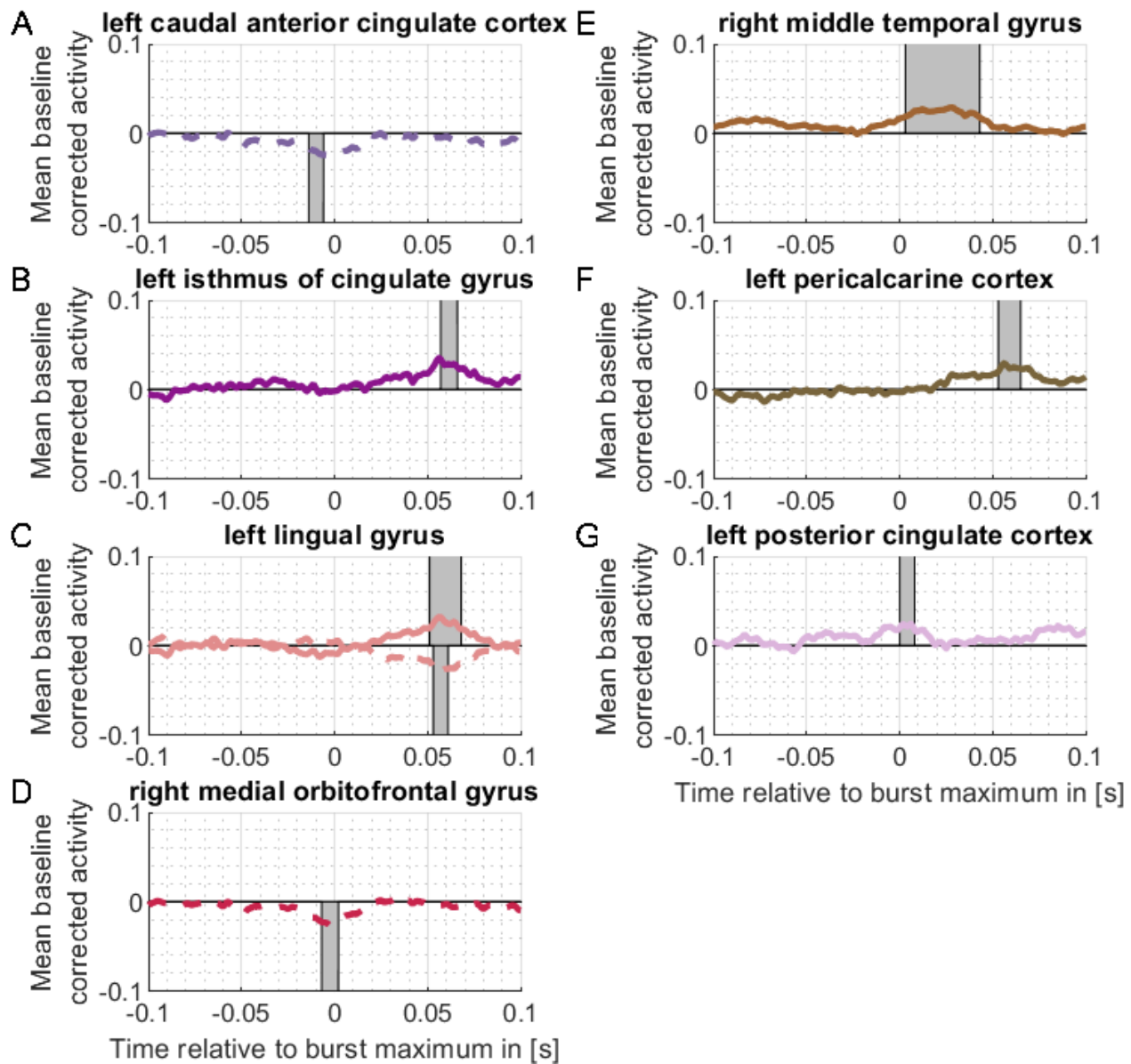


Figure 11.14: Cortical ERFs evoked by beta bursts onset in the left STN with a minimum duration of 200 ms

Cortical ERFs evoked by beta bursts onset in the left STN with a minimum duration of 200 ms. The figure shows temporal dynamics of the ERFs. To each ERF belongs a cluster of at least 10 vertices for at least 5 ms, differed significantly with $|t| > 5.05$ from baseline in the period from 100 ms before to 100 ms after the burst onset. The time-series, with the burst onset at $t = 0$ ms, show for these clusters, the cortical activity averaged on the beta peak and baseline corrected. These averaged time-series were then further averaged across the vertices belonging to one cluster. Clusters were assigned to cortical regions using the Mindboogle atlas, with the primary location of the significant vertices being the determining factor. The plotted time-series were averaged across all subjects and averaged separately across the vertices with a positive deviation (solid line) from baseline and a negative deviation (dashed line). The time windows with a significant deviation from the baseline are highlighted in gray.

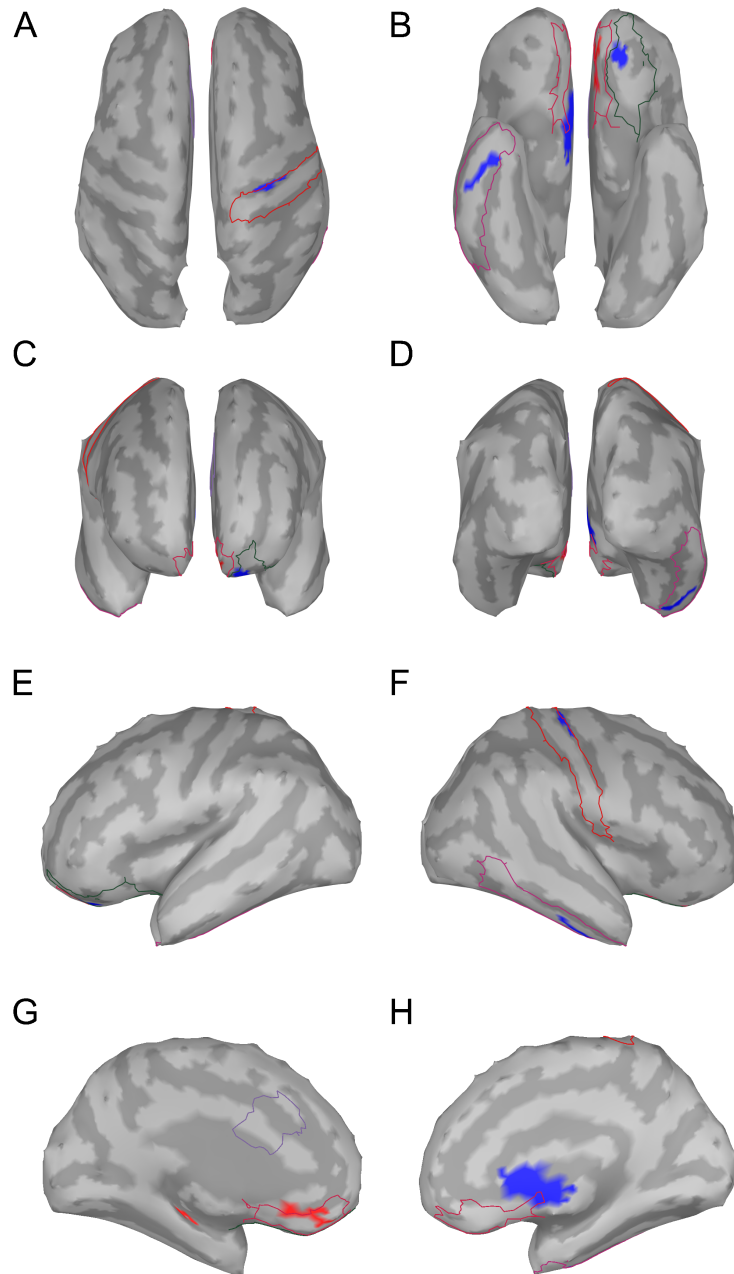


Figure 11.15: Cortical ERFs evoked by beta bursts onset in the right STN with a minimum duration of 200 ms

For detailed description, please refer to Figure 11.13.

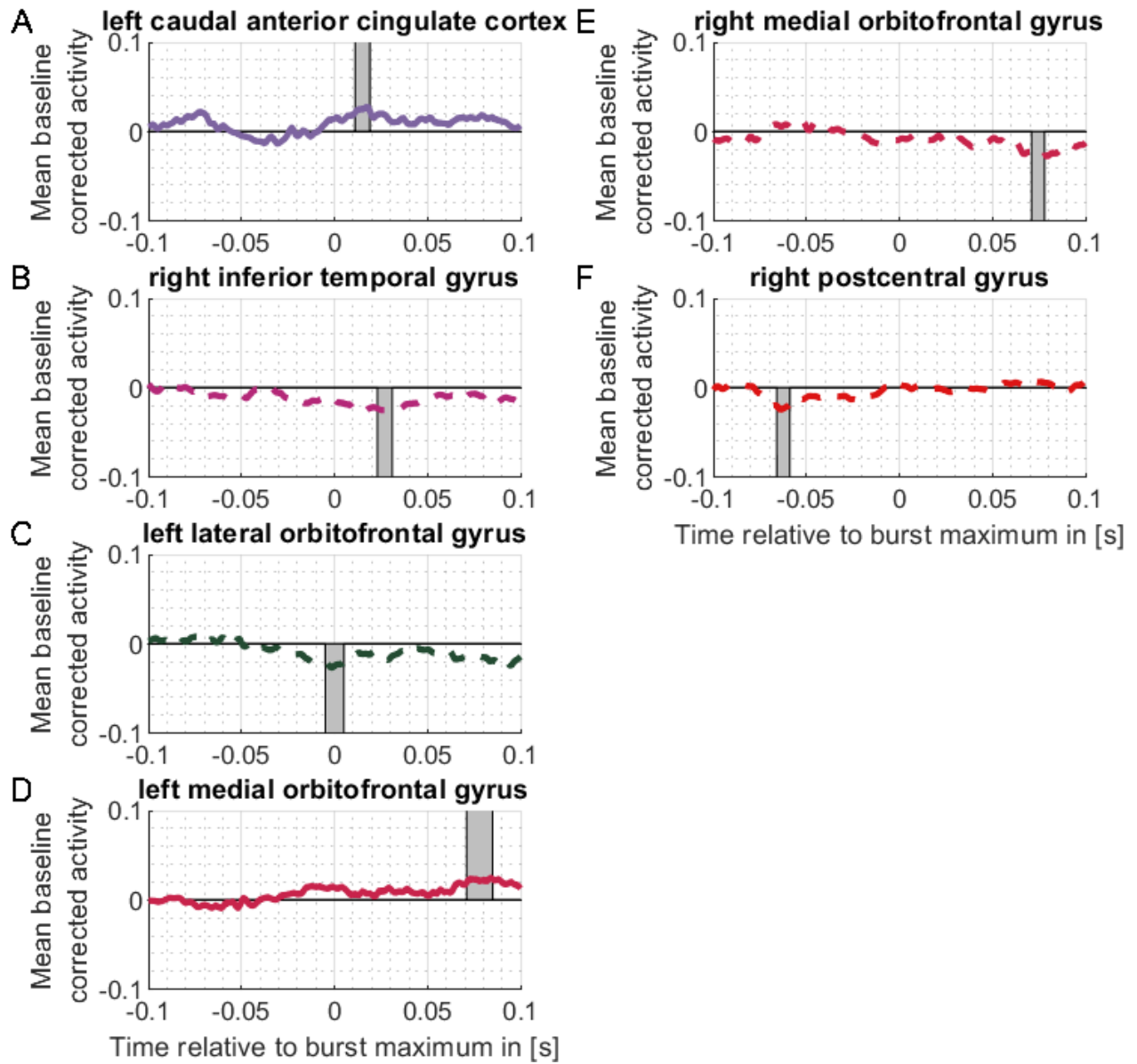


Figure 11.16: Cortical ERFs evoked by beta bursts onset in the right STN with a minimum duration of 200 ms

For detailed description, please refer to Figure 11.14.

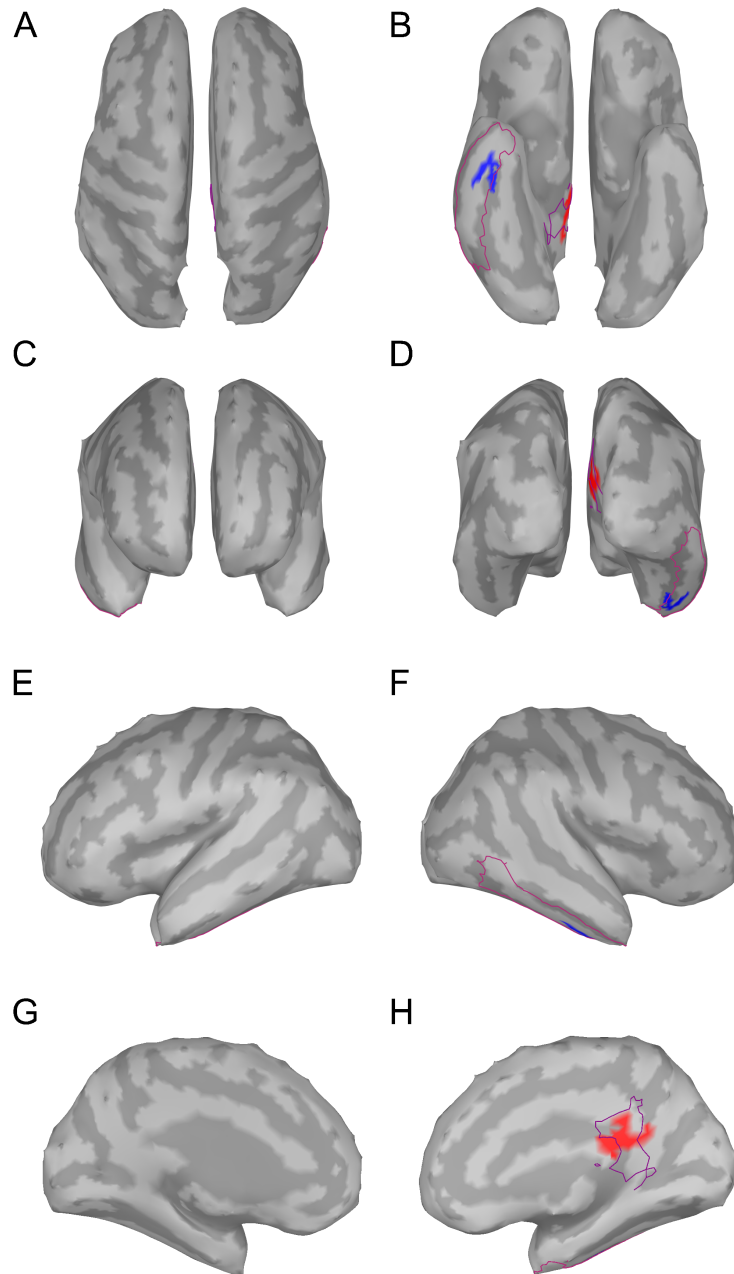


Figure 11.17: Cortical ERFs evoked by beta bursts onset in the right STN with a minimum duration of 500 ms

For detailed description, please refer to Figure 11.13.

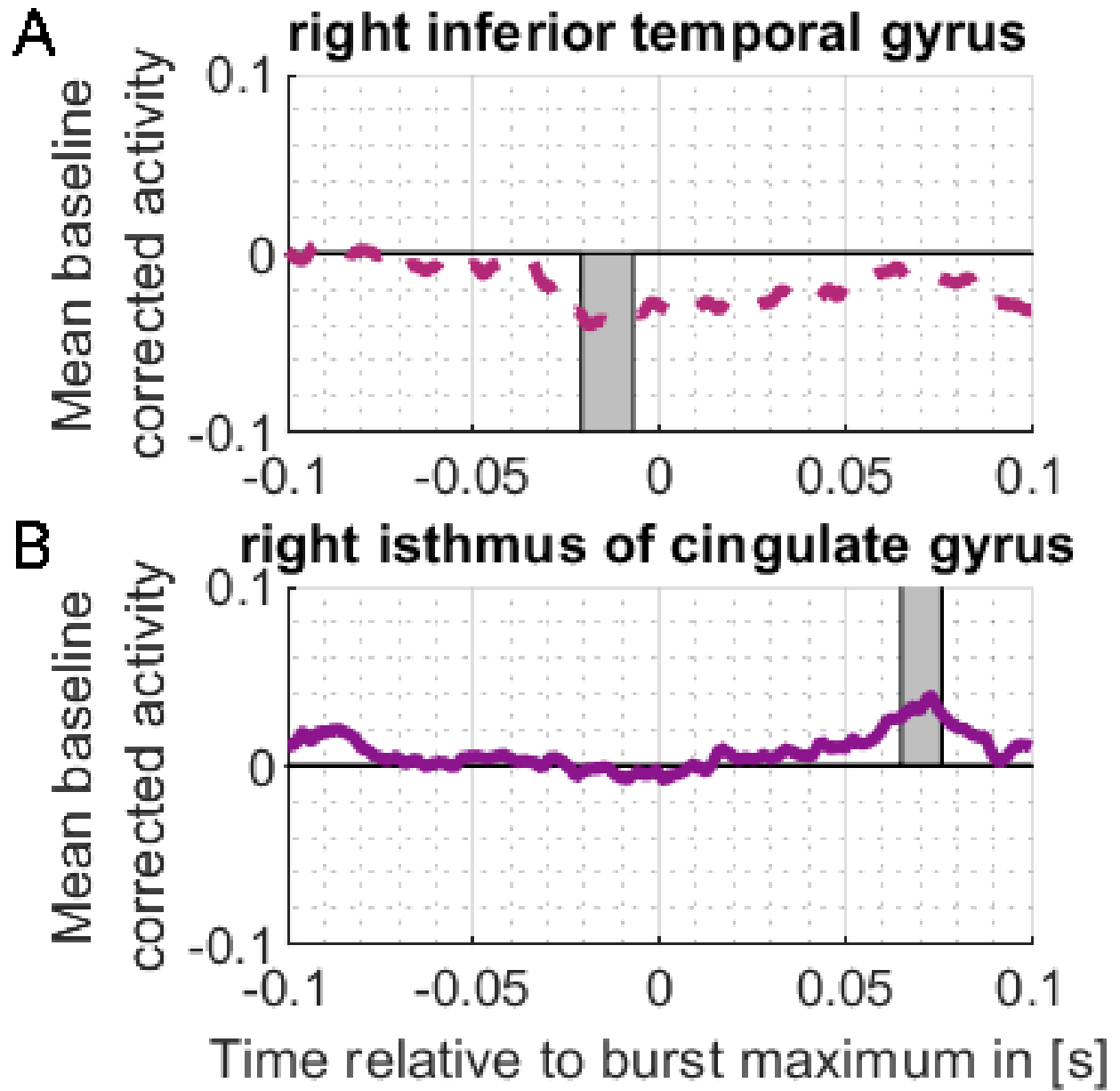


Figure 11.18: Cortical ERFs evoked by beta bursts onset in the right STN with a minimum duration of 500 ms

For detailed description, please refer to Figure 11.14.

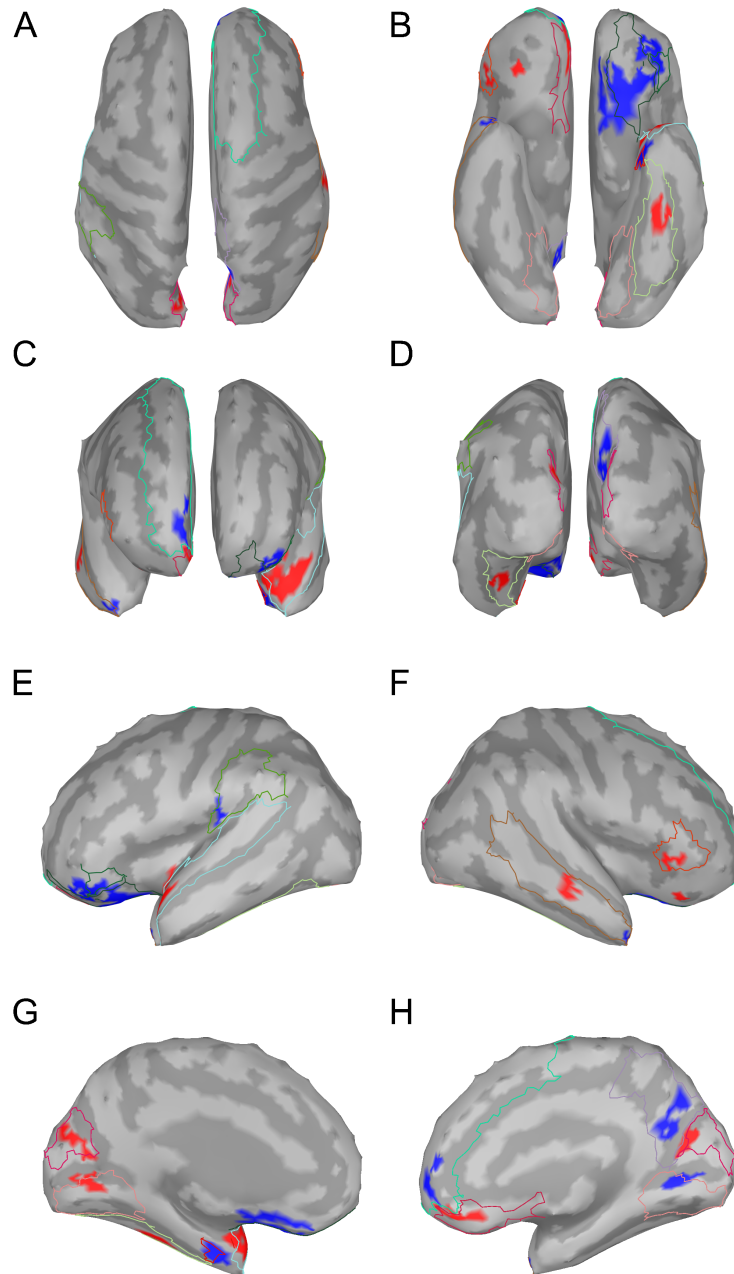


Figure 11.19: Cortical ERFs evoked by beta bursts onset in the left STN with a maximum duration of 300 ms

For detailed description, please refer to Figure 11.13.

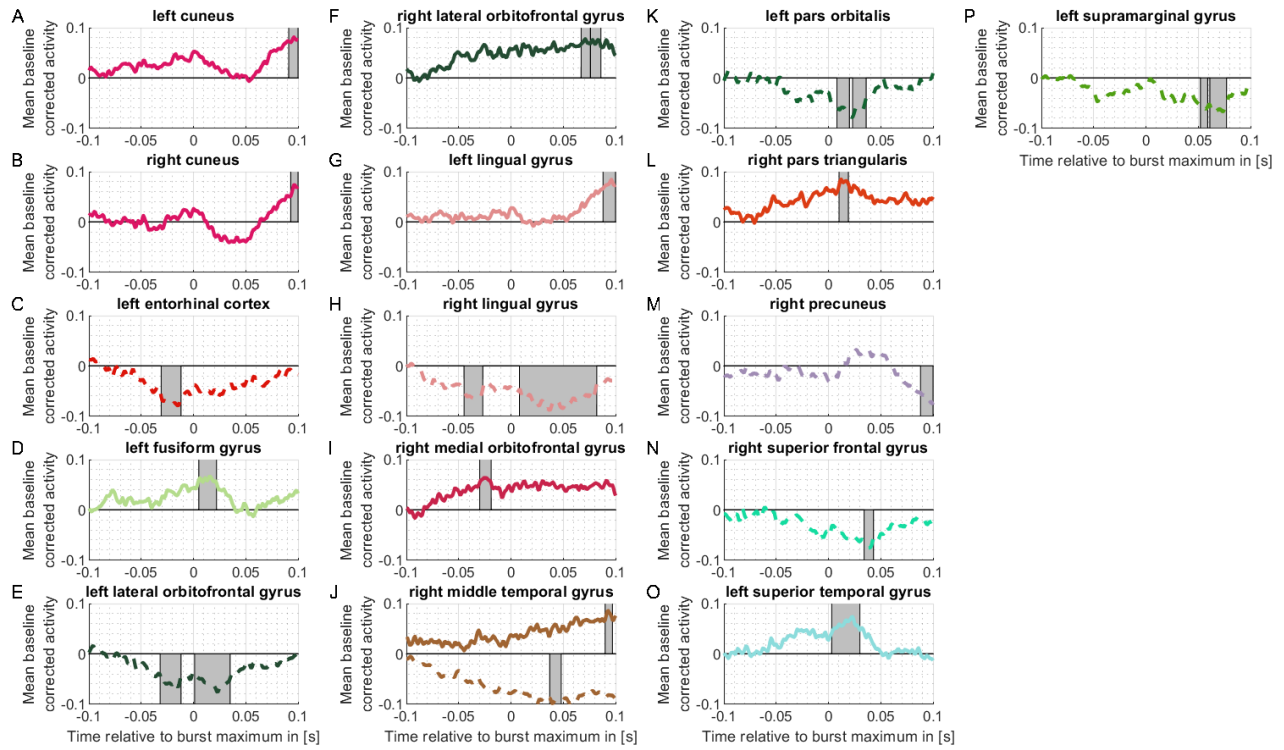


Figure 11.20: Cortical ERFs evoked by beta bursts onset in the left STN with a maximum duration of 300 ms

For detailed description, please refer to Figure 11.14.

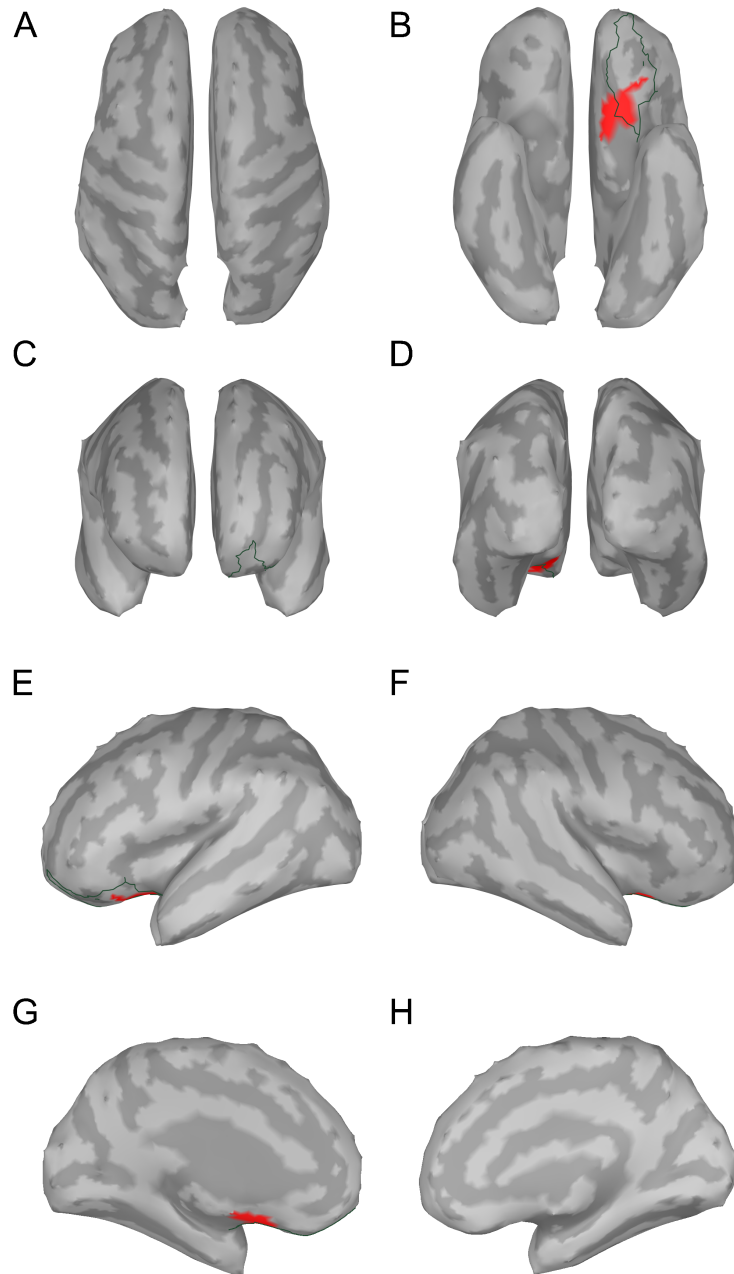


Figure 11.21: Cortical ERPs evoked by beta bursts onset in the right STN with a maximum duration of 300 ms

For detailed description, please refer to Figure 11.13.

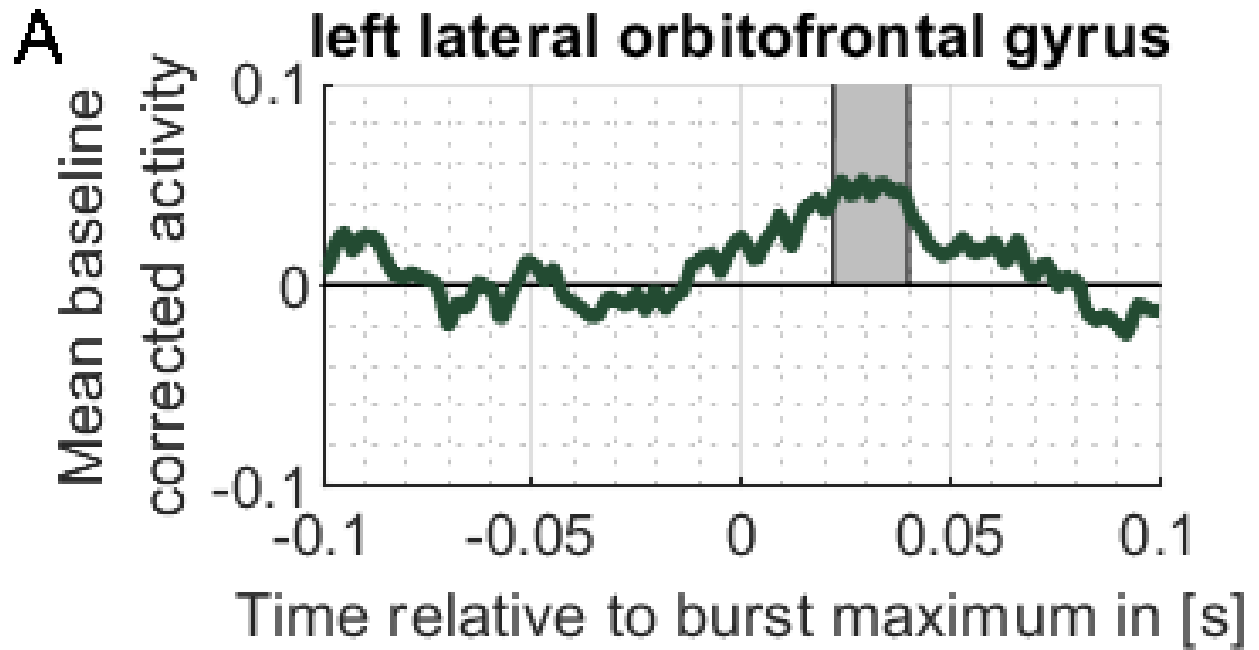


Figure 11.22: Cortical ERFs evoked by beta bursts onset in the right STN with a maximum duration of 300 ms

For detailed description, please refer to Figure 11.14.

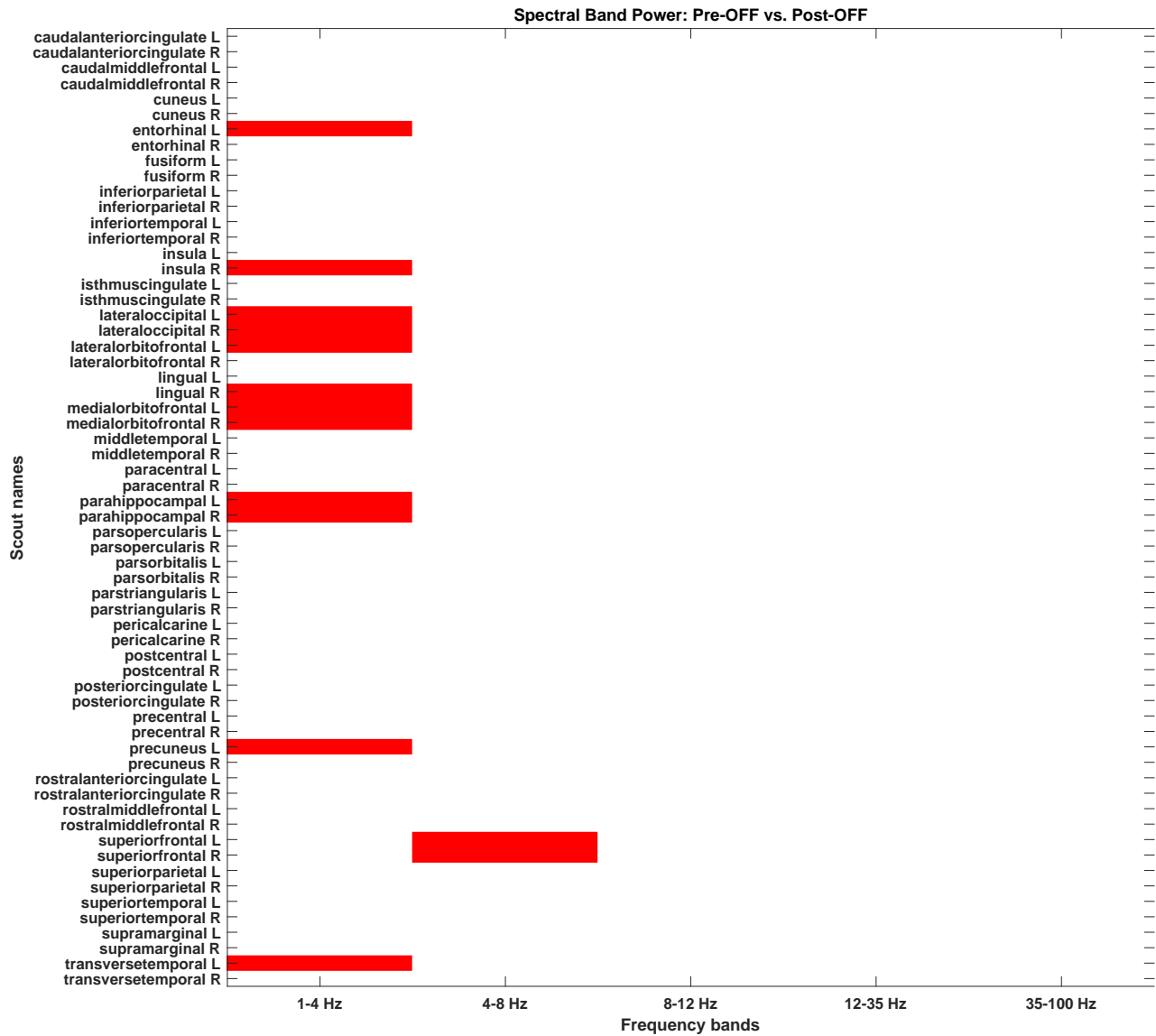


Figure 11.23: Altered spectral band power OFF medication by electrode implantation

For 62 different cortical regions, based on the Mindboggle atlas, significant differences in power are displayed for five different frequency bands before and after electrode implantation in the dopaminergic medication OFF condition. Blue indicates a significant decrease in power after electrode implantation, and red indicates a significant increase. An independent t-test followed by Bonferroni correction for the 62 cortical regions, 5 frequency bands, and 2 medication states was used.

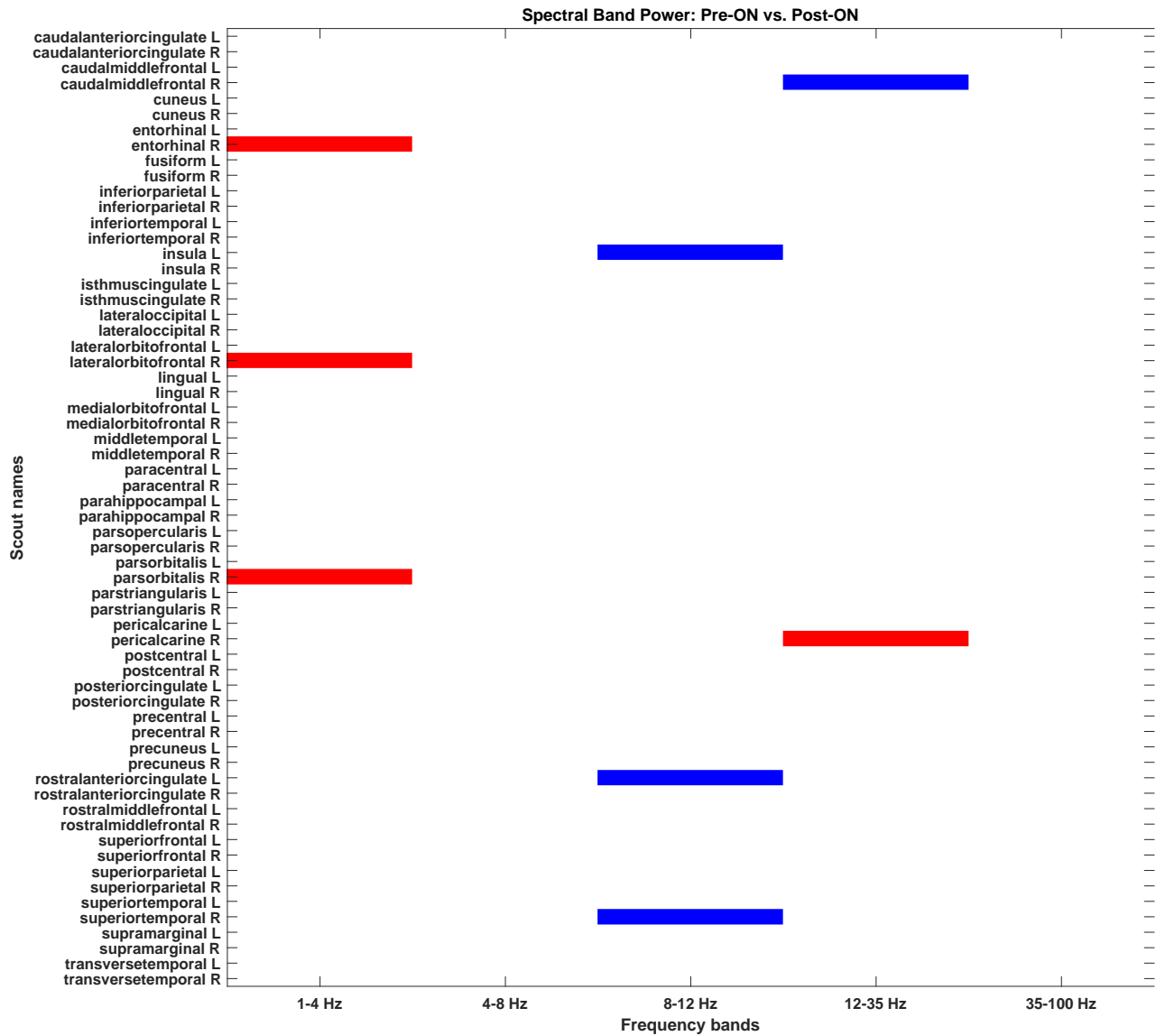


Figure 11.24: Altered spectral band power ON medication by electrode implantation

For 62 different cortical regions, based on the Mindboggle atlas, significant differences in power are displayed for five different frequency bands before and after electrode implantation in the dopaminergic medication ON condition. Blue indicates a significant decrease in power after electrode implantation. No significant increase was found. An independent t-test followed by Bonferroni correction for the 62 cortical regions, 5 frequency bands, and 2 medication states was used.

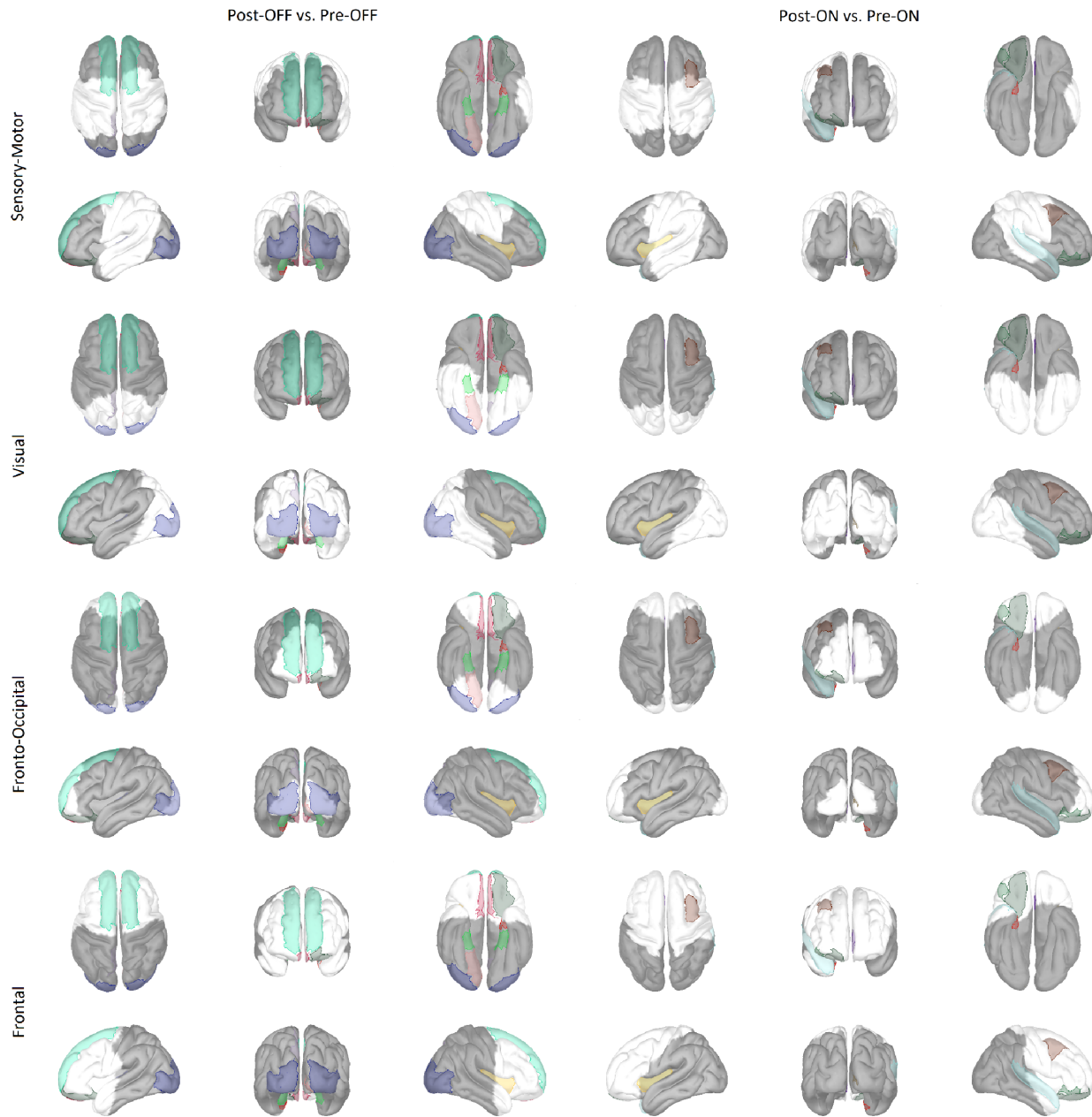


Figure 11.25: Cortical regions with altered power after electrode implantation

Cortical regions with significant differences in power in at least one of five frequency bands (delta: 1-4 Hz, theta: 4-8 Hz, alpha: 8-12 Hz, beta: 12-35 Hz, gamma: 35-100 Hz) emerge in the comparison of post-OFF vs. pre-OFF (three left columns) and post-ON vs. pre-ON (three right columns). Brain areas with significant changes are highlighted. The four resting-state networks (RSN; rows 1 & 2: sensory-motor, rows 3 & 4: visual, rows 5 & 6: fronto-occipital, rows 7 & 8: frontal) are shown for spatial comparison. Areas belonging to either RSN in post- and/or pre-recording are marked in white. Only areas of the RSNs where the coupling strength in one of the two conditions was at least 0.4 are displayed.

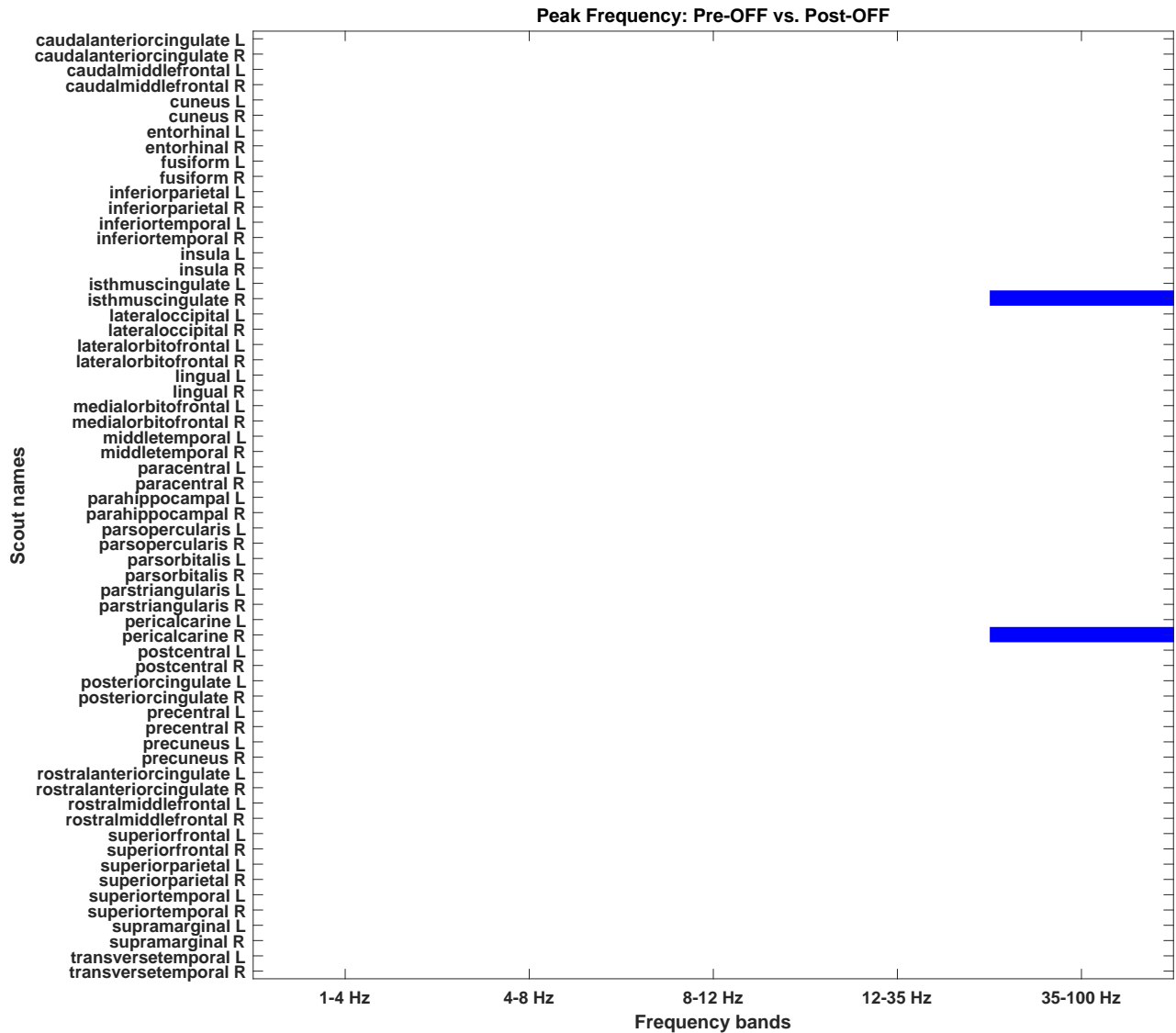


Figure 11.26: Altered peak frequencies OFF medication by electrode implantation

For 62 different cortical regions, based on the Mindboggle atlas, indicates whether the peak frequency of five different frequency bands differs significantly before and after electrode implantation in the dopaminergic medication OFF condition. Blue indicates a significant decrease in power after electrode implantation. No significant increase was found. An independent t-test followed by Bonferroni correction for the 62 cortical regions, 5 frequency bands, and 2 medication states was used.

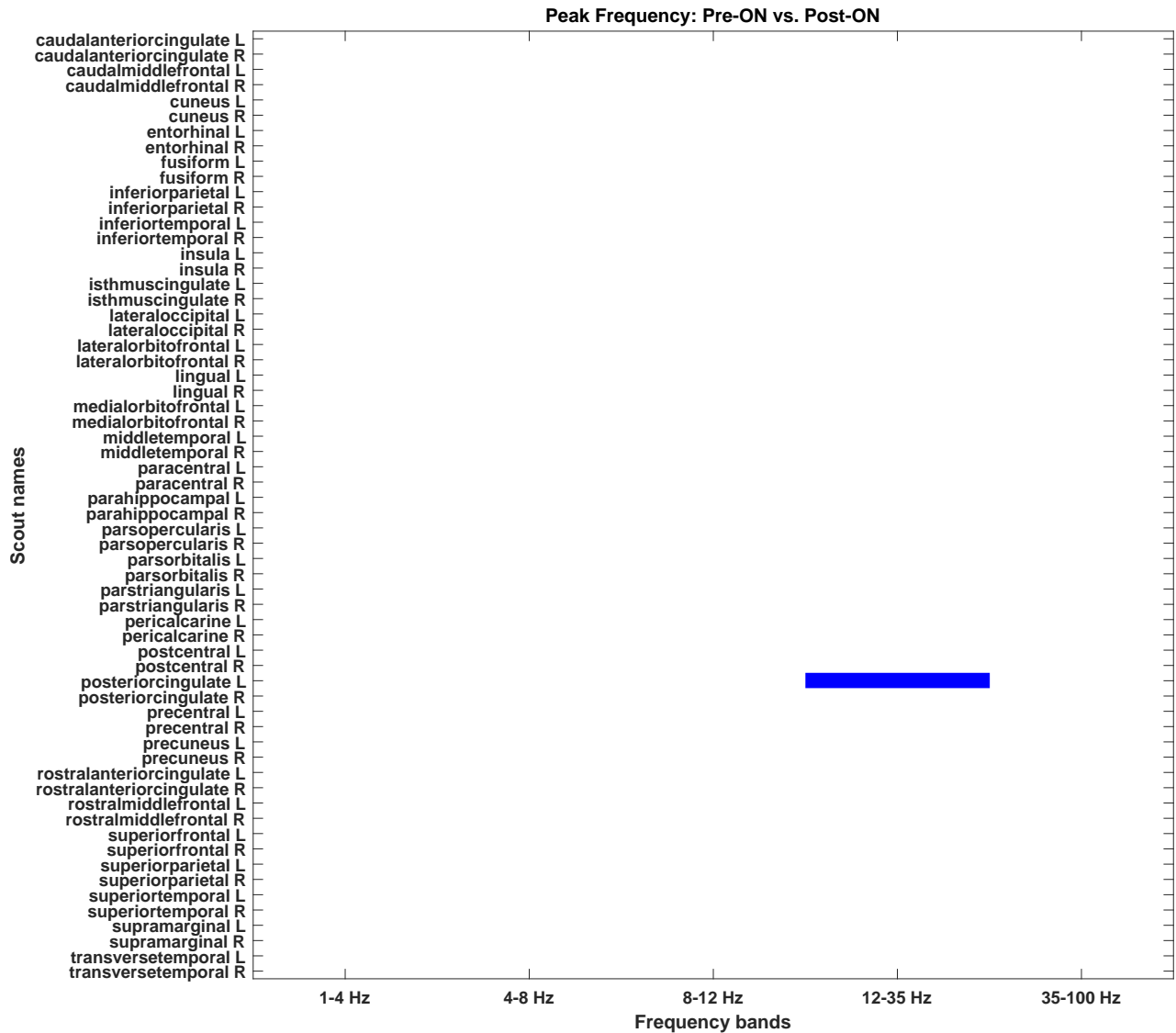


Figure 11.27: Altered peak frequencies ON medication by electrode implantation

For 62 different cortical regions, based on the Mindboggle atlas, indicates whether the peak frequency of five different frequency bands differs significantly before and after electrode implantation in the dopaminergic medication ON condition. Blue indicates a significant decrease in power after electrode implantation. No significant increase was found. An independent t-test followed by Bonferroni correction for the 62 cortical regions, 5 frequency bands, and 2 medication states was used.